EFFECTS OF THE PREDATORY BACTERIUM *BDELLOVIBRIO BACTERIOVORUS* ON MICROBIAL COMMUNITIES: AN INVESTIGATION USING MATHEMATICAL MODELLING AND CHEMOSTAT ARRAYS

by

JOANNA KIMBERLEY SUMMERS

A thesis submitted to the University of Birmingham

for the degree of DOCTOR OF PHILOSOPHY

Institute of Microbiology and Infection
Centre for Systems Biology
School of Biosciences
University of Birmingham
September 2019

ABSTRACT

Increasing antimicrobial resistance creates an urgent need for innovative treatments for bacterial infections. Predatory bacteria, such as *Bdellovibrio bacteriovorus*, hold promise as one alternative, they predate a wide range of Gram-negative bacteria, and are non-toxic to eukaryotic cells. Microbial predators also make excellent model systems to study predator-prey dynamics. To exploit the potential of chemostats in understanding bacterial predation I developed a family of mathematical models and an array of chemostats.

Using the most biologically relevant model I explored predation under a wide range of circumstances and discovered a system prone to extreme oscillations. I predicted optimal values for prey size, predator attack rate and mortality. I used variants of this model to fit data, from the Sockett lab on dual predation of *Escherichia coli* by *B. bacteriovorus* and a bacteriophage. This modelling explained why dual predation was effective at reducing the density of *E. coli* when single predation was not.

Finally, I developed an array of chemostats to test model predictions, and a community of bacterial species, two prey, one decoy and *B. bacteriovorus* that can co-exist as a whole or in combinations for several weeks. These can be used to explore the effects of alternative prey and decoy species on predator effectiveness and give insights into the best ways of treating bacterial infections with *B. bacteriovorus*.

This thesis is dedicated to two remarkable women, my grandmother Daisy Olive Bickerstaff (1909-2005) who shared my love of science and taught me never to stop learning and being curious about the world and my mother Janet Rose Summers (1941 – 2011) who showed me that with enough effort, resilience and determination you can achieve more than you ever thought possible. I love and miss you both so much.

ACKNOWLEDGEMENTS

They say it takes a village to raise a child, well it takes a University to train a PhD student. There are a great many people who have helped me go from a computer programmer with a fascination for biochemistry and microbiology to a microbiologist, but a few of these deserve a special mention. First, Klaus Fütterer, who on receiving an application for the undergraduate biochemistry course from a student whose qualifications were over 20 years old, did not simply reject this, but took the time to discover whether I would be able to cope with the course. So, thank you Klaus Fütterer, without you my journey would not have got started. Secondly, Andy Lovering. By the end of the second year of my undergraduate degree I knew I wanted to study microbiology, but was unsure which area to go into. Then I saw the description for a project involving a predatory bacterium, it blew my mind and I knew this was what I wanted to study. Thank you, Andy Lovering, for letting me spend my third year project studying *Bdellovibrio* in your lab. Much however, as I was fascinated by *Bdellovibrio*, I realised I didn't want to be a structural biologist. What did appeal to me was a series of lectures by Jan Kreft on how bacteria live together in communities, and when I was offered the opportunity to do a PhD studying the effects of *Bdellovibrio* on communities of other bacteria I jumped at the chance. So, thank you Jan for a wonderful PhD project. Finally thank you to all the fantastic people I have worked with, in the Kreft lab, the CCB, the third floor environmental 'omics group and the G7 lab.

Outside of the University I have been supported by a fabulous group of friends and family. Most especially my father Brian Summers, my late step-father Larry Gorton

who always made sure I ate properly and Jackie, the best friend, confidant and often therapist anyone could ever have, I couldn't have done this without you.

CONTENTS

LIST OF FIGURES

LIST OF TABLES

LIST OF ABBREVIATIONS & SYMBOLS

ABC	Approximate Bayesian computation
BALO	*Bdellovibrio* and like organism
B. subtilis	*Bacillus subtilis*
B. bacteriovorus	*Bdellovibrio bacteriovorus*
cfu	Colony forming unit
DDM	Davis minimal medium without citrate
E. coli	*Escherichia coli*
eGFP	Enhanced green fluorescent protein
HEPES	4-(2-hydroxyethyl)-1-piperazineethanesulfonic acid
HI	Host-independent
ID	Internal diameter
LB	Lysogeny broth
MCMC	Markov chain Monte Carlo
MMA	Modified MacConkey agar
OD	Optical density
ODE	Ordinary differential equation
pfu	Plaque forming unit (cf. cfu)
PCA	Principal component analysis
P. putida	*Pseudomonas putida*
P. synxantha	*Pseudomonas synxantha*
qPCR	Quantitative polymerase chain reaction
SMC	Sequential Monte Carlo

CHAPTER 1: INTRODUCTION

"Tyger tyger, burning bright,

In the forests of the night;

What immortal hand or eye,

Could frame thy fearful symmetry?"

With his evocative poem Blake (1794) illustrates the sense of fascination humankind has for predators, from the tiger in the poem, to the wolf pack or a spider waiting in her web. We feel a sense of excitement in the hunt and anthropomorphically identify with both the hunter and the hunted. Microbial predators rarely evoke the same sense of awe, yet they share many properties of larger predator prey ecosystems and can make excellent models, as well as being important in their own right.

Predators are often keystone species in natural ecosystems (Paine, 1969) and predation of bacteria by protists (Fuhrman and Noble, 1995), bacteriophages (Proctor and Fuhrman, 1990) and other bacteria (Williams *et al.*, 2016) plays an important ecological role by regulating the density of bacteria, which are recyclers of carbon and nitrogen (Azam *et al.*, 1983). Investigations into predator-prey dynamics in natural settings are, however, complicated by an array of confounding factors (Krebs *et al.*, 2001). Microbes, by contrast, make attractive models for studying predator-prey interactions in a controlled environment, with millions of individuals in a drop of liquid that can go through many generations in days. A completely separate, but increasingly important, reason for interest in microbial predators is the antimicrobial resistance crisis, with resistance to even last resort antibiotics such as colistin rising (Arcilla *et al.*, 2016). There is an urgent need for 'living antibiotics' as alternatives to antibiotics, and indeed both bacteriophages (Abedon *et al.*, 2011) and bacterial predators (Sockett

and Lambert, 2004) have been proposed as alternative treatments for bacterial infections.

Even within microbial predators, predation by bacteria is less well studied, though of the bacterial predators *Bdellovibrio bacteriovorus* has received the most attention. *B. bacteriovorus* is a small, Gram-negative bacterium with predatory capabilities. It was discovered by accident by Stolp & Petzold (1962) whilst searching for bacteriophages. They had run out of their usual size filters and so used a filter with a slightly larger pore, which allowed the *Bdellovibrio*, to pass through. Normally phage plaques develop to their full size within 24 hours. Stolp and Petzold however saw plaques that did not start to develop for two days and continued to grow for about ten days. Curious about the source of these plaques they examined samples under a phase microscopic, and found fast moving bacteria that were only just big enough to see and which caused neighbouring *Pseudomonas* cells to lyse. *Bdellovibrio* was not the first predatory bacterium to be discovered, the predatory capabilities of *Myxococcus xanthus*, had been known since 1941 (Beebe, 1941). Bacterial predation however, was a little studied area, and *M. xanthus* is an opportunistic, wolf-pack type predator, while *Bdellovibrio* is an intracellular predator that has mechanisms to avoid sharing prey (Lerner *et al.*, 2012). Like *Bdellovibrio*, *M. xanthus* is a δ-proteobacterium and the two are quite closely phylogenetically related (Donze *et al.*, 1991). *M. xanthus* has a complex lifecycle, which includes aggregating into large groups and then forming a fruiting body to disseminate myxospores when facing starvation. It is also considered a model organism for social behaviour in bacteria (Zusman *et al.*, 2007). Unlike *Bdellovibrio*, *M. xanthus* does not possess a flagellum and can only move by gliding

slowly along surfaces. When a colony of *M. xanthus* cells encounters a colony of prey such as *E. coli* it swarms over them in a rippling motion, releasing lytic enzymes that kill and degrade its prey as it goes (Berleman *et al.*, 2006).

Since the discovery of *Bdellovibrio,* other predatory bacteria have been found, with a wide variety of predatory strategies and lifestyles from almost every habitat (Pérez *et al.*, 2016). While still understudied, *Bdellovibrio* has become the best understood intracellular, bacterial predator, and research has clarified many details of its predatory nature (Sockett and Lambert, 2004; Sockett, 2009; Rotem *et al.*, 2014). Other research has looked into the impacts of predatory bacteria in shaping ecosystems, and the evolutionary effects of prey species on their predators (Williams *et al.*, 1982; Piñeiro *et al.*, 2004; Chauhan *et al.*, 2009; Chen *et al.*, 2011, 2018). Recently, with the ever-increasing problem of antibiotic resistance, significant work has gone into evaluating the potential, (Chu and Zhu, 2009; Atterbury *et al.*, 2011; Saxon *et al.*, 2014; Willis *et al.*, 2016; Findlay *et al.*, 2019), safety and immunogenicity of *Bdellovibrio* and other predatory bacteria. Predatory bacteria were found to be non-toxic to rabbit eyes (Romanowski *et al.*, 2016), rats (Shatzkes *et al.*, 2016, 2017) mice (Shatzkes *et al.*, 2015) and mice cell lines (Monnappa *et al.*, 2016), human cell lines (Shanks *et al.*, 2013; Gupta *et al.*, 2016; Monnappa *et al.*, 2016; Romanowski *et al.*, 2016) and human phagocytic cells (Raghunathan *et al.*, 2019). *Bdellovibrio* also induced a much smaller cytokine response than pathogens such as *Klebsiella pneumoniae* (Shatzkes *et al.*, 2015, 2017), probably due to its unusual, neutral lipid A (Schwudke *et al.*, 2003).

1.1 *Bdellovibrio* morphology and lifecycle:

Bdellovibrio And Like Organisms (BALOs) are Gram-negative proteobacteria with a single flagellum and a curved rod shape (Stolp and Starr, 1963). One genus of α-proteobacterial BALOs, the *Micavibrios*, have been found (Lambina *et al.*, 1982), but all other BALOs discovered to date are δ-proteobacteria. *Micavibrio* are epibiotic predators that attach to their prey and suck nutrients out of them (Lambina *et al.*, 1982). Almost all δ-BALOs, by contrast, invade the periplasm of their prey, an exception being *Bdellovibrio exovorus*, which is another epibiotic predator (Koval *et al.*, 2013).

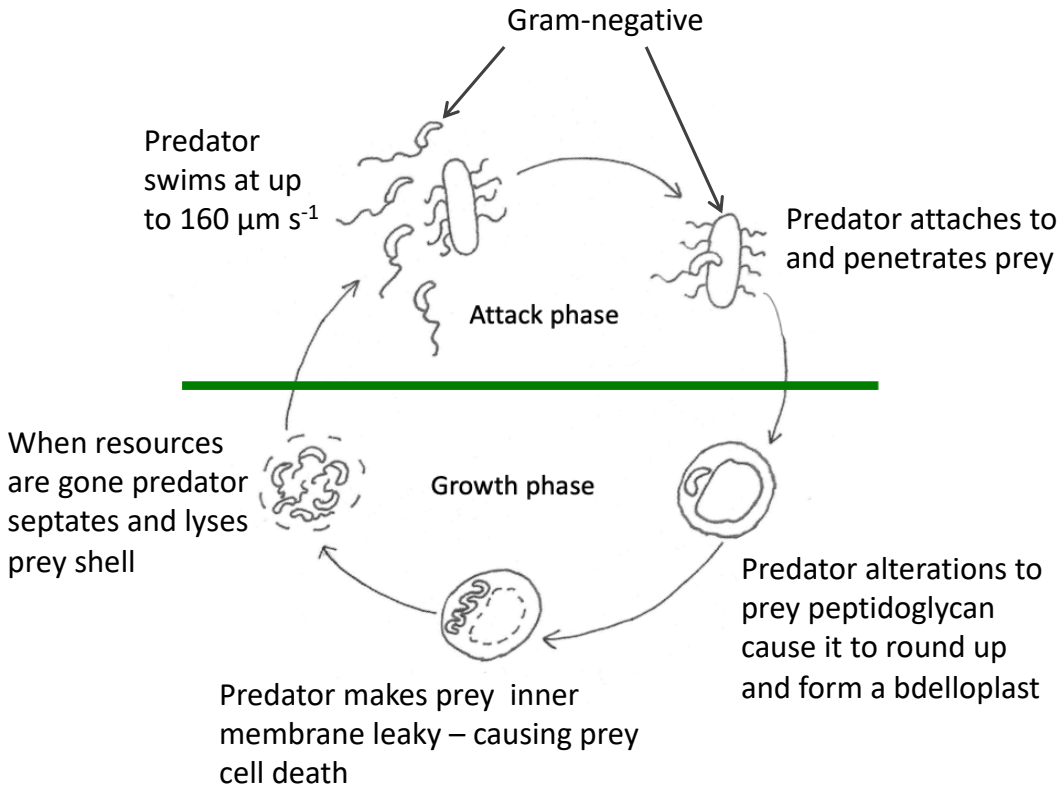

Figure 1.1 – The lifecycle of *Bdellovibrio* and other BALOs.
Figure inspired by (Sockett and Lambert, 2004).

δ-BALOs have an unusual biphasic lifecycle (Fig. 1.1). In their attack phase, some *Bdellovibrios* are capable of swimming at speeds of up to 160 µm second^{-1} in

liquid cultures, (Lambert, Evans, *et al.*, 2006) as they search for prey bacteria. They probably use chemotaxis to aid the search by detecting areas of high bacterial density such as biofilms. The *Bdellovibrio* genome contains genes involved in chemotaxis and knocking out these can reduce predation efficiency (Lambert *et al.*, 2003). It has also been showed that *Bdellovibrio* are chemotactically attracted to yeast extracts (Straley *et al.*, 1974), casamino acids (Chauhan and Williams, 2006), high densities of prey cells (Straley and Conti, 1977), and various other compounds, including certain amino acids (Lamarre *et al.*, 1977), short chain fatty acids, components of the tricarboxylic acid cycle and other key metabolic pathways, inorganic ions and oxygen (Straley *et al.*, 1979). It is unlikely that *Bdellovibrio* can track individual cells as any chemoattractant would likely be at a low concentration and easily diluted away, especially in an environment where there is substantial mixing, such as a chemostat. With a cluster of prey such as a biofilm however, the high density of cells would cause a much stronger signal to be produced, which could be detected. Once in a biofilm the speed of *Bdellovibrio* is much reduced, and movement is via a gliding motion, that is only partially understood (Lambert, Chang, *et al.*, 2010; Lambert *et al.*, 2011; Milner *et al.*, 2014).

When *Bdellovibrio* locate a possible prey bacterium they initially attach loosely to this (Starr and Baigent, 1966). Attachment to a non-suitable target is reversed after a few minutes (Hobley *et al.*, 2006). With suitable prey, attachment becomes permanent and is followed by penetration into the prey periplasm and loss of the flagellum (Starr and Baigent, 1966). Penetration is accomplished by the secretion of lytic enzymes, including peptidases and transglycosylases, to create a pore in the prey outer membrane and cell wall (Thomashow and Rittenberg, 1978a), and the use of

type IV pili, located at the penetration pole, at the opposite end of the *Bdellovibrio* from its flagellum (Lambert, Morehouse, *et al.*, 2006). There is a degree of redundancy in the lytic enzymes, as deletion of the genes for a number of these, including *Bd0816* and *Bd3459*, reduced the efficiency of predation but did not make the bacterium non-predatory (Lerner *et al.*, 2012). The type IV pili however, are essential for predation, as a *pilA* deletion mutant was non-predatory (Evans *et al.*, 2007). Once the predator has entered the periplasm of the prey, it further modifies the prey peptidoglycan. This causes degradation of the peptidoglycan to cease, protecting the structural integrity of the prey cell (Thomashow and Rittenberg, 1978c).

In cases of particularly high multiplicity of infection, it is possible for two *Bdellovibrios* to attach to and penetrate the same prey simultaneously. Tailgating infections, where one *Bdellovibrio* has already established itself in a prey bacterium, and a second *Bdellovibrio* then penetrates the same prey, are rarer. This is likely due to modifications made to the prey cell wall by two carboxypeptidases, encoded by *Bd0816* and *Bd3459*, which are expressed in the 15 to 30 minutes after *Bdellovibrio* has entered the prey. These changes mark the prey out as unsuitable for further predation and cause the rounding up of prey cells. Deletion of either of these genes resulted in slower entry of *Bdellovibrio* into prey, increased numbers of tailgating infections and reduced rounding, with a double knockout mutant showing a more severe phenotype (Lerner *et al.*, 2012). X-ray crystallography of Bd3459, which is structurally similar to type 4 penicillin binding proteins, responsible for normal maintenance of peptidoglycan, showed it lacked a type III domain (Lerner *et al.*, 2012). This domain is responsible for substrate specificity (Lerner *et al.*, 2012) and its absence

may be the reason *Bdellovibrio* can degrade the peptidoglycan of a wide range of prey species.

Penetration takes about 20 minutes (Varon and Shilo, 1968), during which time the prey cell is killed (Rittenberg and Shilo, 1970). To penetrate the prey cell, the predator creates a small pore in the prey outer membrane and peptidoglycan, (Starr and Baigent, 1966) through which it squeezes. Once inside the periplasm, the pore is sealed and further modifications to the prey peptidoglycan cause the prey cell to swell and round up, (Starr and Baigent, 1966; Thomashow and Rittenberg, 1978b) creating a space in which the *Bdellovibrio* can grow. The prey inner membrane becomes porous (Romo *et al.*, 1992), allowing nutrients to leak out into the periplasm where the growing *Bdellovibrio* can absorb them. Leakage out of the periplasm is prevented by modifications to the prey outer membrane, which becomes less porous (Sockett, 2009). The rounded up dead prey cell with the *Bdellovibrio* lodged within, is known as a bdelloplast (Marbach *et al.*, 1976).

Inside the bdelloplast, the *Bdellovibrio* undergoes a change in gene expression, down-regulating many genes associated with its attack phase, and up-regulating others to enter its growth phase (Rendulic *et al.*, 2004; Lambert, Chang, *et al.*, 2010). The time spent in this growth phase varies, but for a typical *E. coli* cell is around 3 hours (Shilo and Bruff, 1965). During this time, the *Bdellovibrio* releases a battery of hydrolytic enzymes, that break down prey macromolecules (Matin and Rittenberg, 1972). These nutrients are taken up by the *Bdellovibrio*, which uses them to fuel its growth and replicate its genome. In the bdelloplast, the *Bdellovibrio* elongates, becoming a twisted spiral shape containing multiple copies of its genome (Lambert, Evans, *et al.*, 2006). When prey resources are largely exhausted the *Bdellovibrio*

septates into multiple new cells, each containing a single copy of its genome and the prey cell is lysed (Burnham *et al.*, 1970). The new predators grow a flagellum, and leave the remnants of the prey cell by gliding (Lambert *et al.*, 2011), before re-entering attack phase and seeking out new prey.

From the first discovery of *Bdellovibrio*, host-independent (HI) mutants that can grow outside of prey cells have been observed (Stolp and Starr, 1963) (Fig. 1.2). These arise spontaneously at a rate of about 1 in 10^6 to 10^7 bacteria (Seidler and Starr, 1969b). They have also been obtained from many species of BALO by inoculating a rich media, supplemented with an antibiotic, with antibiotic resistant BALOs previously grown on antibiotic sensitive prey (Seidler and Starr, 1969b). A rich medium is needed because *Bdellovibrio* is auxotrophic for many compounds, including at least nine amino acids (Rendulic *et al.*, 2004). Some HI strains may retain the ability to predate other cells, albeit at a reduced rate, probably due to a loss of motility, whilst other strains are entirely non-predatory (Varon and Seijffers, 1975). Most HI strains have a mutation in an area of the genome referred to as the *hit*-locus (Cotter and Thomashow, 1992), which comprises genes *Bd0108* and *Bd0109,* involved in pilus formation (Capeness *et al.*, 2013).

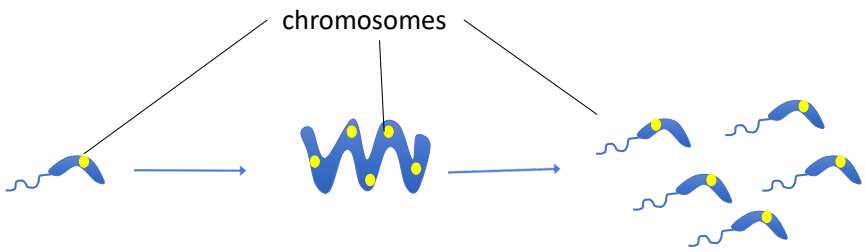

Figure 1.2 – Host-independent BALO lifecycle

Host-independent (HI) mutants have been obtained for several species of BALOs. These grow in rich media to form coenocytic filaments of varying lengths and morphologies, although they are usually spiral in form and lack flagella. After some variable length of time growing as a filament, they septate into new flagellated BALOs, which resemble attack phase host-dependent (HD) BALOs in morphology and which start to once again grow as filaments and lose their flagella. Many HI mutants are capable of predation, but are less efficient at this than HD BALOs.

There is a high degree of heterogeneity in the morphology of populations of HI mutants. They can have spherical, rod-shaped and even spiral forms, but in general are between 1 and 10 µm in length and around 0.3 µm wide (Seidler and Starr, 1969b). They usually grow as coenocytic filaments, which often have reduced mobility (Varon and Seijffers, 1975). Generally they septate on reaching about 10 µm length, which usually happens after about 3 hours (Shilo and Bruff, 1965), similar to the time spent in a bdelloplast, although they can reach a length of 50 µm (Burnham *et al.*, 1970). Septation of a 10 µm filament would be expected to give 7 to 10 new *Bdellovibrio* (Diedrich *et al.*, 1970) (slightly more than from an *E. coli* bdelloplast).

One open question concerns the nature and prevalence of any resister phenotype. While bacterial resistance to bacteriophages is a common phenomenon (Luria and Delbrück, 1943), stable genetically inherited resistance to BALOs is much more unusual. To my knowledge only Varon (1979) and Gallet, Tully and Evans (2009) have reported the occurrence of stably inherited resistance, the former in a continuous culture experiment, the later using serial transfers. A more common occurrence is a ‘plastic’ phenotypic resistance, which has been seen in a variety of prey

species, including *E. coli*, *Erwinia carotovora* and *Pseudomonas syringae* (Shemesh and Jurkevitch, 2004). This can be triggered by exposure to various *Bdellovibrio* strains and is protective against *Bdellovibrio* strains other than that which triggered the plastic resister phenotype. The protection is not absolute, plastic resister cells are still eventually preyed upon, and after a period of time without exposure to predators, the plastic resistance is lost. In particular, if plastic resistant prey cells are grown in the absence of predators their descendants have no resistance to predation (Shemesh and Jurkevitch, 2004). The mechanism by which this resistance occurs is unclear, it is known that the presence of an S-layer is a barrier to predation (Koval and Hynes, 1991), but that capsule is not (Koval and Bayer, 1997) and that changes in the lipopolysaccharide (LPS) of potential prey affects the rate at which predators attach to the prey (Varon and Shilo, 1969). What is also not known is exactly how long plastic resistance lasts, by what factor predation efficiency is reduced, and how plastic resistance affects growth characteristics of the prey. In Chapter 4 of this thesis I have fitted models to an experimental dataset generated by the Sockett lab (Hobley *et al.*, 2019). This model fitting showed strong support for presence of a plastic resistant phenotype and elucidated some of the probable kinetics of the formation and reversion of this phenotype.

1.2 *Bdellovibrio* research in chemostats

Chemostats are environments where nutrients are constantly refreshed and a proportion of the contents are removed through dilution. Bacteria will grow at the same rate as the dilution rate, unless this is faster than their maximal growth rate on the substrate concentration coming into the chemostat (Fig. 1.3a), and will usually consume most of the available nutrients unless the dilution rate is close to their maximal growth rate (Fig. 1.3c). When two species compete for the same niche within a chemostat, such as a single nutrient in limited supply, or a single prey species, generally, only one can survive, and this will be the species which grows fastest on the available substrate (Fig. 1.3b)(Hardin, 1960). There are exceptions to this, the addition of a predator species can allow for the existence of two competing prey species, one slower growing, but less predated and the second faster growing but more heavily targeted by the predator (Becks *et al.*, 2005). Another example would be, if the faster growing species had an incomplete metabolic pathway that resulted in the production of a substance that could act as a nutrient source for a second slower growing species, thus effectively constructing a second ecological niche (Rosenzweig *et al.*, 1994). While no natural system is an ideal chemostat, the gut and wastewater treatment plants both have similarity to chemostats. There is an inflow of fresh nutrients and bacteria are constantly growing and consuming nutrients, keeping nutrient levels within the system low.

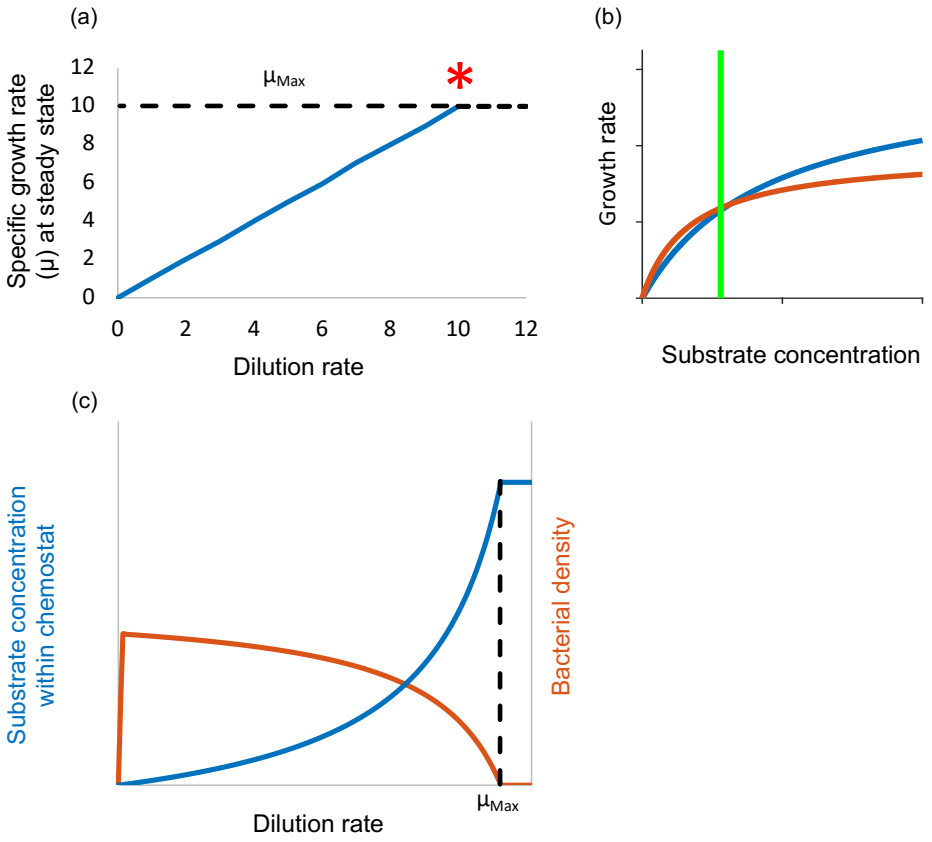

Figure 1.3 – Chemostat kinetics

Panel (a) Relationship between growth rate and dilution rate, units are arbitrary, * marks the point at which the bacteria washout. Panel (b) Growth rates of two bacterial species, blue has a higher maximum growth rate, but also a higher half-saturation constant for prey. At substrate concentrations less than the green line red will outcompete blue and blue will be washed out of the chemostat. At substrate concentrations above the green line the reverse will occur. Panel (c) Relationship between dilution rate and substrate concentration in blue and bacterial density in red (bacterial specific growth rate is constant).

Most experiments with BALOs have been performed in batch cultures, where prey cells are often in stationary phase, due to nutrient depletion, and prey populations decrease due to predation. Chemostats, by contrast, offer an environment where nutrients are constantly renewed, and the prey is in exponential growth phase. As a result of this, the population dynamics and growth kinetics of both predator and prey can be studied over long time periods (in the order of months), equivalent to several thousand generations. Additionally, it is possible to control and adjust both the concentration of nutrients entering the chemostats and their rate of

flow. Despite the above benefits, little work on *Bdellovibrio* has been carried out in chemostats.

Some early laboratory work was undertaken by Whitby in his PhD thesis (Whitby, 1977) on predation of *Spirillum serpens* by *B. bacteriovorus* strain 6-5-S. At low dilution rates (0.05 h^{-1}) the predator and prey were in a stable steady state. At faster dilution rates he observed sustained oscillations of both predator and prey that were out of phase, and which had a period that ranged from ~70 h to ~130 h depending on the dilution rate. At even faster dilution rates (over 0.5 h^{-1}) the *Bdellovibrio* were washed out.

Varon and co-workers, used the marine BALO BM4 and a luminescent prey, *Photobacterium leiognathi* E28 (Varon, 1979; Varon *et al.*, 1984). Varon reported, that in a chemostat the prey diverged into two phenotypes. One was similar to the original strain, the other had a slower specific growth rate, but increased resistance to predation (Varon, 1979). In later experiments Varon, Fine and Stein found that a prey density as low of 2 x 10^5 colony forming units (cfu) ml^{-1} of *Photobacterium leiognathi* E28 could sometimes sustain BALO BM4, but this was erratic and in 60% of cases the predator did not survive.

Dulos and Marchand (1984) used *E. coli* and *B. bacteriovorus* in their chemostats at low dilution rates and obtained oscillations, but these were erratic and not reproducible. Since then little experimental work has been carried out on BALOs in chemostats, and many questions remain to be answered, particularly around the effects of alternative prey species and decoys.

To help with answering some of these questions I have developed an array of small chemostats, detailed in Chapter 5 of this thesis, to facilitate the exploration of

multiple conditions in parallel, with good levels of replication. I have also developed a small community of four bacterial species, that can co-exist for at least three weeks.

1.3 Existing Mathematical Models:

There is a rich history over the last century of mathematical modelling, of predator-prey dynamics. One of the earliest models (Eq. 1.1a and 1.1b), was developed independently by Lotka (1925) and Volterra (1926) the latter inspired by catches of fish in the Adriatic Sea. The density of prey is N and the density of the predator P. The prey has a specific growth rate μ and the predator a mortality rate of λ. Predation occurs at a rate proportional to the density of both predator and prey and results in the production of β units of predator for each α units of prey consumed. Using this simple system, they showed that predator-prey models could produce sustained oscillations in the densities of both populations without the need for external fluctuations (e.g. in environmental conditions).

$$\frac{dN}{dt} = \mu N - \alpha NP \quad (1.1a)$$

$$\frac{dP}{dt} = \beta NP - \lambda P \quad (1.1b)$$

These oscillations however were not stable, as they were neutral cycles about an equilibrium point at $N = \frac{\lambda}{\beta}, P = \frac{\mu}{\alpha}$, that was neither an attractor, nor a repeller, therefore the amplitude of the oscillations depended upon the initial conditions (Fig. 1.4a) (Edelstein-Keshet, 2005). Any subsequent perturbations, as would be seen in any real-world situation, would result in a change to the amplitude of the oscillations. The oscillations were not robust to perturbations, because the system did not contain any negative feedback mechanisms. The Lotka-Volterra model assumed prey grew exponentially without constraint, which destabilises the system, as in the absence of predation, there is no control on infinite prey growth. Predation was assumed to be proportional to the density of prey, and did not saturate even at very high prey

densities, implying the predator could consume prey at an infinitely fast rate. These over simplifications lead to results that were neither biologically interesting, nor realistic.

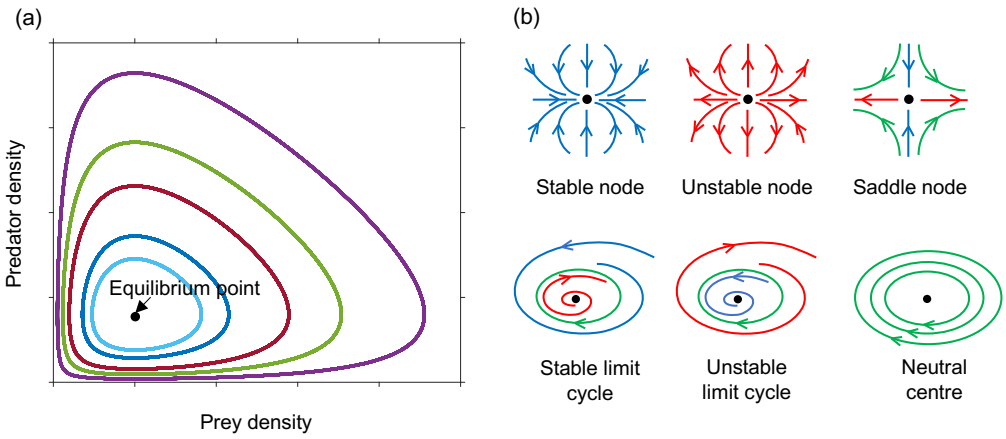

Figure 1.4 – Phase plane diagram of equilibrium points

Panel (a) Phase plane diagram of a Lotka-Volterra system with varying initial conditions (b) Phase plane diagram of various types of equilibria. Arrows indicate direction of flow over time, blue towards the equilibrium point (black dot), red away from equilibrium, green around the equilibrium.

More realistic functions for prey growth include the logistic function and the Gompertz function. The logistic function was first developed by Pierre Verhulst (1838) to model growth in human populations, and was subsequently shown by Gause (1934) to be a good fit to the growth of *Saccharomyces cerevisiae*. The logistic function takes the form:

$$\frac{dN}{dt} = kN\left(1 - \frac{N}{C}\right) \qquad (1.2)$$

Where k is the growth rate constant and C is the carrying capacity. The logistic function gives a sigmoidal curve, with growth being slowest at both very low prey densities, and at densities close to the carrying capacity.

The Gompertz function was first used in population dynamics by Gompertz (1825) to model human mortality figures and has since been adapted for predator-prey models. The Gompertz function takes the form:

$$\frac{dN}{dt} = kN \ln \frac{C}{N} \quad (1.3)$$

While the logistic and Gompertz functions successfully constrain prey growth at high prey densities, they also result in low growth rates at low prey densities. This phenomenon, known as the Allee effect (Allee and Bowen, 1932) has been seen in many animal systems, and may in part be due to low species density making it harder to find a mating partner for reproduction, or to co-operative group behaviour increasing reproductive success. In bacterial cultures however, finding a mating partner is not an issue as growth is by binary fission of a single individual. An alternative means of constraining prey growth, developed specifically for bacteria by Monod (1949), is for growth rates to saturate at high nutrient concentrations. In the Monod equation growth rate takes the form:

$$\frac{dN}{dt} = \frac{\mu_{max} NS}{S+K} \quad (1.2)$$

Where μ_{max} is the maximum specific growth rate, S the nutrient or substrate concentration and K, the prey half-saturation constant, that is the concentration of substrate required for the prey specific growth rate to be half its maximal value. The Monod equation gives a hyperbola with increases in substrate concentration having the largest effect when substrate concentrations are low and very little effect at already high substrate concentrations.

For the predator, similar constraints on growth are required in order for a system to realistically model biology, as no predator can consume prey at infinitely fast rates, as is implied by the Lotka-Volterra equations. Alternative forms for the predation rate were developed by Holling whilst studying the predation of sawflies by small mammals (Holling, 1959b), and subsequently tested in a disk experiment, with

human volunteers taking the role of predators (Holling, 1959a). Holling proposed three forms of predation rate or functional responses. In the type I functional response the predation rate is linearly proportional to prey density until it hits a certain value, at which point it saturates and does not change with further increase in prey density. This type of functional response is found in filter feeders (Jeschke *et al.*, 2004). The type II functional response takes the same form as the Monod equation (Eq. 1.2) and results from a handling time when prey is caught, that limits the maximum predation rate at high prey density. The type III function response has a sigmoidal form and arises from the presence of an alternative prey. Which if any of these functional responses best matches the actual predation rate of a system depends on the nature of both predator, prey and their environment, and indeed Holling saw live predation patterns that fitted all three proposed forms (Holling, 1959b).

Alternative modifications proposed for the predation rate include using a logistic function (Leslie, 1948), which introduces a ratio-dependence on prey, and using a per-capita predation rate (Arditi and Ginzburg, 1989), which is most useful when there is a large difference in the time scales of predation time and generation time. Both ratio-dependence and per-capita predation rates solve the paradox of enrichment, where increasing nutrients at the lowest trophic level destabilise the system (Rosenzweig, 1971), and the biological control paradox (Luck, 1990), where models predict a low prey density cannot be stable (Berryman, 1992). This may be advantageous for some systems as it is certainly possible for low prey densities to still be apparently stable (Turnbull and Chant, 1961; Hagen and Franz, 1973). Additionally, while there are circumstances where enrichment does not result in a reduction in stability (Arditi and Ginzburg, 1989; Ginzburg and Akçakaya, 1992), there are also

cases where it does have a destabilising effect (Huffaker *et al.*, 1963). Furthermore, whilst mechanisms such as ratio-dependent and per-capita predation rates, which effect predation rates at high prey densities are sufficient to solve the paradox of enrichment, they are not necessary. Other mechanisms, such as predator mortality, which have the greatest effect on overall predation at low prey densities, also give a stabilising effect (Nisbet *et al.*, 1983). The conclusion from this is that care should be taken when choosing growth and predation rate functions to select the most appropriate functions for the type of system being modelled, no one function has been found that is best for all scenarios.

Adding saturation to prey growth or predation rates in any of the above forms alters the stability of the system, making oscillations more or less likely, depending on the precise functions chosen. Many real animal predator-prey systems have also been shown to display oscillations, including snowshoe hares and lynx (Maclulich, 1936), lemmings (Elton, 1942), moths (Bigger, 1973) and protists (Luckinbill, 1973) to name but a few. Understanding the nature of these oscillations, and how they are likely to be impacted by interventions, such as nutrient enrichment or the reduction of predators has implications for both species conservation and bio-control of pest species, as well as the use of predators to reduce or eliminate pathogens. May contends that almost all predator prey models contain either a stable node or a stable limit cycle (Fig. 1.4b), for all parameters where both species can co-exist (May, 1972). Although the oscillations associated with a stable limit cycle may be so extreme that at their nadir prey (or predator) densities may be become so low that stochastic fluctuations will cause the removal of the last of the species and the system will collapse (May, 1972).

Given the lack of robust permanence (Jansen and Sigmund, 1998) of limit cycles with extreme oscillations, it is important to be able to predict when they are likely to occur and replace a stable node. Determining the global stability of a predator prey system can be an unfeasible task, which only increases in complexity with the addition of further interacting species. It is however possible to determine the local stability of a system, and therefore its dynamic behaviour, around equilibrium points using linear stability analysis (Edelstein-Keshet, 2005). It should be noted that linear stability analysis applies linear tools to nonlinear systems, and as such is only strictly true at the equilibrium point. Linear stability analysis shows whether an equilibrium point of a particular system is a stable, unstable or saddle node or if it is a centre of oscillations and if so whether these oscillations will be damped or stable oscillations, the latter resulting from the presence of a stable limit cycle (Fig 1.4b).

As an alternative to linear stability analysis Rosenzweig and MacArthur developed a graphical analysis technique to predict the stability of predator-prey models and the conditions (parameters) that would cause that stability to change (Rosenzweig and MacArthur, 1963). They plotted the nullclines of each species (points at which the rate of change of that species over time is zero) against the density of predator and prey (with the predator plotted on the y-axis and the prey on the x-axis). The points at which the nullclines intersect is an equilibrium point of the system and the nature of the prey nullcline at that point determines the stability of the system. If the prey nullcline is decreasing with respect to increasing prey density at the equilibrium point, i.e. $\frac{\delta P^*}{\delta N} < 0$, where P^* is the density of the predator when $\frac{dN}{dt} = 0$ and N is the density of prey, the system will be stable, that is it will either have an asymptotically stable node or damped oscillations. On the other hand, if the slope is

positive the result will be an unstable equilibrium point, resulting in sustained oscillations and a stable limit cycle. Points at which $\frac{\delta P^*}{\delta N} = 0$ result in neutral cycles, as seen in the Lotka-Volterra model (Rosenzweig and MacArthur, 1963).

In the Lotka-Volterra model the prey nullcline is horizontal and the predator nullcline vertical. Changing the prey growth rate to a logistic form, whilst keeping predation unchanged results in the prey nullcline being a straight line with a negative slope throughout ensuring that the equilibrium point (where it exists) is always stable (Berryman, 1992). Using a Gompertz equation for prey growth gives a logistic curve of $\frac{1}{[N]}$ for the prey nullcline, again resulting in the slope of the nullcline always being negative.

Using a Holling type II functional response for the predation term, along with a logistic or Monod function for the prey growth, destabilises the system resulting in the prey nullcline taking the form of a parabola. This means that when equilibrium points occur at low prey density the prey nullcline is increasing and the equilibrium point is unstable, resulting in a stable limit cycle and sustained oscillations. While at higher prey densities the prey nullcline has a decreasing slope (Rosenzweig and MacArthur, 1963), resulting in either an asymptotically stable node or damped oscillations. (For an explanation of precisely why the prey curve is parabolic the reader is directed to the excellent explanation given by Rosenzweig (1969)). This system is vulnerable to a paradox of enrichment effect, because increasing nutrient levels result in an increase in the maximum prey density and a shift to the right of the prey nullcline, whilst having no effect on the predator nullcline. This results in an increased likelihood of the nullclines intersecting in a region where the prey nullcline has a positive slope

(Rosenzweig, 1971). Rosenzweig believed that such systems could not persist (Rosenzweig, 1971), however May showed that these systems did persist in the form of a stable limit cycle, albeit potentially one where at their nadir, prey population densities were so low that they were vulnerable to extinction, due to stochastic fluctuations (May, 1972).

The point at which the slope of the prey nullcline at its intersection with the predator nullcline goes from negative to positive is of particular interest. Before and after this point changes to the parameters result in quantitative differences of predator and prey populations over time, but do not affect the qualitative picture. At the point of transition however the system bifurcates from a stable node (possibly with damped oscillations) to an unstable node associated with a stable limit cycle, resulting in stable oscillations. When a system tips from a regime of damped oscillations, associated with a stable node, to one of stable oscillations, caused by an unstable node and its associated stable limit cycle, the resulting bifurcation is referred to as a Hopf bifurcation (Hopf, 1948). At a Hopf bifurcation the conjugate pair of complex eigenvalues, associated with the Jacobian matrix of the system, cross the imaginary axis and the sign of their real parts changes from negative to positive.

1.4 Microbial Predator-Prey Models:

Much of the work done on microbial predator-prey relationships in chemostats has been theoretical, in the form of mathematical modelling. Most of these centred upon protist predation of bacteria (Curds and Bazin, 1980) or bacteriophage infection (Krysiak-Baltyn *et al.*, 2016). Only a few studies have involved predatory bacteria, the earliest of which, by Varon and Zeigler (1978), used a simple Lotka-Volterra model. Using this they predicted a minimum prey density of 7×10^5 cfu ml^{-1} was required to sustain *Bdellovibrio*. Later models have introduced increasingly complexity, including Monod growth kinetics for prey species (Monod, 1949), more realistic kinetics for predator attack rate and the introduction of decoy species. For more information on these the reader is referred to the introduction to Chapter 2 of this thesis. Detailed in Chapter 2, I have developed a family of models for bacterial predation in a chemostat and used these to explore the effects of different modelling choices. The most biologically relevant of these models (most appropriate predation kinetics and inclusion of bdelloplast stage and predator mortality) predicted that *Bdellovibrio* when predating a single prey species is a system that is prone to extreme and long time period oscillations which would, in an experimental system, result in the extinction of the predator. I also found that *Bdellovibrio* would, under the conditions tested in my model, be outcompeted by a bacteriophage, which is specialist predator. Together these findings suggest why *Bdellovibrio* needs to be a generalist predator.

1.5 Aims and objectives:

This thesis sets out to describe a body of work investigating predator-prey population dynamics of the bacterial predator *Bdellovibrio bacteriovorus*. It aims to determine the conditions under which predation is most effective and to understand the effects of a secondary prey and/or a decoy species on the effectiveness of the predator to eliminate a target species. To further this investigation, I have used a combination of theoretical mathematical models and bacterial culturing techniques, mostly centred around chemostats. Chapter 2 describes a purely theoretical, ordinary differential equation (ODE) model of *Bdellovibrio* predation on a single prey species in a chemostat. It uses this model to investigate the types of dynamic behaviours that can be expected from this system and the conditions under which these behaviours occur. Chapter 2 also compares *Bdellovibrio* predation to protist and bacteriophage predation, to put the dynamics seen in a wider ecological context. Chapter 3 gives a mathematical analysis of the stability of model used in Chapter 2. Chapter 4 details the fitting of several variants extending the base model from Chapter 2 to experimental data of *Bdellovibrio* and a bacteriophage jointly predating *E. coli*, gathered by a collaborator. The fitting process used a combination of approximate Bayesian computation and a sequential Monte Carlo process to both select models and fit parameters to them. Chapter 5 details the construction and optimisation of an array of chemostats, designed to allow the testing of many conditions in parallel. I also demonstrate that *Bdellovibrio* can be cultured for over a month within these chemostats. As the presence of alternative prey and decoy species could affect predation dynamics, and such species may well be present in a real-world environment, I developed a small community of three bacterial species, two prey and

one decoy, that could be maintained in a mixed culture in a chemostat with or without *Bdellovibrio*.

CHAPTER 2: PREDATION STRATEGIES OF THE BACTERIUM *BDELLOVIBRIO BACTERIOVORUS*: ATTACK RATE, SIZE EFFECTS AND A RATE VERSUS YIELD TRADE-OFF

An earlier version of this chapter has been deposited on BioRxiv – DOI: 10.1101/621490

With increasing levels of antimicrobial resistance alternative means of treating bacterial infections are urgently needed. The use of predatory bacteria, such as *Bdellovibrio bacteriovorus*, and phage therapies are highly attractive options for filling this gap. In order to make best use of these however, we need to better understand the dynamics of microbial predator-prey interactions. We developed mass action mathematical models of *B. bacteriovorus* predation in chemostats, which have the low nutrient levels and slow growth rates associated with intended application environments such as the gut, aquaculture or wastewater treatment plants. Our model predicted that under a wide range of biologically relevant conditions extreme oscillations will lead to population bottlenecks. We also show that the system exhibits many classical traits of predation models, including two predators being able to survive on a single prey species, a paradox of enrichment and a tragedy of the commons. Predator mortality had a stabilising effect on the system and there were optimal mortality and attack rate constants. As might be expected we found that a T4 bacteriophage could outcompete *Bdellovibrio*, due largely to its much greater burst size. More surprisingly we found, in contrast to most chemostat systems, that a predator that takes longer to fully consume its prey would out compete a faster, but more wasteful competitor. Our model predicted an ideal prey: predator size ratio for maximum predator productivity, offering an explanation why *Bdellovibrio* is considerably smaller than its prey. Combined, these results suggest that *Bdellovibrio* needs to be a semi-generalist predator to survive in natural environments while under competition from specialist phages.

2.1 Introduction

Predator-prey relationships are some of the oldest and most important interactions in nature and occur at every level, from the smallest virus infecting a bacterium, to lions attacking wildebeest. At the microscopic level, bacteria are under attack from a wide range of predators from protists such as amoebae and ciliates to bacteriophages and even other bacteria, such as *Bdellovibrio bacteriovorus*.

B. bacteriovorus is a small, highly motile, Gram-negative bacterium, which predates a wide range of other Gram-negative bacteria (Stolp and Starr, 1963), including many pathogens. Gram-negative bacteria are a large group that have an outer membrane in addition to the normal cytoplasmic membrane, and a periplasmic space in between. This periplasmic space also contains the peptidoglycan - a rigid, cross-linked polymer, found in almost bacteria, which provides structure to the cell. *Bdellovibrio* is around one seventh the volume of an *Escherichia coli* (Cover *et al.*, 1984), and can swim at speeds of up to 160 μm s^{-1} (Lambert, Morehouse, *et al.*, 2006). Wild type *Bdellovibrio* replicates within the periplasm of its prey and displays a bi-phasic lifestyle. When free-living and hunting prey, it has a high metabolic rate, resulting in a loss of viability within 10 hours, if fresh prey is not encountered (Hespell *et al.*, 1974). When *Bdellovibrio* first encounters a cell it spends several minutes investigating the suitability of the potential prey (Hobley *et al.*, 2006). After this time, it either detaches from an unsuitable prey or enters the prey cell, if suitable, by creating a pore in the outer membrane and peptidoglycan, through which it squeezes in order to enter the prey periplasm (Starr and Baigent, 1966). Once inside the periplasm, *Bdellovibrio* alters the prey peptidoglycan, stopping further degradation

and causing the prey cell to round up, forming a structure known as a "bdelloplast". *Bdellovibrio* also makes the prey's inner membrane leaky (Romo *et al.*, 1992), thereby both killing the prey cell and causing the cytoplasmic nutrients to leak into the periplasm. *Bdellovibrio* uses these nutrients to grow into a coiled, coenocytic filament (Lambert, Morehouse, *et al.*, 2006). When the nutrients have been used up, the filament septates into as many new cells as resources allow for, typically between 3 and 6 new predators from one *E. coli* cell (Seidler and Starr, 1969a). Using normal binary fission, it could only produce 2^n offspring, potentially wasting prey resources if they would suffice for 5 predator offspring, rather than 4 or 8. The new *Bdellovibrio* grow flagella, and the remains of the prey cell are lysed, allowing the new predators to burst out in search of fresh prey.

The first models of predator prey interactions developed separately by Lotka (1925) and Volterra (1926) showed that these interactions could result in oscillatory behaviour without the need for any external variations. These oscillations are not stable however, as the equations produce neutral cycles, where the period and amplitude depend on the initial conditions (Fig. 1.4a). Additionally, any perturbations would result in a different cycle with an altered period and amplitude.

$$\frac{dN}{dt} = \mu N - \alpha NP \qquad (2.1a)$$

$$\frac{dP}{dt} = \beta NP - \lambda P \qquad (2.1b)$$

Where N is the prey and P the predator. The specific growth rate of the prey is μ and the predator has a mortality rate of λ. α and β are constants that reflect the amount of prey consumed in order to produce a certain number of predators.

These initial models assumed that prey growth is exponential (μ_N) and unlimited and that predation is proportional to predator and prey population sizes and is again unlimited. More realistic models, allowing for saturation of bacterial appetites were developed by Monod (1949):

$$Prey\ growth = \frac{\mu_{max} NS}{S+K_M} \quad (2.2)$$

Where μ_{max} is the maximum specific growth rate of the prey and K_M the level of substrate needed for half of this maximum specific growth rate. This was extended to also apply to predator consumption of prey by Holling (1959), in the form of the type II functional response.

Most models of microbial predator prey interactions have been tailored to protist predation of bacteria, or bacteriophage infection. Only a few studies considered predatory bacteria. See Table 2.1 for an overview of these, for more details the reader is referred to the review by Wilkinson (2006). Varon & Zeigler (1978) applied a Lotka-Volterra scheme to model their experimental results and used this to predict that a minimum prey density of 7 x 10^5 cfu ml^{-1} was required to sustain the predator. Crowley (1980) created a model that tracked substrate levels and used Monod kinetics for prey growth, as well as introducing a delay between predation and the production of new predators, reflecting the lengthy bdelloplast phase of *Bdellovibrio* predation. This model found that the population dynamics were destabilised by increased nutrient concentrations, leading to extreme oscillations. Models based on Monod kinetics and Holling type II predator functional response have been developed for protist predation of bacteria (Nisbet *et al.*, 1983), which showed that incorporating predator mortality had a stabilising effect, however, protists are different to bacterial predators. In particular, multiple prey bacteria must be

consumed to produce a single protist. In contrast, consumption of a single prey bacterium supports the production of multiple *B. bacteriovorus* cells (Seidler and Starr, 1969a). Additionally, when *B. bacteriovorus* predates a prey cell it enters a bdelloplast stage where for some period of time it is converting prey biomass into new predators and until this is completed it does not seek out fresh prey (Starr and Baigent, 1966). By contrast a protist will predate one prey cell, and whilst this is still being converted into protist biomass, will continue hunting and predating more prey. Wilkinson (2001) developed several *Bdellovibrio* models, including one based on a Holling type II functional response, but without specifically modelling the bdelloplast stage or allowing for the delay between the removal of prey and the birth of new predators in any other way. Another model did include a combined predator-prey complex, but used a Holling type I functional response (Wilkinson, 2001). Wilkinson again concluded from these models that increased nutrients destabilised the system, but also that both predator mortality and the presence of decoys reduced this effect, making long-term predator survival more likely. Similarly Hobley et al., (2006), Baker et al., (2017) and Said et al. (2019) also used a predator-prey complex and a Holling type I functional response, in models which were fitted to experimental data. Two further models, also fitted to experimental data, have been developed by Hol et al. (2016) and Dattner et al. (2017), both including spatial structure. Those previous microbial predator prey models that dealt with chemostats (those by Crowley, Nisbet and Wilkinson) focussed on the effects of dilution rate and substrate inflow on the dynamics of the chemostat systems. However, the effects of prey and predator characteristics such as prey size, attack kinetics and predation efficiency have not been studied.

Table 2.1 – Previous models of *Bdellovibrio,* and other relevant microbial, predation

Bdelloplast stage?	Predator Mortality?	Prey Growth	Holling type	Batch or chemostat	Notes	Source
No	No	Exponential	I	Batch	Lotka-Volterra model	(Varon and Zeigler, 1978)
No	Yes	Monod	I	Chemostat	Delay between predation and birth of predators	(Crowley *et al.*, 1980) Model 1
No	Yes	Monod	I	Chemostat	As Crowley Model 1, but also includes bdellophage (phage that infect *Bdellovibrio*)	(Crowley *et al.*, 1980) Model 2
No	Yes	Monod	II	Chemostat	Protist predation	(Nisbet *et al.*, 1983)
No	Yes	Monod	II	Chemostat		(Wilkinson, 2001) Model 1
Yes	No	Monod	I	Chemostat	As Wilkinson Model 1, but also contains decoys	(Wilkinson, 2001) Model 2
Yes	Yes	Exponential	I	Batch	Contains decoys and nutrient recycling	(Hobley *et al.*, 2006)
Yes	Yes	Monod	I	Batch	Includes effects of serum	(Baker *et al.*, 2017)
Yes	No	Exponential	I	Batch	Gaussian function for bdelloplast maturation time	(Said *et al.*, 2019)
Yes	Yes	Monod	II	Chemostat	Family of models with various ingredients examined	Model 6 of this study

In this study, we developed a family of models, based on 'ingredients' from previous models, to identify a unique combination that generates realistic outcomes from realistic model assumptions in order to ask many novel questions. This model predicts that *Bdellovibrio* has to be much smaller than its prey to survive, which is in agreement with empirical evidence (Cover *et al.*, 1984). We also found that high attack rate constants, large prey sizes and low predator mortality, which might be expected to help the predator, are in fact detrimental for predator survival. Instead, these parameters have optimal values that maximize predator density. These optima occurred at the tipping points into oscillations, and were often very narrow relative to the natural variation of these parameters. Moreover, we found that the system was prone to extreme oscillations in bacterial densities, leading to bottlenecks that would result in stochastic extinction. Additionally, *Bdellovibrio* would easily be outcompeted by a bacteriophage. Together, these three key predictions (narrow optima, population bottlenecks and phage superiority) suggest that *Bdellovibrio* would struggle to survive on a single prey species in a natural environment full of phages, and where conditions are unlikely to be optimal, and if so, not for long. Our findings are consistent with the fact that *Bdellovibrio* is a generalist predator so we posit that our model explains why *Bdellovibrio* is a generalist predator and why it has to be as small as it is.

2.2 Methods

2.2.1 Model development

We developed models to investigate the effects of a microbial predator, either *Bdellovibrio bacteriovorus* or a bacteriophage, on the population levels of a prey bacterium under continuous culture conditions in a chemostat. Under these conditions, nutrients are limited, and growth while continuous is often slow, mimicking conditions often found in the natural environment (Jannasch, 1969). Chemostats also allow population dynamics to be studied over long time periods as, unlike in batch cultures, nutrients are constantly renewed. We developed a family of models to determine the effect of structural changes and model assumptions on the types of behaviour observed. This analysis identified model 6 as being the most realistic in its assumptions and we therefore decided to explore this model in greater detail (see Table 2.2). Model 6 is described in Fig. 2.1 and its parameters are listed in Table 2.3. It consisted of a simple chemostat with a single abiotic resource (S), single prey species (N), and a single obligate predator (P). The prey species displayed Monod growth kinetics, and the predator had a Holling type II functional response, bdelloplast (for *Bdellovibrio*) or infected cell (for bacteriophage) stage and mortality. The bdelloplast (B) is a distinct stage in the *Bdellovibrio* life cycle that usually lasts for 2 to 4 hours. There are distinct parallels between this bdelloplast stage and a bacteriophage infected cell. For both systems, during the infection time the prey, which makes up the majority of the bdelloplast or infected cell, does not grow or replicate and the predator making up the remainder of the structure does not infect more prey. Due to this delay and the combining of the predator and its prey we

modelled the bdelloplast or infected cell stage as a separate 'species'. For simplicity from here on the species will be referred to as a bdelloplast, but the principles apply equally to an infected cell.

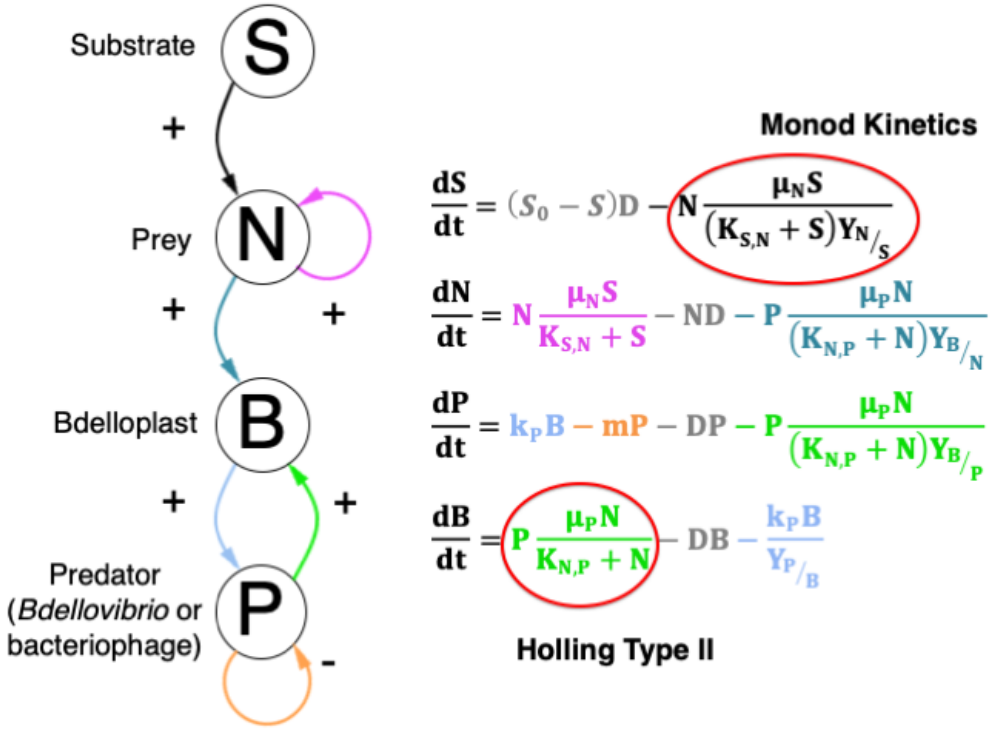

Figure 2.1 – Model 6 for chemostats

Used to track predator and prey densities. Substrate is consumed by prey to fuel prey growth. Prey and predators combine to form a bdelloplast. The bdelloplast matures to give new predators. Predators have mortality.

2.2.2 Structural Sensitivity Analysis

Several versions of our model were run on the same set of test conditions to determine the effects of each part of the model (Table 2.2). In Model 1, there was no predator mortality and no bdelloplast stage. Model 2 was like Model 1 but used delay differential equations (DDE) to implicitly model the delay between prey death and the birth of new predators. Model 3 was like Model 1 but had predator mortality. Models 4 to 6 had both mortality and a bdelloplast stage. In Model 4, the predator had a

Holling type I functional response whereas in Models 5 and 6, a Holling type II functional response was implemented. Unlike all the other models, Model 5 replaces substrate dynamics with constant inflow of prey, as if the prey were grown in a separate chemostat feeding into the chemostat with the predator.

Table 2.2 – Differences between model variants

Model	Substrate		Prey			Predator				Bdelloplast		
	Dilution	Prey Growth	Dilution	Growth	Predation	Dilution	Predation	Bdelloplast maturation	Mortality	Dilution	Predation	Maturation
1	$(S_0 - S)D$	$\frac{-SN\mu_N}{(K_{S,N}+S)Y_{N/S}}$	$-ND$	$\frac{SN\mu_N}{K_{S,N}+S}$	$\frac{-NP\mu_P}{(K_{N,P}+N)Y_{P/N}}$	$-PD$	$\frac{NP\mu_P}{K_{N,P}+N}$					
2	$(S_0 - S)D$	$\frac{-SN\mu_N}{(K_{S,N}+S)Y_{N/S}}$	$-ND$	$\frac{SN\mu_N}{K_{S,N}+S}$	$\frac{-NP\mu_P}{(K_{N,P}+N)Y_{P/N}}$	$-PD$	$\frac{NP\mu_P}{K_{N,P}+N}$	Implicit via DDE				
3	$(S_0 - S)D$	$\frac{-SN\mu_N}{(K_{S,N}+S)Y_{N/S}}$	$-ND$	$\frac{SN\mu_N}{K_{S,N}+S}$	$\frac{-NP\mu_P}{(K_{N,P}+N)Y_{P/N}}$	$-PD$	$\frac{NP\mu_P}{K_{N,P}+N}$		$-mP$			
4	$(S_0 - S)D$	$\frac{-SN\mu_N}{(K_{S,N}+S)Y_{N/S}}$	$-ND$	$\frac{SN\mu_N}{K_{S,N}+S}$	$\frac{-NP\mu_P}{Y_{B/N}}$	$-PD$	$\frac{-NP\mu_P}{Y_{B/P}}$	k_pB	$-mP$	$-BD$	$NP\mu_P$	$\frac{-k_pB}{Y_{P/B}}$
5			$(N_0 - N)D$		$\frac{-NP\mu_P}{(K_{N,P}+N)Y_{B/N}}$	$-PD$	$\frac{-NP\mu_P}{(K_{N,P}+N)Y_{B/P}}$	k_pB	$-mP$	$-BD$	$\frac{NP\mu_P}{K_{N,P}+N}$	$\frac{-k_pB}{Y_{P/B}}$
6	$(S_0 - S)D$	$\frac{-SN\mu_N}{(K_{S,N}+S)Y_{N/S}}$	$-ND$	$\frac{SN\mu_N}{K_{S,N}+S}$	$\frac{-NP\mu_P}{(K_{N,P}+N)Y_{B/N}}$	$-PD$	$\frac{-NP\mu_P}{(K_{N,P}+N)Y_{B/P}}$	k_pB	$-mP$	$-BD$	$\frac{NP\mu_P}{K_{N,P}+N}$	$\frac{-k_pB}{Y_{P/B}}$

2.2.3 Model 6 description

The differential equations developed to track the concentrations of each species are set out below.

$$\frac{dS}{dt} = (S_0 - S)D - N\frac{\mu_N S}{(K_{S,N}+S)Y_{N/S}} \quad (2.3a)$$

$$\frac{dN}{dt} = N\frac{\mu_N S}{K_{S,N}+S} - ND - P\frac{\mu_P N}{(K_{N,P}+N)Y_{B/N}} \quad (2.3b)$$

$$\frac{dP}{dt} = k_P B - (D+m)P - P\frac{\mu_P N}{(K_{N,P}+N)Y_{B/P}} \quad (2.3c)$$

$$\frac{dB}{dt} = P\frac{\mu_P N}{K_{N,P}+N} - BD - \frac{k_P B}{Y_{P/B}} \quad (2.3d)$$

S_0 is the concentration of substrate flowing into the system and D is the dilution rate of the system. The maximum growth rate of the prey is μ_N and its half-saturation constant for substrate is $K_{S,N}$. The attack rate constant of the predator is μ_P and its half-saturation constant for prey is $K_{N,P}$. The rate of maturation of bdelloplasts into new *Bdellovibrio* is k_P and the mortality of the *Bdellovibrios* is m. All yields are expressed in the form $Y_{A/B}$, which is the yield of species A per species B consumed. The half-saturation constant of species B for species A is expressed as $K_{A,B}$.

In most animal predator-prey models, the yield terms would be expressed as the gain of Y predators at the expense of 1 prey (where Y is likely to be less than 1). The model developed here however has to be different to account for the unusual biology, in that both predator and prey are 'consumed' to produce a bdelloplast (which will later mature into new predators). This combined prey-predator entity does not exist in canonical predator prey models and as is shown here, requires special treatment. If a single yield term were to be placed on the bdelloplast resulting from predation, then identical amounts of predator and prey would have to go into making

up that bdelloplast, which is not biologically accurate. Placing two yield terms, one on each producer species (prey and predator), by contrast, allows the ratios of producers going into the bdelloplast to be varied, which also facilitates varying the relative sizes of prey and predator. Thus, a single yield term on the 'product' species needs to be replaced by two separate yield terms on the two 'reactant' species to use a chemical analogy.

The standard approach in animal predator prey models is to track species in terms of individuals and not to attempt to balance biomass as this is not tractable in the wild. In contrast, the approach of studies of microbial growth and physiology in the laboratory is based on substrate and product concentrations rather than individual molecules and biomass is often more conveniently determined than cell numbers. Moreover, for understanding metabolic pathways and energy metabolism as well as process modelling in biotechnology, the mass balance is an essential tool and growth and product yields are of primary interest. These two traditions collide when modelling the predator prey dynamics of a bacterial prey and a bacterial predator, suggesting the use of either particle-based or biomass-based unit systems. In this thesis, the biomass-based system is used predominantly, but for modelling phage, the particle-based system was found to be more suitable so both systems were compared for a subset of the results and found to be in agreement. When tracking numbers of individuals of a species no attempt is made to explicitly balance biomass, as one prey cell combines with one predator cell to give one bdelloplast, so the two yields of bdelloplast per prey and bdelloplast per predator are both unity ($Y_{B/_N} = Y_{B/_P} = 1$). When the units are in terms of biomass however, mass is tracked explicitly, so care must be taken to ensure that the equations satisfy conservation of mass of prey and

predator when forming a bdelloplast. For this it is required that the mass of the bdelloplast not exceed the combined mass of the predator cell and prey cell from which it is formed. For simplicity it is assumed that the conversion of predator and prey into a bdelloplast occurs without loss, such that the mass of the bdelloplast equals the combined mass of the predator cell and the prey cell. Any loss is best accounted for in the following conversion of bdelloplast into predator offspring, as this is more tractable experimentally. To enforce this mass balance constraint, it is necessary (for mass-based units) that the sum of the inverse yields is one (the inverse of the yield of bdelloplast mass formed per predator mass is the 'yield' of predator mass consumed per bdelloplast mass formed, analogously for the prey):

$$\frac{1}{Y_{B/P}} + \frac{1}{Y_{B/N}} = 1 \qquad (2.4a)$$

Hence

$$Y_{B/N} = \frac{Y_{B/P}}{Y_{B/P} - 1} \qquad (2.4b)$$

2.2.4 Model Parameters

Details of the model parameters are shown in Table 2.3. Parameters for the substrate and prey interactions of the model were based on *E. coli* as the prey species, growing on glucose as the substrate. The kinetics of this are relatively well studied and understood, and the parameters were taken from the literature (Kreft *et al.*, 1998).

For the predator, certain information is also well known. *Bdellovibrio* is approximately 1/7th the size of *E. coli* (Stolp and Starr, 1963; Kubitschek and Friske, 1986) and is assumed to be of a similar density. As a result, when one predator and one prey cell combined to give a bdelloplast each g of dry mass of bdelloplast formed

was at the expense of 0.125 mg dry mass of predator and 0.875 mg dry mass of prey. This gave a yield of bdelloplast per prey ($Y_{B/N}$) of 1.143 and a yield of bdelloplast per predator ($Y_{B/P}$) of 8. The burst size of *Bdellovibrio* from a bdelloplast formed from *E. coli* prey is usually an average of 3.5 cells (Seidler and Starr, 1969a), each 1/8th the size of the bdelloplast, since a bdelloplast contains the mass of both the predator and the prey that formed it. Hence the yield of predator per bdelloplast ($Y_{P/B}$) was set to 0.438.

Predator mortality rate (m) was based on observations by Hespell (1974). The maturation rate (k_P) was calculated from the time required for bdelloplasts to mature, and release new predators, which when formed from *E. coli* prey, was observed to be between two and four hours (Seidler and Starr, 1969a). The attack rate constant (μ_P) and half-saturation constant for prey ($K_{N,P}$) of the predator were set to values determined from modelling experimental data (see Chapter 4), as no literature values were available for these parameters.

Table 2.3 – Baseline parameters for the main model.

Minimum and maximum values refer to the range over which global sensitivity analysis was performed.

Parameter	Units	Value	Minimum	Maximum	Source
Inflow substrate concentration (S_0)	mg ml^{-1}	5×10^{-3}	5×10^{-3}	2.5	Assumed to be ~2 × $K_{S,N}$
Prey maximum specific growth rate (μ_N)	h^{-1}	1.23	¾ ln(2)	3 ln(2)	(Kreft *et al.*, 1998)
Predator attack rate constant (μ_P)	mg bdelloplast mg $predator^{-1}$ h^{-1}	0.38	0.3	6	See Chapter 4
Predator half-saturation constant for prey ($K_{N,P}$)	mg prey ml^{-1}	8.6×10^{-4}	1.5×10^{-6}	6.5×10^{-3}	See Chapter 4
Yield of bdelloplasts from predators ($Y_{B/P}$)	mg bdelloplast mg $predator^{-1}$	8	5	20	Relative sizes of *E. coli* and *Bdellovibrio* cells (Stolp and Starr, 1963; Kubitschek and Friske, 1986)
Bdelloplast maturation rate (k_P)	mg predator mg $bdelloplast^{-1}$ h^{-1}	0.109	0.075	0.3	(Seidler and Starr, 1969a)
Predator mortality rate (m)	h^{-1}	0.06	0.03	0.09	(Hespell *et al.*, 1974)
Dilution rate (D)	h^{-1}	Always 0.05			
Prey half-saturation constant for substrate ($K_{S,N}$)	mg ml^{-1}	Always 2.34×10^{-3}			(Kreft *et al.*, 1998)
Yield of prey from substrate ($Y_{N/S}$)	mg dry mass prey mg $substrate^{-1}$	Always 0.4444			(Kreft *et al.*, 1998)
Yield of bdelloplasts from prey ($Y_{B/N}$)	mg $bdelloplast^{-1}$ mg $prey^{-1}$	Always $\frac{Y_{B/P}}{Y_{B/P}{}^{-1}}$			Relative sizes of *E. coli* and *Bdellovibrio* cells (Stolp and Starr, 1963; Kubitschek and Friske, 1986)
Yield of predators from bdelloplasts ($Y_{P/B}$)	mg predator mg $bdelloplast^{-1}$	Always 0.438			Relative sizes of *E. coli* and *Bdellovibrio* cells and burst size (Stolp and Starr, 1963; Seidler and Starr, 1969a; Kubitschek and Friske, 1986)

2.2.5 Model Simulation

The model was run in MatLab (8.6.0.267246 (R2015b)) using the ode45 solver, which implements an explicit Runge-Kutta method. The relative and absolute tolerances were set to 1 x 10^{-9}, all species values were forced to be non-negative and all other options left as default. After every 100 hours of simulated time (or 5 volume changes at a dilution rate of 0.05 h^{-1}) the system was checked to see if it had reached a steady state, was in sustained oscillations or had still to reach its final state. The system was considered to be in a steady state if for the last n hours, where n is a parameter, for each species the maximum and minimum values for that species were within a relative tolerance (set as a parameter) of each other. The system was considered to be in sustained oscillations if two consecutive peaks in the substrate species values were within a (parameterizable) relative tolerance of each other. If after 8000 hours (equivalent to 400 volume changes at 0.05 h^{-1} dilution rate) the system was still not in either steady state or sustained oscillations, it was deemed that it was unstable and would likely never reach a stable state.

2.2.6 Parameter Sweeping

Parameter sweeps were performed for both the simulations and analytical calculations. For the simulation sweeps the final concentration of each species was plotted, unless the system was displaying sustained oscillations, when instead the average value over the oscillatory cycle was used. This average was calculated over a period between two consecutive peaks and was obtained by averaging all values recorded during this period, weighted by the simulated time gap between recordings. For analytical sweeps the calculated steady state values for the parameter settings

were plotted, as were the eigenvalues of the system and the type of regime predicted, e.g. damped oscillations. Sweeps were made in small increments through various parameters. Other parameters were set according to Table 2.3.

2.2.7 Global Sensitivity Analysis

A sensitivity analysis was carried out on all seven parameters revealed by the dimensional analysis (detailed in the Results). In order to avoid bias in the analysis it was important to select sampling points that were both randomly chosen and well distributed. A Latin hypercube design (Mckay *et al.*, 1979) creates randomly selected tuples of points in as many dimensions as is required and ensures that these are well distributed in each dimension. For this sensitivity analysis 10,000 tuples of points were selected at random in a Latin hypercube design. The tuples were obtained by using the MatLab function lhsdesign, which created five sets of tuples and selected the best of these according to a maximin comparison. This maximised the minimum distance between any two points and so reduced clumping. Each of these sets of points was scaled evenly across the realistic parameter range (see Table 2.3 for minimum and maximum values), to give a set of parameter values (parameter value = minimum value + design point value * parameter range).

For each set of parameters created, the species steady state values were calculated using equations 3.4a-d. Each of the parameters was varied up, and down

by 1%. The difference between the perturbed values and the baselines values, as a percentage of that baseline, was stored for further analysis.

2.2.8 Competitions

Competing two species following different strategies is an unbiased and unequivocal way to compare the fitness of their strategies. This meant we could compare effects such as a change in prey cell biomass, or an increase in the rate at which *Bdellovibrio* consumes prey, at the expense of its efficiency in utilising prey resources. The competition assays also allowed a comparison of the effectiveness of *Bdellovibrio* and a bacteriophage. This in particular was of interest because both *Bdellovibrio* and bacteriophages have been proposed as potential alternatives to antibiotics. The assays were developed by introducing a second predator species, with a second bdelloplast or infected cell stage. Equation (2.3a) for the substrate was unaffected. Equation (2.3b) for the prey species became:

$$\frac{dN}{dt} = N\frac{\mu_N S}{K_{S,N}+S} - ND - P_1\frac{\mu_{P_1}N}{(K_{N,P_1}+N)Y_{B1/N}} - P_2\frac{\mu_{P_2}N}{(K_{N,P_2}+N)Y_{B2/N}} \qquad (2.5)$$

Equations (2.3c & 2.3d) were duplicated for P_2 and B_2, the second predator and its bdelloplast or infected cell stage.

2.2.9 High Rate Predator Adjustments

For the high rate vs. high yield experiments, the standard settings were used for the high yield predator. As the high rate predator is assumed to lyse the bdelloplast before all the available nutrients are consumed, (in order to more quickly release new predators into the environment to locate and prey upon more prey cells), the yield of predators from a bdelloplast ($Y_{P/B}$) was halved to 0.313 mg predator mg bdelloplast^{-1}. To reflect the faster maturation rate of bdelloplasts in this model, the k_p was

increased to 0.278 mg predator mg bdelloplast^{-1} hour^{-1}. This higher rate of predator growth has not been observed in *Bdellovibrio*. However, chemostats generally select for microbial strains which can grow more quickly, as these rapidly consume the available nutrients and therefore outcompete slower growing competitors. Long term growth of predators in a chemostat might therefore be expected to select for faster growing predators, if this proved to give them a competitive advantage.

2.2.10 Bacteriophage models

For modelling bacteriophage predation, the bdelloplast stage was assumed to become an infected cell stage. There are obvious similarities between these two situations. In both cases, there is a lag between predator penetration of the prey cell and production of new predators, and in both cases (although for different reasons) prey cell growth effectively terminates during this time.

Attempts to run the model using biomass-based units with parameters suitable for a bacteriophage were unsuccessful. All the ODE solvers tried were unable to resolve the rate equations in a reasonable time period (most probably due to the differences in timescales over which species densities were changing meaning that a suitable timestep could not be found). All bacteriophage predation assays were therefore run using particle-based units. When converting between biomass and particle-based units, a prey cell is assumed to be 1 fl in size (Kubitschek and Friske, 1986). 20% of a cell is assumed to be dry biomass, giving dry mass per prey cell of 0.2 pg. Predator dry mass per cell is assumed to be 1/7th that of the prey, based on their relative sizes (Stolp and Starr, 1963; Kubitschek and Friske, 1986).

One bdelloplast, or one infected cell, is formed from one predator cell, or one virion, and one prey cell ($Y_{B/P} = Y_{B/N} = 1$). One bdelloplast is assumed to yield on average 3.5 *Bdellovibrio* (Seidler and Starr, 1969a), so $Y_{P/B} = 3.5$ and one cell infected by a T4 phage is assumed on average to give 64 phage virions ($Y_{P/B} = 64$) (Hadas *et al.*, 1997).

The average lysis time for a phage is assumed to be 36 minutes (Hadas *et al.*, 1997), giving a rate of virion production (k_P) of 107 hour^{-1}. Data from a study by Stent (Stent and Wollman, 1952) was used to calculate an attack rate constant (μ_P) of 19.3 infected cells predator^{-1} hour^{-1} and half-saturation constant for prey ($K_{N,P}$) of 1.32 x 10^8 prey cells ml^{-1}, for a T4 virulent bacteriophage of *E. coli*.

2.3 Results

2.3.1 Model implementation and validation

2.3.1.1 Structural sensitivity analysis

To gain a better understanding of the impact of various modelling choices, we first compared a number of ordinary differential equation (ODE) and delay differential equation (DDE) models. In all cases, the same set of standard conditions, based on *Bdellovibrio* predating *E. coli* that are growing on glucose (0.05 mg ml^{-1}) and a dilution rate of 0.0333 h^{-1} (equivalent to a 30 hour retention time) were used. For each case, we first ran the simulation without predators until the prey had reached a steady state, and then simulated the addition of the predator. In all instances, the system without a predator reached a steady state, with the same density of prey bacteria (Fig. 2.2a). (Model 1) The addition of a predator, in a model system without a bdelloplast stage, or any other form of delay between prey killing and predator birth, gave rise to sustained, extreme oscillations (Fig. 2.2b). (Model 2) Incorporating an explicit delay approximately doubled the oscillatory period from ~150 hours to ~300 hours (Fig. 2.2c). (Model 3) Adding mortality reduced the oscillatory period to approximately 100 hours (Fig. 2.2d). (Models 4 – 6) The addition of a bdelloplast stage stabilised the system and caused it to come to a stable steady state of co-existing predator and prey, regardless of the predator Holling type functional response (Fig. 2.2e-g). (Model 4) With a Holling type I predator functional response (Fig. 2.2e), the final prey density was more than 3 times lower, and the predator density higher, than (Model 6) with a type II response (Fig. 2.2g). (Model 5) Having a constant input of prey to the system is akin to growing the prey on its own in one chemostat feeding into a second chemostat

with prey and predator. This gave (Fig. 2.2f) a very similar response to the single chemostat with constant input of substrate (Fig. 2.2g).

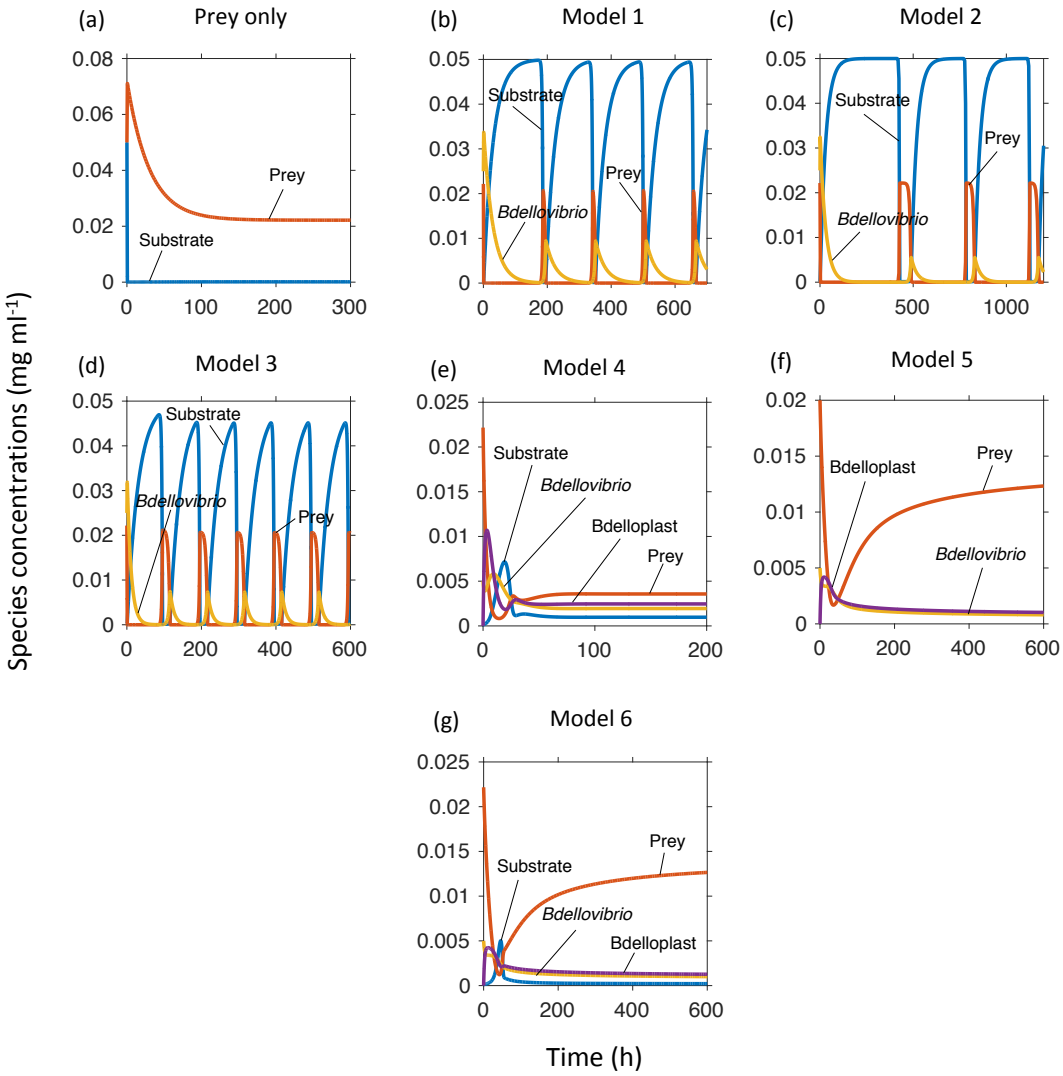

Figure 2.2 – Modelling choices affect the qualitative dynamics.

All models were run with a dilution rate = 0.0333 h^{-1} (equivalent to a volume change every 30 hours), S_0 = 0.05 mg ml^{-1} and all other parameters at default settings. All models had a Holling type II predator functional response unless otherwise stated. (a) Model 1 run without any predators (the same result was obtained for all models). (b) Model 1, without bdelloplast stage. (c) Model 2, with delay equations. (d) Model 3 – as Model 1, but with predator mortality. (e) Model 4 – incorporating a bdelloplast stage, predator mortality and a Holling type I functional response. (f) Model 5 – as Model 4, but with constant prey input, (g) Model 6 – Final model with bdelloplast stage and predator mortality.

Model 6 was chosen as the best model for all further work, for several biological reasons. Firstly, the time taken for a *Bdellovibrio* to penetrate prey is in the region of ten minutes (Hespell, 1976). This is the minimum time for a successful attack

in a prey-saturated environment. By contrast, the time required for a *Bdellovibrio* to consume the contents of a prey cell, convert these into new *Bdellovibrio* predators, septate and finally lyse the prey cell to release new predators is in the region of four hours (Seidler and Starr, 1969a). As the prey is killed very shortly after penetration (Rittenberg and Shilo, 1970), this difference in timescales meant there is a significant delay between prey killing, and the birth of new predators. We felt this difference was best modelled by treating the bdelloplast stage as a separate species. Secondly, *Bdellovibrio* has a high endogenous respiration rate, and a correspondingly low life span in the absence of suitable prey (Hespell *et al.*, 1974). This meant it was appropriate to include a mortality factor in the model. Thirdly, the saturating Holling type II functional response results from the 'handling time' of a predator (Jeschke *et al.*, 2002). This would correspond to the minimum time for a successful attack in a prey-saturated environment, i.e., the attachment and penetration time of *Bdellovibrio* of ~10 minutes (Hespell, 1976).

2.3.2 Dynamic regimes

Model 6 has six dynamic regimes and 12 parameters (Table 2.4 and Fig. 2.3). In order to gain a better understanding of the factors determining which of these regimes were observed for any particular parameter setting, we conducted a sweep through a range of inflow substrate concentrations (S_0) and dilution rates. We performed a linear stability analysis on the steady state of the system and the eigenvalues of its Jacobian matrix for these parameter settings (Fig. 2.3a). As expected, at the highest dilution rates and lowest S_0, all biological species washed out. Reducing the dilution rate or increasing S_0 enabled survival of first the prey and then

the predator. Further increases in S_0 destabilised the system, resulting in first damped and then sustained oscillations, before finally reaching a linearly unstable state (Fig. 2.3a).

Table 2.4 – Possible dynamical outcomes and associated eigenvalues of the four species co-existence state where it exists.

Dynamical regimes	**Real parts of eigenvalues**	**Imaginary parts of eigenvalues**
Complete washout of all bacteria	N/A as four species co-existence state does not exist	
Prey only survival	N/A as four species co-existence state does not exist	
Stable co-existence of all species (stable node)	All negative	All zero
Co-existence of all species with damped oscillations (stable focus)	All negative	Not all zero
Co-existence of all species with sustained, stable oscillations (stable limit cycle)	At least two positive	Not all zero
Co-existence of all species, but linearly unstable (saddle node or unstable node)	At least one positive	All zero

To confirm that there was a good agreement between the outcomes predicted from the linear stability analysis, and those generated by running simulations, we ran a series of simulations, with parameters for which the linear stability analysis predicted each type of regime (white crosses in Fig. 2.3a). The analytically predicted states matched those observed in the corresponding simulations, except where the analytical results predicted a linearly unstable state (Fig. 2.3b-g). In that latter case the simulation gave sustained, extreme yet stable oscillations (Fig. 2.3d).

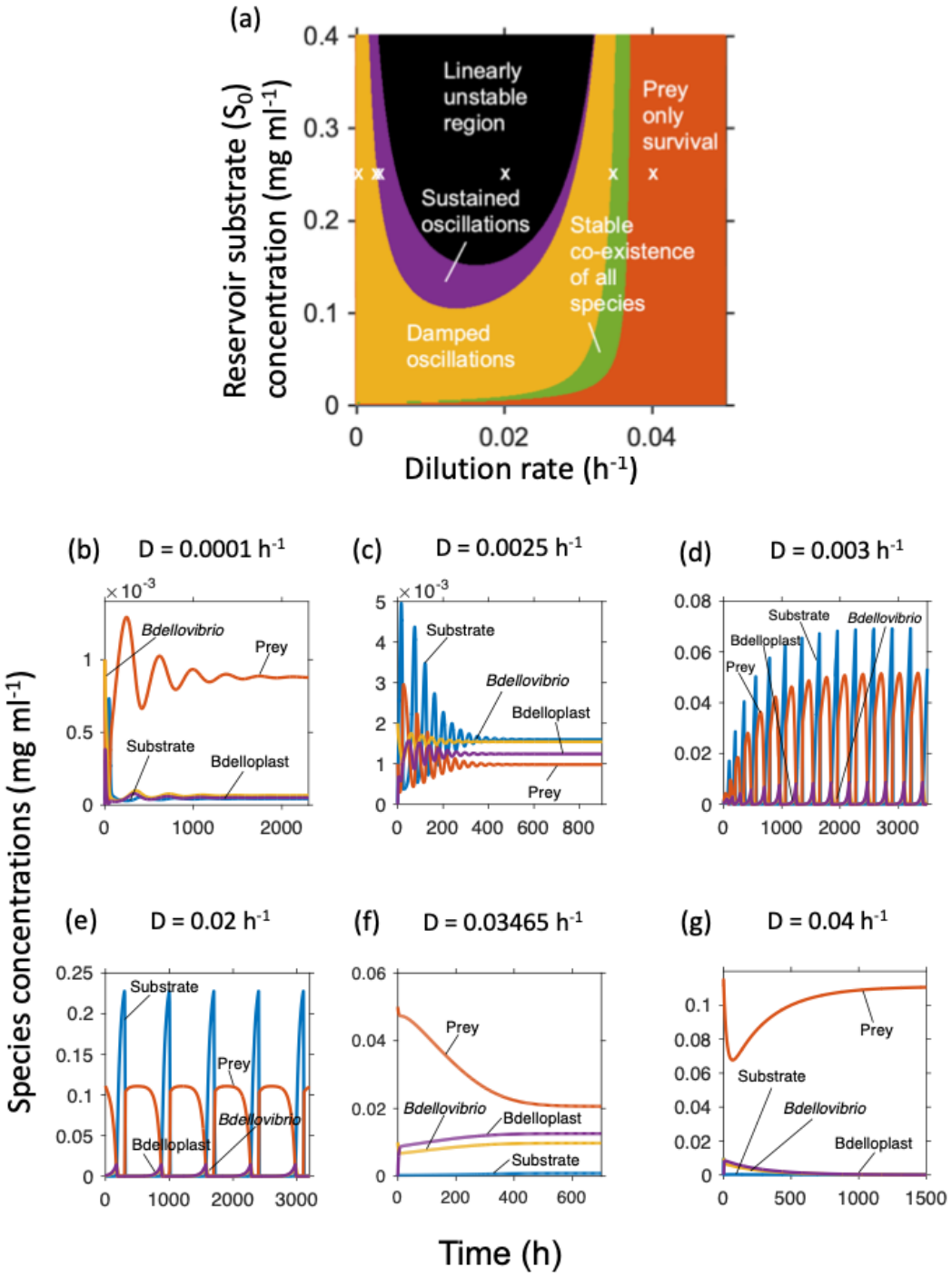

Figure 2.3 – Dynamic regimes of Model 6.

(a) Analytically calculated regimes, as depending on the inflow substrate concentration S_0 and dilution rate D. (b-g) Simulations at S_0 = 0.25 mg ml^{-1} and increasing dilution rates, indicated by white crosses in (a). (b) Damped oscillations that ended in steady state co-existence. (c) Damped oscillations of much shorter period than (b). (d) Amplifying oscillations that ended in sustained, extreme oscillations. (e) The analytically predicted linearly unstable region gave sustained, extreme oscillations in the numerical simulations. (f) Stable co-existence of predator and prey. (g) Predator extinction.

2.3.3 Protist model

The population dynamics generated by our model are qualitatively different from those generated by typical Lotka-Volterra models for animal populations (Curds and Bazin, 1980). In Lotka-Volterra models, the oscillations are gentle and fairly similar to sine waves, whereas in our model the waves are very asymmetric, approach zero very closely and rise and fall abruptly. Such extreme oscillations were also seen by Curds and Bazin when they modelled protist predation (Curds and Bazin, 1980), but their oscillations had a much shorter period. We hypothesised that this was due either to environmental factors (Curds and Bazin had a higher dilution rate in their model), biological factors (the two predators differed in their attack kinetics), or a combination of these. To understand which of these was responsible for the differences in period length we recreated their model, then introduced parameters relevant to *Bdellovibrio* predation (Fig. 2.4). We found that decreasing the dilution rate, decreasing the prey half-saturation constant of the predator and reducing the attack rate constant all increased the period length.

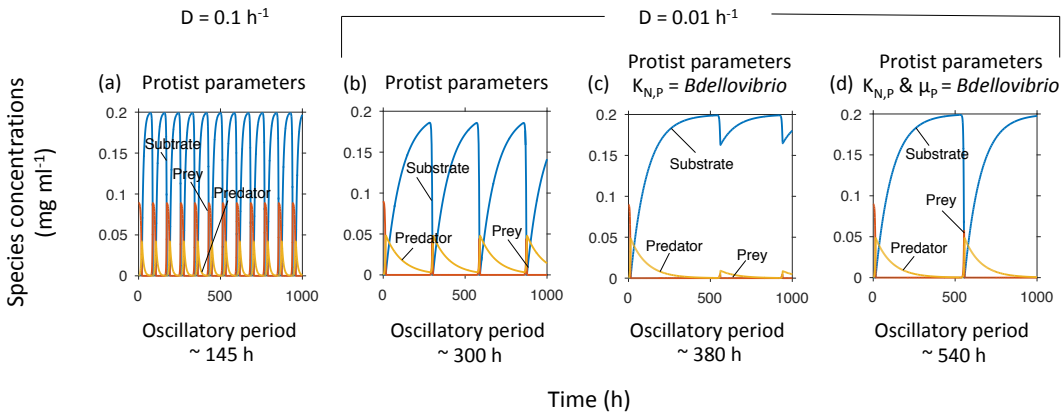

Figure 2.4 – The protist model of predation (Curds and Bazin, 1980)**.**

Shows similarly extreme oscillations as the *Bdellovibrio* model but shorter periods. (a) The protist predation model without predator mortality, or the equivalent to a bdelloplast stage, gave a similar pattern of behaviour to that seen in our model. With a dilution rate of 0.1 h^{-1}, the value used in (Curds and Bazin, 1980), the oscillatory period was shorter than seen in our model. (b) Reducing the dilution rate lengthened the period. (c) Adjusting the much higher prey half-saturation constant of the protist ($K_{N,P}$ = 1.2 x 10^{-2} mg dry mass ml^{-1}) to that of *Bdellovibrio* ($K_{N,P}$ = 8.6 x 10^{-4} mg dry mass ml^{-1}) lengthened the oscillatory period and reduced the prey recovery, resulting in a different pattern of oscillations. (d) When the attack rate constant was also adjusted from the protist rate (μ_P = 0.43 h^{-1}) to that of *Bdellovibrio* (μ_P = 0.38 h^{-1}), the original pattern was restored but the period further lengthened.

We concluded that the difference in oscillatory period between our model and that of Curds and Bazin was partly due to the different dilutions rates modelled. However, even when the same dilution rate was applied to both systems the oscillatory period of the Curds and Bazin model was still only approximately half that seen in our model. This additional difference was due to the different predation kinetics between the two predators. *Bdellovibrio* has a lower attack rate constant, but also a lower prey half-saturation constant meaning the predator comes close to its maximal predation rate at lower prey densities. The lengthy oscillation period of both the protist and *Bdellovibrio* models results in both the predator and its prey being at very low levels for an extended period of time, meaning that neither system would show robust permeance under the conditions modelled.

2.3.4 Biological questions

2.3.4.1 Bdellovibrio has a minimal and optimal attack rate constant

To our knowledge, Varon & Zeigler (1978) is the only study of predation kinetics of a relative of *Bdellovibrio*. They used the marine strain BM4, with *Photobacterium leiognathi* E28 as prey. *P. leiognathi* can grow at rates of up to 0.2 h^{-1} (Dunlap, 1985), however nothing beyond the study by Varon and Zeigler is known about the growth kinetics of BALO BM4. We used this study to calculate our default values for the attack kinetics. This however is a different BALO targeting a different prey species and as such predation kinetics may vary considerably from *Bdellovibrio* predating *E. coli*. To better understand how any such changes may affect system behaviour we investigated the effects of varying the attack rate constant at a number of different S_0 and dilution rate values. The attack rate constant in the Holling type II functional response gives the fastest rate at which predation can occur in the presence of a saturating density of prey. The ratio of attack rate constant (μ_P) and half-saturation constant ($K_{N,P}$) give the initial slope of the Holling type II function, which determines the predation rate at low prey densities. We hypothesised that the faster the predator was at locating and attacking its prey the more successful it would be, particularly given its high mortality rate, that meant it would quickly starve (half-life of 10 hours) if it did not rapidly find fresh prey. This would suggest that *Bdellovibrio*'s attack rate constant was constrained by a biological inability to be any faster (at up to 160 μm s^{-1} it is already one of the fastest swimming bacteria, especially considering its small size). To test this proposition, we examined the final densities of predator and

prey when the predator had a range of attack rate constants at various dilution rates and reservoir substrate concentrations.

Surprisingly the highest attack rate constant did not give the greatest levels of predator density. Instead there was an optimal attack rate constant for the predator (this also gave the lowest level of prey density) (Fig. 2.5). The optimal value occurred just above the minimum attack rate constant for the predator survival and increased at faster dilution rates (Fig. 2.5b, d) from around 0.5 mg bdelloplast mg predator^{-1} h^{-1} (depending on S_0) at a dilution rate of 0.03 h^{-1} to 1 mg bdelloplast mg predator^{-1} h^{-1} at a dilution rate of 0.1 h^{-1}. This is somewhat less than the 1.67 mg bdelloplast mg predator^{-1} h^{-1}, calculated based on the data from Varon and Zeigler (1978), but more than the 0.31 to 0.36 mg bdelloplast mg predator^{-1} h^{-1} predicted in Chapter 4 by fitting to the model to experimental data. The difference in attack rate constants from the studies is understandable given that the predatory BALO and the prey species differed between the studies and the Varon and Zeigler study was conducted in a chemostat, whilst the experimental data used in Chapter 4 was obtained from batch cultures. Increasing levels of S_0 caused the peak to narrow towards the minimal attack rate constant, which hardly changed (Fig. 2.5a-c), decreasing the range of μ_P at which the predator could achieve near maximal density. Below the optimal μ_P, there was a sharp drop to predator extinction. Above the optimal, predator density slowly declined with increasing μ_P. The optimal μ_P was also the rate at which the system underwent a Hopf bifurcation (Hopf, 1948) from a stable steady state co-existence into an oscillatory regime (Fig. 2.5e, g). This difference from our original proposition, that the highest attack rate constant would be best, can be understood by realising that the food source for the predator is a living organism, and therefore potentially renewable, if it

is given time to regrow. Hence, a too aggressive predator kills off too much of its food source and will starve, due to a lack of available resources to exploit. This in turn suggests that whilst there are undoubtable limits on how fast a bacterium can swim, in this case these limits may not be the only reason why *Bdellovibrio* is not even faster, but instead it may have evolved to be at or near the optimal speed to maximally exploit its prey.

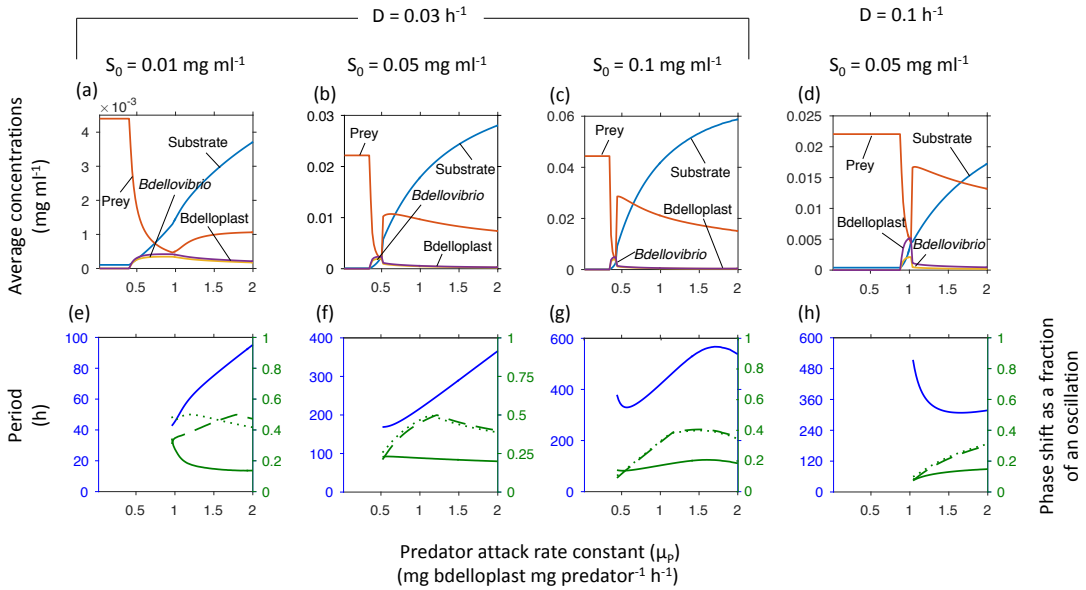

Figure 2.5 – Minimal and optimal attack rate constant (μ_P).

The average population densities and substrate concentrations, oscillatory periods and phase shifts strongly depend on the attack rate constant, shown at increasing inflow substrate concentrations (S_0) and two dilution rates (cf. phase diagram in Fig. 2.3a). Top row shows concentrations at steady state or averaged over one oscillatory cycle (see methods 2.2.6). Bottom row shows the oscillatory period (blue, left axis) and phase shifts (green, right axis) from substrate peak to peak of prey (solid line), free *Bdellovibrio* (dashed line) or bdelloplast (dotted line). Note that oscillations start above the optimal attack rate constant. In order to obtain accurate simulation results at all parameter values, the absolute tolerance of the ode45 solver had to be reduced from 1 x 10^{-9} to 1 x 10^{-12}.

2.3.4.2 Higher prey growth rate does not benefit prey

Given that the predator had an optimal attack rate constant, due to a need to allow the prey to regrow, we speculated that an increased prey growth rate would be to the benefit of both predator and prey. The parameters used in our model were based on the prey species being *E. coli* growing on glucose as its sole carbon source.

Bdellovibrio however has a wide potential prey range, with most Gram-negative bacteria being vulnerable to some BALO. As different bacterial species have different growth rates, we next sought to investigate the effects of different values of prey growth rate (μ_N) and determine which species actually benefitted from an increase in prey growth rate. We chose growth rates from 0.2 h^{-1} to 2 h^{-1}, equivalent to a doubling time of between 21 minutes and 210 minutes. For comparison the minimum doubling time of *E. coli* growing on glucose in a minimal medium is 34 minutes (Kreft *et al.*, 1998).

Contrary to what we had expected, increasing prey growth rate benefitted only the predator and never the prey. At the lowest S_0 the system was always in stable co-existence and increasing μ_N had little or no effect on the densities of any of the biological species, although it did cause the levels of substrate within the chemostat to fall (Fig. 2.6b). At higher S_0 increasing μ_N caused the density of the predator to increase at the expense of the prey, and resulted in a transition from oscillations to stable co-existence (Fig. 2.6a, c). Increasing the dilution rate caused this Hopf bifurcation to occur at a lower value of μ_N. The transition from oscillations to stable co-existence was accompanied by a sharp drop in prey species density, and increase in predator density.

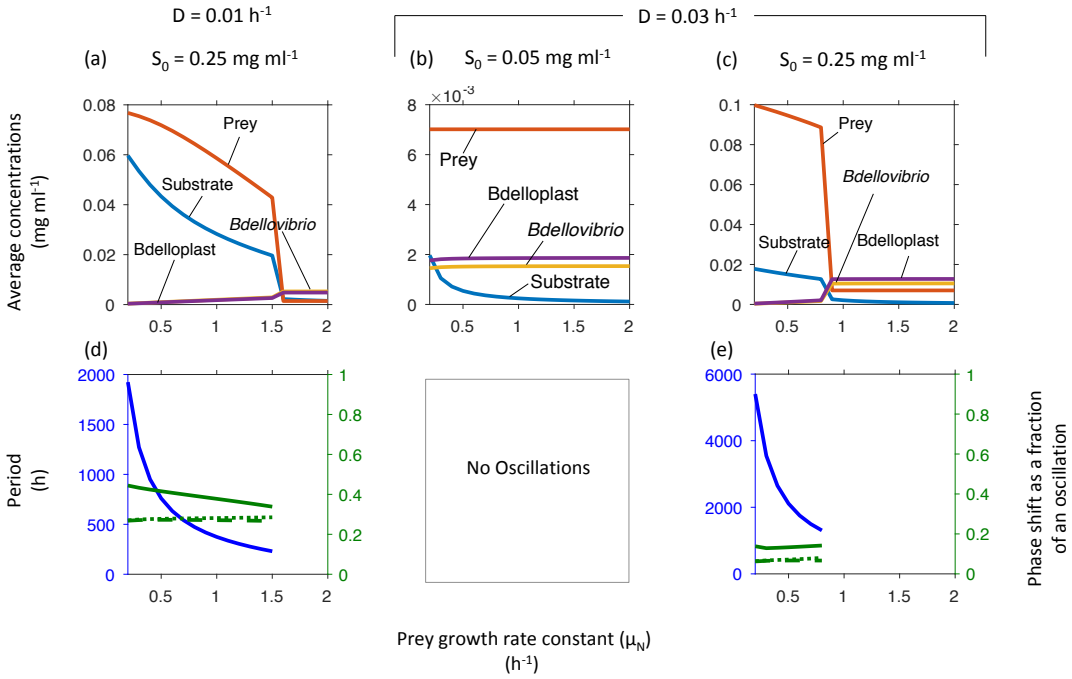

Figure 2.6 – Effects of prey growth rate (μ_N)

Increasing the maximum specific growth rate of the prey (μ_N) leads to a sharp drop in prey density and stabilizes the system at high inflow substrate concentrations (S_0). The system was more stable at low S_0 (cf. phase diagram in Fig. 2.3a). Top row shows concentrations at steady state or averaged over one oscillatory cycle (see methods 2.2.6). Bottom row shows the oscillatory period (blue, left axis) and phase shifts (green, right axis) from substrate peak to peak of prey (solid line), free *Bdellovibrio* (dashed line) or bdelloplast (dotted line). Note that oscillations occur at the higher inflow substrate concentration and below a critical μ_N. Prey density is much higher in the oscillatory regimes where it decreases with increasing prey growth rates. Since prey density will of course be zero if μ_N is zero, there is an optimal prey growth rate.

2.3.4.3 Predators benefit from mortality

Bdellovibrio has a mortality that is much higher than other bacteria, due to its high endogenous respiration rate and limited energy reserves (Hespell *et al.*, 1974). It would seem logical that if *Bdellovibrio* were able to reduce its mortality rate it would be able to grow to increased densities. To investigate this supposition we included the process of predator death in our model, and swept a range of mortality values, from zero (no mortality) to 0.2 h^{-1} – substantially more than had been reported for *Bdellovibrio* (Hespell *et al.*, 1974). Contrary to our expectations, predator mortality was found to stabilise the system by preventing oscillations, and we found that a certain amount of mortality benefited the predator, resulting in an optimal predator

mortality for maximum predator biomass. This optimum was just below the maximum mortality before predator washout and was the rate at which the system underwent a Hopf bifurcation from steady state to extreme oscillations (Fig. 2.7). The level of mortality which was optimal for the predator increased with increasing nutrient inflow to the system, from 0.02 to 0.08 h^{-1}, which is comparable to the 0.06 h^{-1} mortality observed for *Bdellovibrio* (Hespell *et al.*, 1974). Whilst the system was in an oscillatory regime further reduction in predator mortality caused the densities of both the predator and the prey to decrease. Increasing S_0 levels resulted in a narrower peak in predator and trough in prey density, as did increasing the dilution rate.

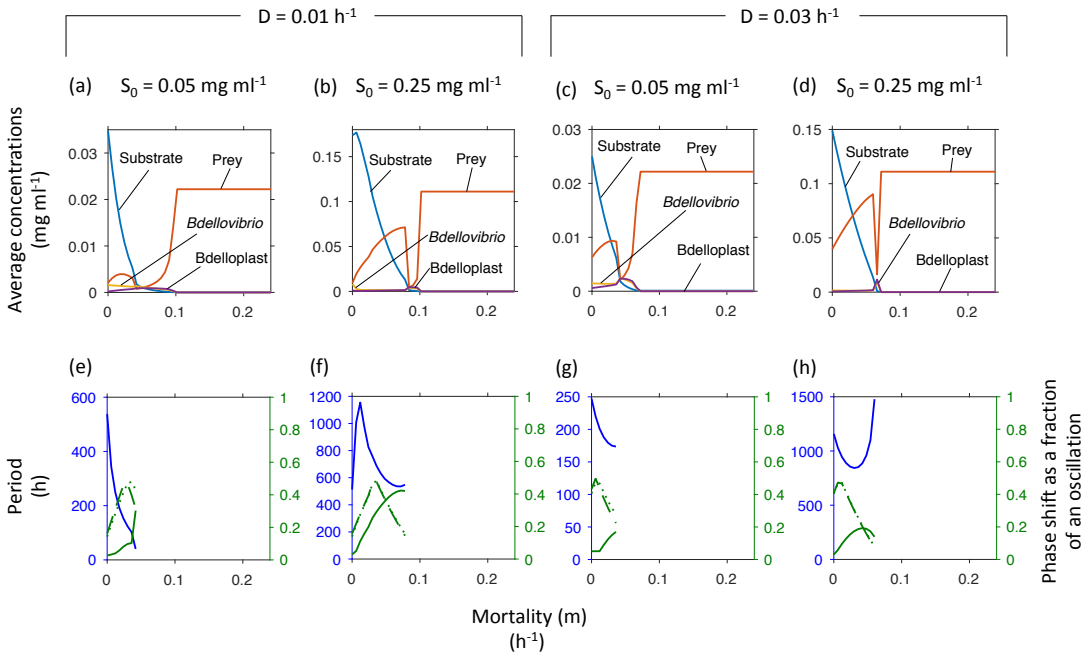

Figure 2.7 – Optimal predator mortality

Above a critical predator mortality rate, the population densities no longer oscillated, prey density dropped and predator density reached a maximum, which was higher than at zero mortality. At even higher mortality, the predator died out, leading to a prey only steady state. At higher substrate inflow concentrations (S_0) and dilution rates, the predator abundance peak narrowed. Top row shows concentrations at steady state or averaged over one oscillatory cycle (see methods 2.2.6). Bottom row shows the oscillatory period (blue, left axis) and phase shifts (green, right axis) from substrate peak to peak of prey (solid line), free *Bdellovibrio* (dashed line) or bdelloplast (dotted line).

We concluded that while a certain amount of *Bdellovibrio* mortality is likely to be inevitable, due to life style (small size and high speed), this mortality is also actually advantageous to the predator as it allows the prey a degree of respite in which to regrow and support further new predators.

2.3.4.4 There is an optimal rate of bdelloplast maturation

The final biological process involved in our model was maturation of the bdelloplast to give new predators. The bdelloplast is a unique entity made up of a dead prey cell and a *Bdellovibrio* replicating within it. It takes about three hours for *Bdellovibrio* to consume prey such as a standard size *E. coli*, during which time it does not predate more prey and the prey cell being dead does not consume further nutrients. Clearly, there is a biological limit on how quickly *Bdellovibrio* can convert the prey material into more predators. Given the presence of optimal values for predator attack rate constant and mortality however, we hypothesised that even if a faster rate of conversion were possible it might not be to the benefit of the predator. To test this proposal, we swept a range of maturation rates for the bdelloplast. We found that, as with predator attack rate constant and mortality, there is also an optimal bdelloplast maturation rate to optimise predator biomass. Once again, this optimum occurs just above the minimum rate to allow the predator to survive, and is the rate at which a Hopf bifurcation occurs from a steady state regime to extreme oscillations (Fig. 2.8). The optimal maturation rate at a dilution rate of 0.03 h^{-1} was around 0.1 mg predator mg bdelloplast^{-1} h^{-1}, depending on S_0, which is about the expected rate (0.109 mg predator mg bdelloplast^{-1} h^{-1}) for the maturation rate of a bdelloplast formed from *Bdellovibrio* predation of a typical *E. coli* cell. At low S_0 and

dilution rate it was possible for all species to stably co-exist without oscillations at all values of k_P tested (Fig. 2.8a). A faster maturation rate here caused a small increase in the density of free predators, combined with a decline in the density of both bdelloplasts and prey. Increasing the dilution rate caused an increase in the minimum value of k_P required for predator survival, but otherwise did not affect the trends seen (Fig. 2.8a, e). Increasing S_0 destabilised the system and resulted in oscillations (Fig. 2.8 b-d & f-h). Under these conditions increasing k_P reduced prey density, but had little effect on predators, except at the higher (0.03 h^{-1}) dilution rate (Fig. 2.8d). These results confirm that, as with predator attack rate constant, too fast a rate of predation is to the detriment of the predator, as it hampers prey regrowth.

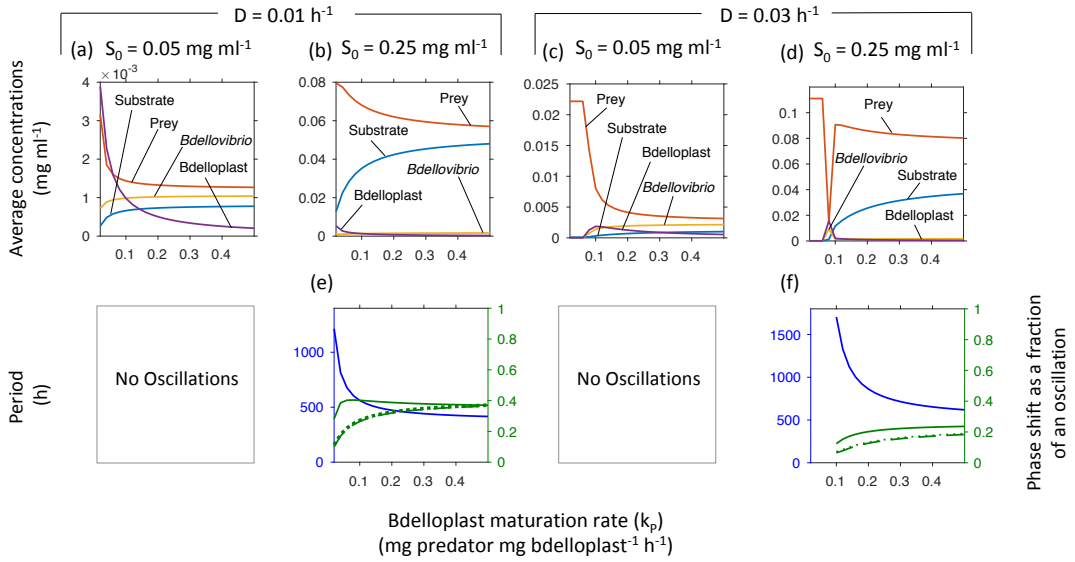

Figure 2.8 – Effects of bdelloplast maturation rate

Varying the maturation rate of the bdelloplast (k_P) from 0.02 to 0.5 mg predator mg bdelloplast^{-1} h^{-1} had a plethora of effects. (a, c) At low inflow substrate concentrations (S_0), the populations did not oscillate regardless of maturation rate. The minimal maturation rate for predator persistence and the optimal maturation rate are visible in (c). (b, d) At higher S_0, populations oscillated above a threshold maturation rate; the optimal maturation rate was just below this threshold (visible in d). (a-d) Concentrations at steady state or averaged over one oscillatory cycle (see methods 2.2.6). (e, f) Oscillatory period (blue, left axis) and phase shifts (green, right axis) from substrate peak to peak of prey (solid line), free *Bdellovibrio* (dashed line) or bdelloplast (dotted line).

2.3.4.5 Lowest half-saturation constant of the predator by its prey is not always optimal

One of the fundamental system parameters identified from the dimensional analysis was $K'_R = \frac{K_{N,P}}{K_{S,N}\, Y_{N/S}}$, the ratio of predator half-saturation constant for prey ($K_{N,P}$), to prey half-saturation constant for substrate ($K_{S,N}$), scaled by the productivity of the prey ($Y_{N/S}$). While more is known about $K_{S,N}$ and $Y_{N/S}$, $K_{N,P}$ has been studied very little. To our knowledge a literature value for this has not previously been available. We obtained an estimate from modelling a batch culture experiment (cf. Chapter 4) and we reanalysed data from a chemostat experiment conducted by Varon & Zeigler (1978) using a marine BALO (BM4) and *Photobacterium leiognathi* E28 as prey to obtain a second estimate from this data. We wanted however to understand the effects of any errors in these estimates, so we swept a range of values for $K_{N,P}$ to observe how changes in this parameter altered the system dynamics. Given the optimal value found for the attack rate constant we expected to find a similar pattern for the half-saturation constant, although in this instance we expected to find a maximum value for survival and a lower optimal value, as a higher half-saturation constant results in a lower effective attack rate at any particular substrate concentration. As expected, we found that a low half-saturation constant of the predator by its prey (low $K_{N,P}$) resulted in extreme oscillations (Fig. 2.9). Increasing that half-saturation level (increasing $K_{N,P}$) resulted in a Hopf bifurcation to steady state co-existence of predator and prey. The rate at which this transition occurred was also the optimal value for the predator. Increasing the half-saturation constant further resulted in a reduction in the biomass of the predator and an increase in that of the

prey. As would be expected, increasing S_0 increased the prey density, resulting in an increase in the value of $K_{N,P}$ at which the Hopf bifurcation occurred.

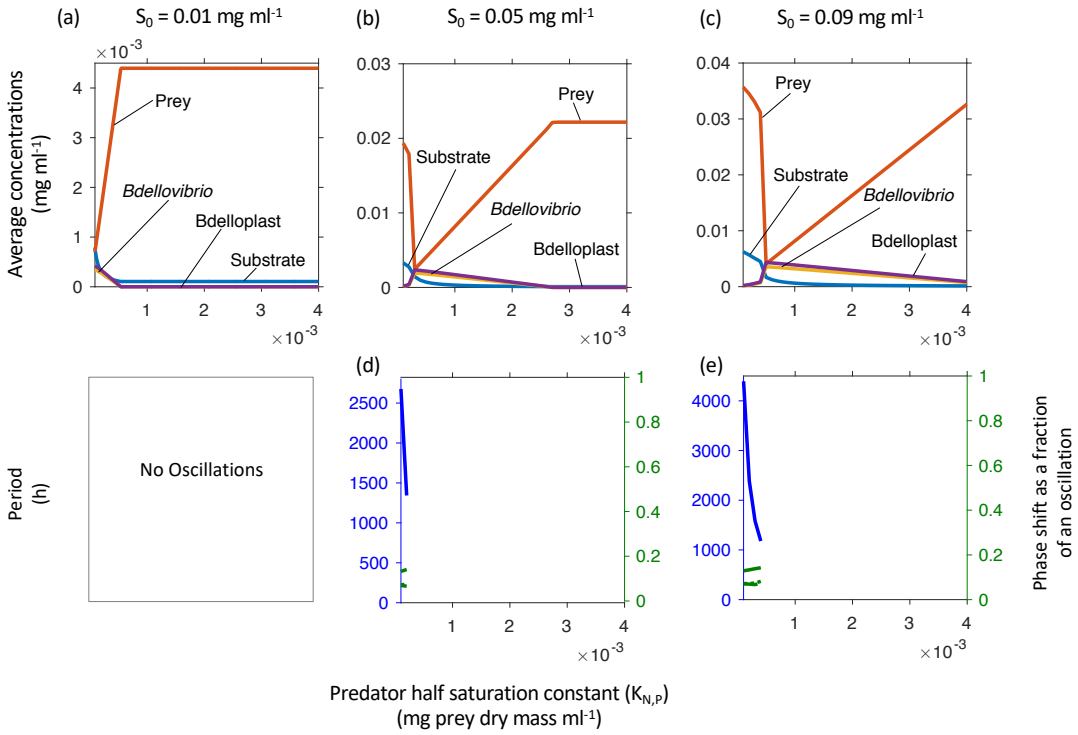

Figure 2.9 – Effects of predator half-saturation constant

Change in average bacterial densities, oscillatory period and species phase shifts with changing $K_{N,P}$ at various S_0 and dilution rates. Top - Species concentrations at steady state or average concentrations over an oscillatory cycle (see methods 2.2.6). Bottom – Blue line is oscillatory period and Green lines are phase shifts from peak substrate to peak of other species; solid – prey, dashed – free *Bdellovibrio*, dotted – bdelloplast.

2.3.4.6 Increasing prey productivity benefits predator until an optimum is reached

S_0' is a ratio of S_0 to $K_{S,N}$ and is in essence a measure of the biomass availability to the lowest biological level of our food web, the prey. It might be expected that increasing the amount of nutrients coming in to a system would be of benefit to all species within that system, especially those, such as predators, at the top of the food chain. On the other hand it has been seen that increased nutrients levels can destabilise an ecosystem in a paradox of enrichment effect (Rosenzweig, 1971). We sought to determine which of these effects would be observed in our system. As

varying the $K_{S,N}$ would have altered a second dimensionless parameter, K_R', we instead varied S_0. Increasing S_0, as previously seen, destabilised the system and caused oscillations. The optimal S_0 concentration for the predator was just less that than which resulted in these oscillations (Fig. 2.10) and occurred at values between 0.1 to 0.25 mg ml^{-1}, depending on dilution rate. By comparison the amount of carbon entering the human gut is much higher and has been estimated to be about 55 mg ml^{-1} (Cremer *et al.*, 2017), although not all of this may be in a form digestible to many species of enteric bacteria. The amount of readily digestible nutrients entering a wastewater treatment plant is much less at about 0.01 mg ml^{-1} (Henze *et al.*, 1987), which is lower than the optimum values predicted by our model. Once oscillations were seen, further increases in S_0 increased the oscillatory period up to a maximal value (Fig. 2.10c, d). Over the range during which the period increased, the benefit of extra resources was almost exclusively felt by the prey species (Fig. 2.10a). Once the maximal period had occurred, further increases in S_0 benefited both the predator and the prey.

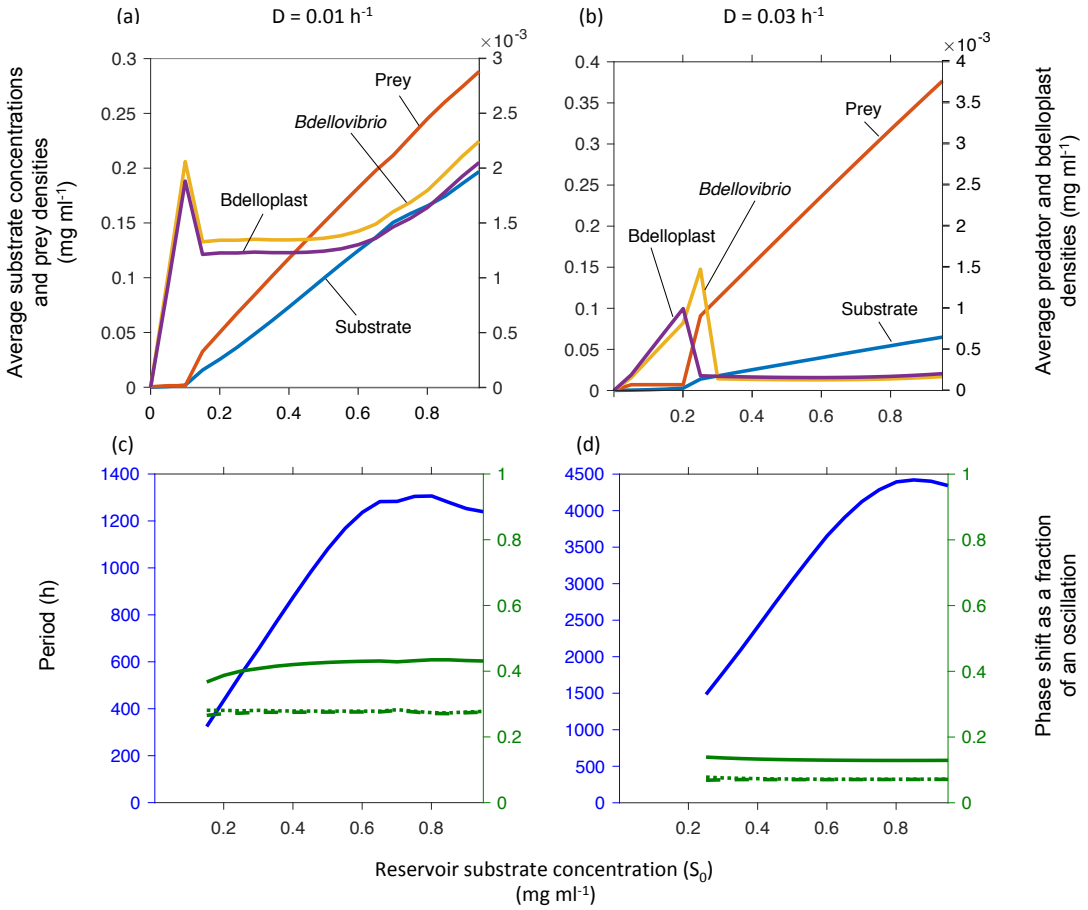

Figure 2.10 – Effects of nutrient levels

Change in average bacterial densities, oscillatory period and species phase shifts with changing S_0 at various dilution rates. Top - Species concentrations at steady state or average concentrations over an oscillatory cycle (see methods 2.2.6). Bottom – Blue line is oscillatory period and Green lines are phase shifts from peak substrate to peak of other species; solid – prey, dashed – free *Bdellovibrio*, dotted – bdelloplast.

2.3.4.7 There is an optimal predator burst size

The final dimensionless parameter Y'_{B*P} corresponded to the *Bdellovibrio* burst size, which varies with the biomass of the prey species. We hypothesised that increased burst sizes would be to the benefit of the predator as it is effectively using its prey more efficiently, whilst lower burst sizes reflect a more wasteful use of prey. There was an issue with attempting to vary this parameter, as the two components $Y_{B/P}$ and $Y_{P/B}$ are also components of other parameters. Varying either of these parameters alone would have caused a second dimensionless parameter to also vary,

confounding the results. To compensate for this, we varied both $Y_{B/P}$ and μ_P at the same time, such that the ratio between the two values was kept constant. This ensured that Y'_{B*P} was varied without altering any other parameters. At the lowest burst sizes the predator could only survive at very low (0.01 h^{-1}) dilution rates (Fig. 2.11). Increasing the burst size resulted in predator survival, and a sharp drop in prey density. As with μ_P, there was also an optimal burst size, which occurred between 4 and 6 *Bdellovibrio* per prey cell, within the observed ranged for an *E. coli* prey cell (Seidler and Starr, 1969a). Increasing the burst size above this value resulted in a Hopf bifurcation to extreme oscillations, corresponding with a sharp rise in prey and drop in predator density. Further increases caused the density of both predator and prey to decline. Increasing the dilution rate resulted in a sharper peak in predator density, which also occurred at a higher burst size (Fig. 2.11b, c). Contrary to initial expectations, we found that once again that whilst a certain burst size is required for predator survival, too large a burst size, i.e. too efficient a predator results in a boom in the predator population that cannot be supported by the prey, as it cannot reproduce quickly enough to make up for losses due to predation.

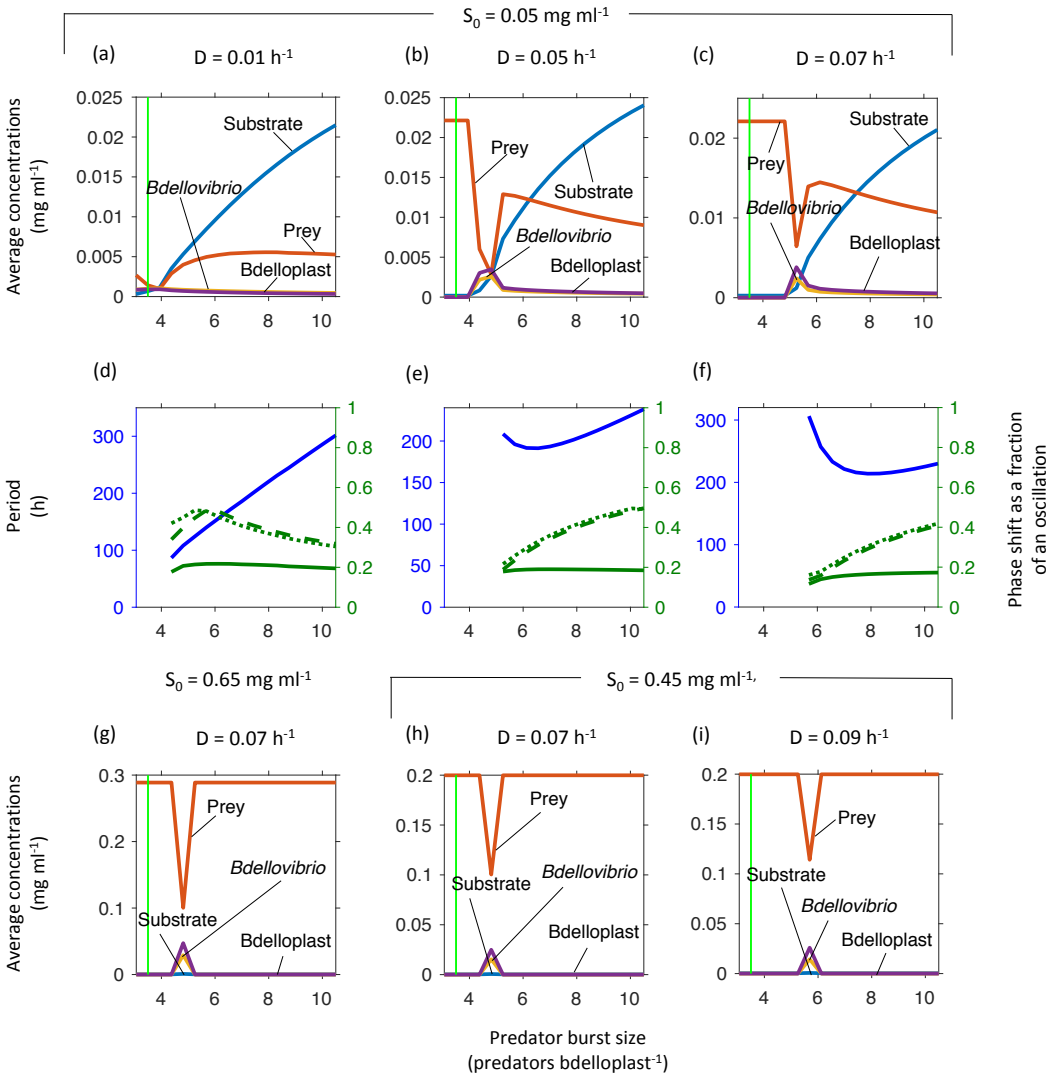

Figure 2.11 – Effects of predator burst size

Change in average bacterial densities, oscillatory period and species phase shifts with changing Y'_{B*P} at various S_0 and dilution rates. Top and bottom – Species concentrations at steady state or average concentrations over an oscillatory cycle (see methods 2.2.6). Middle row – Blue line is oscillatory period and Green lines are phase shifts from peak substrate to peak of other species; solid – prey, dashed – free *Bdellovibrio*, dotted – bdelloplast. The green line is the burst size of a bdelloplast formed from an average *E. coli* and similar to most prey used in laboratory studies or for isolating *Bdellovibrio* from the environment.

2.3.4.8 Bdellovibrio and bacteriophages

We asked whether bacteriophages would outcompete *Bdellovibrio* on single prey populations and if so, under which conditions and why. The bacteriophage was parameterised based on the well-studied T4 phage infecting *E. coli*. Under both inflow substrate concentrations (S_0) tested, T4 bacteriophage caused oscillations and

outcompeted *Bdellovibrio* (Fig. 2.12). The bacteriophage is hampered by a higher prey half-saturation constant (higher $K_{N,P}$), but helped by a lack of mortality, higher attack rate constant (μ_P) and improved kinetics of prey consumption (increased k_P and burst size). To find out which of these advantage(s) allowed the phage to outcompete *Bdellovibrio*, we ran competitions where the phage kept the prey saturation disadvantage and had one or more of the advantages. We found that increased burst size ($Y_{P/B}$) alone was sufficient to allow the phage to outcompete the *Bdellovibrio* (Fig. 2.13d). Increased attack rate constant (μ_P) and reduced mortality were also sufficient, but only in combination (Fig. 2.13a, b, e). Increased maturation rate (k_P) was insufficient even in the presence of either an increased attack rate constant (μ_P) or reduced mortality (Fig. 2.13c, f, g). In conclusion, bacteriophages outcompete *Bdellovibrio* in spite of the latter having a lower half-saturation constant for their mutual prey, largely due to the large burst size of the phages, with some additional effects from the increased attack rate constant of the phage and its lack of mortality.

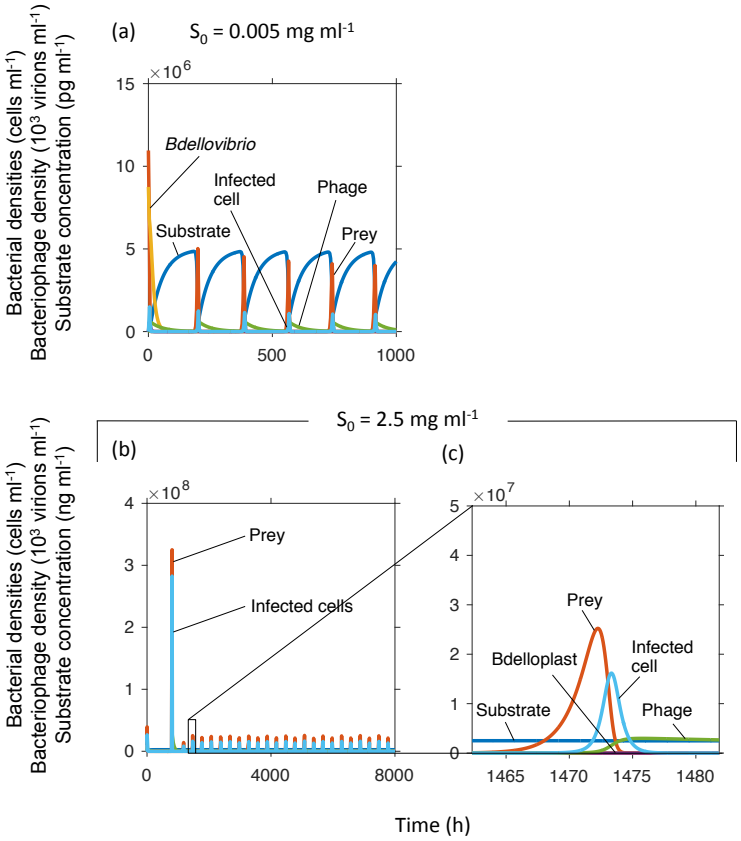

Figure 2.12 – T4 phage vs. *Bdellovibrio.*

T4 phage caused oscillations and outcompeted *Bdellovibrio* at two very different inflow substrate concentrations. Dilution rate was 0.02 h^{-1}. Note that units had to be changed to particle densities from the biomass densities used in the other sections. Panel (c) shows a zoomed in version of a peak in panel (b), the substrate concentration appears to be constant on the scale needed to show the other variables.

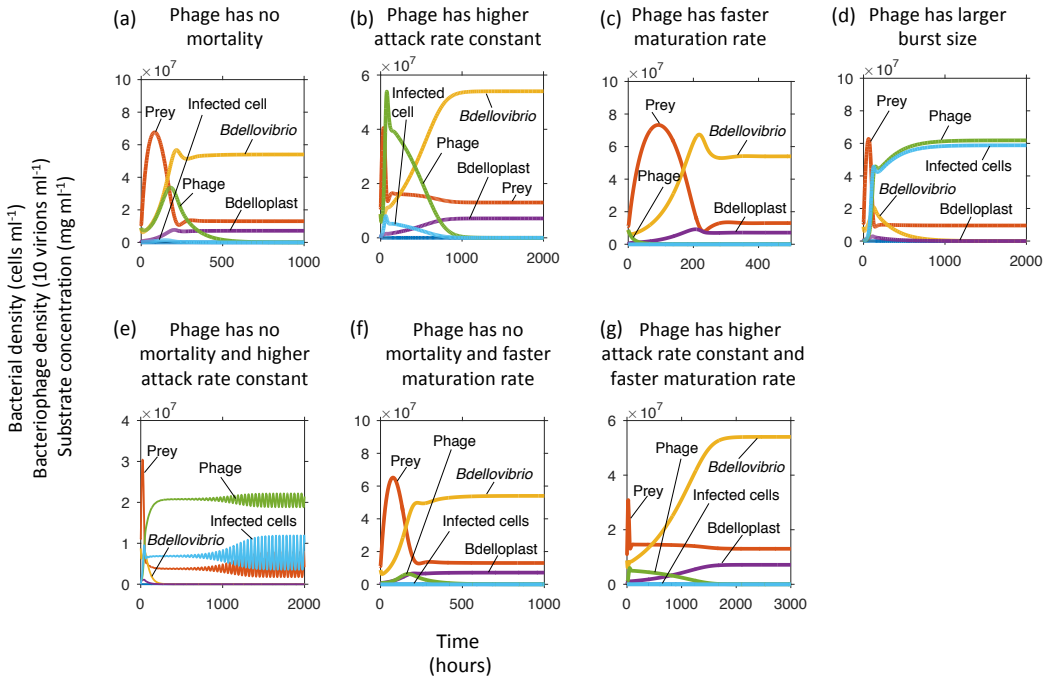

Figure 2.13 – Why phage outcompetes *Bdellovibrio*

Competitions between *Bdellovibrio* and a phage that has one disadvantage, an increased prey half-saturation constant (higher $K_{N,P}$), but one or more compensating advantages. The phage wins if it has a larger burst size (panel d) or a combination of immortality and higher attack rate constant (panel e). All competitions were carried out at a dilution rate of 0.02 h^{-1} and an inflow substrate concentration (S_0) of 0.05 mg ml^{-1}. To enable all data to be shown on the same axis, the phage data values were divided by 10, so 1 axis unit represents 10 virions.

2.3.4.9 Prey spiking in a batch system

Williams and co-workers spiked a seawater mesocosm with *Vibrio parahaemolyticus* and observed that the naturally resident *Halobacteriovorax* (a marine predatory bacterium with the same lifecycle as *Bdellovibrio*) spiked in numbers, whilst no resident bacteriophages did (Williams *et al.*, 2016). Given that we had previously found bacteriophage to outcompete *Bdellovibrio* when growing on the same prey we set out to electronically reproduce the spiking experiment. We used our model, with the dilution set to 0 h^{-1} to mimic the batch culture setting of the mesocosm, to explore the response of *Bdellovibrio* and bacteriophage to a spike in prey numbers. We observed that in the absence of bacteriophage, *Bdellovibrio* densities spiked in response to the spike in prey (Fig. 2.14a). When both *Bdellovibrio*

and bacteriophage where present, however, only the bacteriophage spiked in numbers, as was expected given our results on *Bdellovibrio* versus phage competitions, though this is in contrast to the findings in (Williams *et al.*, 2016). Presumably, their mesocosm did not contain suitable phages that could infect the non-indigenous strain of *V. parahaemolyticus* added to the microcosm.

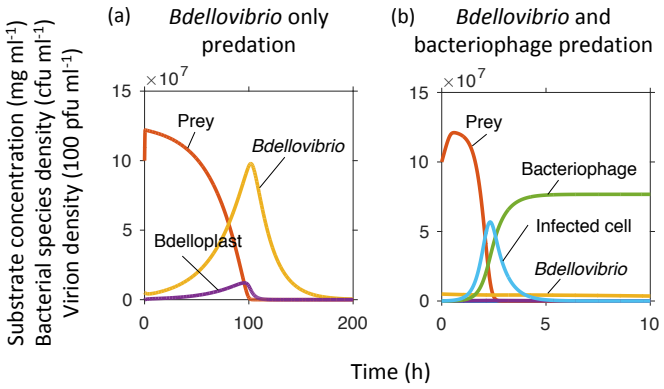

Figure 2.14 – Predator response to a spike in prey in a closed batch system
Dilution rate = 0 h^{-1}.

2.3.4.10 Trade-off between high rate versus high yield for predators

Generally, in a chemostat competition experiment the fastest growing species utilising a resource will outcompete a more efficient, but slower growing species. To see whether this was true in our system, we competed two predatory species. The first species was capable of converting bdelloplasts into new free predators at a higher rate (higher k_P), but had a lower burst size (lower $Y_{P/B}$) to reflect a reduced yield. The second predator had a lower k_P, but higher $Y_{P/B}$. In contrast to simpler systems, with our model, the high yield predator outcompeted the high rate species, driving it to extinction under all S_0 and dilution rate conditions tested (Fig. 2.15). At the lower S_0 the more efficient predator was able to stably co-exist with the prey (Fig. 2.15a). As with the bacteriophage higher S_0 resulted in oscillations with varying amplitude,

without a discernible pattern (Fig. 2.15b). In this case however, the relative changes in amplitude were smaller than with the bacteriophage and could have been caused by small inaccuracies in the precision of the solver.

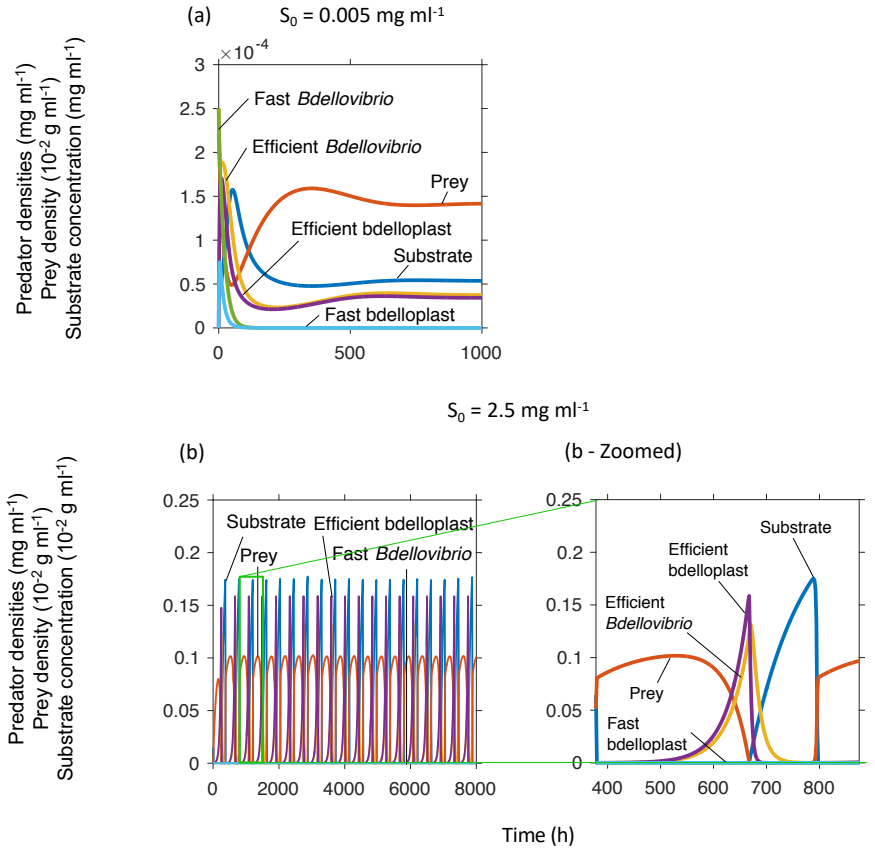

Figure 2.15 – Rate vs. yield trade-off
Simulations of competitions between a predator with a fast maturation rate (high k_P) and one with a high burst size (high $Y_{P/B}$), at (a) S_0 = 0.005 mg ml^{-1} and (b) S_0 = 0.25 mg ml^{-1}. Dilution rates = 0.02 h^{-1}. Panel (c) shows a zoomed in version of a peak of panel (b).

2.3.4.11 Co-existence of two predators on one prey

Another expectation of a chemostat is that only one species can occupy each niche. Therefore, with a predator prey system each prey species present should only be able to support a single predator species. We sought to test if this was true of our system by having two predators, one with a fast attack rate (high μ_P) and the other a low prey half-saturation constant (low $K_{N,P}$). We found that it was possible for both

predators to co-exist on the same prey (Fig. 2.16). Depending on the S_0 value and the differences in μ_P and $K_{N,P}$ it was possible for the species to either stably co-exist (Fig. 2.16a) or display sustained oscillations (Fig. 2.16d). When substrate was in low abundance it also limited the maximal prey density, and prey half-saturation constant of the predator was key (Fig. 2.16a, b). At higher substrate concentrations there was more prey, so predators encountered prey more often and the limiting factor became how fast the predator could handle (penetrate and kill) the prey (Fig. 2.16c, d).

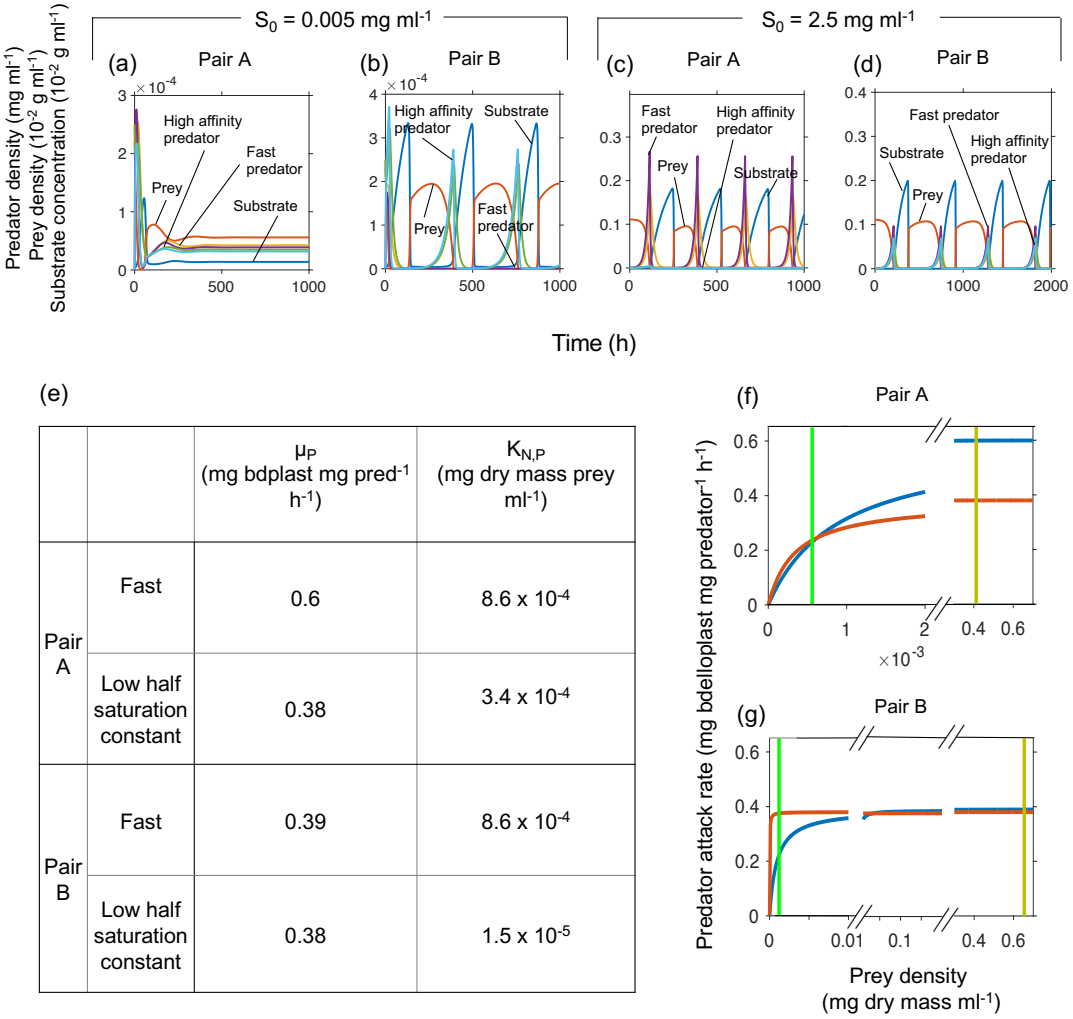

		μ_P (mg bdplast mg pred^{-1} h^{-1})	$K_{N,P}$ (mg dry mass prey ml^{-1})
Pair A	Fast	0.6	8.6 x 10^{-4}
	Low half saturation constant	0.38	3.4 x 10^{-4}
Pair B	Fast	0.39	8.6 x 10^{-4}
	Low half saturation constant	0.38	1.5 x 10^{-5}

Figure 2.16 – Co-existence of two predators

Simulations of competitions between a predator with a high attack rate constant (high μ_P) and one with a low prey half-saturation constant (low $K_{N,P}$) at a dilution rate of 0.02 h^{-1}. Panels (a, c) – Pair A – Predator 1 μ_P = 0.6 mg bdelloplast mg predator^{-1} h^{-1}, predator 2 $K_{N,P}$ = 3.4 x 10^{-4} mg prey ml^{-1}. Panels (b, d) – Pair B – Predator 1 μ_P = 0.39 mg bdelloplast mg predator^{-1} h^{-1}, predator 2 $K_{N,P}$ = 1.5 x 10^{-5} mg prey ml^{-1}. Panel (e) μ_P and $K_{N,P}$ for all predators. Panels (f, g) comparison of predator growth rates for both pairs of predators over a range of prey densities.

2.3.4.12 Prey cell biomass

Bacterial cells can have a large range of sizes (and therefore biomass) from ultra-small species such as the marine bacterium *Pelegabacter ubique* (Giovannoni *et al.*, 2005) to *Thiomargarita namibiensis*, a sulphur bacterium, which is large enough to be seen with the naked eye (Schulz *et al.*, 1999). Clearly, there is biologically a lower limit to the size of cell *Bdellovibrio*, as a periplasmic predator, could physically enter

and predate, however, it is not clear whether there is any upper size constraint. A *Bdellovibrio* cell is around seven times smaller than an *E. coli* cell and many other known prey species such as *Pseudomonas putida* (Huang and Starr, 1973) and *Klebsiella pneumoniae* (Dashiff *et al.*, 2010) are of a similar size to *E. coli*. There are however, examples of *Bdellovibrio* species predating much larger cells such as filamentous *E. coli* (Kessel and Shilo, 1976) and *aquaspirillum* (Núñez *et al.*, 2003) The relatively small size of *Bdellovibrio* could allow it to predate a wider range of cells, however there is a potential for the predator cell to prey cell biomass ratio to affect the kinetics of predation and alter the population dynamics.

Given the same amount of nutrients coming into a system, in the absence of predators, it can support a certain number of cells of low biomass, or a smaller number of cells of a higher biomass. When a predator is added into this system it will encounter prey cells more often when there are many smaller cells (encounter rate is proportional to the surface area of the prey cells, which increase with square of the cell radius, whilst biomass increases with the cube of the radius). However, when the predator does encounter a larger cell it will acquire more resources with which to reproduce. This trade-off between more frequent, but less profitable encounters with prey and rarer, but more profitable encounters means it is difficult to predict whether a larger prey cell biomass is to the benefit of the predator. To investigate the possible effects of this trade-off, we examined final biomass density of both predator and prey over a range of prey to predator cell biomass ratios and a variety of S_0 and dilution rate conditions. We found that there was both a minimum prey : predator biomass ratio required in order for the predator to survive, which under the conditions tested was between 5.25 and 15, depending on dilution rate, and an optimal value for

maximal predator biomass of between 8.75 and 32.5, again dependent on dilution rate (Fig. 2.17). This means that a typical *E. coli* would be slightly smaller than the optimal value, but larger than the minimum value for at least some conditions. Higher prey : predator biomass ratios caused the system to display extreme oscillations and the optimal ratio for the predator was just less than that which would cause these oscillations. Increases in S_0 resulted in a decrease in the optimal ratio value (Fig. 2.17 a-c) and a narrowing of the range of values that gave predator biomass close to the maximum achievable. Increases in the dilution rate gave a similar narrowing of the optimal range, but caused the optimal value to increase (Fig. 2.17c, d).

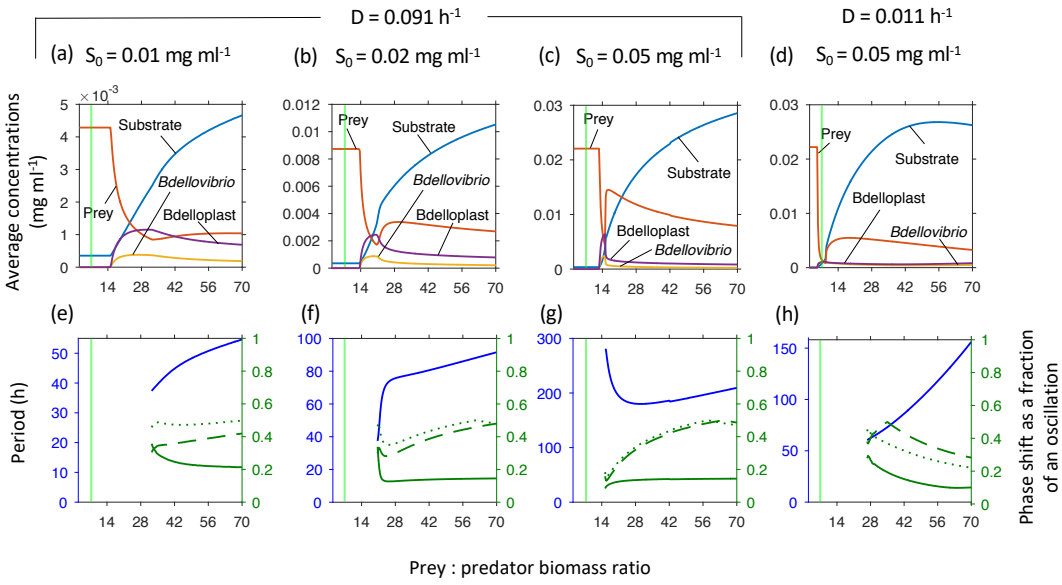

Figure 2.17 – Minimal and optimal prey biomass

Prey biomass relative to predator biomass (0.028 pg dry biomass). Predator density showed a broad optimum at low inflow substrate concentrations (S_0) that became narrower at higher S_0 and dilution rate. Too large prey caused oscillations. Top row shows concentrations at steady state or averaged over one oscillatory cycle (see methods 2.2.6). Bottom row shows the oscillatory period (blue, left axis) and phase shifts (green, right axis) from substrate peak to peak of prey (solid line), free *Bdellovibrio* (dashed line) or bdelloplast (dotted line). The green line is the biomass ratio between an average *E. coli* and *Bdellovibrio* and similar to most prey used in laboratory studies or for isolating *Bdellovibrio* from the environment.

From this we can conclude there is an optimal prey cell biomass for the predator, which varies depends on the conditions (dilution rate and inflow of

nutrients), but is usually somewhat larger than an *E. coli* cell, which is typical in size and biomass of many cells predated by *Bdellovibrio*. This would seem to indicate that *Bdellovibrio* should ideally be smaller than it already is however, this may not be possible due to biological constraints. *Bdellovibrio* already has quite a large genome (3.6 Mb) to biomass ratio when compared to *E. coli* (4.5 Mb), which has approximately seven times as much biomass. Additionally, lack of energy storage is thought to be a factor in the relatively high mortality of *Bdellovibrio* (Hespell *et al.*, 1974) and any further reduction in cell biomass would likely result in a reduction in the already limited capacity for energy storage.

2.3.4.13 Conditions for robust co-existence and paradox of enrichment

When studying the conditions under which the maximum density of predator biomass could be obtained, it became clear that for many of the conditions tested the system displayed an oscillatory regime, with periods in the region of hundreds of hours. These oscillations had such an extreme amplitude (minimum values < 1×10^{-30} mg dry mass ml^{-1}) that the stochastic noise present in any real system would result in the extinction of the predator, or both the predator and the prey. We therefore examined more closely the range of values that would allow for predator survival, without either the washout of the predator or the presence of extreme oscillations.

As can be seen from Fig. 2.18 there was a paradox of enrichment effect. At low levels of S_0 there was a wide range of prey to predator biomass ratios at which predator survival was possible. Higher values of S_0 destabilised the system, reducing the gap between the ratio needed to prevent predator washout, and that which caused oscillations. As previously seen (Fig. 2.17c, d) increasing the dilution rate

resulted in an increase in the minimum prey : predator ratio at which the predator could survive. It also caused a narrowing of the survival range between predator washout and extreme oscillations. At nutrients levels of 0.01 mg ml^{-1}, typical of the inflow into waste water treatment plants (Henze *et al.*, 1987), there is a wide range of prey : predator biomass ratios at which robust co-existence of the predator and prey can occur, especially at lower dilution rates. It should be note that at higher dilution rates in particular a typical *E. coli* cell is predicted to be too small to sustain the presence of *Bdellovibrio*, although *E. coli* can grow into long filaments (Maki *et al.*, 2000), which would be large enough to sustain *Bdellovibrio*.

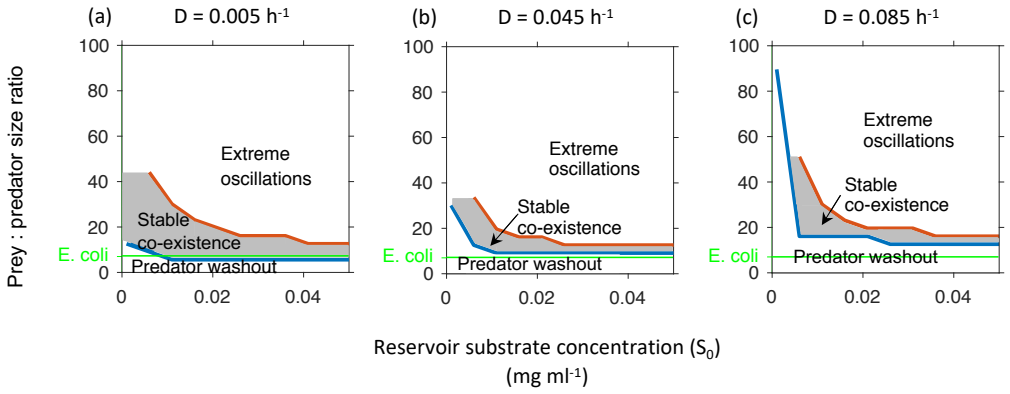

Figure 2.18 – Paradox of enrichment.

The range of prey to predator biomass ratios enabling permanence or stable co-existence of predator and prey (here including the regions of stable co-existence and damped oscillations in Fig. 2.3a) shrank with increasing productivity (inflow substrate concentration S_0). At higher dilution rates, prey had to be unrealistically large for permanence; also, the prey biomass range for permanence shrank. Below the blue line, the predator is washed out. Within the shaded area permanence occurred. Above the red line, extreme oscillations occurred resulting in bottlenecks and predator extinction due to stochastic dynamics. The green line is the biomass ratio between an average *E. coli* and *Bdellovibrio* and similar to most prey used in laboratory studies or for isolating *Bdellovibrio* from the environment.

2.3.4.14 Tragedy of the commons

Similarly, to with S_0, increasing μ_P likewise reduced the survival gap of prey to predator biomass ratios (Fig. 2.19). This was a tragedy of the commons effect, as the predator was eating its prey faster than the prey could regrow. Increases in S_0 caused a large decrease in the size of the survival gap for the predator (Fig. 2.19a-c), whilst

increases in dilution rate caused an increase in the gap (Fig. 2.19a, d & e). Fitting of our model to experimental data (see Chapter 4), indicates *B. bacteriovorus* HD100 has an attack rate constant of about 0.38 mg bdelloplast mg predator^{-1} h^{-1}. At this value there is a wide range of prey : predator size ratios at which *Bdellovibrio* survival is possible, for all but the highest concentration of nutrients tested, although a typical *E. coli* cell is near or below the minimum prey size required to sustain *Bdellovibrio*.

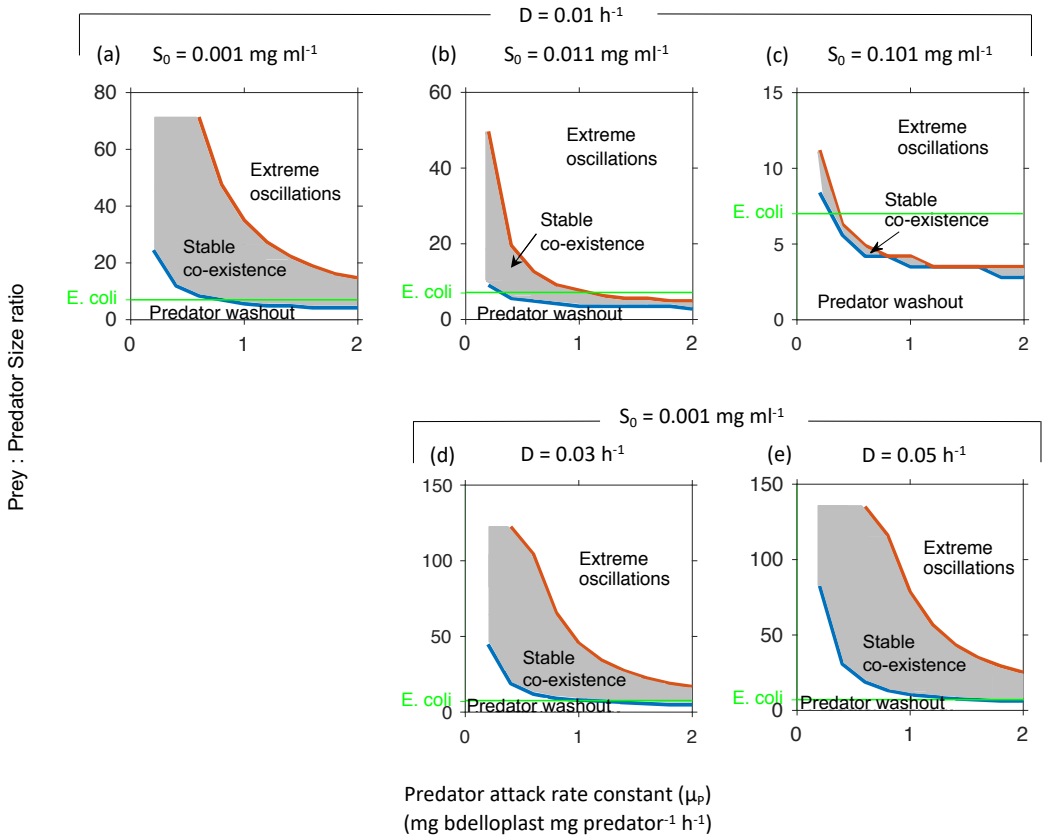

Figure 2.19 – Tragedy of the commons

The prey biomass range for permanence of the predator (robust co-existence with prey) shrinks rapidly as the predator's attack rate constant increases, as a too effective predator overexploits the prey, and then becomes extinct. This large drop in survival range occurs over a small increase in attack rate constant, illustrating the sensitivity of the system to the predator attack rate constant (see Fig. 2.5). Increased inflow substrate concentration S_0 narrowed the prey biomass range for co-existence (top row), whilst increased dilution rate expanded the range (panel a and bottom row). Below the blue line, the predator is washed out. Within the shaded area permanence occurred. Above the red line, extreme oscillations occurred resulting in bottlenecks and predator extinction due to stochastic dynamics. The green line is the biomass ratio between an average *E. coli* and *Bdellovibrio* and similar to most prey used in laboratory studies or for isolating *Bdellovibrio* from the environment.

2.3.5 Global parameter sensitivity analysis

When parameterising our model, we based our values on literature values for the best-studied predator, *B. bacteriovorus* strain HD100, predating the best-studied prey, *E. coli*, growing on glucose, as a sole carbon and energy source (Table 2.3). This meant that some aspects of this system such as prey growth rate are reasonably well-studied and understood, however others, such as the predator attack rate constant, have hardly been studied. To better understand the effects of inaccuracies in parameter estimations, as well as the differences that would be observed if the model were used for a different prey species and/or carbon source, we conducted a global sensitivity analysis for each of the parameters identified from the dimensional analysis.

Note one parameter Y'_{B*P} could not be varied independently of the other dimensionless parameters as it consists of two standard parameters $Y_{B/P}$ and $Y_{P/B}$, both of which are also part of another dimensionless parameter. To allow for this we included both $Y_{B/P}$ and $Y_{P/B}$ in the global sensitivity analysis along with the rest of the dimensionless parameters making a total of eight parameters. Each parameter was increased and decreased by 1% for 10,000 settings of the other parameters over the ranges given in Table 2.3 and the relative change of substrate concentration or population densities was calculated.

For most parameter values a small change in the input value caused only a modest change in the species concentrations (Fig. 2.20), however in a small number of cases a very large response (several orders of magnitude) was observed (Fig. 2.21). These extremely large responses occurred with parameter sets close to bifurcation points between a species survival and its washout.

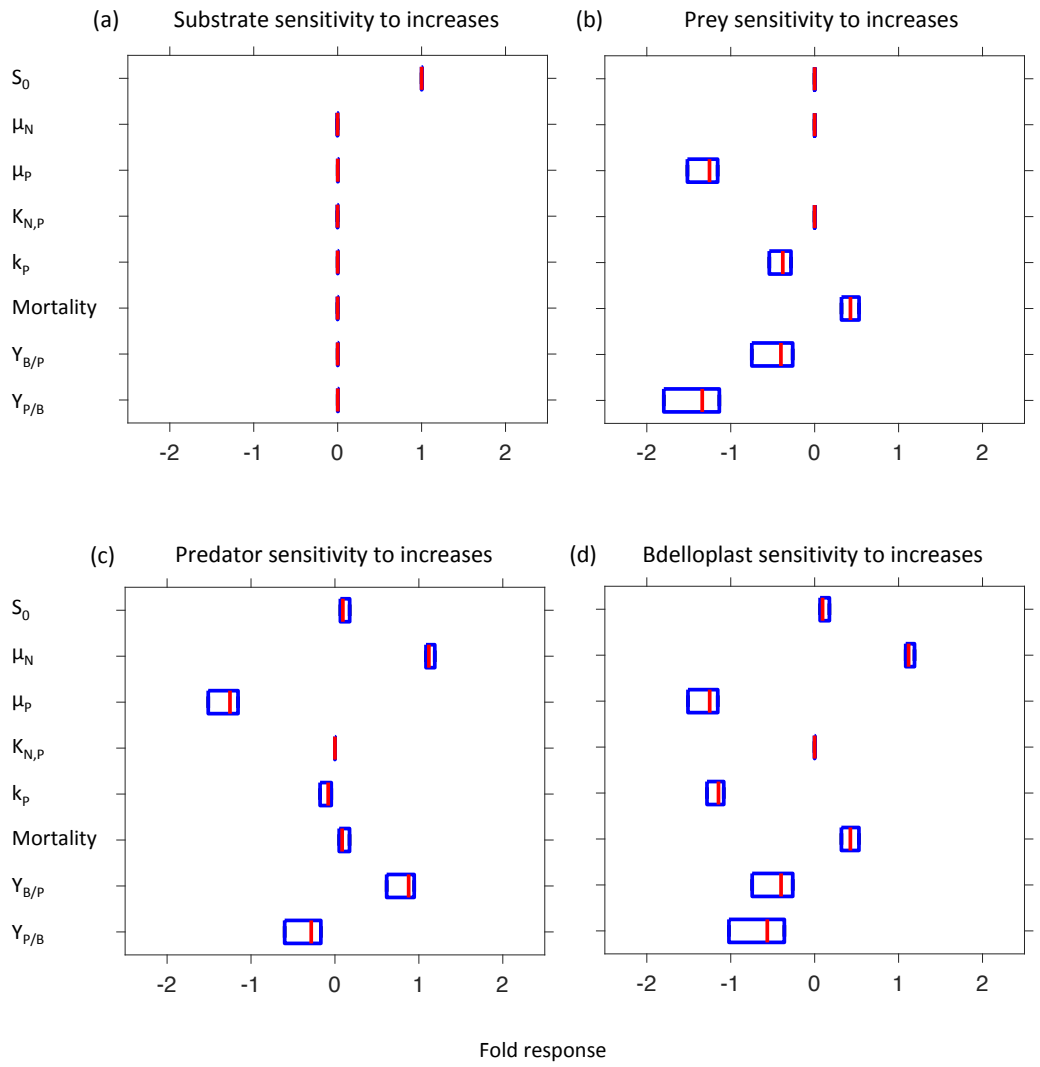

Figure 2.20 – Global sensitivity analysis without outliers

Global sensitivity of (a) substrate concentration, (b) prey, (c) predator and (d) bdelloplast population densities to small changes of a given model parameter (at 10,000 settings of the other model parameters). The distributions of the 10,000 sensitivities of outcomes to a 1% increase of the given model parameter are shown as box plots. Here, only median (red line) and 25th and 75th percentiles (blue lines) are shown; Fig. 2.21 includes the sometimes orders of magnitude different sensitivities outside the box.

In the majority of cases, substrate concentrations showed little response to changes in parameter values, the largest response was to S_0 where the response was usually equal to the change in parameter value (Fig. 2.20a). For parameter sets near the boundaries between dynamic regimes however extremely large changes in substrate concentration could be observed (Fig. 2.21a). This was especially true with

changes in predator attack rate constant (μ_P) and the yield of bdelloplast biomass per predator ($Y_{B/P}$) and predator biomass per bdelloplast ($Y_{P/B}$).

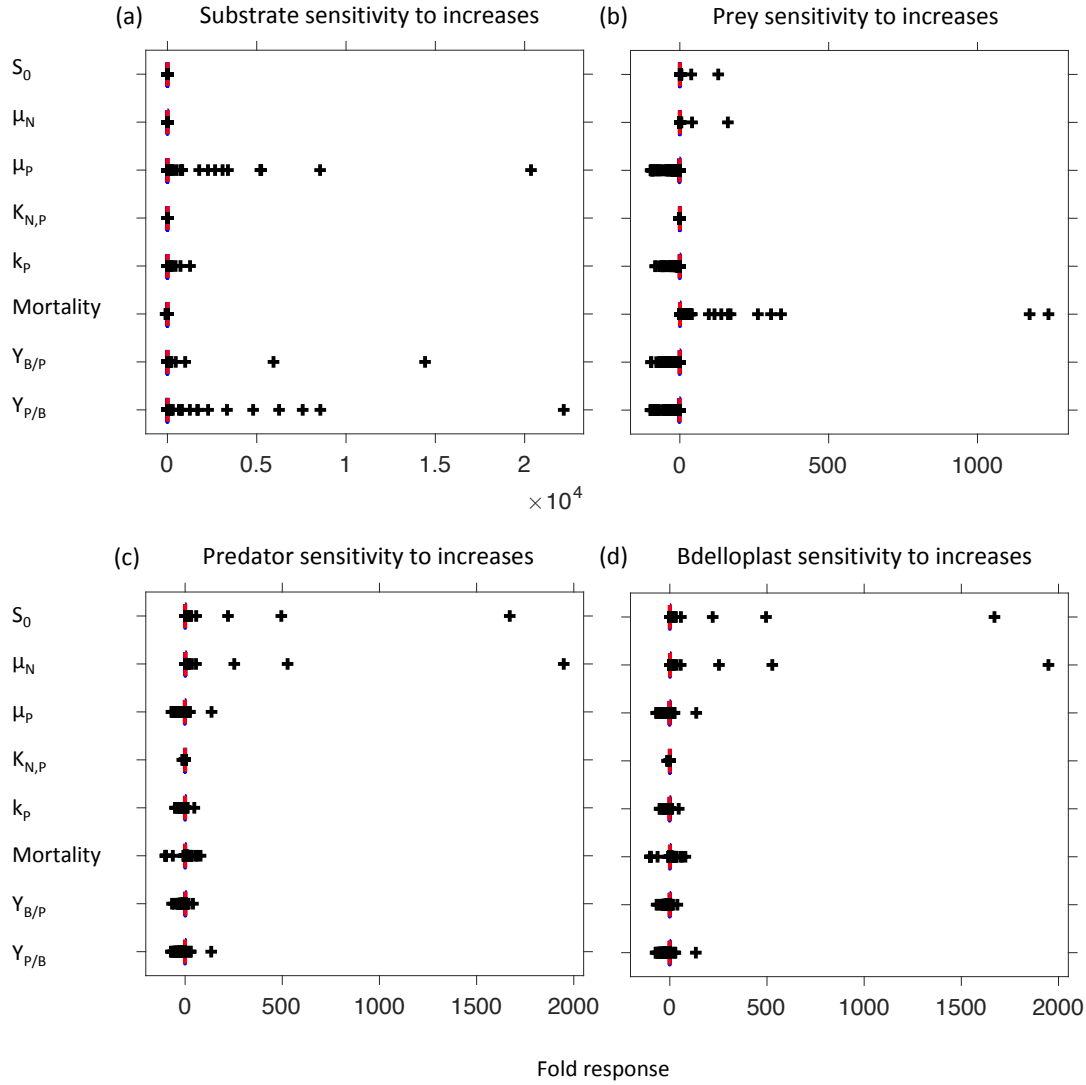

Figure 2.21 – Global sensitivity analysis with outliers

Global sensitivity of model parameters including outlier values. Response is to a 1% increase in the parameter value. Red line is the median response value. Blue box shows values from the 25th to the 75th percentile response. Black crosses are outlier values.

Prey densities were a little more sensitive to parameter changes, but in most cases the response was no more than twice the change in parameter value (Fig. 2.20b). The most common response was to changes in predator efficiency, especially to predator attack rate constant (μ_P) and to burst size ($Y_{P/B}$), increases in either of which, as might be predicted, caused a decrease in prey density. Once again, in certain

parameter sets close to the boundaries of regimes, large changes in prey densities were observed (Fig. 2.21b). This was especially true of all predator attack kinetics, except the predator's half-saturation constant ($K_{N,P}$).

With the predator and bdelloplast densities there was generally a very similar pattern of responses to changes in parameter values (Fig. 2.20c, d and Fig. 2.21c, d). When including the extreme responses, the predator and bdelloplast results were the same for all parameters. Increases in prey productivity in the form of increased nutrients into the system and faster prey growth rate, were capable of causing very large increases in the densities of both free predators and bdelloplasts (future predators). Changes in predator kinetics by contrast could cause increases or decreases in predator numbers. When these extreme responses were excluded the patterns of predator and bdelloplast density changes were still very similar. Both predator and bdelloplast benefitted from faster prey growth and suffered if the predator was too fast at attacking prey. The main differences were that increases in the maturation rate (k_P) did not affect predator numbers, but caused a small decrease in the density of the bdelloplasts and that decreases in the proportion of the bdelloplast that came from the predator (increased $Y_{B/P}$) caused a small decrease in bdelloplast densities and a larger increase in predator numbers (Fig. 2.20c & d).

2.4 Discussion

Our results suggest that *Bdellovibrio* consuming a single prey species can only survive permanently within a very narrow range of conditions. Over a wide range of conditions, the system is prone to extreme oscillations with periods of over a hundred hours and bacterial densities dropping below 0.1 pg ml^{-1}. In a deterministic mathematical model, species densities can eventually recover from even the smallest positive number but in a biological system, there has to be at least a single cell left (~1 pg). More importantly, when a system contains just a few cells over a long time, stochastic fluctuations will almost inevitably result in the loss of those cells, leading to local extinction. For most system parameters, there was a narrow range of values that allowed the predator to reproduce fast enough to avoid being washed out without triggering these oscillations, and the optimal value to maximise predator numbers occurred just above or below the threshold triggering oscillations.

Clearly, a periplasmic predator, such as *Bdellovibrio,* must be smaller than its prey to squeeze inside the periplasm. Additionally, it would be expected that a prey cell would need to be large enough to produce at least two *Bdellovibrio* progeny, although it has been reported that it is possible for *Bdellovibrio* to start replication within one prey cell and complete this in a second prey (Makowski *et al.*, 2019). Our model however predicts that *Bdellovibrio* needs to be even smaller relative to its prey in order to survive. The minimum viable prey size predicted by our model was around 7 times larger than the predator, about the difference in size between *Bdellovibrio* and *E. coli* (Cover *et al.*, 1984), which is of a similar size to other typical prey species. However, the optimal prey size is predicted to be larger than this. *Bdellovibrio* may be

larger than is optimal relative to its prey, because it cannot be any smaller than it already is.

Our model also predicts that a predator that kills its prey too efficiently (has too high an attack rate constant, or too little mortality) will drive that prey to extinction and will then become extinct itself, resulting in a tragedy of the commons (Hardin, 1968). *Bdellovibrio* does have a high mortality rate compared to other bacteria, correlating with a high endogenous respiration rate (Hespell *et al.*, 1974). While this may make over exploitation of prey less likely, this is likely to be a side effect, with the raised mortality being primarily due to *Bdellovibrio*'s life style, including its fast movement rate (Lambert, Morehouse, *et al.*, 2006) and its small size and lack of energy storage vesicles (Hespell *et al.*, 1974).

In conclusion, our model predicts a system that is prone to extreme, destabilising oscillations. This, together with the fact that *Bdellovibrio* and other BALOs need to compete with specialist bacteriophage means they need to be semi-generalist predators with a wide prey range in order to survive long term in natural environments. Additionally, they should be hotspot specialists capable of migrating between regions of high prey density which they can likely detect through chemotaxis (Lambert *et al.*, 2003; Chauhan and Williams, 2006). This has implications for the use of *Bdellovibrio* either as a therapeutic in agriculture and aquaculture or to reduce numbers of pathogens in an environmental setting. BALOs are likely to be most effective when there are alternative prey species present that may act to boost predator numbers.

CHAPTER 3: PREDATION STRATEGIES OF THE BACTERIUM *BDELLOVIBRIO BACTERIOVORUS*: ATTACK RATE, SIZE EFFECTS AND A RATE VERSUS YIELD TRADE-OFF – MATHEMATICAL ANALYSIS

An earlier version of this chapter has been deposited on BioRxiv – DOI: 10.1101/621490 as supplementary information

3.1 Model implementation and validation

3.1.1 Solver choice

Results from ODE model simulations can be affected by the choice of ODE solver. Different solvers exist because the best choice of solver depends on the nature of the ODEs and parameters of the particular model being investigated. In particular, MatLab solvers Ode15s, Ode23s and Ode23tb are designed to handle stiff systems, where there are significant differences in the timescales over which changes in different species values change. By contrast, solvers Ode45 and Ode113 are designed for non-stiff systems and Ode23 and Ode23t are best in situations of intermediate stiffness. Additionally, Ode23, Ode23s, Ode23t and Ode23tb solvers can be faster when less strict tolerances are used, while Ode113 is often fastest for particularly strict tolerances. The Ode23 and Ode45 solvers use an explicit Runge-Kutta methodology, while Ode113 uses an Adams-Bashford-Moulton method and Ode15 uses numerical differentiation formulae with variable order and step size and can also optionally implement backwards differentiation using Gear's method (Shampine and Reichelt, 1997).

Unless otherwise stated, results here were obtained with the MatLab Ode45 solver. In order to evaluate whether this was the most appropriate solver for this model, we ran simulations with a number of parameter settings (corresponding to the different dynamic regimes observed in Fig. 2.3) using several MatLab solvers. All solvers were tested with absolute and relative tolerances set to 1×10^{-9}, and all species constrained to be non-negative (if the solver permitted such a non-negative constraint). While all the solvers tested could correctly handle conditions where the

stability analysis had predicted a steady state, solvers Ode113, Ode15, Ode23t and Ode23tb were not capable of handling conditions where sustained oscillations were predicted (Fig. 3.1). Solvers Ode23 and Ode23s could handle all the scenarios, except for predicted sustained oscillations when the initial predator numbers were increased to 5×10^{-2} mg ml^{-1} for Ode23 or to 1×10^{-1} mg ml^{-1} for Ode23s. Under these conditions, simulations with the Ode23 solver incorrectly showed an abiotic state, in which all bacteria had been eliminated (Fig. 3.1e). Solver Ode23s (which cannot be set to not allow negative values) showed exponential growth of substrate concentrations to the order of 2×100^{154} mg ml^{-1} with negative density of prey in the order of -1×100^{154} mg ml^{-1} (Fig. 3.1f). In both cases, solver Ode45 (Fig. 3.1g) correctly showed the system to give sustained, extreme oscillations.

Although we expected the solvers for stiff systems (ending in s) to be appropriate, we found that the Ode45 solver was the only one that was reliable under all the tested conditions, so it was used for all further investigations.

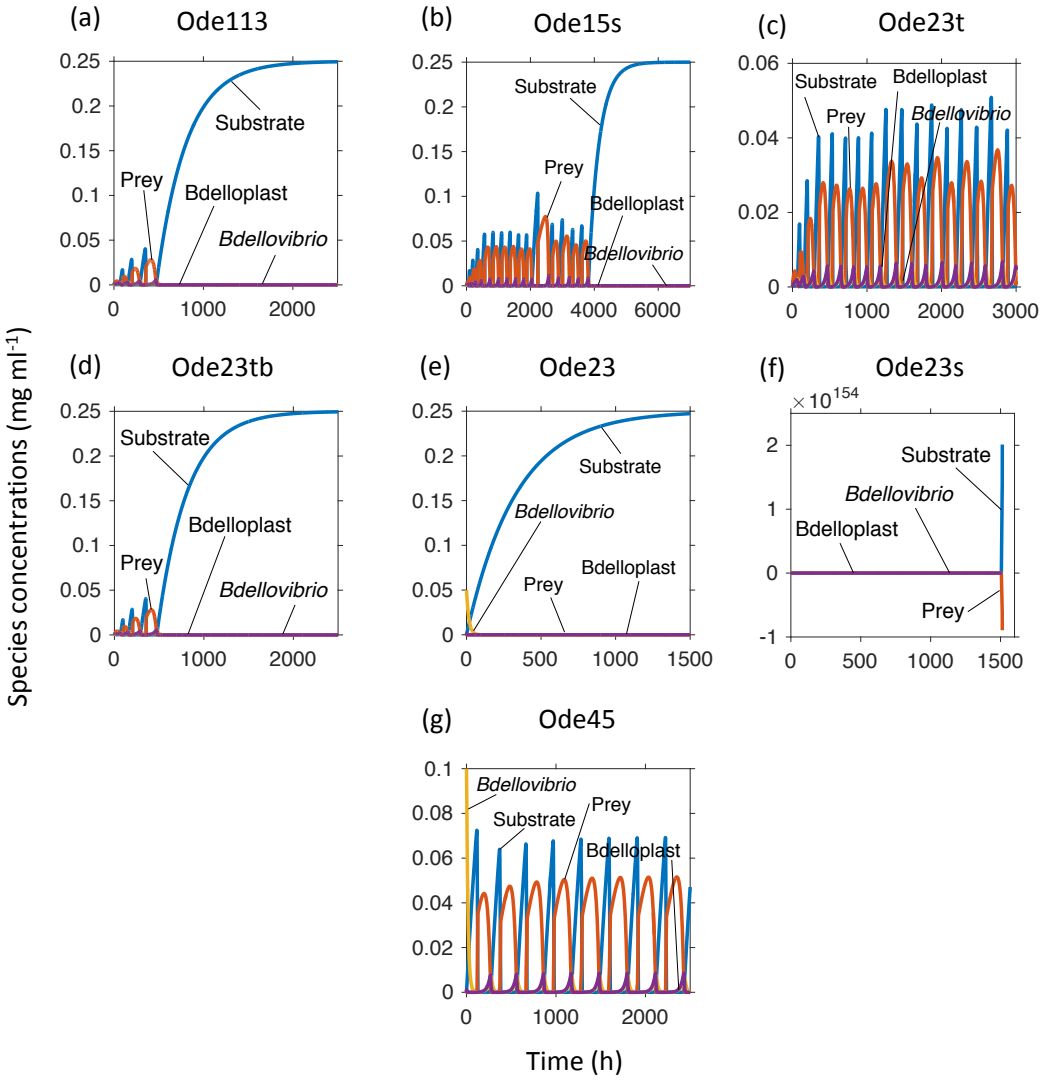

Figure 3.1 – Effects of solver choice on simulation performed with standard parameters.
S_0 = 0.25 mg ml^{-1} and a dilution rate = 0.003 h^{-1}.

3.1.2 Solver options

We also tested a range of tolerance settings for the Ode45 solver, as these can influence the outcome of a simulation (Fig. 3.2). In particular, tolerances that are too loose can result in inaccurate simulations, whilst overly strict tolerances are inefficient. The absolute tolerance setting had a much stronger influence than the relative tolerance. An absolute tolerance of 1 x 10^{-9} is needed to achieve an accurate simulation. With this absolute tolerance, a relative tolerance of 1 x 10^{-6} or lower was needed. Reducing the relative tolerance to 1 x 10^{-9} produced a small improvement in

the final result. Based on these finding, all further simulations were run with both absolute and relative tolerances of 1 x 10^{-9}, unless otherwise noted.

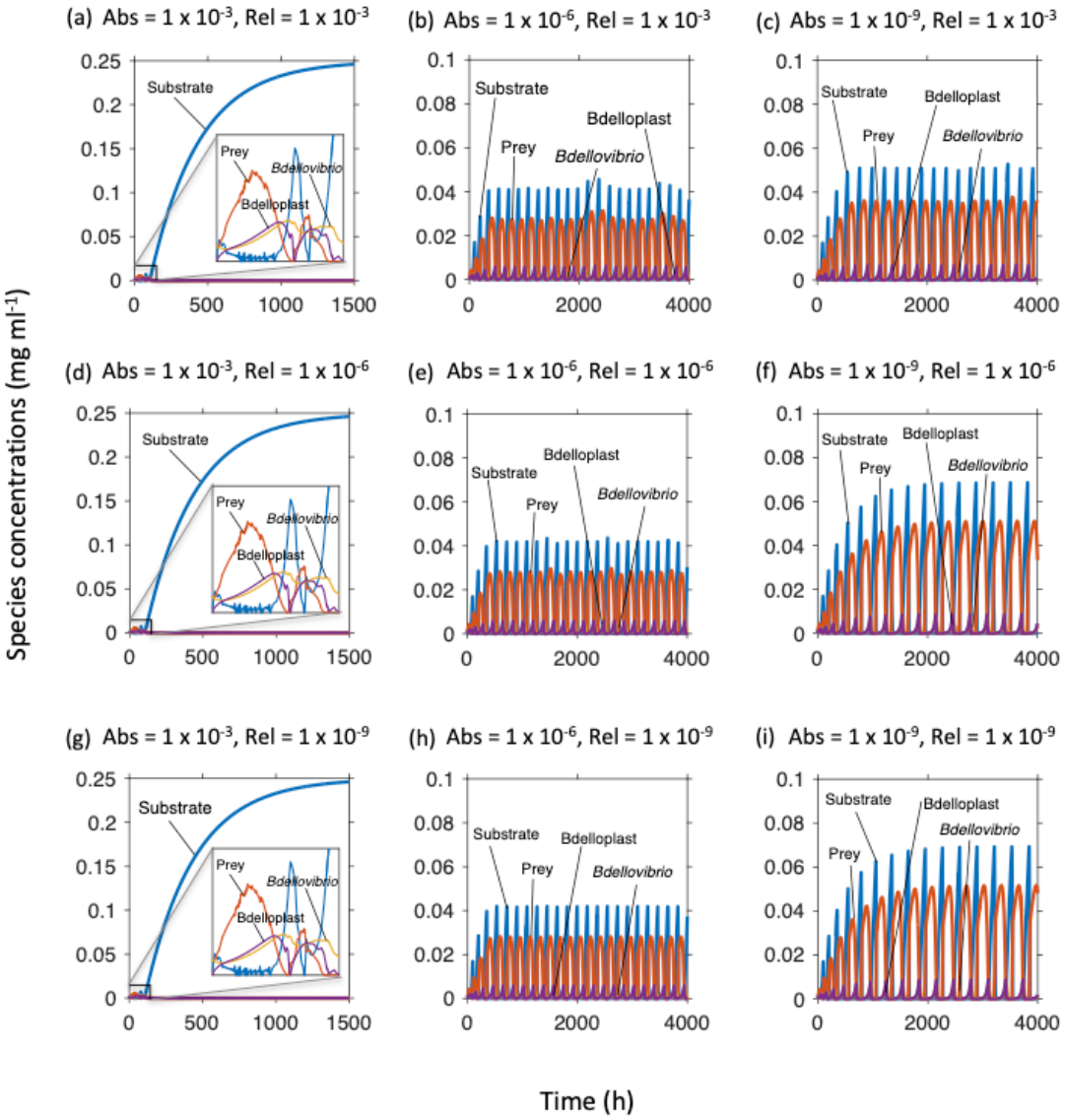

Figure 3.2 – Effects of solver tolerances on simulations with standard parameters.
S_0 = 0.25 mg ml^{-1} and dilution rate = 0.003 h^{-1}. Absolute tolerance decreases (becomes stricter) from left to right; relative tolerance decreases from top to bottom. The strict settings of panel (i) were used for all simulations in this study unless stated otherwise.

3.1.3 Particle-based units versus biomass-based units versus dimensionless equations

As seen in Fig. 2.3, there was usually a good agreement between the type of regime predicted from the eigenvalues of the Jacobian matrix (Table 3.1) and those

observed by running simulations. Exceptions were at the boundaries between regimes and in the region predicted by the eigenvalues to be linearly unstable, where the simulations resulted in very long-period, extreme oscillations. The calculations based on the eigenvalues of the Jacobian matrix were using the dimensionless form of the ODEs, whilst the simulations were performed using standard equations. To check that any differences seen were not due to differences in the use of dimensionless equations, all scenarios from Fig. 2.3 were also run with dimensionless equations. The results from these simulations (data not shown) were identical to those from the standard equations, showing that for these cases the choice of standard or dimensionless equations did not affect the outcome of the simulations. For all further work, the standard equations were used for simulations.

Most simulations were run using units of biomass density (mg dry mass ml^{-1}). When this was attempted with bacteriophage predators, the simulation ran for several days without completing and eventually caused the MatLab program to crash. This was most probably due to the system being unable to find a suitable time step, as the large differences in densities of the species lead to large differences in the rate of change of species over a time step. To handle these scenarios the units were changed from biomass-based to particle-based densities (cells, virions or particles ml^{-1}). This resulted in simulations completing within minutes, to at most a few hours. We wanted to check that the only effect of the change of units was to allow simulations that would otherwise cause a crash of MatLab, to be successfully completed. To check this, test scenarios previously run for biomass-based units, were rerun using particle-based units. The results from the simulations with particle-based units (Fig. 3.3) were the same as those from the biomass-based densities, with two exceptions. Firstly, the

relative proportions of the species had changed. This was inevitable as prey cells were set to be seven times larger than predator cells. This meant that each cell ml^{-1} of a prey cell resulted in seven times more mg dry mass ml^{-1} than a predator cell. Secondly, for a dilution rate of 0.0025 h^{-1}, the pattern observed differed between particle-based and biomass-based units. This dilution rate was very close to the boundary of a Hopf bifurcation between damped and sustained oscillations, and was very sensitive to initial conditions. For both unit settings it was possible by adjusting the initial species values to get either damped or sustained oscillations. For the simulation using particle-based densities, the initial conditions were adjusted slightly, to get the best match possible to the outcome from using biomass-based units.

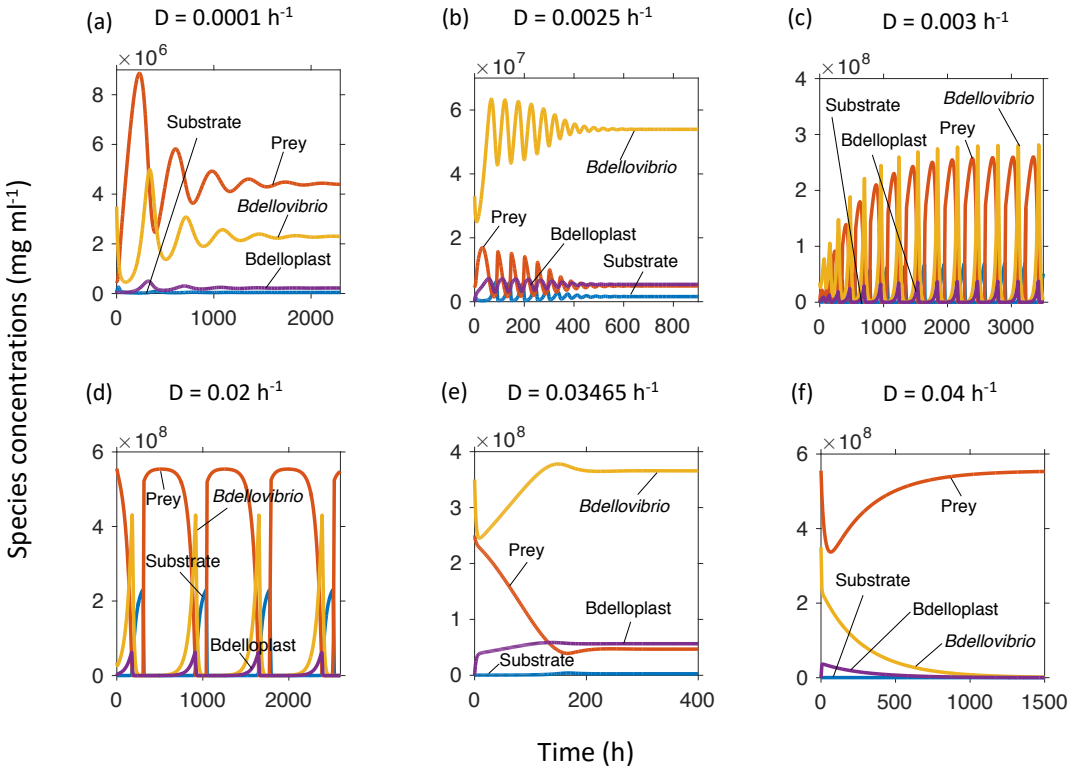

Figure 3.3 - Standard simulations in particle-based units

S_0 = 0.25 mg ml^{-1}, using particle-based units (cells, virions or particles ml^{-1}). Dilution rates are the same as in panels (b-g) of Fig. 2.3 and the same dynamic regimes are observed.

3.2 Model analysis

3.2.1 Dimensional Analysis

Model 6 has twelve parameters, many of which are interconnected in various ways. The more parameters a model has, the more difficult it is to determine which parameters, or combinations of parameters, have the biggest effect on model outcomes. In order to reduce the number of parameters that had to be considered independently, and deduce something about the relationships between parameters, a dimensional analysis was performed. The set of dimensional equations for Model 6 were already given in Chapter 2, but are shown again for convenience:

$$\frac{dS}{dt} = (S_0 - S)D - N\frac{\mu_N S}{(K_{S,N}+S)Y_{N/S}} \quad (2.3a)$$

$$\frac{dN}{dt} = N\frac{\mu_N S}{K_{S,N}+S} - ND - P\frac{\mu_P N}{(K_{N,P}+N)Y_{B/N}} \quad (2.3b)$$

$$\frac{dP}{dt} = k_P B - (D+m)P - P\frac{\mu_P N}{(K_{N,P}+N)Y_{B/P}} \quad (2.3c)$$

$$\frac{dB}{dt} = P\frac{\mu_P N}{K_{N,P}+N} - BD - \frac{k_P B}{Y_{P/B}} \quad (2.3d)$$

First the variables were explicitly written as products of numbers and units to give:

$$\frac{d(S' S\hat{})}{d(t' \tau)} = (S_0 - S' S\hat{})D - N' N\hat{}\frac{\mu_N S' S\hat{}}{(K_{S,N}+S' S\hat{})Y_{N/S}} \quad (3.1a)$$

$$\frac{d(N' N\hat{})}{d(t' \tau)} = N' N\hat{}\frac{\mu_N S' S\hat{}}{K_{S,N}+S' S\hat{}} - N' N\hat{}D - P' P\hat{}\frac{\mu_P N' N\hat{}}{(K_{N,P}+N' N\hat{})Y_{B/N}} \quad (3.1b)$$

$$\frac{d(P' P\hat{})}{d(t' \tau)} = k_P B' B\hat{} - (D+m)P' P\hat{} - P' P\hat{}\frac{\mu_P N' N\hat{}}{(K_{N,P}+N' N\hat{})Y_{B/P}} \quad (3.1c)$$

$$\frac{d(B' B\hat{})}{d(t' \tau)} = P' P\hat{}\frac{\mu_P N' N\hat{}}{K_{N,P}+N' N\hat{}} - B' B\hat{}D - \frac{k_P B' B\hat{}}{Y_{P/B}} \quad (3.1d)$$

where primes denote numbers, carets denote units and τ is the time unit.

Next the equations were divided by $S^{\wedge}$, $N^{\wedge}$, $P^{\wedge}$ and $B^{\wedge}$ and multiplied by τ to remove these from the left-hand side of the equations.

$$\frac{dS'}{dt'} = \left(\frac{S_0}{S^{\wedge}} - S'\right)\tau D - \tau N' N^{\wedge} \frac{\mu_N S'}{(K_{S,N} + S' S^{\wedge}) Y_{N/S}} \quad (3.2a)$$

$$\frac{dN'}{dt'} = N' \frac{\tau \mu_N S' S^{\wedge}}{(K_{S,N} + S' S^{\wedge})} - N' \tau D - P' P^{\wedge} \frac{\tau \mu_P N'}{(K_{N,P} + N' N^{\wedge}) Y_{B/N}} \quad (3.2b)$$

$$\frac{dP'}{dt'} = \frac{\tau k_P B' B^{\wedge}}{P^{\wedge}} - (D\tau + m\tau)P' - P' \frac{\tau \mu_P N' N^{\wedge}}{(K_{N,P} + N' N^{\wedge}) Y_{B/P}} \quad (3.2c)$$

$$\frac{dB'}{dt'} = \frac{P' P^{\wedge}}{B^{\wedge}} \frac{\tau \mu_P N' N^{\wedge}}{(K_{N,P} + N' N^{\wedge})} - B' \tau D - \frac{\tau k_P B'}{Y_{P/B}} \quad (3.2d)$$

Then we chose units to eliminate parameters ($\tau = \frac{1}{D}$, $S^{\wedge} = K_{S,N}$, $N^{\wedge} = K_{N,P}$, $P^{\wedge} = \frac{K_{N,P} Y_{B/N}}{Y_{B/P}}$ and $B^{\wedge} = K_{N,P} Y_{B/N}$) to give:

$$\frac{dS'}{dt'} = \left(\frac{S_0}{K_{S,N}} - S'\right) - N' \frac{\mu_N S' K_{N,P}}{D K_{S,N} (1 + S') Y_{N/S}} \quad (3.3a)$$

$$\frac{dN'}{dt'} = N' \frac{\mu_N S'}{D(1 + S')} - N' - P' \frac{\mu_P N'}{D(1 + N') Y_{B/P}} \quad (3.3b)$$

$$\frac{dP'}{dt'} = \frac{k_P B' Y_{B/P}}{D} - \left(1 + \frac{m}{D}\right) P' - P' \frac{\mu_P N'}{D(1 + N') Y_{B/P}} \quad (3.3c)$$

$$\frac{dB'}{dt'} = \frac{\mu_P N' P'}{Y_{B/P} D(1 + N')} - B' - \frac{k_P B'}{D Y_{P/B}} \quad (3.3d)$$

Finally, we identified seven independent parameters of the Model 6:

DP1 $\mu_N' = \frac{\mu_N}{D}$

DP2 $\mu_P' = \frac{\mu_P}{D Y_{B/P}}$

DP3 $k_P' = \frac{k_P}{D Y_{P/B}}$

DP4 $m^{'} = \frac{m}{D}$

DP5 $S_0^{'} = \frac{S_0}{K_{S,N}}$

DP6 $K_R^{'} = \frac{K_{N,P}}{K_{S,N} Y_{N/S}}$

DP7 $Y_{B*P}^{'} = Y_{P/B} Y_{B/P}$

To give dimensionless ODEs:

$$\frac{dS}{dt} = S_0^{'} - S - \frac{SN\mu_N^{'} K_R^{'}}{1+S} \quad (3.4a)$$

$$\frac{dN}{dt} = \frac{SN\mu_N^{'}}{1+S} - N - \frac{NP\mu_P^{'}}{1+N} \quad (3.4b)$$

$$\frac{dP}{dt} = k_P^{'} BY_{B*P}^{'} - \left(1 + m^{'}\right)P - \frac{NP\mu_P^{'}}{1+N} \quad (3.4c)$$

$$\frac{dB}{dt} = \frac{NP\mu_P^{'}}{1+N} - B - k_P^{'} B \quad (3.4d)$$

Four of the seven dimensionless parameters (DP1 – DP4) are related to the dilution rate of the system as they are ratios of rates relating to the four intrinsic biological processes occurring: prey growth (DP1), predation of prey to form a bdelloplast (DP2), maturation of that bdelloplast into new predators (DP3) and predator mortality (due to starvation – DP4).

The other three parameters are mass ratios. S_0' (DP5) is the ratio of substrate concentration entering the chemostat, to the half-saturation constant for prey growing on the substrate. K_R' (DP6) is the ratio of half-saturation constants of the predator and prey for their respective diets, adjusted for the efficiency with which the prey converts substrate. The final parameter Y_{B*P}' (DP7) is the burst size of the *Bdellovibrio*, i.e., the number of new predators formed from a single bdelloplast.

3.2.2 Analytical Determination of Steady States

Simulating a system shows how population densities vary over time, and gives the final state of the system. Such analysis however, can be relatively slow, and dependent on an appropriate choice of initial conditions. It is also possible to calculate the nullclines of an ODE system. Each nullcline is the set of values for which one of the differential equations equals zero, and the species described by that equation does not vary over time. Where all the nullclines intersect none of the species' values change over time and the system is in a steady state, albeit one which may be unstable, and lost if small perturbations occur. Calculating the values that produce an intersection of the nullclines did not give any information on how the final state was approached, but it was independent of initial conditions and much quicker to perform than a simulation. This speed made it feasible to study how the steady state varied over a very large range of parameter values.

Analysis showed that for any particular set of parameters there were up to three points at which the nullcline would intersect. One intersection was abiotic with only substrate present. A second point had substrate and prey, but no predators or bdelloplasts, and the final potential steady state had substrate, prey, predator and bdelloplast co-existing. We were particularly interested in this final four species co-existence state. To calculate the species values at the co-existence state we first rearranged equation 9d to describe B in terms of N and P.

$$\frac{NP\mu_P^{'}}{1+N} - B - k_P^{'} B = 0 \qquad (3.5)$$

$$B = \frac{NP\mu_P^{'}}{(1+N)\left(1+k_P^{'}\right)} \qquad (3.6)$$

This value was substituted into equation 3.4c to give

$$k_P^{'} \frac{Y_{B*P}^{'} NP\mu_P^{'}}{(1+N)\left(1+k_P^{'}\right)} - \left(1+m^{'}\right)P - \frac{NP\mu_P^{'}}{1+N} = 0 \quad 3.7)$$

Which could be rearranged into:

$$N = \frac{\left(1+m^{'}\right)\left(1+k_P^{'}\right)}{k_P^{'}\mu_P^{'}Y_{B*P}^{'} - \mu_P^{'}\left(1+k_P^{'}\right) - \left(1+m^{'}\right)\left(1+k_P^{'}\right)} \quad (3.8)$$

Equation 3.4a was used to give S in terms of N.

$$S_0^{'} - S - \frac{SN\mu_N^{'}K_R^{'}}{1+S} = 0 \quad (3.9)$$

$$S^2 + S\left(1 + N\mu_N^{'}K_R^{'} - S_0^{'}\right) - S_0^{'} = 0 \quad (3.10)$$

This quadratic equation has two solutions, however only the physically possible non-negative solution was recorded as a genuine steady state.

Finally, equation 3.4b was used to get P in terms of N and S.

$$\frac{SN\mu_N'}{1+S} - N - \frac{NP\mu_P'}{1+N} = 0 \quad (3.11)$$

$$P = \left(\frac{S\mu_N'}{1+S} - 1\right)\frac{(1+N)}{\mu_P'} \quad (3.12)$$

This meant the three equilibrium points or steady states of the system were, in order S, N, P, B:

Abiotic state:

$$\left(S_0^{'}, 0, 0, 0\right)$$

Predator free state (prey and substrate only):

$$\left(\frac{1}{\mu_N^{'}-1}, \frac{S_0^{'}\left(\mu_N^{'}-1\right)-1}{K_R^{'}\left(\mu_N^{'}-1\right)}, 0, 0\right)$$

All species co-existence (note only 1 possible value for S is non-negative):

$$\left(\frac{-(1+N\mu_N'K_R'-S_0')\pm\sqrt{(1+N\mu_N'K_R'-S_0')^2-4S_0'}}{2},\ \frac{(1+m')(1+k_P')}{k_P'\mu_P'Y_{B*P}'-\mu_P'(1+k_P')-(1+m')(1+k_P')},\left(\frac{S\mu_N'}{1+S}-1\right)\frac{(1+N)}{\mu_P'},\frac{NP\mu_P'}{(1+N)(1+k_P')}\right)$$

3.2.3 Jacobian Matrix and Hopf Bifurcations

The Jacobian matrix is the set of all first order partial derivatives of all differential equations of a system with respect to all variables, evaluated at steady state. It can be used for linear stability analysis, although it should be noted that results of this may only be valid near the steady state as it represents a linearization of an intrinsically non-linear system. The linearized system can be solved. The solution consists of sums of exponential functions of the form $\boldsymbol{x}(t) = \boldsymbol{v}e^{\lambda t}$ with the eigenvalues λ of the Jacobian matrix in the exponents determining the time evolution of perturbations $\boldsymbol{x}(t)$ of the steady state and therefore the local stability of steady states (Edelstein-Keshet, 2005). Any complex eigenvalues indicate that the system will display some form of oscillations. If the common real part of the complex conjugate eigenvalue pair is negative, the oscillations will be damped, and the equilibrium point is a stable focus, while for a positive real part, the oscillations are sustained and the equilibrium point is an unstable node with an associated stable limit cycle. If all the eigenvalues are real and negative this indicates a stable steady state with the equilibrium point being a stable node. While all real and at least one positive is an unstable state and the equilibrium point is either a saddle node or an unstable node. In order to calculate these eigenvalues for various system parameters the Jacobian matrix was determined for the dimensionless equations. The rows of the Jacobian

matrix were derived for the substrate S, prey N, predator P and bdelloplast B rates of change in this order (Eqs. 3.4a-d) by partially differentiating by S, N, P and B in turn for each column:

	$\frac{\delta}{\delta S}$	$\frac{\delta}{\delta N}$	$\frac{\delta}{\delta P}$	$\frac{\delta}{\delta B}$
$\frac{dS}{dt}$	$-1-\frac{N\mu'_N K'_R}{(1+S)^2}$,	$-\frac{S\mu'_N K'_R}{1+S}$,	0,	0,
$\frac{dN}{dt}$	$\frac{N\mu'_N}{(1+S)^2}$,	$\frac{S\mu'_N}{1+S}-1-\frac{P\mu'_P}{(1+N)^2}$,	$-\frac{N\mu'_P}{1+N}$,	0
$\frac{dP}{dt}$	0,	$-\frac{P\mu'_N}{(1+N)^2}$,	$-1-m'-\frac{N\mu'_P}{1+N}$	$k'_P Y'_{B*P}$
$\frac{dB}{dt}$	0,	$\frac{P\mu'_N}{(1+N)^2}$,	$\frac{N\mu'_P}{1+N}$,	$-1-k'_P$

(3.13)

Figure 3.4 – Jacobian matrix for model 6

Zero entries, circled in brown, indicate independence, i.e., changing a variable had no effect on the rate of change of the other variable. Entries that were always negative, circled in red, mean that an increase in one variable caused a decrease in the rate of change of the corresponding variable. Entries that were always positive, circled in blue, meant that an increase in one variable caused an increase in the rate of change of the other. Entries circled in green, could be positive or negative depending on parameter values.

Each entry in the Jacobian matrix (Eq. 3.13) describes the effect of a small change in one species on the rate of change of another species, when the system was initially at steady state. The values on the main diagonal, are the effects of a change in the density of a variable on its own rate of change. The eigenvalues of the Jacobian matrix are found using equation 3.14, where λ is the eigenvalues, J the Jacobian matrix and I the identity matrix (Edelstein-Keshet, 2005).

$$J - \lambda I = 0 \tag{3.14}$$

This can in theory be solved analytically, but gives rise to a quartic equation that is intractable and has to be evaluated numerically. Instead taking inspiration from the graphical analysis method of Rosenzweig and MacArthur (1963) I examined the $\frac{\delta}{\delta N}$

of $\frac{dN}{dt}$ entry of the Jacobian matrix (Eq. 3.13). This is the rate of change of the prey nullcline with respect to prey density. In a two-dimensional predator prey system, when this is positive, the equilibrium point is unstable, and the result is stable oscillations, resulting from a stable limit cycle. When it is negative, the equilibrium point is stable. The point at which the steady state of the system goes from being a stable limit cycle, surrounding an unstable node, to damped oscillations around a stable node, is a Hopf bifurcation of the system. A four-dimensional system, such as described by my model 6 is inherently more complex than a two-dimensional system, but similar principles may apply. Substituting the equilibrium value of:

$$P = \left(\frac{S\mu'_N}{1+S} - 1\right)\frac{(1+N)}{\mu'_P} \tag{3.15}$$

into the equation for the $\frac{\delta}{\delta N}$ of $\frac{dN}{dt}$ entry in the Jacobian matrix (Eq. 3.13):

$$\frac{S\mu'_N}{1+S} - 1 - \frac{P\mu'_P}{(1+N)^2} \tag{3.16}$$

Gave:

$$\left(\frac{S\mu'_N}{1+S} - 1\right) - \frac{\left(\frac{S\mu'_N}{1+S} - 1\right)}{1+N} \tag{3.17}$$

Which can only be zero if either $N = 0$, which is not a point at which all four species are co-existing, as prey density is zero, or when $\frac{S\mu'_N}{1+S} - 1 = 0$. Substituting the equilibrium value for S

$$S = \frac{-\left(1+N\mu'_N K'_R - S'_0\right) \pm \sqrt{\left(1+N\mu'_N K'_R - S'_0\right)^2 - 4S'_0}}{2} \tag{3.18}$$

into equation 3.17 gave an equation that could be solved for inflow substrate concentration (S_0). Inputting the default parameters (Table 2.3) and a dilution rate of 0.02 h^{-1} and solving gave a negative impossible value for S_0 of -0.00607 mg ml^{-1},

indicating that there is no value of S_0 that, with these parameter values, would make the $\frac{\delta}{\delta N}$ of $\frac{dN}{dt}$ entry in the Jacobian matrix zero (or negative). This is not entirely surprising, as this is an unusual four species system in which predator and prey densities both decrease when predation events occur and only bdelloplast densities increase.

Fig. 2.3a shows, the system does in fact undergo Hopf bifurcations. Take as an example the series of points indicated by the series of white crosses in Fig. 2.3a, whose Jacobian matrix values and eigenvalues ate listed in Table 3.1. The inflow substrate concentration (S_0) was set to 0.25 mg ml^{-1} (and all other parameters to their default values). When the dilution rate was set to 0.04 h^{-1}, the predator washed out of the system and only the prey remained (Fig. 2.3a, g). When the dilution rate was reduced to 0.03465 h^{-1}, the predator could multiple fast enough to survive within the chemostat and a four species equilibrium point occurred, the eigenvalues for which were all real and negative, indicating the equilibrium point was a stable node (Table 3.1 and Fig 2.3a, f). When the dilution rate was lowered further to 0.003 h^{-1} two of the eigenvalues were negative real numbers, the other two were a complex conjugate pair, with a positive real part, indicating the equilibrium point was an unstable node, with an associated stable limit cycle (Table 3.1 and Fig 2.3a, d). Driving the dilution rate still lower to 0.0025 h^{-1} resulted in the system passing through a Hopf bifurcation. The complex conjugate pair of eigenvalues associated with the equilibrium point of this system had crossed the imaginary axis and now had negative real parts, while the other two eigenvalues were both still negative real numbers, indicating the equilibrium point was a stable focus, with associated damped oscillations (Table 3.1 and Fig 2.3a, c).

Table 3.1 – Eigenvalues and Jacobian matrix for selected points

Parameters all had default values (Table 2.3), except S_0=0.25 mg ml^{-1} and dilution rate was as shown.

Dilution rate (h^{-1})	Jacobian matrix				Eigenvalues	Type of node
0.0001	-5.6511x10^3	-0.1045x10^3	0	0	-5.5230 -3.3445 -0.0255+0.1665i -0.0255-0.1665i	Stable focus (with damped oscillations)
	6.8320x10^3	0.0634 x10^3	-0.2402 x10^3	0		
	0	-0.0620 x10^3	-0.0841 x10^3	0.8720 x10^3		
	0	0.0620	0.2402	-2.4896		
0.0025	-93.3560	-93.0502	0	0	-139.12 -0.0540+0.6661i -0.0540-0.6661i -19.67	Stable focus (with damped oscillations)
	111.6752	59.4252	-10.1249	0		
	0	-52.0894	-35.1249	348.8000		
	0	52.0894	10.1249	-100.5434		
0.003	-62.5338	-90.7286	0	0	-117.43 7.10 + 57.10i 7.10 - 57.10i -14.22	Unstable node (with associated limit cycle)
	74.4055	58.5560	-8.5287	0		
	0	-50.1513	-29.5287	290.6667		
	0	50.1513	8.5287	-83.9528		
0.02	-1.1386	-27.5136	0	0	23.9566 -20.0333 -1.0442 0.9826	Unstable node
	0.1675	24.2262	-1.7831	0		
	0	-8.0427	-5.7831	43.6000		
	0	8.0427	1.7831	-13.4429		
0.03465	-227.2689	-4.2668	0	0	-222.1058 -12.2486 -0.6788 -0.4388	Stable node
	273.6001	3.9991	-1.3142	0		
	0	-0.1602	-4.0409	25.0935		
	0	0.1602	1.3142	-8.1614		

CHAPTER 4: MODELLING DUAL PREDATION BY *BDELLOVIBRIO BACTERIOVORUS* AND A BACTERIOPHAGE WHICH TOGETHER SUCCESSFULLY ELIMATE *E. COLI* PREY

A version of this chapter comprises the modelling section of a paper that has been published in Journal of Bacteriology. A copy of the main text of that paper as submitted is included as appendix A.

Bdellovibrio bacteriovorus is a small, predatory Gram-negative bacterium that exclusively targets other Gram negative bacteria. As such it holds promise as a means of treating antibiotic resistant infections. Previous studies have shown this bacterium to be non-toxic to eukaryotic cells and only mildly immunogenic, its effectiveness in treating bacterial infections however has been mixed. In order to boost this effectiveness, previous studies have combined *B. bacteriovorus* treatment with antibiotics and the effects of the immune system. To our knowledge however no previous study has looked into combination treatment involving *B. bacteriovorus* and a bacteriophage. The Sockett lab at the University of Nottingham have successfully isolated a bacteriophage infecting *E. coli* growing in slurry samples taken from a dairy farm. The *E. coli* isolated from these samples were also infected with *B. bacteriovorus*, and the Socket lab have investigated the effects of dual predation by these two predators on a population of *E. coli*. We have taken this data set and used model selection and parameter fitting to explain aspects of the data. We found that three types of prey, completely sensitive, phage resistant and plastic *B. bacteriovorus* resistant were needed to explain the data. We also found that the results of dual predation can be explained by the combined actions of the two predators without needing to include additional interactions between them.

4.1 Introduction

With the increase in antimicrobial resistance, new safe and effective treatments are constantly being sought to treat bacterial infections. *B. bacteriovorus*, a small, Gram-negative, predatory bacterium that predates other Gram-negative bacteria has been proposed as one such treatment. Several studies have addressed the issue of safety of *Bdellovibrio* and like organisms (BALOs) (Lenz and Hespell, 1978; Shatzkes *et al.*, 2015; Gupta *et al.*, 2016; Monnappa *et al.*, 2016) and found BALOs to be non-toxic to eukaryotic cells and only mildly immunogenic (Gupta *et al.*, 2016; Shatzkes *et al.*, 2016, 2017), probably due to their unusual lipid A (Schwudke *et al.*, 2003). There have also been investigations into the effectiveness of BALOs in treating various bacterial infections, in plants (Scherff, 1973), fungi (Saxon *et al.*, 2014) and animals (Chu and Zhu, 2009; Atterbury *et al.*, 2011; Emmert *et al.*, 2014; Li *et al.*, 2014; Shatzkes *et al.*, 2016; Russo *et al.*, 2018), as well as studies explicitly investigating the effectiveness of *B. bacteriovorus* in combination with the immune system (Willis *et al.*, 2016) or with antibiotics (Im *et al.*, 2017). Meanwhile a great many studies have explored the possibilities of treating infections with bacteriophages over the last 100 years (Abedon *et al.*, 2011). To our knowledge however no previous study has looked at the effects of combining *B. bacteriovorus* with a bacteriophage to control or eliminate bacterial populations.

The Sockett lab at the University of Nottingham, while attempting to isolate *B. bacteriovorus* from a poultry farm, also isolated a bacteriophage that caused ‘halos’ around *B. bacteriovorus* plaques on an *E. coli* prey lawn. They isolated the bacteriophage causing these halos and found it to be a rosette tailed phage. They also

investigated the effects of *B. bacteriovorus* HD100 and this bacteriophage on population dynamics of *E. coli*, both in isolation and in combination.

Mathematical models have been used extensively to model bacteriophage predation (Levin *et al.*, 1977; Bohannan and Lenski, 2000; Krysiak-Baltyn *et al.*, 2016). Fewer models have been developed for *B. bacteriovorus* predation, for a fuller review of these see Chapter 2. Before a mathematical model can be used to explain experimental data or make useful predictions an appropriate model must be developed. This inevitably involves a balance between a model that is complex enough to capture details of the experimental data, without including variable or parameters that can neither be inferred from the data, nor known with any degree of certainty from previous studies.

When attempting to fit parameters to models, various Monte Carlo methods are frequently used to sample the parameter space. The Markov Chain Monte Carlo (MCMC) method creates a chain of sets of parameter values by taking the previous parameter set and perturbing the parameter values to give a new candidate parameter set (parameters may be updated sequentially or simultaneously). The fit of the model to the data using the candidate parameter set is then compared to the fit from the previous parameter set. If the candidate fit is an improvement over the previous fit the candidate set is accepted and added to the chain and is used as the starting point for the next candidate parameter set. If the candidate parameter set gives a less good fit to the data it may still be accepted. The probability of accepting a less good fit is based on how much worse the fit is compared to the previous parameter set, such that parameter sets that are almost as good a fit as the previous set are more likely to be accepted. Typical MCMC chains consist of two phases, a burn

in section where the fit is improving and a sampling phase where the range of parameters that give close to the best fit found is explored. The typical number of iterations required to complete the burn in phase varies, both with the model being fitted and the choice of starting position, but can be at least hundreds of thousands or millions of iterations, particularly for higher dimensional parameter sets. MCMC can be sensitive to initial conditions and depending on the choice of these may find a local best fit rather than the global optimal solution. MCMC can be used for model selection where the model is treated as an additional parameter to fit. This works best with models with very similar parameter sets, but is problematic when models have very different types of parameters.

Sequential Monte Carlo (SMC) methods (Halton, 1960) can be used to objectively choose which model or models of those proposed best describe a dataset. They also fit parameters to the data, to give a range of reasonable values for each parameter. SMC consists of several rounds of parameter and model selection, with increasingly strict tolerances, and with the selected model and parameter sets in one round forming the base pool for future rounds. SMC methods require suitable priors on the parameters, but are better than MCMC methods at sampling the entire parameter space, and do not have the same sensitivity to initial conditions, making them more likely to find globally optimal solutions. With SMC the choice of tolerance levels is particularly important, too loose and the range of parameters chosen is too broad, too tight and the selection will take too long and there is a risk of overfitting. When competing models with different numbers of parameters there is also a risk of overfitting. With SMC however, each additional parameter adds an extra dimension to the parameter space to search, making it less likely that when a more complex

model is chosen the corresponding parameter set selected gives a fit to the data that is good enough for inclusion into the next round of selection. Approximate Bayesian Computation – Sequential Monte Carlo (ABC-SMC) is an extension of SMC that avoids the need for an explicit likelihood function and is particularly well suited for time series data (Toni *et al.*, 2009).

We have taken the data produced by the Sockett lab and fitted it a family of ordinary differential equation (ODE) mathematical models based on the model described in Chapter 2. We then used ABC-SMC methodology to determine the most appropriate model and fit suitable parameters to this. In doing so we found that three different prey phenotypes: completely sensitive to predation; phage resistant, but predatable by *B. bacteriovorus;* and *B. bacteriovorus* plastic resistant (but still predatable by phage) were required to explain the experimental data. We also inferred some of the details of how resistance to phage and plastic resistance to *B. bacteriovorus* may arise. Finally, we discovered that models fitted to single predator data only, could be a good fit to dual predation data, meaning that the response seen to the two predators in combination can be explained without requiring any direct interactions between the predators.

4.2 Methods

4.2.1 Model description

A family of ordinary differential equation (ODE) models was developed for the population dynamics because the data were on the population rather than the individual level and the model could be simulated in a fraction of a second, which was important as model selection and fitting requires millions of simulations. Fig. 4.1 visualizes the variables, their interactions and the equations of the base model and Fig. 4.2 shows different model variants. Parameters are defined in Table 4.1.

A Base model variables and interactions

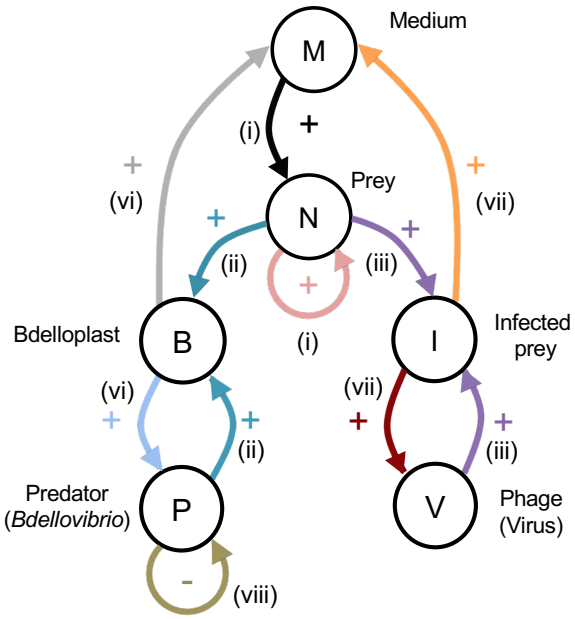

B Differential Equations (colours match arrows)

Rate of change	(i) Prey growth	(iv) Bdelloplast maturation	(ii) *Bdellovibrio* predation	(v) Infected prey *maturation*	(iii) Phage predation	(viii) *Bdello-vibrio* mortality	(vi) and (vii) Nutrient release
$\frac{dM}{dt} =$	$-N\frac{\mu_N M}{(K_{M,N}+M)Y_{N/M}}$						$+Y_{M/P}k_P B$ $+Y_{M/V}k_V I$
$\frac{dN}{dt} =$	$N\frac{\mu_N M}{K_{M,N}+M}$		$-P\frac{\mu_P N}{(K_{N,P}+N)Y_{B/N}}$		$-V\frac{\mu_V N}{Y_{I/V}}$		
$\frac{dP}{dt} =$		$k_P B$	$-P\frac{\mu_P N}{(K_{N,P}+N)Y_{B/P}}$			$-mP$	
$\frac{dB}{dt} =$		$-\frac{k_P B}{Y_{P/B}}$	$+P\frac{\mu_P N}{K_{N,P}+N}$				
$\frac{dV}{dt} =$				$k_V I - V\frac{\mu_V N}{Y_{I/V}}$			
$\frac{dI}{dt} =$				$-\frac{k_V I}{Y_{V/I}} + V\mu_V N$			

Figure 4.1 – Base model with one prey type

(A) Diagram of the model variables (populations and chemicals) in circles and their positive or negative interactions. The arrow colours match the colours of the terms in the equations in panel **(B)**, and the roman numerals refer to the list of processes in the text. **(B)** Set of differential equations defining the base model.

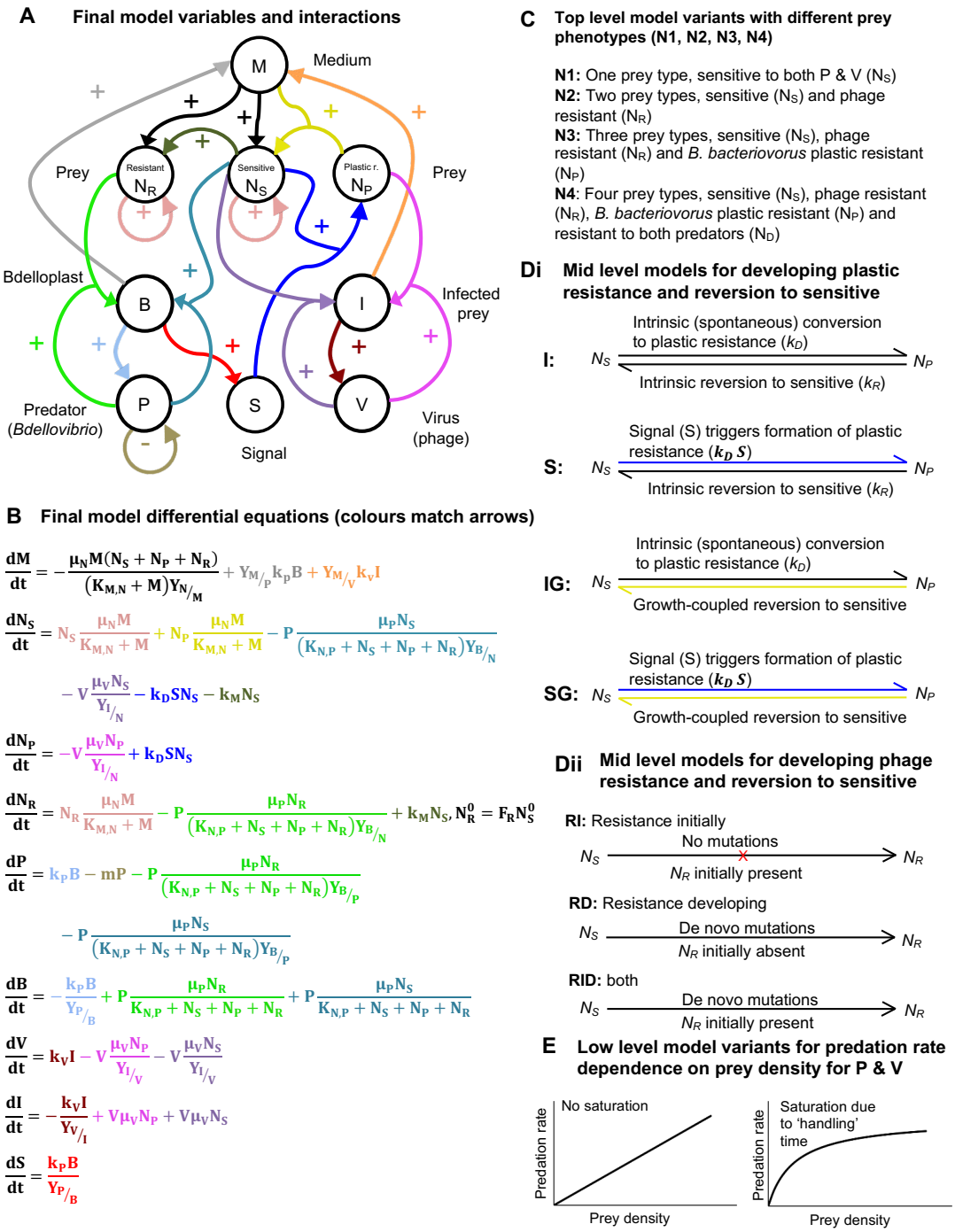

Figure 4.2 – Final model and model variants

(A) Diagram of the final model variables (populations and chemicals) and their positive or negative interactions. The arrow colours match the colours of the terms in the equations in panel **(B)**. **(B)** Set of differential equations defining the final model. **(C)** Top-level model variants with different prey phenotypes (models **N1**, **N2**, **N3,** and **N4**). **(D)** Mid-level model variants – **(Di)** Methods of development of plastic resistance to *B. bacteriovorus*, **(Dii)** Methods of development of phage resistance. **(E)** Low-level model variants. The predation rate either saturates at high prey densities or not (can differ between *B. bacteriovorus* and phage).

Table 4.1 – Model parameters with their symbols and units.

The prior values used for parameter fitting were uniformly distributed over the ranges shown. The results of ABC-SMC fitting are also given. Typical fitted parameters were identified using Principal component analysis (PCA), see Fig. 4.10 for an explanation.

Parameters	Units	Priors for fitting		Statistics of fitted parameters		Typical fitted parameters	
		Minimum value	Maximum value	Median	25th – 75th percentile	Using all data for fitting	Without using dual predator data
Initial phage resistant fraction of prey (F_R)	dimensionless	1.0×10^{-6}	1.0×10^{-4}	3.6×10^{-6}	2.3×10^{-6} 5.4×10^{-6}	8.6×10^{-6}	3.9×10^{-6}
Prey maximum growth rate (μ_N)	h^{-1}	¼ ln(2)	3 ln(2)	0.47	0.38 0.60	0.46	1.3
Prey half-saturation constant for medium ($K_{M,N}$)	pg ml^{-1}	1.0×10^{7}	4.0×10^{10}	3.8×10^{7}	1.9×10^{7} 6.7×10^{7}	4.2×10^{7}	1.6×10^{8}
Growth rate scaling for plastic resistant prey (η_P)	dimensionless	0.4	2	0.98	0.72 1.3	Parameter not in final model	
Yield of prey per medium ($Y_{N/M}$)	prey cells pg $substrate^{-1}$	1	10	2.2	1.5 3.0	1.2	1.8
B. bacteriovorus attack rate constant – non-saturating (μ_P)	bdelloplast cells *B. bacteriovorus* $cells^{-1}$ prey $cells^{-1}$ h^{-1}	2.1×10^{-9}	5.1×10^{-7}	2.3×10^{-8}	1.6×10^{-8} 3.0×10^{-8}	Parameter not in final model	
B. bacteriovorus attack rate constant – Holling type II (μ_P)	bdelloplast cells *B. bacteriovorus* $cells^{-1}$ h^{-1}	8.1×10^{-2}	2.1×10^{1}	0.36	0.31 0.43	0.33	0.36
B. bacteriovorus half-saturation constant for prey ($K_{N,P}$)	prey cells ml^{-1}	2.0×10^{4}	1.0×10^{9}	3.2×10^{6}	2.5×10^{6} 4.2×10^{6}	3.2×10^{6}	3.6×10^{6}
Bdelloplast maturation rate (k_P)	*B. bacteriovorus* cells bdelloplast $cells^{-1}$ h^{-1}	7.0×10^{-1}	2.5×10^{0}	0.86	0.78 0.98	1.1	1.1
Bacteriophage halo attack rate constant – non-saturating (μ_V)	infected cells bacteriophage $virions^{-1}$ prey $cells^{-1}$ h^{-1}	1.0×10^{-10}	1.0×10^{-7}	1.6×10^{-9}	1.2×10^{-9} 2.2×10^{-9}	3.9×10^{-9}	1.9×10^{-9}
Bacteriophage halo attack rate constant – Holling type II (μ_V)	infected cells bacteriophage $virions^{-1}$ h^{-1}	3.2×10^{-3}	3.2×10^{0}	0.43	0.22 0.91	Parameters not in final model	
Bacteriophage halo half-saturation constant for prey ($K_{N,V}$)	prey cells ml^{-1}	1.3×10^{5}	1.3×10^{10}	1.0×10^{8}	4.2×10^{8} 5.0×10^{8}		
Infected cell lysis rate (k_V)	bacteriophage virions infected $cells^{-1}$ h^{-1}	1.0×10^{0}	5.0×10^{2}	12	8.1 18	4.2	8.7

Parameters	Units	Priors for fitting		Statistics of fitted parameters		Typical fitted parameters	
		Minimum value	Maximum value	Median	25th – 75th percentile	Using all data for fitting	Without using dual predator data
Bacteriophage halo burst size ($Y_{V/I}$)	bacteriophage virions infected cells^{-1}	$5.0x10^{0}$	$2.0x10^{2}$	23	20 27	24	34
Nutrients released on *B. bacteriovorus* lysis ($Y_{M/P}$)	pg nutrients *B. bacteriovorus* cell^{-1}	$2.0x10^{-5}$	$2.0x10^{-1}$	$1.2x10^{-3}$	$2.7x10^{-4}$ $5.5x10^{-3}$	$3.3x10^{-3}$	$2.8x10^{-3}$
Nutrients released on phage lysis ($Y_{M/V}$)	pg nutrients bacteriophage virion^{-1}	$1.0x10^{-4}$	$3.2x10^{-1}$	$1.7x10^{-2}$	$8.8x10^{-3}$ $3.8x10^{-2}$	$2.1x10^{-2}$	$6.9x10^{-3}$
Rate of developing *B. bacteriovorus* plastic resistance – without signal (k_D)	h^{-1}	$5.0x10^{-8}$	$5.0x10^{-4}$	$5.0x10^{-5}$	$2.0x10^{-5}$ $1.1x10^{-4}$	Parameter not in final model	
Rate of developing *B. bacteriovorus* plastic resistance – with signal (k_D)	prey cells^{-1} h^{-1}	$5.0x10^{-14}$	$5.0x10^{-10}$	$1.7x10^{-12}$	$9.4x10^{-13}$ $2.9x10^{-12}$	$4.0x10^{-12}$	$1.3x10^{-12}$
Rate of reversion to sensitive prey (k_R)	h^{-1}	$5.0x10^{-7}$	$5.0x10^{-3}$	$2.9x10^{-5}$	$6.4x10^{-5}$ $1.7x10^{-4}$	Parameter not in final model	
Rate of *de novo* phage resistance mutations (k_M)	h^{-1}	$1x10^{-10}$	$1x10^{-8}$	$7.0x10^{-10}$	$3.5x10^{-10}$ $1.6x10^{-9}$	7.5×10^{-10}	$4.9x10^{-9}$
Predator mortality rate (m)	h^{-1}	0.04	0.15	$6.1x10^{-2}$	$5.2x10^{-2}$ $7.2x10^{-2}$	$6.4x10^{-2}$	$9.5x10^{-2}$
B. bacteriovorus burst size ($Y_{P/B}$)	*B. bacteriovorus* cells bdelloplast^{-1}	Fixed to literature value of 4.17 (Fenton, 2010)					

The model was for a batch culture with a single abiotic resource (M for medium) comprising of materials released during lysis of prey cells, a single prey species with up to four phenotypes (N_S, N_R, N_P, N_D), all displaying Monod growth kinetics, and two predators *B. bacteriovorus* (P for predator) and a bacteriophage (V for virus). The rate of predation of the predators was described either by a linear, non-saturating response (type I) or by a saturating functional response (Holling type II) (Fig. 4.2E). Initial assumptions (that were later tested as described below) included that *B. bacteriovorus* predation followed saturating kinetics, whereas bacteriophage predation kinetics were non-saturating. *B. bacteriovorus* has a bi-phasic lifestyle

consisting of a free-living attack phase, and a growth phase which occurs within a dead prey cell termed a bdelloplast. The bdelloplast is a distinct stage in the predation cycle, lasting from two to four hours. During this stage the prey, which makes up the majority of the bdelloplast, did not grow or replicate and did not contribute to the viable counts when considering the experimental data, and the predator making up the remainder of the structure did not carry out further predations. Due to its distinct properties we decided to model this stage as a separate entity (variable), (B for bdelloplast). There are also parallels between the bdelloplast and a bacteriophage infected cell. When infected by a bacteriophage the prey cell no longer grew, consumed nutrients nor contributed to the viable cell count, and until the prey cell was lysed the phage did not infect further prey cells. Accordingly, we also modelled the infected cell as a separate entity (I for infected cell) with properties similar to a bdelloplast. *B. bacteriovorus* is known to have an unusually high mortality rate for a bacterium so we included a mortality term. As regrowth of prey was seen in the experiments (Fig. 4.3B), there must have been some source of nutrients supporting growth, as the calcium HEPES buffer does not support growth, and any spent medium carried over with the prey cells would have been insufficient to account for the level of regrowth that occurred. It was assumed that the source of these nutrients was 'waste' products released during the lysis of the prey cells by both *B. bacteriovorus* and the halo-phage.

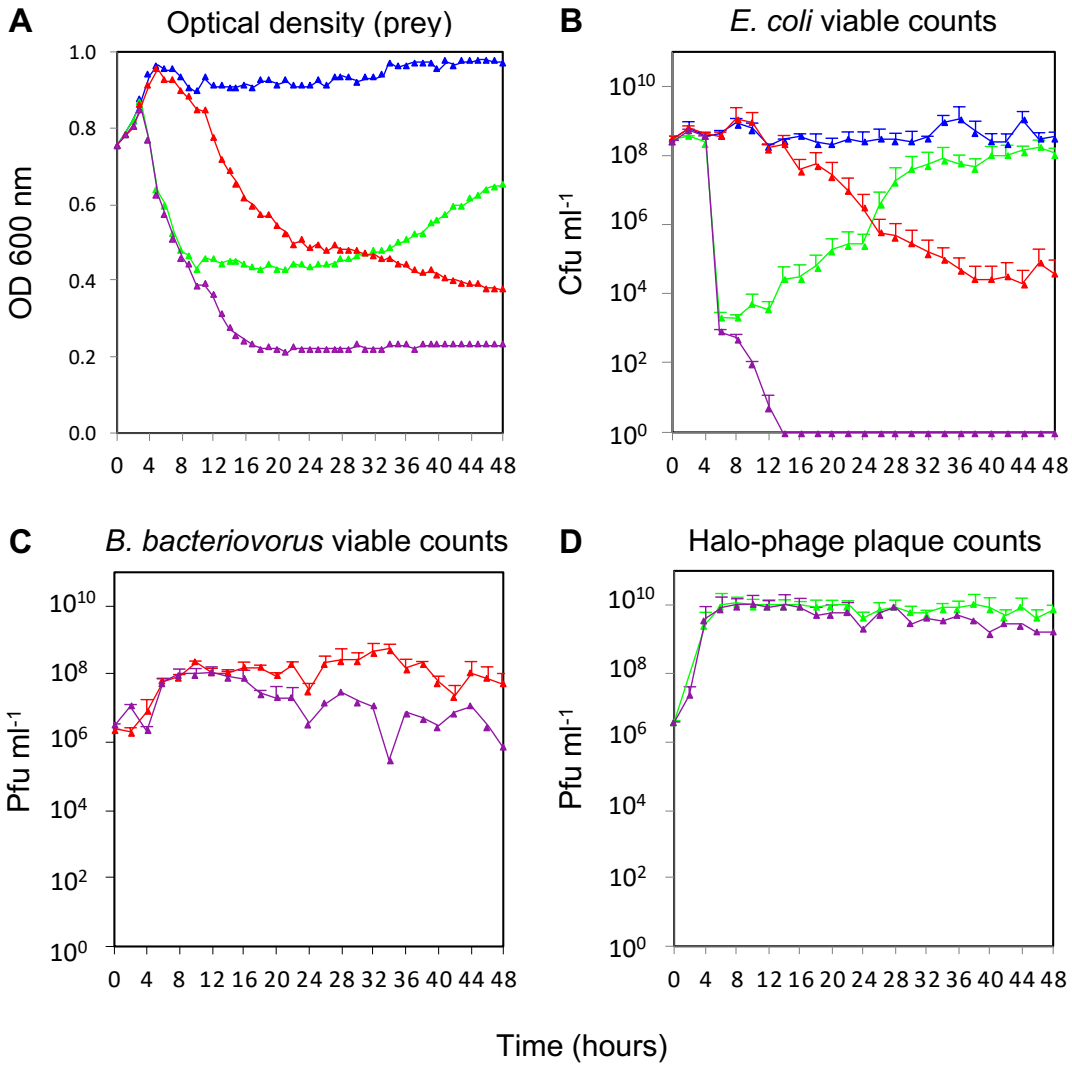

Figure 4.3 – Experimental results of *B. bacteriovorus* and bacteriophage predation of *E. coli*.

These graphs were produced from data generated by the Sockett lab at the University of Nottingham (Hobley *et al.*, 2019) and show optical densities and viable counts measured over 48 hours. Predation was on late log-phase *E. coli* S17-1 by halo-phage alone (green), *B. bacteriovorus* HD100 alone (red); both halo-phage and *B. bacteriovorus* HD100 (purple) versus *E. coli* plus buffer control (blue). (**A**) *E. coli* measured by optical density (OD_{600} nm) (*B. bacteriovorus* are too small to register at OD_{600} nm). (**B**) *E. coli* viable counts. (**C**) *B. bacteriovorus* HD100 enumeration by plaque counts. (**D**) bacteriophage halo enumeration by plaque counts.

4.2.2 Model simulation

All model variants were implemented in MatLab (8.6.0.267246 (R2015b)) and simulated using the ordinary differential equation solver ode45, which implements an explicit Runge-Kutta method.

4.2.3 Model selection and parameter fitting

Each model variant was fitted to experimental data from several 48-hour time series with high resolution – data points every 2 hours (Fig. 4.3). These time series measured *E. coli* numbers in the prey only experiment, *E. coli* and *B. bacteriovorus* for *B. bacteriovorus* only predation, *E. coli* and halo-phage for halo-phage only predation and *E. coli, B. bacteriovorus* and halo-phage in the dual predation experiment.

A Bayesian framework for model selection and parameter inference was used to obtain estimates of the uncertainty of the model and parameters. As explicit likelihood functions cannot be derived, Approximate Bayesian Computation (ABC) was used. Selection of the various model variants and parameter fitting was performed using an ABC Sequential Monte Carlo (ABC-SMC) algorithm as described by Stumpf and co-workers (Toni *et al.*, 2009) using increasingly strict selection criteria (tolerance levels). As the priors were uniformly distributed, and the perturbation kernels were symmetric, all parameter sets carried equal weight. In each competition, model and parameter set selection was performed multiple times (referred to as generations). For each generation, 1,000 'particles' (model with a parameter set) that produced simulation results within the tolerance distance, for that generation, of the experimental results, were selected. Models were competed for up to 15 generations, and the tolerance levels for the distance between observed and simulated data were reduced from generation to generation.

The simulation results for each parameter set were evaluated for their fit to the experimental data using the distance function:

$$average\ distance = \frac{\sqrt[2]{sum[(point\ distance)^2]}}{number\ of\ data\ points}$$

where for each pair of data points (experimental and simulated) the point distance was calculated as:

$$point\ distance = \big(log(simulation\ datum) - log(experimental\ datum)\big)$$

The data points were log transformed to prevent small relative errors in large data values from having an excessive influence as the data values ranged over ten orders of magnitude. The distances between experimental and simulation data were also squared to emphasis a few large errors, which were likely to be caused by a poor model fit, over many smaller errors which could result from noise in the experimental data.

As the tolerance limit decreased from generation to generation, the distribution of distances for accepted fits became increasingly narrow, indicating that the model parameter set combinations were approaching the best fit possible for the model variants and parameter ranges being tested (Fig. 4.4).

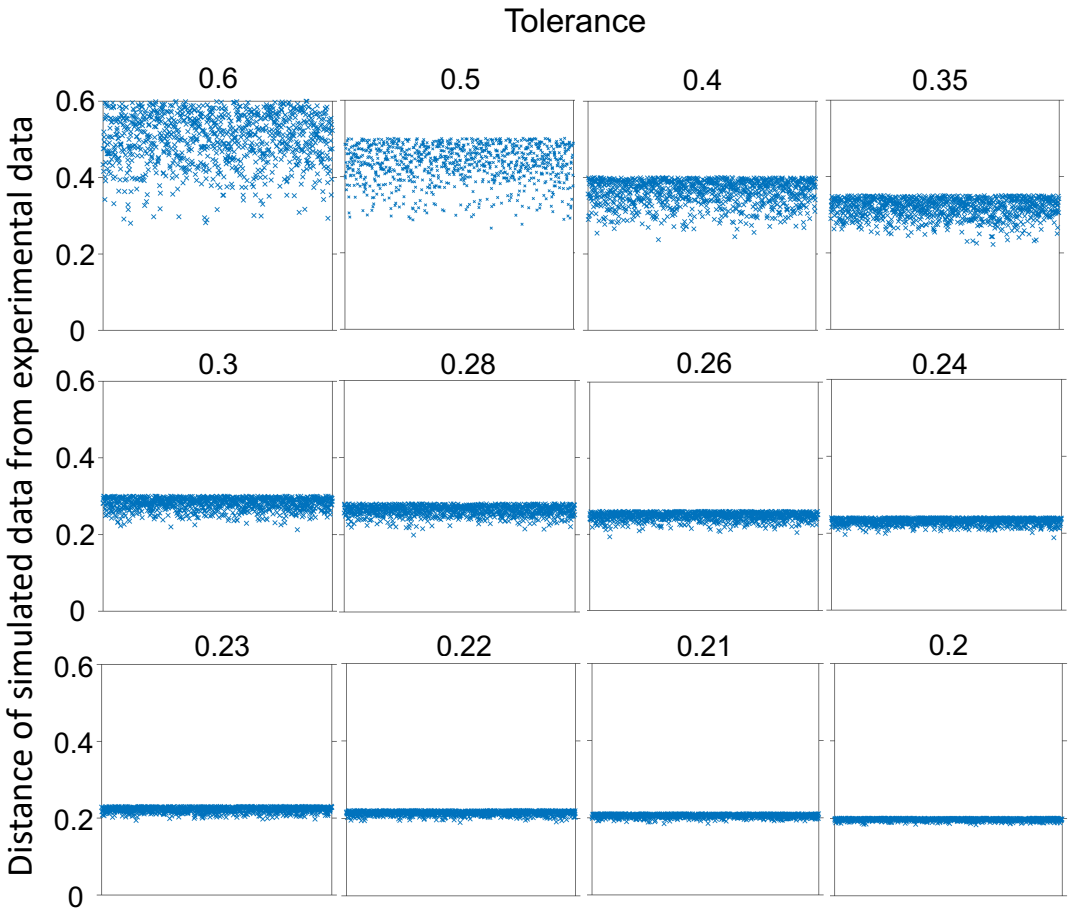

Figure 4.4 – Distances between simulated and experimental data over successive generation

The fit of the final model improves from generation to generation in the ABC-SMC method. Each generation lowered the threshold for accepting a fit. In the final generation, all accepted fits have a similar distance between simulated and experimental data, showing that fits with further reduced distance did not occur. None of the accepted fits in the first generation would have been accepted in the last generation. The x axis has no meaning and is simply used to spread out the data. See methods 4.2.3 for the distance measure.

We repeated the model selection and fitting process ten times to test for the reproducibility of its outcomes (Fig. 4.5).

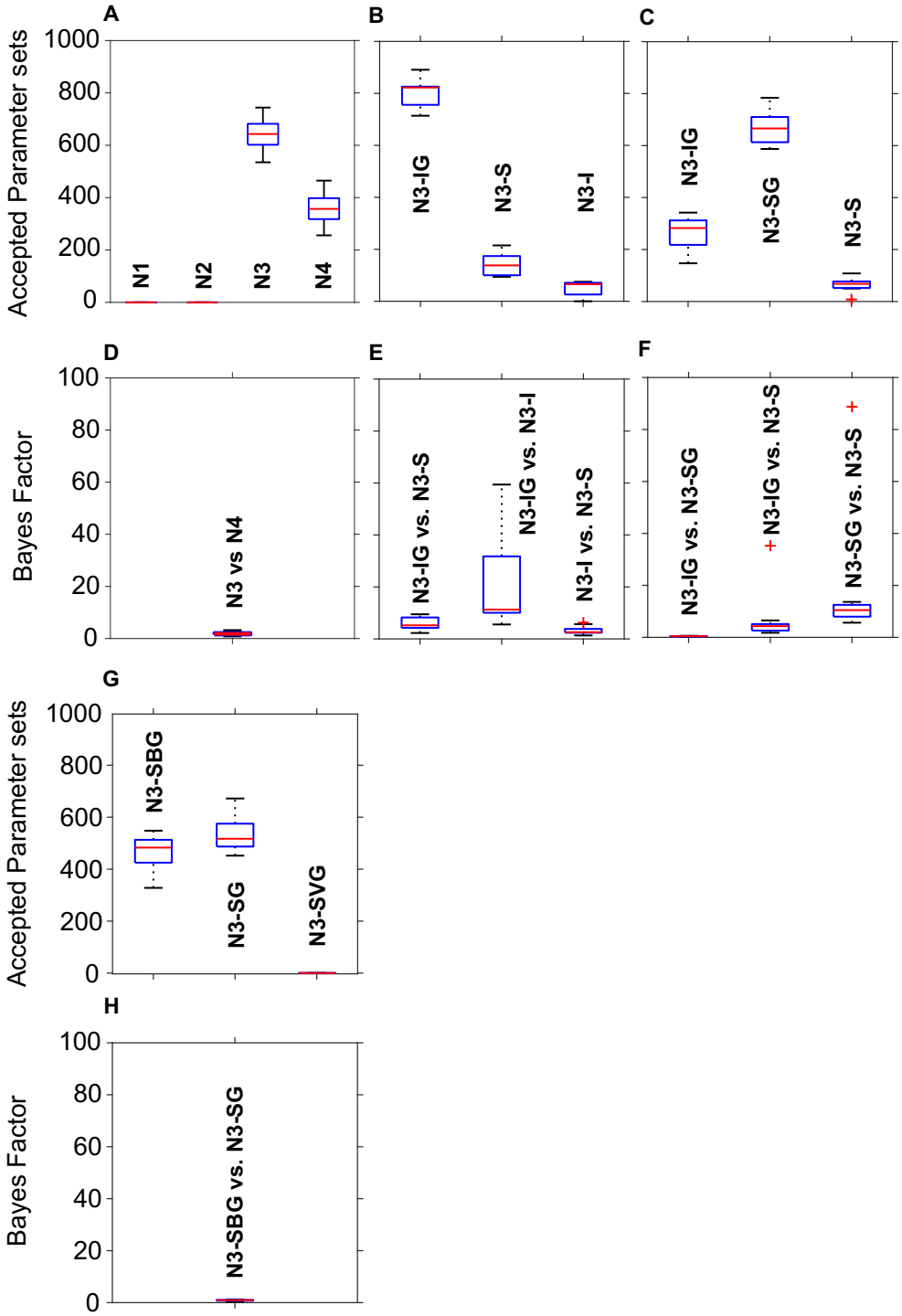

Figure 4.5 - Box plots showing the variation amongst the 10 repeats of model selection.

We repeated the model selection procedure shown in Fig. 4.6A-D ten times because finding 1,000 acceptable parameter sets with a Monte Carlo method could lead to some variation between runs of the ABC-SMC algorithm and it is good to check whether these differences are large. Box plots show the variation amongst the 10 repeats. We only show repeats for sub-model selections where the outcome was not 100% in favour of one model variant. The Bayes factor is the ratio of the times model X was accepted versus model Y. A factor of 1 indicates equally well supported models. A factor above 1 indicates greater support for the first model, below 1 for the second model. Where a model received no support, the Bayes factors comparing this model are not shown as these would be either zero or infinity.

4.2.4 Model equations

4.2.4.1 An explanation of symbols.

The maximum specific growth rate of the prey and attack rate constants of the predators are μ_N , μ_P and μ_V respectively and their half-saturation constants for substrate and prey are $K_{M,N}$ (read as half-saturation of N by M), $K_{N,P}$ and $K_{N,V}$ respectively. The rates of maturation of bdelloplasts into new *B. bacteriovorus* and of infected cells into new phages are $k_{P,}$ and k_V and the mortality of *B bacteriovorus* is m. All yields are expressed in the form $Y_{A/B}$, i.e., the yield of A per B consumed (Table 4.1).

4.2.4.2 Top level model variants – prey types

We performed the model selection in a hierarchical manner. The first level of selection was the number of prey sub-types or phenotypes. We competed four different models, with one, two, three or four prey phenotypes as set out below.

N1. The equations for the base model with a single prey phenotype (**N1**) that is sensitive to predation from both *B. bacteriovorus* and halo-phage (N_S). This model has a type II saturating functional response for *B. bacteriovorus* and type I non-saturating response for the halo-phage:

$$\frac{dM}{dt} = -N_S \frac{\mu_N M}{(K_{M,N} + M)\, Y_{N/M}} + Y_{M/P} k_p B + Y_{M/V} k_v I \qquad \text{(N1-a)}$$

$$\frac{\mathrm{dN_S}}{\mathrm{dt}} = \mathrm{N_S} \frac{\mu_N \mathrm{M}}{\mathrm{K_{M,N}} + \mathrm{M}} - \mathrm{P} \frac{\mu_P \mathrm{N_S}}{(\mathrm{K_{N,P}} + \mathrm{N_S})\, \mathrm{Y_{B/N}}} - \mathrm{V} \frac{\mu_V \mathrm{N_S}}{\mathrm{Y_{I/N}}} \qquad \text{(N1-b)}$$

$$\frac{dP}{dt} = k_P B - mP - P \frac{\mu_P N_S}{(K_{N,P} + N_S)\, Y_{B/P}} \qquad \text{(N1-c)}$$

$$\frac{\mathrm{dB}}{\mathrm{dt}} = \mathrm{P} \frac{\mu_P \mathrm{N_S}}{\mathrm{K_{N,P}} + \mathrm{N_S}} - \frac{\mathrm{k_P B}}{\mathrm{Y_{P/B}}} \qquad \text{(N1-d)}$$

$$\frac{dV}{dt} = k_V I - V\frac{\mu_V N_S}{Y_{I/V}} \quad \text{(N1-e)}$$

$$\frac{dI}{dt} = V\mu_V N_S - \frac{k_V I}{Y_{V/I}} \quad \text{(N1-f)}$$

N2. The equations for the two prey phenotype model (**N2**), with one type sensitive to both predators (N_S) and one type resistant to phage predation only (N_R). This phage resistant type is assumed to be present at the beginning of the experiment and the simulation at a very low frequency given by the parameter F_R. Further conversion from sensitive to resistant prey (via *de novo* mutations) continues over the course of the experiment at a rate k_M. In terms of predation by *B. bacteriovorus*, both types are assumed to be the same. In terms of growth kinetics, we assume that the phage resistance does not change the growth kinetics as experimental results by the Sockett lab (Hobley *et al.*, 2019) show that phage resistance is due to a mutation in the ferric hydroxamate uptake gene *fhuA* that had no effect on growth in the iron sufficient conditions of the experiment. The equations are as below (functional response types as above):

$$\frac{dM}{dt} = -(N_S + N_R)\frac{\mu_N M}{(K_{M,N} + M)\,Y_{M/S}} + Y_{M/P}k_p B + Y_{M/V}k_v I \quad \text{(N2-a)}$$

$$\frac{dN_S}{dt} = N_S\frac{\mu_N M}{K_{M,N} + M} - P\frac{\mu_P N_S}{(K_{N,P} + N_S + N_R)\,Y_{B/N}} - V\frac{\mu_V N_S}{Y_{I/N}} - k_M N_s \quad \text{(N2-b)}$$

$$\frac{dN_R}{dt} = N_R\frac{\mu_N M}{K_{M,N} + M} - P\frac{\mu_P N_R}{(K_{N,P} + N_S + N_R)\,Y_{B/N}} + k_M N_s,$$

$$N_R(t=0) = F_R N_S(t=0) \quad \text{(N2-c)}$$

$$\frac{dP}{dt} = k_P B - mP - P\frac{\mu_P(N_S + N_R)}{(K_{N,P} + N_S + N_R)\,Y_{B/P}} \quad \text{(N2-d)}$$

$$\frac{dB}{dt} = P\frac{\mu_P(N_S + N_R)}{K_{N,P} + N_S + N_R} - \frac{k_P B}{Y_{P/B}} \quad \text{(N2-e)}$$

$$\frac{dV}{dt} = k_V I - V\frac{\mu_V N_S}{Y_{I/V}} \quad \text{(N2-f)}$$

$$\frac{dI}{dt} = V\mu_V N_S - \frac{k_V I}{Y_{V/I}} \quad \text{(N2-g)}$$

N3. There were a few different variants of the three prey phenotype model (**N3**). They all had one type sensitive to both predators, one type resistant to phage predation and one type exhibiting 'plastic' phenotypic resistance to *B. bacteriovorus* predation. They differed in the way the plastic resister types formed and reverted and in the way phage resistance occurred. At this level plastic resistance was modelled to arise intrinsically (spontaneously) at a rate k_D and reversion to sensitivity was coupled to growth of the plastic resistant type. The equations for model variant **N3** with these specifics are shown further below (equation set **N3-IG**).

N4. The equations for the four prey phenotype model (**N4**), with the prey types from the **N3** model and an additional type resistant to both phage predation and *B. bacteriovorus* (N_D):

$$\frac{dM}{dt} = -(N_S + N_R + N_P + N_D)\frac{\mu_N M}{(K_{M,N} + M)\,Y_{N/M}} + Y_{M/P}k_p B + Y_{M/V}k_v I \quad \text{(N4-a)}$$

$$\frac{dN_S}{dt} = (N_S + N_P)\frac{\mu_N M}{K_{M,N} + M} - P\frac{\frac{\mu_P N_S}{(K_{N,P} + N_S + N_P + N_R + N_D)\,Y_{B/N}}}{-V\frac{\mu_N N_S}{Y_{I/N}} - k_M N_S - k_D N_S} \quad \text{(N4-b)}$$

$$\frac{dN_P}{dt} = -V\frac{\mu_V N_P}{Y_{I/N}} + k_D N_S - k_M N_P \quad \text{(N4-c)}$$

$$\frac{dN_R}{dt} = (N_R + N_D)\frac{\mu_N M}{K_{M,N} + M} - P\frac{\mu_P N_R}{(K_{N,P} + N_S + N_P + N_R + N_D)Y_{B/N}} + k_M N_S - k_D N_R,$$

$$N_R(t=0)\; F_R N_S(t=0) \quad \text{(N4-d)}$$

$$\frac{dN_D}{dt} = k_D N_R + k_M N_P \quad \text{(N4-e)}$$

$$\frac{dP}{dt} = k_P B - mP - P\frac{\mu_P(N_S + N_R)}{\left(K_{N,P} + N_S + N_P + N_R + N_D\right) Y_{B/P}} \quad \text{(N4-f)}$$

$$\frac{dB}{dt} = P\frac{\mu_P(N_S + N_R)}{K_{N,P} + N_S + N_P + N_R + N_D} - \frac{k_P B}{Y_{P/B}} \quad \text{(N4-g)}$$

$$\frac{dV}{dt} = k_V I - V\frac{\mu_V(N_S + N_P)}{Y_{I/V}} \quad \text{(N4-h)}$$

$$\frac{dI}{dt} = V\mu_V(N_S + N_P) - \frac{k_V I}{Y_{V/I}} \quad \text{(N4-i)}$$

Competing the top-level model variants with one, two, three or four prey types (Fig. 4.3C) gave clear results (Fig. 4.6A). The model variant **N1** with prey sensitive to both predators (N_S) and variant **N2** with only N_S and bacteriophage-resistant prey (N_R) were not supported by the experimental data at all. The variant **N3** with N_S, N_R, and prey exhibiting the "plastic" phenotypic resistance to *B. bacteriovorus* predation (N_P) was best supported by the experimental data, while variant **N4**, including the doubly resistant prey (N_D), was less supported (Fig. 4.6A). **N3** and **N4** are nested models with the same number of parameters, so fitting variant **N4** is not intrinsically more difficult.

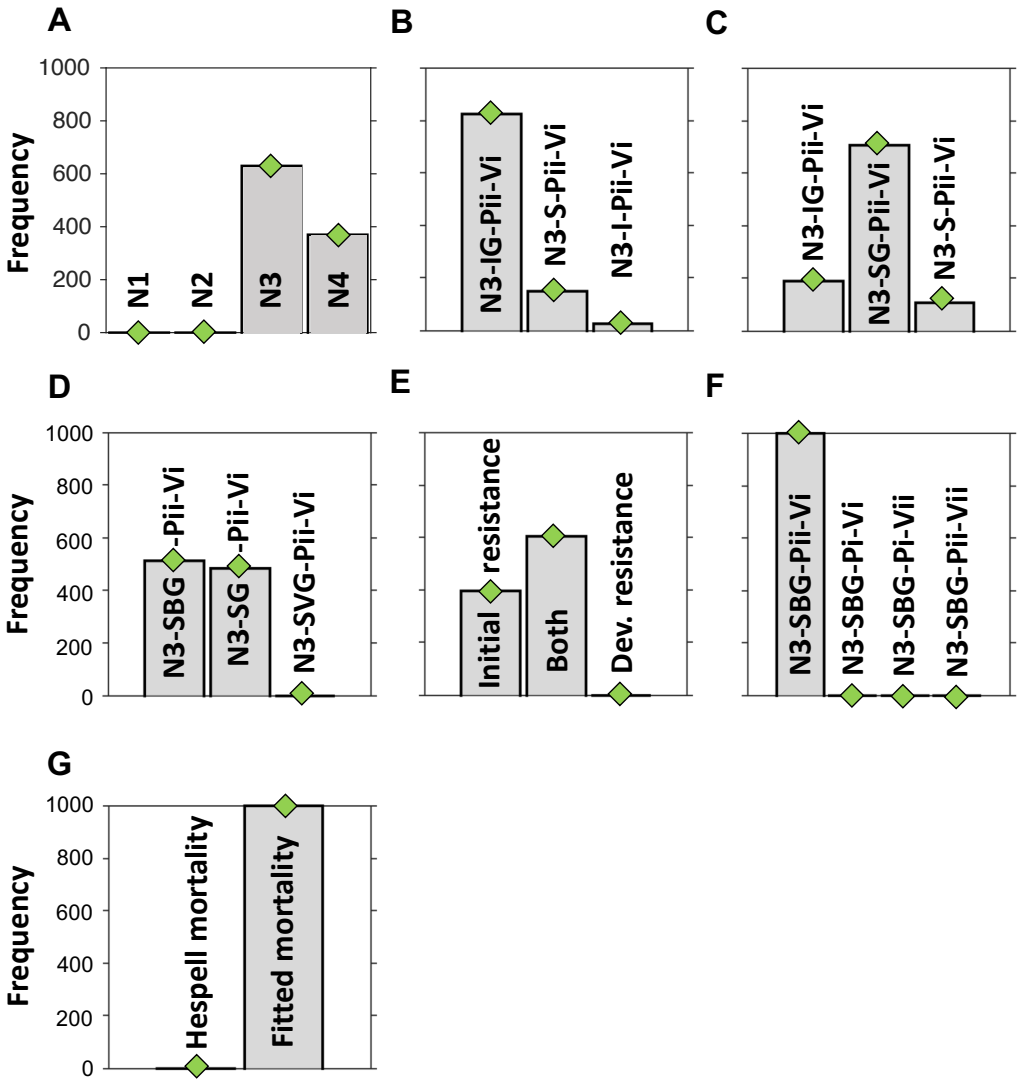

Figure 4.6 - Hierarchical model selection process.

This infers which model variants from Fig. 4.2 are best supported by the data (frequency of a variant winning out of 1000). **(A)** Competition of models with different number of prey phenotypes. **N1**: one prey type sensitive to both predators (N_S), **N2**: two prey types, N_S and phage resistant prey (N_R), **N3**: three prey types, N_S, N_R and prey with plastic phenotypic resistance to *B. bacteriovorus* (N_P), **N4:** four prey types, N_S, N_R, N_P and prey with dual resistance (N_D). **(B)** Competition of models with different ways of converting between sensitive prey (N_S) and plastic resistant prey (N_P) but the same saturating *B. bacteriovorus* attack rate (**Pii**) and non-saturating phage attack rate (**Vi**). **N3-IG-Pii-Vi**: N_S intrinsically (spontaneously) converts to N_P and back conversion is coupled to growth. **N3-S-Pii-Vi**: N_S conversion to N_P is triggered by a signal and back conversion is spontaneous. **N3-I-Pii-Vi**: spontaneous conversion both ways. **(C)** The best variants from panel (**B**) were combined to give **N3-SG-Pii-Vi,** which was competed against its 'parent' variants. **N3-SG-Pii-Vi**: N_S conversion to N_P is triggered by a signal and back conversion is coupled to growth. **(D)** Model variants, derived from the combined model in panel **(C)**, but differing in the way the signal is produced. **N3-SBG-Pii-Vi**: Signal derives from interaction of prey and *B. bacteriovorus* only. **N3-SG-Pii-Vi**: Signal derives from interaction of prey with both predators. **N3-SVG-Pii-Vi**: Signal derives from prey interaction with virus (phage) only. **(E)** Different ways of generating phage resistance. Phage resistant prey were already present initially or prey developed resistance *de novo* or both. **(F)** Model variants, based on **N3-SBG** from panel **(D)**, but differing in attack rate saturation. **Pii**: *B. bacteriovorus* attack rate saturates at high prey density while **Pi** does not saturate. Likewise, with **Vii** and **Vi** for the virus (phage). **(G)** Mortality of *B. bacteriovorus* (phage assumed to be stable) was either set to Hespell et al. (1974) or fitted by the ABC-SMC method. Less decisive competitions **(B-D)** were repeated 10 times, see Fig. 4.5.

4.2.4.3 Mid-level model variants – Generating plastic resistance to B. bacteriovorus predation.

Before investigating the mechanism by which phage resistance arose, we first looked into the possible ways in which prey could become phenotypically resistant to *B. bacteriovorus* predation and how these plastic resisters could revert to a sensitive phenotype.

N3-I. The simplest assumed mechanism of plastic persister formation is that sensitive prey cells become resistant spontaneously or intrinsically, so that the rate was proportional to their density (first order kinetics) with a certain specific rate (k_D). Likewise, the back conversion to sensitive prey followed first order kinetics with a rate of k_R. Growth rates between sensitives and plastic resisters were allowed to differ by a factor η_P, which could be smaller or larger than one. The equations for this model variant (**N3-I** for Intrinsic conversions) were as below (functional response types as above):

The equations for variant **N3-I** are:

$$\frac{dM}{dt} = -(N_S + N_R + N_P\eta_P)\frac{\mu_N M}{(K_{M,N}+M)\,Y_{N/M}} + Y_{M/P}k_p B + Y_{M/V}k_v I \qquad \text{(N3-I-a)}$$

$$\frac{dN_S}{dt} = N_S\frac{\mu_N M}{K_{M,N}+M} - P\frac{\mu_P N_S}{(K_{N,P}+N_S+N_P+N_R)\,Y_{B/N}} - V\frac{\mu_V N_S}{Y_{I/N}} - k_M N_s$$

$$-k_D N_S + k_R N_P \qquad \text{(N3-I-b)}$$

$$\frac{dN_P}{dt} = N_P\frac{\eta_P\mu_N M}{K_{M,N}+M} - V\frac{\mu_V N_P}{Y_{I/N}} + k_D N_S - k_R N_P \qquad \text{(N3-I-c)}$$

$$\frac{dN_R}{dt} = N_R\frac{\mu_N M}{K_{M,N}+M} - P\frac{\mu_P N_R}{(K_{N,P}+N_S+N_P+N_R)\,Y_{B/N}} + k_M N_s,$$

$$N_R(t=0) = F_R N_S(t=0) \qquad \text{(N3-I-d)}$$

$$\frac{dP}{dt} = k_P B - mP - P\frac{\mu_P(N_S+N_R)}{(K_{N,P}+N_S+N_P+N_R)\,Y_{B/P}} \qquad \text{(N3-I-e)}$$

$$\frac{dB}{dt} = P\frac{\mu_P(N_S + N_R)}{K_{N,P} + N_S + N_P + N_R} - \frac{k_P B}{Y_{P/B}} \quad \text{(N3-I-f)}$$

$$\frac{dV}{dt} = k_V I - V\frac{\mu_V(N_S + N_P)}{Y_{I/V}} \quad \text{(N3-I-g)}$$

$$\frac{dI}{dt} = V\mu_V(N_S + N_P) - \frac{k_V I}{Y_{V/I}} \quad \text{(N3-I-h)}$$

N3-S. Another mechanism assumed that plastic resisters form due to the production of a signal (S) somehow produced by predation. Such signals could be released during the lysis of prey, so this model includes terms for a signal being released from both the lysis of bdelloplasts and the lysis of phage-infected prey. Back conversion is intrinsic as in **N3-I**. The equations for this model (**N3-S**) are as below (functional response types as above):

$$\frac{dM}{dt} = -(N_S + N_R + N_P\eta_P)\frac{\mu_N M}{(K_{M,N} + M)\,Y_{N/M}} + Y_{M/P}k_p B + Y_{M/V}k_v I \quad \text{(N3-S-a)}$$

$$\frac{dN_S}{dt} = N_S\frac{\mu_N M}{K_{M,N} + M} - P\frac{\mu_P N_S}{(K_{N,P} + N_S + N_P + N_R)\,Y_{B/N}} - V\frac{\mu_V N_S}{Y_{I/N}} - k_M N_s$$

$$-k_D S N_S + k_R N_P \quad \text{(N3-S-b)}$$

$$\frac{dN_P}{dt} = N_P\frac{\eta_P\,\mu_N M}{K_{M,N} + M} - V\frac{\mu_V N_P}{Y_{I/N}} + k_D S N_S - k_R N_P \quad \text{(N3-S-c)}$$

$$\frac{dN_R}{dt} = N_R\frac{\mu_N M}{K_{M,N} + M} - P\frac{\mu_P N_R}{(K_{N,P} + N_S + N_P + N_R)\,Y_{B/N}} + k_M N_s,$$

$$N_R(t = 0) = F_R N_S(t = 0) \quad \text{(N3-S-d)}$$

$$\frac{dP}{dt} = k_P B - mP - P\frac{\mu_P(N_S + N_R)}{(K_{N,P} + N_S + N_P + N_R)\,Y_{B/P}} \quad \text{(N3-S-e)}$$

$$\frac{dB}{dt} = P\frac{\mu_P(N_S + N_R)}{K_{N,P} + N_S + N_P + N_R} - \frac{k_P B}{Y_{P/B}} \quad \text{(N3-S-f)}$$

$$\frac{dV}{dt} = k_V I - V\frac{\mu_V(N_S + N_P)}{Y_{I/V}} \quad \text{(N3-S-g)}$$

$$\frac{dI}{dt} = V\mu_V(N_S + N_P) - \frac{k_V I}{Y_{V/I}} \quad \text{(N3-S-h)}$$

$$\frac{dS}{dt} = \frac{k_P B}{Y_{P/B}} + \frac{k_V I}{Y_{V/I}} \quad \text{(N3-S-i)}$$

N3-IG. A third three prey phenotype model variant assumed that the formation of plastic resisters is intrinsic as in **N3-I**, but that sensitive prey were generated from persisters in a growth coupled manner rather than by a spontaneous back conversion, model **N3-IG**. This is because plastic resisters are assumed to grow at a slow rate and resistance is assumed not to be heritable. This is the sub-model of **N3** used for the top-level model selection and given by the equations below (functional response types as above):

$$\frac{dM}{dt} = -(N_S + N_R + N_P)\frac{\mu_N M}{(K_{M,N} + M)\, Y_{N/M}} + Y_{M/P} k_p B + Y_{M/V} k_v I \quad \text{(N3-IG-a)}$$

$$\frac{dN_S}{dt} = (N_S + N_P)\frac{\mu_N M}{K_{M,N} + M} - P\frac{\mu_P N_S}{(K_{N,P} + N_S + N_P + N_R)\, Y_{B/N}}$$

$$-V\frac{\mu_N N_S}{Y_{I/N}} - k_M N_s - k_D N_S \quad \text{(N3-IG-b)}$$

$$\frac{dN_P}{dt} = -V\frac{\mu_V N_P}{Y_{I/N}} + k_D N_S \quad \text{(N3-IG-c)}$$

$$\frac{dN_R}{dt} = N_R\frac{\mu_N M}{K_{M,N} + M} - P\frac{\mu_P N_R}{(K_{N,P} + N_S + N_P + N_R) Y_{B/N}} + k_M N_s,$$

$$N_R(t = 0)\; F_R N_S(t = 0) \quad \text{(N3-IG-d)}$$

$$\frac{dP}{dt} = k_P B - mP - P\frac{\mu_P (N_S + N_R)}{(K_{N,P} + N_S + N_P + N_R)\, Y_{B/P}} \quad \text{(N3-IG-e)}$$

$$\frac{dB}{dt} = P\frac{\mu_P (N_S + N_R)}{K_{N,P} + N_S + N_P + N_R} - \frac{k_P B}{Y_{P/B}} \quad \text{(N3-IG-f)}$$

$$\frac{dV}{dt} = k_V I - V\frac{\mu_V (N_S + N_P)}{Y_{I/V}} \quad \text{(N3-IG-g)}$$

$$\frac{dI}{dt} = V\mu_V (N_S + N_P) - \frac{k_V I}{Y_{V/I}} \quad \text{(N3-IG-h)}$$

N3-SG. Competing these three variants (Fig. 4.6B and Fig. 4.5B) revealed that the data gave very little support for model **N3-I**, some support (between 9.4% and

27% of accepted parameter sets) for variant **N3-S**, and stronger support for variant **N3-IG** (between 62% to 89% of accepted parameter sets).

We then decided to try a combination of the two variants that were supported by the data. Here development of plastic resistance was triggered by a signal and therefore proportional to the numbers of dead prey cells. Plastic resisters did not intrinsically revert to sensitives or suffer any growth penalty, but when they grew, they become new sensitive bacteria. The equations for this model (**N3-SG**) are as below (functional response types as above):

$$\frac{dM}{dt} = -(N_S + N_R + N_P)\frac{\mu_N M}{(K_{M,N} + M)\,Y_{N/M}} + Y_{M/P}k_p B + Y_{M/V}k_v I \quad \text{(N3-SG-a)}$$

$$\frac{dN_S}{dt} = (N_S + N_P)\frac{\mu_N M}{K_{M,N} + M} - P\frac{\mu_P N_S}{(K_{N,P} + N_S + N_P + N_R)\,Y_{B/N}} - V\frac{\mu_V N_S}{Y_{I/N}}$$

$$-k_M N_S - k_D S N_S \quad \text{(N3-SG-b)}$$

$$\frac{dN_P}{dt} = -V\frac{\mu_V N_P}{Y_{I/N}} + k_D S N_S \quad \text{(N3-SG-c)}$$

$$\frac{dN_R}{dt} = N_R\frac{\mu_N M}{K_{M,N} + M} - P\frac{\mu_P N_R}{(K_{N,P} + N_S + N_P + N_R)\,Y_{B/N}} + k_M N_s,$$

$$N_R(t=0) = F_R N_S(t=0) \quad \text{(N3-SG-d)}$$

$$\frac{dP}{dt} = k_P B - mP - P\frac{\mu_P(N_S + N_R)}{(K_{N,P} + N_S + N_P + N_R)\,Y_{B/P}} \quad \text{(N3-SG-e)}$$

$$\frac{dB}{dt} = P\frac{\mu_P(N_S + N_R)}{K_{N,P} + N_S + N_P + N_R} - \frac{k_P B}{Y_{P/B}} \quad \text{(N3-SG-f)}$$

$$\frac{dV}{dt} = k_V I - V\frac{\mu_V(N_S + N_P)}{Y_{I/V}} \quad \text{(N3-SG-g)}$$

$$\frac{dI}{dt} = V\mu_V(N_S + N_P) - \frac{k_V I}{Y_{V/I}} \quad \text{(N3-SG-h)}$$

$$\frac{dS}{dt} = \frac{k_P B}{Y_{P/B}} + \frac{k_V I}{Y_{V/I}} \quad \text{(N3-SG-i)}$$

Competing variants **N3-S**, **N3-IG** and **N3-SG** showed that the data supported the (re)combined variant **N3-SG** much better than its parents **N3-S** and **N3-IG** (Fig. 4.6C and 4.5C). Thus, we can infer from the modelling that plastic resistance arises as a result of some signal(s) released upon lysis of infected prey, and that the growth of plastic resistant prey results in the production of sensitive prey.

4.2.4.4 Mid-level model variants – source of plastic resistance signal.

We next investigated potential sources of the signal that triggered the plastic resistance phenotype. We developed three sub-variants of this model that differed in source of the signal (see Eq. N3-SG-i). In model **N3-SG**, both predation by *B. bacteriovorus* and by phage contributed to the formation of the signal.

Model **N3-SBG** assumed only predation by *B. bacteriovorus* produced the signal. Here, the equations were the same as variant **N3-SG** except that equation N3-SG-i was replaced by N3-SBG-i:

$$\frac{dS}{dt} = \frac{k_P\, B}{Y_{P/B}} \qquad \text{(N3-SBG-i)}$$

In the third alternative **N3-SVG**, the signal only came from predation by phage, again the equations were the same as variant **N3-SG** except that equation N3-SG-i was replaced by N3-SVG-i:

$$\frac{dS}{dt} = \frac{k_V\, I}{Y_{V/I}} \qquad \text{(N3-SVG-i)}$$

Competing these three variants (Fig. 4.6D and 4.5D) showed no support for the model where the signal was generated by lysis of the bacteriophage-infected prey only. The support for the other two variants was almost equal. Since there was no evidence for phage involvement in signal generation, model **N3-SBG** where all signal is derived from *B. bacteriovorus* predation was the logical choice.

4.2.4.5 Mid-level model variants – Source of phage resistant prey.

The successful model variant **N3-IG** was then used as a basis to infer how phage resistance could arise. One variant assumed that all prey were sensitive to phage at the outset of the experiment, but that the resistant population N_R could develop by *de novo* mutations during the experiment, with mutation rate k_M (Table 4.1), giving model **N3-IG-RD** (Resistance developing):

$$\frac{dM}{dt} = -(N_S + N_R + N_P)\frac{\mu_N M}{(K_{M,N} + M)\,Y_{N/M}} + Y_{M/P}k_p B$$

$$+Y_{M/V}k_v I \qquad \text{(N3-IG-RD-a)}$$

$$\frac{dN_S}{dt} = (N_S + N_P)\frac{\mu_N M}{K_{M,N} + M} - P\frac{\mu_P N_S}{(K_{N,P} + N_S + N_P + N_R)\,Y_{B/N}}$$

$$-V\frac{\mu_V N_S}{Y_{I/N}} - k_M N_S - k_D N_S \qquad \text{(N3-IG-RD-b)}$$

$$\frac{dN_P}{dt} = -V\frac{\mu_V N_P}{Y_{I/N}} + k_D N_S \qquad \text{(N3-IG-RD-c)}$$

$$\frac{dN_R}{dt} = N_R\frac{\mu_N M}{K_{M,N} + M} - P\frac{\mu_P N_R}{(K_{N,P} + N_S + N_P + N_R)\,Y_{B/N}} + k_M N_S,$$

$$N_R(t = 0) = 0 \qquad \text{(N3-IG-RD-d)}$$

$$\frac{dP}{dt} = k_P B - mP - P\frac{\mu_P(N_S + N_R)}{(K_{N,P} + N_S + N_P + N_R)\,Y_{B/P}} \qquad \text{(N3-IG-RD-e)}$$

$$\frac{dB}{dt} = P\frac{\mu_P(N_S + N_R)}{K_{N,P} + N_S + N_P + N_R} - \frac{k_P B}{Y_{P/B}} \qquad \text{(N3-IG-RD-f)}$$

$$\frac{dV}{dt} = k_V I - V\frac{\mu_V(N_S + N_P)}{Y_{I/V}} \qquad \text{(N3-IG-RD-g)}$$

$$\frac{dI}{dt} = V\,\mu_V(N_S + N_P) - \frac{k_V I}{Y_{V/I}} \qquad \text{(N3-IG-RD-h)}$$

Another variant assumed that a fraction F_R (Table 4.1) of the prey population was already resistant initially, but that further resistance via mutation did not develop (model **N3-RI**):

$$\frac{dM}{dt} = -(N_S + N_R + N_P)\frac{\mu_N M}{(K_{M,N} + M)\,Y_{N/M}} + Y_{M/P}k_p B + Y_{M/V}k_v I \quad \text{(N3-IG-RI-a)}$$

$$\frac{dN_S}{dt} = (N_S + N_P)\frac{\mu_N M}{K_{M,N} + M} - P\frac{\frac{\mu_P N_S}{(K_{N,P} + N_S + N_P + N_R)\,Y_{B/N}}}{}$$

$$-V\frac{\mu_V N_S}{Y_{I/N}} - k_D N_S \quad \text{(N3-IG-RI-b)}$$

$$\frac{dN_P}{dt} = -V\frac{\mu_V N_P}{Y_{I/N}} + k_D N_S \quad \text{(N3-IG-RI-c)}$$

$$\frac{dN_R}{dt} = N_R\frac{\mu_N M}{K_{M,N} + M} - P\frac{\mu_P N_R}{(K_{N,P} + N_S + N_P + N_R)\,Y_{B/N}},$$

$$N_R(t = 0) = F_R\,N_S(t = 0) \quad \text{(N3-IG-RI-d)}$$

$$\frac{dP}{dt} = k_P B - mP - P\frac{\mu_P(N_S + N_R)}{(K_{N,P} + N_S + N_P + N_R)\,Y_{B/P}} \quad \text{(N3-IG-RI-e)}$$

$$\frac{dB}{dt} = P\frac{\mu_P(N_S + N_R)}{K_{N,P} + N_S + N_P + N_R} - \frac{k_P B}{Y_{P/B}} \quad \text{(N3-IG-RI-f)}$$

$$\frac{dV}{dt} = k_V\,I - V\frac{\mu_V(N_S + N_P)}{Y_{I/V}} \quad \text{(N3-IG-RI-g)}$$

$$\frac{dI}{dt} = V\,\mu_V(N_S + N_P) - \frac{k_V\,I}{Y_{V/I}} \quad \text{(N3-IG-RI-h)}$$

The combined variant **N3-IG-RID** where phage resistance is both present as an initial subpopulation of the prey and also arises due to *de novo* mutations during the course of the experiment was better supported by the data than **N3-IG-RI**; **N3-IG-RD** was not supported at all (Fig. 4.6E). Model **N3-IG-RID** is identical to the original model variant **N3-IG** described above.

4.2.4.6 Low level model variant – saturating or non-saturating predation kinetics.

The model was initially constructed assuming that bacteriophage predation would not saturate with increasing prey density but that *B. bacteriovorus* predation would saturate (Holling type II kinetics) due to its longer handling time (time for attachment and prey entry). This assumption was challenged by testing all four

combinations of saturating and non-saturating functional responses for the two predators (Fig. 4.6F). The previously used model variant **N3-SBG** (see above) was in fact **N3-SBG-Pii-Vi** where **Pii** means Predator follows saturating kinetics and **Vi** means that the Virus follows non-saturating or type I kinetics. This original model was competed against variants with both predators following non-saturating kinetics (**N3-SBG-Pi-Vi**):

$$\frac{dM}{dt} = -(N_S + N_R + N_P)\frac{\mu_N M}{(K_{M,N} + M)\,Y_{N/M}}$$

$$+Y_{M/P}k_p B + Y_{M/V}k_v I \qquad \text{(N3-SBG-RID-Pi-Vi-a)}$$

$$\frac{dN_S}{dt} = (N_S + N_P)\frac{\mu_N M}{K_{M,N} + M} - P\frac{\mu_P N_S}{Y_{B/N}}$$

$$-V\frac{\mu_V N_S}{Y_{I/N}} - k_M N_S - k_D S N_S \qquad \text{(N3-SBG-RID-Pi-Vi-b)}$$

$$\frac{dN_P}{dt} = -V\frac{\mu_V N_P}{Y_{I/N}} + k_D S N_S \qquad \text{(N3-SBG-RID-Pi-Vi-c)}$$

$$\frac{dN_R}{dt} = N_R\frac{\mu_N M}{K_{M,N} + M} - P\frac{\mu_P N_R}{Y_{B/N}} + k_M N_s,$$

$$N_R(t=0) = F_R N_S(t=0) \qquad \text{(N3-SBG-RID-Pi-Vi-d)}$$

$$\frac{dP}{dt} = k_P B - mP - P\frac{\mu_P(N_S + N_R)}{Y_{B/P}} \qquad \text{(N3-SBG-RID-Pi-Vi-e)}$$

$$\frac{dB}{dt} = P\mu_P(N_S + N_R) - \frac{k_P B}{Y_{P/B}} \qquad \text{(N3-SBG-RID-Pi-Vi-f)}$$

$$\frac{dV}{dt} = k_V I - V\frac{\mu_V(N_S + N_P)}{Y_{I/V}} \qquad \text{(N3-SBG-RID-Pi-Vi-g)}$$

$$\frac{dI}{dt} = V\mu_V(N_S + N_P) - \frac{k_V I}{Y_{V/I}} \qquad \text{(N3-SBG-RID-Pi-Vi-h)}$$

$$\frac{dS}{dt} = \frac{k_P B}{Y_{P/B}} \qquad \text{(N3-SBG-RID-Pi-Vi-i)}$$

B. bacteriovorus following non-saturating and phage saturating kinetics (**N3-SBG-RID-Pi-Vii**):

$$\frac{dM}{dt} = -(N_S + N_R + N_P)\frac{\mu_N M}{(K_{M,N} + M)\,Y_{N/M}}$$

$$+Y_{M/P}k_p B + Y_{M/V}k_v I \qquad \text{(N3-SBG-RID-Pi-Vii-a)}$$

$$\frac{dN_S}{dt} = (N_S + N_P)\frac{\mu_N M}{K_{M,N} + M} - P\frac{\mu_P N_S}{Y_{B/N}} - V\frac{\mu_V N_S}{(K_{N,V} + N_S + N_P + N_R)\,Y_{I/N}}$$

$$-k_M N_S - k_D S N_S \qquad \text{(N3-SBG-RID-Pi-Vii-b)}$$

$$\frac{dN_P}{dt} = -V\frac{\mu_V N_P}{(K_{N,V} + N_S + N_P + N_R)\,Y_{I/N}}$$

$$+k_D S N_S \qquad \text{(N3-SBG-RID-Pi-Vii-c)}$$

$$\frac{dN_R}{dt} = N_R\frac{\mu_N M}{K_{M,N} + M} - P\frac{\mu_P N_R}{Y_{B/N}} + k_M N_s,$$

$$N_R(t=0) = F_R N_S(t=0) \qquad \text{(N3-SBG-RID-Pi-Vii-d)}$$

$$\frac{dP}{dt} = k_P B - mP - P\frac{\mu_P(N_S + N_R)}{Y_{B/P}} \qquad \text{(N3-SBG-RID-Pi-Vii-e)}$$

$$\frac{dB}{dt} = P\mu_P(N_S + N_R) - \frac{k_P B}{Y_{P/B}} \qquad \text{(N3-SBG-RID-Pi-Vii-f)}$$

$$\frac{dV}{dt} = k_V I - V\frac{\mu_V(N_S + N_P)}{(K_{N,V} + N_S + N_P + N_R)\,Y_{I/V}} \qquad \text{(N3-SBG-RID-Pi-Vii-g)}$$

$$\frac{dI}{dt} = \frac{V\mu_V(N_S+N_P)}{K_{N,V} + N_S + N_P + N_R} - \frac{k_V I}{Y_{V/I}} \qquad \text{(N3-SBG-RID-Pi-Vii-h)}$$

$$\frac{dS}{dt} = \frac{k_P B}{Y_{P/B}} \qquad \text{(N3-SBG-RID-Pi-Vii-i)}$$

Both predators following saturating kinetics (**N3-SBG-RID-Vii-Pii**):

$$\frac{dM}{dt} = -(N_S + N_R + N_P)\frac{\mu_N M}{(K_{M,N} + M)\,Y_{N/M}}$$

$$+Y_{M/P}k_p B + Y_{M/V}k_v I \qquad \text{(N3-SBG-RID-Pii-Vii-a)}$$

$$\frac{dN_S}{dt} = (N_S + N_P)\frac{\mu_N M}{K_{M,N} + M} - P\frac{\mu_P N_S}{(K_{N,P} + N_S + N_P + N_R)\,Y_{B/N}}$$

$$-V\frac{\mu_V N_S}{\left(K_{N,V}+N_S+N_P+N_R\right)Y_{I/N}}-k_M N_S$$

$$-k_D S N_S \qquad \text{(N3-SBG-RID-Pii-Vii-b)}$$

$$\frac{dN_P}{dt}=-V\frac{\mu_V N_P}{\left(K_{N,V}+N_S+N_P+N_R\right)Y_{I/N}}$$

$$+k_D S N_S \qquad \text{(N3-SBG-RID-Pii-Vii-c)}$$

$$\frac{dN_R}{dt}=N_R\frac{\mu_N M}{K_{M,N}+M}-P\frac{\mu_P N_R}{\left(K_{N,P}+N_S+N_P+N_R\right)Y_{B/N}}+k_M N_s,$$

$$N_R(t=0)=F_R N_S(t=0) \qquad \text{(N3-SBG-RID-Pii-Vii-d)}$$

$$\frac{dP}{dt}=k_P B-mP$$

$$-P\frac{\mu_P(N_S+N_R)}{\left(K_{N,P}+N_S+N_P+N_R\right)Y_{B/P}} \qquad \text{(N3-SBG-RID-Pii-Vii-e)}$$

$$\frac{dB}{dt}=\frac{P\mu_P(N_S+N_R)}{K_{N,P}+N_S+N_P+N_R}-\frac{k_P B}{Y_{P/B}} \qquad \text{(N3-SBG-RID-Pii-Vii-f)}$$

$$\frac{dV}{dt}=k_V I-V\frac{\mu_V(N_S+N_P)}{\left(K_{N,V}+N_S+N_P+N_R\right)Y_{I/V}} \qquad \text{(N3-SBG-RID-Pi-Vii-g)}$$

$$\frac{dI}{dt}=\frac{V\mu_V(N_S+N_P)}{K_{N,V}+N_S+N_P+N_R}-\frac{k_V I}{Y_{V/I}} \qquad \text{(N3-SBG-RID-Pi-Vii-h)}$$

$$\frac{dS}{dt}=\frac{k_P B}{Y_{P/B}} \qquad \text{(N3-SBG-RID-Pi-Vii-i)}$$

The previously used variant **N3-SBG-RID-Pii-Vi** consistently outcompeted all other variants (Fig. 4.6F).

4.2.4.7 Low level model variants – fixed or fitted B. bacteriovorus mortality.

There remained some discrepancy in the best fitting model with regards to the decline in *B. bacteriovorus* numbers seen in the experimental data. Therefore, we allowed *B. bacteriovorus* mortality, which had previously been fixed at 0.06 h^{-1}, a value taken from Hespell and co-workers (1974), to be fitted as an additional parameter.

The **N3-SBG-RID-Pii-Vi** model with fitted *B. bacteriovorus* mortality clearly outcompeted the variant with fixed mortality (Fig. 4.6G).

4.2.4.8 Final model

The variant with fitted mortality became the final model, **N3-SBG-RID-Pii-Vi-fitted-mortality** or **N3-SBG** for short, which was used in the simulations of the experimental data shown in Fig. 4.7. Fitted parameters are given in Table 4.1. The equations are shown in Fig. 4.1B and are the same as **N3-SBG-RID-Pii-Vi** above.

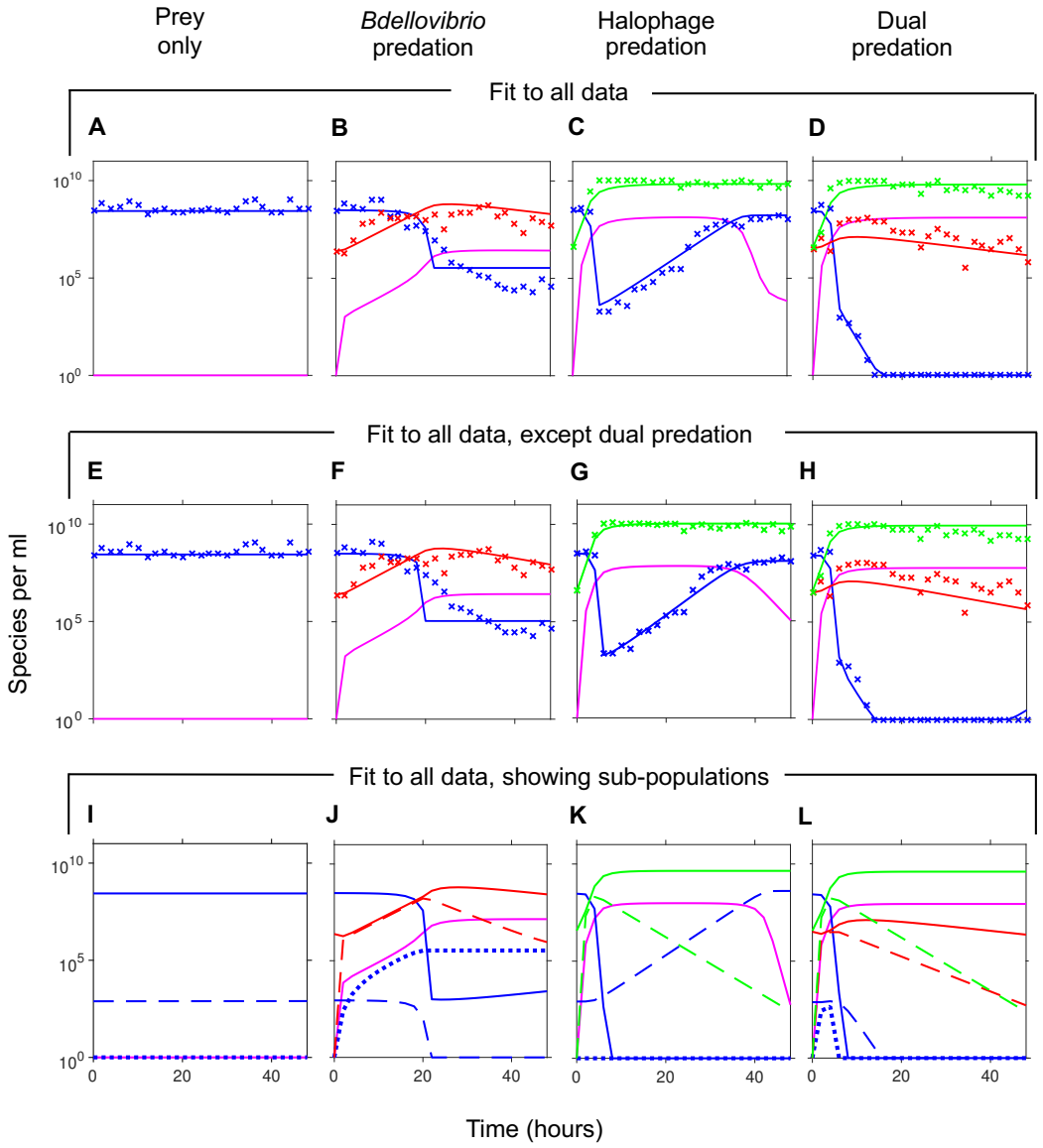

Figure 4.7 – Comparison of experimental data (mean values) with fits of the best model variant

The model was either fitted using **(A-D)** all experimental data or **(E-H)** all data without dual predation and then used to predict the outcome of dual predation (shown in **H**). The parameter values for each case are given in Table 4.1. Experimental data is shown by symbols, lines represent model simulations. **(A-H)** Blue – *E. coli* prey, Red – *B. bacteriovorus*, Green – bacteriophage halo, Pink – substrate (not experimentally measured). **(I-L)** Dynamics of the sub-populations of prey and predators predicted by the model that was fitted to all data, corresponding to panels **(A-D)**. **(I-L)** Blue – *E. coli* prey: solid line – susceptible prey N_S, dotted line – plastic resistant prey N_P, dashed line – bacteriophage resistant prey N_R. Red – *B. bacteriovorus*: solid line – free *B. bacteriovorus* P, dashed line – bdelloplasts B. Green – bacteriophage halo: solid line – free bacteriophage V, dashed line – bacteriophage-infected cells I. Pink – substrate.

4.2.4.9 Picking typical parameters with PCA

In order to objectively pick a typical parameter set to be used in model simulations shown in Fig. 4.7 from the many accepted fits, we used Principal

Component Analysis (PCA) to find the parameter sets in the centre of the cloud of points, which we regard as 'typical' or 'average'. We applied this PCA idea to the parameter sets obtained by fitting the final model to all the experimental data (fitting 15 parameters, one (*B. bacteriovorus* burst size) was fixed). We selected four such 'typical' parameter sets and ran simulations for each of them. These sets all gave very similar simulation results. The values for one of these parameter sets are given in Table 4.1 and the fit to the experimental data is shown in Fig. 4.7A-D. We did the same for the parameter sets fitted to all data without dual predation, the resulting typical parameter set is also given in Table 4.1 and the fit to experimental data is shown in Fig. 4.7E-H. The two fits, to all data or to all data without dual predation, are very similar, suggesting that the combined action of the two predators did not require any additional terms for direct interactions between the two, and that the observed kinetics of dual predation can be predicted from the actions of each predator alone.

4.3 Results

A family of mathematical models was developed (Fig. 4.2) based on the predator prey model described in Chapter 2. Unlike that chemostat model this family described a batch culture system and so did not include the effects of dilution. Additionally, we added into these models, resistance to bacteriophage predation and plastic phenotypic resistance to *B. bacteriovorus* predation. The model was fitted to data generated by the Sockett lab (Hobley *et al.*, 2019) (Fig. 4.3). Briefly, a lab strain of *E. coli* (S17-1) was grown to late-log phase before being placed in HEPES buffer with 2 mM $CaCl_2$ (calcium HEPES). To this was added either a – calcium HEPES (predator free control), b – attack phase *B. bacteriovorus*, c – halo-phage, or d – both *B. bacteriovorus* and halo-phage (dual predation). These cultures were followed for 48 hours with prey counts determined by optical density at 600 nm (OD_{600}) every hour and viable counts every two hours. *B. bacteriovorus* and halo-phage counts were determined by plaquing assays every two hours. All measurements were taken in triplicate and two biological repeats of the experiment were performed.

We initially attempted to determine parameter ranges using an MCMC method. This resulted in some success in defining certain parameter ranges, however the MCMC method struggled with other parameters and was not particularly suited for model selection. As a result, we moved to using an SMC methodology (Toni *et al.*, 2009) to select and fit those models which best matched the experimental data. Approximate Bayesian Computation – Sequential Monte Carlo (ABC-SMC) is an extension of SMC that avoids the need for an explicit likelihood function and is particularly well suited for time series data (Toni *et al.*, 2009). We used a hierarchical selection process to determine first the number of prey phenotypes required,

followed by the mechanisms by which resistance to phage and plastic resistance to *B. bacteriovorus* predation arose and finally the kinetics of predation. In the event that lower level model competitions selected a model that differed from the higher-level selection, the selection process for the higher-level models was repeated with the better fitting sub model.

We found that three prey phenotypes, one sensitive to predation by both predators (N_S), one displaying plastic resistance to *B. bacteriovorus* predation only (N_P) and one resistant to phage predation only (N_R) were required to explain the experimental results (Fig. 4.6A).

The population dynamics in the presence of two predators can be predicted by a model fitted only to single predator data, showing that the experimental results can be explained without invoking any interactions between the two predators (Fig. 4.7E-H).

4.3.1 Number of prey phenotypes

We first competed four top-level models (**N1**, **N2**, **N3** and **N4**) with one, two, three or four prey phenotypes (Fig. 4.2C). **N1** had a single phenotype (N_s) that was sensitive to predation by both *B. bacteriovorus* and halo-phage. **N2** had the sensitive phenotype (N_S) along with a second phenotype that was resistant to predation by halo-phage only (N_R). We assumed that a small fraction of the prey population (F_R) was initially resistant to phage predation and that further resistance occurred due to *de novo* mutations during the course of the experiment at a rate k_M. **N3** had the two phenotypes from **N2** and a third phenotype (N_P) that was plastically resistant to predation by *B. bacteriovorus*. We assumed that this plastic resistance arose

spontaneously (at a rate k_D) and that reversion to a sensitive phenotype (N_S) was coupled to growth. **N4** had the three phenotypes from **N3** and a fourth phenotype (N_D) that was resistant to predation by both *B. bacteriovorus* and halo-phage. None of the 1,000 successful fits of a model together with its parameter set (distance between model prediction and data below threshold) were for models **N1** or **N2**, indicating that these models were not supported by the experimental data. Variant **N3** was best supported by the experimental data, whilst variant **N4** received less support (Fig. 4.6A). Using the parameter values generated by fitting either of variant **N3** or variant **N4** predicted similarly low levels of doubly resistant prey at the end of the experiment when applied to the equations of variant **N4**. Variant **N4** fitted to all data predicted 0.26 colony forming units (cfu) ml^{-1}, while the same variant using parameters from fitting variant **N3** to all data predicted 0.0084 cfu ml^{-1}. Both are well below the detection threshold in the experiments (10 cfu ml^{-1}). Variant **N4** predicts double resistance to occur, albeit at a very low level; however, the data could not provide information to constrain this density. Due to these considerations and the aim to choose the minimum adequate model, the **N3** model variant was selected for further study.

4.3.2 Mechanism of plastic resistance generation

We then competed different variants of model **N3**, the best top-level model. These variants differed in the way the *B. bacteriovorus* plastic resistant prey (N_P) were generated from and reverted to sensitive prey (N_S) (Fig. 4.2Di). The simplest assumption termed **N3-I** (I for intrinsic conversion) was that the conversion process was intrinsic rather than triggered and that it occurred with certain rates in both directions. The 'plastic' resisters were allowed to grow at a rate that differed from sensitive prey by a factor η_P, which was fitted (Table 4.1) and could be smaller or larger than one. A second **N3** model variant **N3-IG** (IG for intrinsic conversion and growth coupled reversion of plastic resisters) also assumed that plastic resisters arose spontaneously, but that reversion to the sensitive phenotype was coupled to growth. The third model variant **N3-S** assumed that conversion to plastic resistance was triggered by a signal generated during the lysis of prey cells and that reversion to sensitive was again intrinsic. At this initial stage in the modelling, the signal was assumed to be generated by the lysis of bdelloplasts and phage infected cells. Plastic resistance has been previously described (Shemesh and Jurkevitch, 2004) as developing to *B. bacteriovorus* in predatory cultures, due to (as yet unidentified) molecular signals changing prey metabolism/development but it is not due to genetic changes in the prey as when those prey are grown in new cultures and re-challenged with *B. bacteriovorus* they are susceptible once more (Lambert, Chang, *et al.*, 2010).

As shown in Figs. 4.6B and 4.5B, the data gave no support for the simplest model **N3-I** but good support for the other two models, with model **N3-IG** being somewhat more likely than **N3-S**, given our experimental results. Since these two models had reasonable support, we constructed a new variant by combining the signal

assumption with the assumption of plastic resisters growing into sensitive prey at a certain rate (**N3-SG** for signal and growth coupled reversion). This merged model outcompeted the parent models (Figs. 4.6C and 4.5C), suggesting that signals triggering plastic resister formation are being generated and that reversion from plastic resisters back to sensitive cells is coupled to growth.

4.3.3 Source of signal

Since the merged **N3-SG** model was best supported by the data, we then compared sub-variants that differed in the source of the signal (see Fig. 4.2Di). This signal could in principle arise from prey actively responding to phage attack (**N3-SVG**, **SV** for Signal response to Virus) (or phage attack passively generating the signal – we do not distinguish these cases) or from prey actively responding to *B. bacteriovorus* attack (**N3-SBG**, **SB** for Signal response to *B. bacteriovorus*) (likewise, we do not distinguish active response from passive generation here), or both (the original **N3-SG** above). Competing these sub-variants, it is clear that phage generated signal alone cannot explain the data (Figs. 4.6D, 4.5D). This is expected as the plastic resisters do arise in cultures that contain only *B. bacteriovorus*. The other two sub-variants (**N3-SG** and **N3-SBG**) were both supported by the data (Figs. 4.6D, 4.5D). As the **N3-SG** model is a combination of the supported **N3-SBG** model and the unsupported **N3-SVG** model the **N3-SBG** model is logically the best choice.

4.3.4 Phage resistance mechanisms

We next investigated the mechanisms of phage resistance. We considered three possibilities (see Fig. 4.2Dii). Firstly that a small fraction (F_R) of the prey was already phage resistant at the start of the experiment, presumably having occurred

when the prey culture was grown overnight prior to the start of the experiment, consistent with the findings of Luria and Delbrück (1943) and that no further mutations occurred (**N3-SBG-RI**). Secondly, that at the start of the experiment all prey was sensitive and that resistance mutations arose *de novo* during the experiments, (**N3-SBG-RD**). Finally, a combination of these two possibilities, that there were phage resistant bacteria initially present, and that further mutations occurred over the course of the experiment (**N3-SBG-RID**). We found that a combination model (**N3-SBG-RID**) was best supported (Fig. 4.6E). There also was evidence of support for resistance being present initially only, but none for the model where all prey was initially phage sensitive (**N3-SBG-RD**).

4.3.5 Selection of predation kinetic response types

Finally, with the best resistance generating model variant (**N3-SBG-RID**), we asked whether the predator response would become saturated at high prey density. In the ecological literature, this is known as a Holling type II response, whereas the simpler mechanism that we refer to as type I assumes that rate of predation is proportional to the density of prey and predator without any saturation. Holling type II is mathematically identical to Michaelis-Menten kinetics, and shows saturation of predation at high prey densities. Competing the four possible combinations **Pi-Vi** (Predator and Virus of type I), **Pii-Vi**, **Pi-Vii** and **Pii-Vii**, we found that the combination **Pii-Vi** was the only one supported by the data (Fig. 4.6F). This suggests that *B. bacteriovorus* becomes saturated at higher prey densities but that the phage does not, at least in the range of prey densities used. Since the type II response can be derived by assuming that the predator requires a certain time to handle the prey (Jeschke *et*

al., 2002), this suggests that *B. bacteriovorus* requires a significant handling time while the phage's handling time is negligible, consistent with observations of *B. bacteriovorus* predation requiring between 10 and 30 minutes to attach to prey and enter the periplasm (Varon and Shilo, 1968; Hespell *et al.*, 1975). Once it had been established that the **Pii-Vi** type gave the best results, the previous levels of model selection were all re-run with this **Pii-Vi** type combination. This change of response type combination did not affect which of the higher-level models were best supported by the data. Fig. 4.6 actually shows the results of this rerun.

4.3.6 B. bacteriovorus mortality

As there was some discrepancy between the decline in *B. bacteriovorus* numbers predicted by the model and that seen in the experimental data, we decided to take the best model from the previous section (**N3-SBG-RID-Pii-Vi**) but now allowed *B. bacteriovorus* mortality to be fitted as an additional parameter. To confirm the improvement in fit justified the addition of an extra parameter we competed the model with and without variation in mortality and saw that all 1,000 successful fits came from the model where mortality had been fitted (Fig. 4.6G).

4.3.7 Performance of the best model

4.3.7.1 Fit of the best model variant to the complete data set

The best model (**N3-SBG-RID-Pii-Vi** with fitted mortality) was fitted to the whole data set. This was run for 13 generations to a final tolerance of 0.2, which was lower than the tolerances used for model selection. Using PCA of the parameter space (see section 4.3.11) a 'typical' parameter set was selected. Running a simulation with this parameter set shows how well the model fits the data (Fig. 4.7). Note that the

predicted substrate concentration was not measured experimentally. While the fit to prey decline in the presence of phage (Fig. 4.7C) and in the presence of both *B. bacteriovorus* and phage (Fig. 4.7D) is quite good, the fit of the prey decline in the presence of *B. bacteriovorus* only (Fig. 4.7B) is not as close as we would like. However, any other parameter sets that fitted this curve any better gave poorer fits to the other traces. Clearly, the best model did not give a completely satisfactory fit in all curves as the prey decline in Fig. 4.7B is too steep and the plateau level too high. Since none of the many models of plastic resister generation and back conversion to sensitive prey was able to produce a more gradual decline and entry into the plateau level (Fig. 4.7B), we suggest that differences between individual prey cells may cause a more gradual change, which could be investigated with an individual-based model in the future.

4.3.7.2 Fit of the best model variant to single predator data only

We asked whether fitting the best model (**N3-SBG-RID-Pii-Vi**) to single predator data only would produce a reasonable prediction for the dual predation experiment. As above, we used PCA to identify typical parameter sets. Fig. 4.7E-H shows that the model fitted to single predator data produces as good a fit as the same model fitted to all data. Both fits are very similar, the main difference is the fit to prey decline in the presence of *B. bacteriovorus* (panels B & F), which as discussed is not satisfactory in either case. This suggests that single predator experiments can predict dual predator experiments so there is no need to assume any interactions between the two predators.

4.3.8 Sub populations

The modelling also allowed for insights to be made into the individual sub-populations that comprised each bacterial population (Fig. 4.7I-L). The model for *B. bacteriovorus* only predation reveals that between 2 and 20 hours the *B. bacteriovorus* population is evenly split between equal numbers of free *B. bacteriovorus* and bdelloplasts. At 20 hours the numbers of bdelloplasts decline exponentially whilst free *B. bacteriovorus* increase a little (due to progeny release from bdelloplasts) and then decline again due to their mortality (Fig. 4.7J). This correlates to the rapid decline in prey numbers predicted by the model at 20 hours. Both the fully-susceptible and phage-resistant prey populations are significantly reduced at 20 hours, whilst the numbers of 'plastic'-resistant prey increase to become the predominant prey sub-population from this point onwards.

Modelling of predation by phage alone revealed that most prey killing (and conversion of prey into the 'infected prey' population happened within the first six hours (Fig. 4.7K). Whilst the susceptible prey population was reduced to below detectable levels by eight hours, the increase in phage-resistant prey started from the four hour timepoint, resulting in a final resistant prey population of approximately equal size to the initial predation-susceptible population. In Figs. 4.3B and 4.7L it is clear that *B. bacteriovorus* predation is responsible for clearing these phage resistant *E. coli* after they arise and that this action reduces the *E. coli* numbers to below 10 ml^{-1} by 14 h in the experimentation and by 16 h in the model (Fig. 4.3B and 4.7L).

In the modelling of dual predation, the phage is mostly responsible for the rapid drop in the concentration of the susceptible prey and the removal of the intermittently arising plastic *B. bacteriovorus* resistant prey, whilst *B. bacteriovorus* is

responsible for the removal of the phage resistant prey. All three prey populations are eradicated by the two predators together (Fig. 4.7L). Whilst the phage sub-population kinetics were very similar to those in the single predator model, the kinetics of the *B. bacteriovorus* population was significantly different to that for the *B. bacteriovorus* alone cases. The early transition of free *B. bacteriovorus* into bdelloplasts resembled that seen for the *B. bacteriovorus* alone up to the four hour timepoint. However, after four hours the bdelloplast population started to decline (as the bdelloplasts formed early on, lysed releasing free *B. bacteriovorus*) but the free *B. bacteriovorus* population did not rise to the same extent as in the *B. bacteriovorus* alone situation. This is likely due to the significant reduction in available prey for subsequent rounds of predation.

4.3.9 Dependence on initial densities

To understand the dependence of predation success on the initial densities of prey and predators, we used the model to predict the outcome if we varied one population at a time, increasing as well as decreasing initial densities 10-fold (Fig. 4.8). The time series of the three related traces (10-fold lower, normal and 10-fold higher initial densities) showed similar qualitative behaviour for cases with prey only and prey with a single predator. Here, the three traces either converged in the end, or their separation was less than the 10-fold initial separation. Prey could survive during dual predation if (i) the initial density of prey was too high, (ii) the initial density of B. bacteriovorus was too low, or (iii) the initial density of the phage was too high (Fig. 4.8F to H). The model can thus identify suitable densities of the predators to add for effective predation.

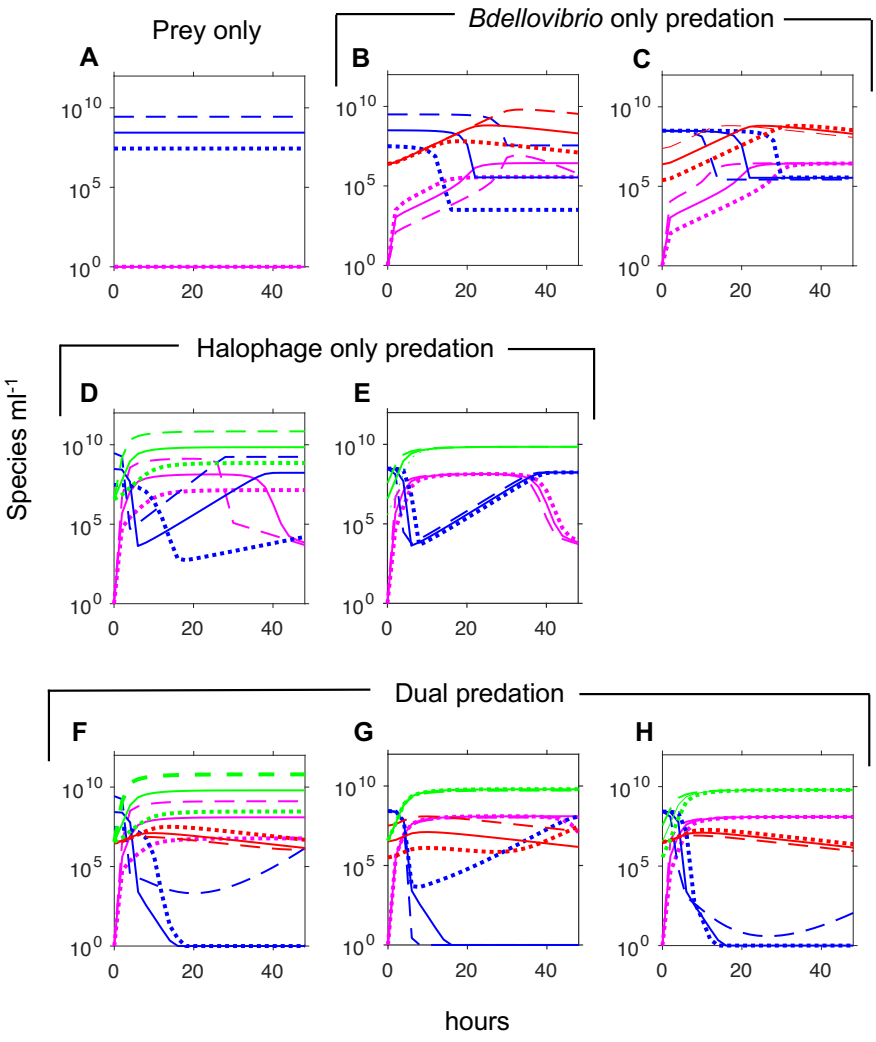

Figure 4.8 – Effect of varying initial densities.

The final model (**N3-SBG-RID-Pii-Vi**) was simulated using the typical parameter values fitted to all data in Table 4.1, with either initial values from the experimental data (solid lines), one order of magnitude higher than these values (dashed lines) or one order of magnitude lower (dotted lines). Blue: *E. coli* prey, Red: *B. bacteriovorus*, Green: bacteriophage halo, Pink: medium. **(A)** Effects of initial prey density on prey only scenario. **(B-C)** Effects of varying either initial prey **(B)** or initial *Bdellovibrio* **(C)** densities on *Bdellovibrio* only predation. **(D-E)** Effects of varying either initial prey **(D)** or initial halophage **(E)** densities on halo-phage only predation. **(F-H)** Effects of varying either initial prey **(F)**, initial *Bdellovibrio* **(G)** or initial halo-phage **(H)** densities on dual predation.

4.3.10 Validation of SMC-ABC fitting methodology

SMC works by selecting models and their parameter sets against an increasingly strict selection criterion (tolerance level). The models and parameter sets that met one tolerance level became the pool of models and parameters to draw upon for the next, stricter tolerance level. In our procedure, for each tolerance setting (generation), we selected for 1,000 parameters sets that were below the tolerance

set. To confirm that our selection process was working correctly, we examined a number of selection diagnostics. Firstly, for each generation, we constructed plots of the distance (see methods 4.3.2) between the data simulated based on each accepted parameter set and the experimental data set. These distances will always be less than the tolerance for that generation (as this is the criterion for their acceptance), however, with a well-chosen set of tolerance levels, the distances should initially be well spread-out, then gradually become closer to the tolerance setting with increasingly strict tolerance levels. Additionally, the minimum distance of the simulated data obtained from any accepted parameter set should decrease with increasingly stricter tolerance. A levelling of this trend would indicate that the tolerance level is close to the best fit that can be expected from this model within the parameter space being searched. As can be seen in Fig. 4.4, the distances of the simulated data from the observed data clustered closer to the tolerance limit as that limit decreased. Additionally, the lowest distance found decreased from approximately 0.36 at a tolerance limit of 0.6 to approximately 0.18 at a tolerance limit of 0.2.

As the model fitting procedure progressed through the generations, the range for each parameter that gave an acceptable match decreased. For certain parameters, this decrease was particularly noticeable, whereas for others the fitting procedure narrowed down acceptable values from the initial priors to a lesser extent (Fig. 4.9). The parameters for a type II functional response, i.e., the attack rate constant of the *B. bacteriovorus* (μ_P) and its half-saturation constant for its prey ($K_{N,P}$), both of which were not available in the literature, were significantly narrowed down and estimated for the first time. In contrast, the maturation rate of the bdelloplast (k_P), which was

already reasonably well known, and the nutrient release upon prey lysis by *B. bacteriovorus* ($Y_{M/P}$), which was poorly defined in the literature, were narrowed down to a lesser extent.

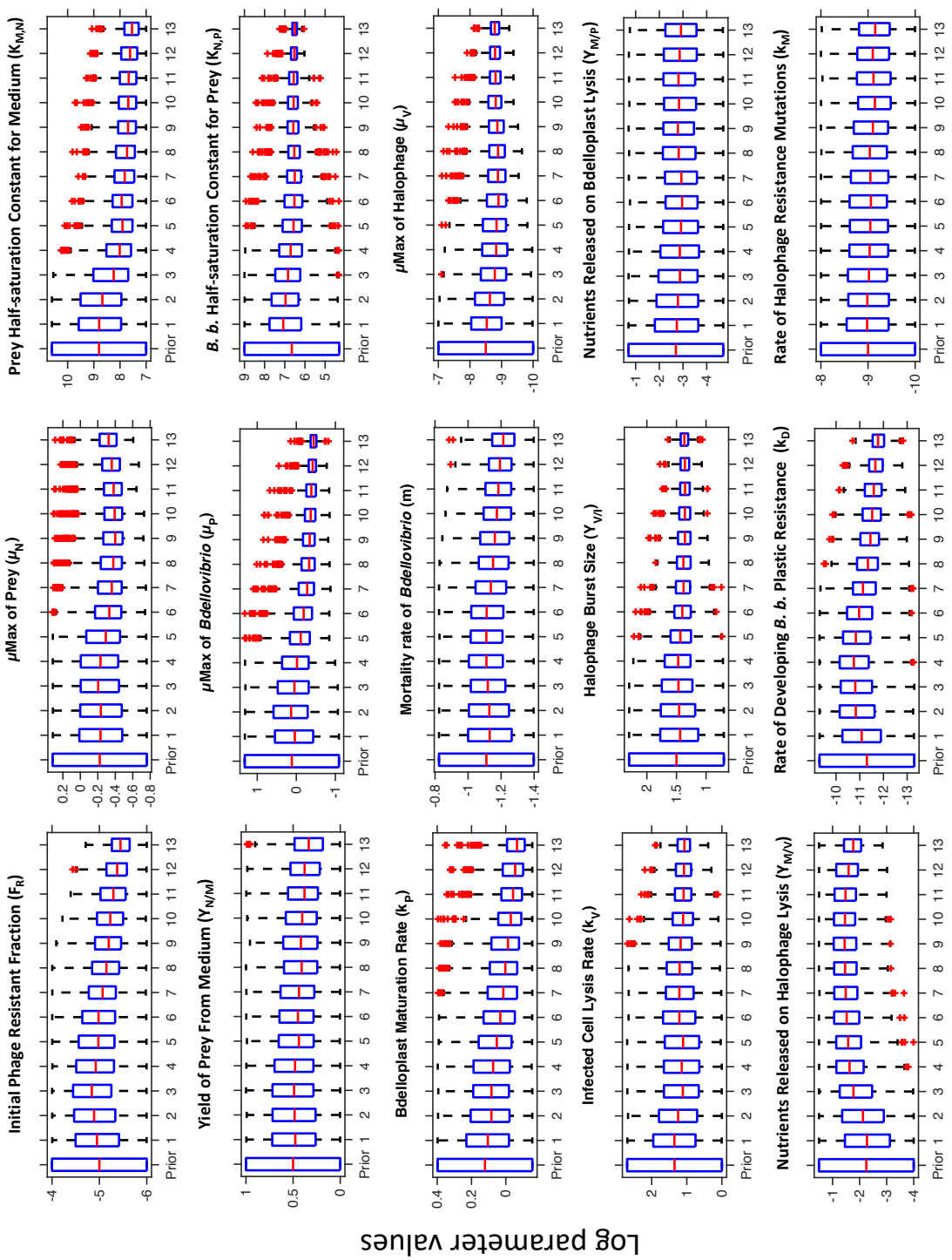

Figure 4.9 – Convergence of fitted parameters from generation to generation

Parameters are from fitting to final model (**N3-SBG-RID-Pii-Vi**). We started from the uniform priors to the values after the final generation 12. Parameters that are better informed by the experimental data reach a narrower spread of fitted values. Medians and quartiles from the final generation are shown in Table 4.1. Note the log scale for the parameters.

4.3.11 Choosing 'typical' parameter sets objectively

We also performed PCA of the accepted parameter sets for each generation, in order to objectively identify typical parameter sets (Fig. 4.10), for figures showing typical simulation results. From this analysis we selected four parameter sets as 'typical' (these were sets whose position in a plot of the first two principle components was nearest to the origin). With these parameter sets we simulated the model and plotted the results of these simulations against the observed data.

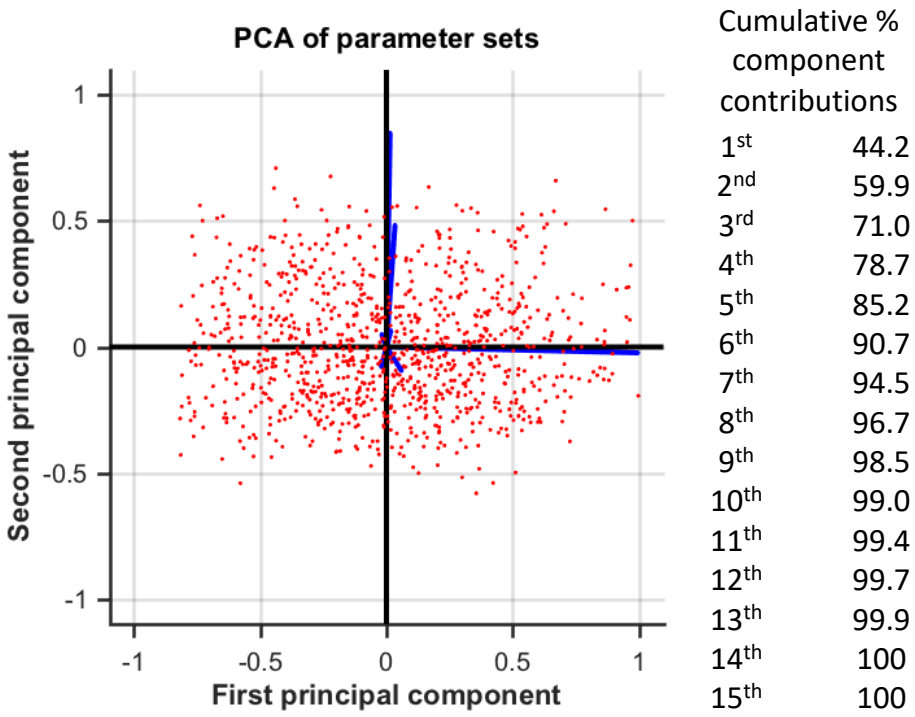

Figure 4.10 - Objective selection of a typical parameter set.

Selection was from the hundreds of parameter sets that gave acceptable fits and were nearly equally good (see Fig. 4.4). PCA was used to find the centre of the cloud of parameter sets in 15-dimensional parameter space. Four parameter sets that were closest to the centre were picked and used to run simulations. Results of these four simulations were indistinguishable by eye and one of these four parameter sets was then chosen as 'typical' and used in Fig. 4.7 and reported in Table 4.1.

4.3.12 Simulations fit better from generation to generation

Fig. 4.11 shows the results of simulations using such typical parameter sets from the first, two intermediate and the last generation. It can be seen that the simulations matched the observed data more closely with each generation of the fitting process.

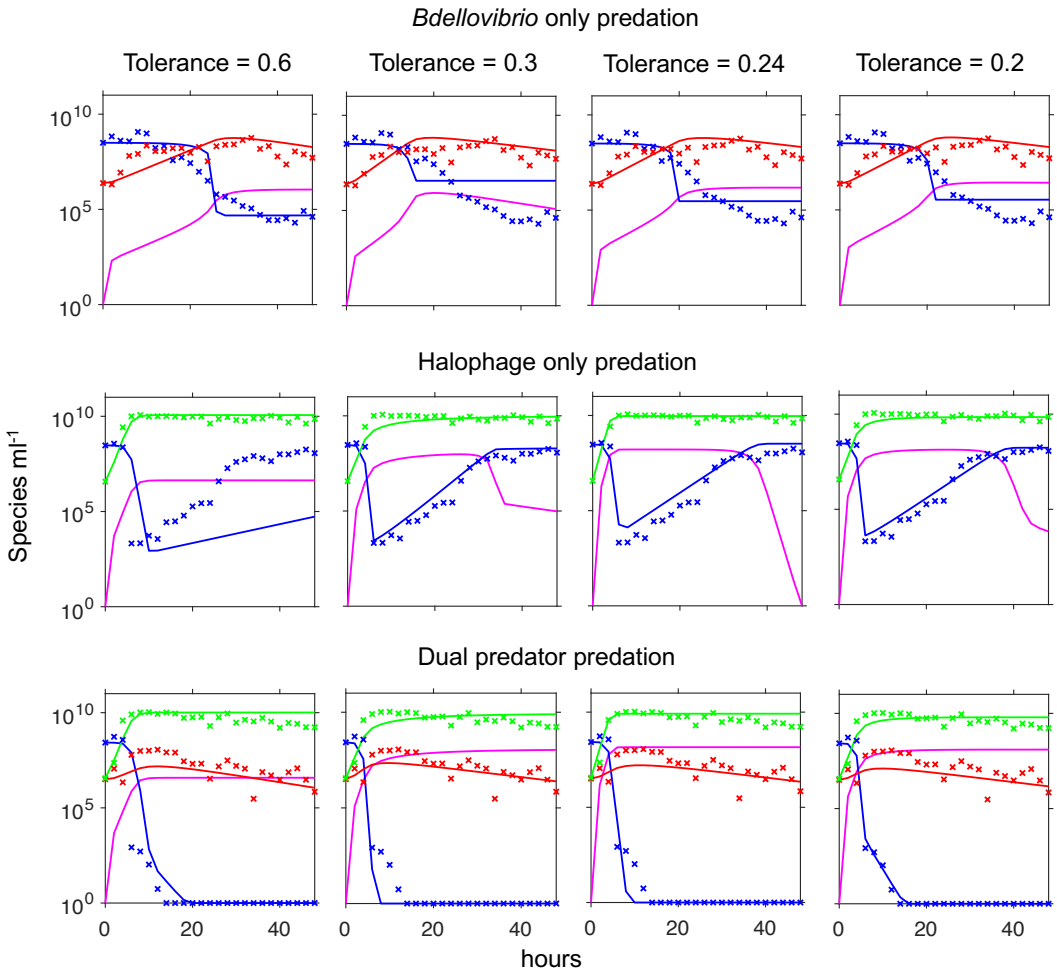

Figure 4.11 – Comparison of simulated and experimental data

Comparison shows that with increasingly strict (lower) tolerances the simulated data more closely matched the experimental data. Fitting is to final model **N3-SBG-RID-Pii-Vi** Left to right: simulation results based on a typical parameter set meeting increasingly strict tolerances. Pink – substrate, Blue – Prey, Red – *B. bacteriovorus*, Green – halo-phage. Solid lines are simulation results, symbols are experimental data.

4.3.13 Reproducibility of SMC Model Selection Results

Model selection by SMC or other procedures has an inherent element of stochasticity. This can result in either only one model receiving all the support, or that model receiving the strongest support, but there being some small element of support for a competing model. When two models have similar performance levels it can be down to chance which model is the most successful. To test for the reproducibility of model selection, each level of model selection was repeated ten times. With the final model selection level, deciding on the Holling types, all successful parameter sets corresponded to the *B. bacteriovorus* Holling type II and halo-phage Holling type I (**Pii-Vi**) model. For the other levels of model selection, the picture was more mixed with more than one model contributing to the final generation (Fig. 4.5).

The model selection process was also found to be robust with regard to small variations in the models. Model selection was first run with an initial fraction of the prey bacteria being resistant to phage, but no further resistance arising. Later all competitions were rerun with a combination of an initial phage resistant fraction and an ongoing rate of development of resistance (as this had outcompeted the initial resistance only model). In both these cases the outcome of subsequent lower level model selection was the same. Additionally, the model selection process was run with two different fixed values for the *B. bacteriovorus* burst size 3.5 (Seidler and Starr, 1969a) and 4.17 (Fenton, 2010) in both cases the same pattern of outcomes was observed.

4.3.14 Long term species trajectories

The laboratory experiments tracked the concentrations of bacteria and viruses over a 48-hour period, and the model is likewise valid over a similar time frame. However, we also ran the 'winning' **N3-SBG-RID-Pii-Vi** model with a typical parameter set over a 100-hour time period, to check whether the model would predict any unreasonable behaviour at a later time. As can be seen from Fig. 4.12, there was little change after 48 hours, except for *B. bacteriovorus,* which due to its mortality, continued to decline slowly, and the *E. coli* numbers in the dual predator scenario, which started to rebound after 48 hours. Further investigation of this rebound in the dual predator scenario revealed a range of behaviours for the *E. coli* concentrations. For some of the accepted parameter sets, prey numbers started to rebound soon after the initial 48-hour period. For others, simulations showed a prey rebound close to 100 hours, and for the final group of parameter sets, there was no sign of a rebound within 100 hours. This rebound is caused by a fall in the density of *B. bacteriovorus*, due to its intrinsically mortality, resulting in it being unable to control the phage resistant sub population of *E. coli*. A similar pattern is observed when initial densities of *B. bacteriovorus* are 10-fold lower (Fig. 4.8G). Note that a rebound from very low concentrations is possible in a mathematical model, but with real bacteria at least one cell is required and at very low concentrations stochastic noise is likely to result in complete extinction, especially if this situation continues over a substantial period of time.

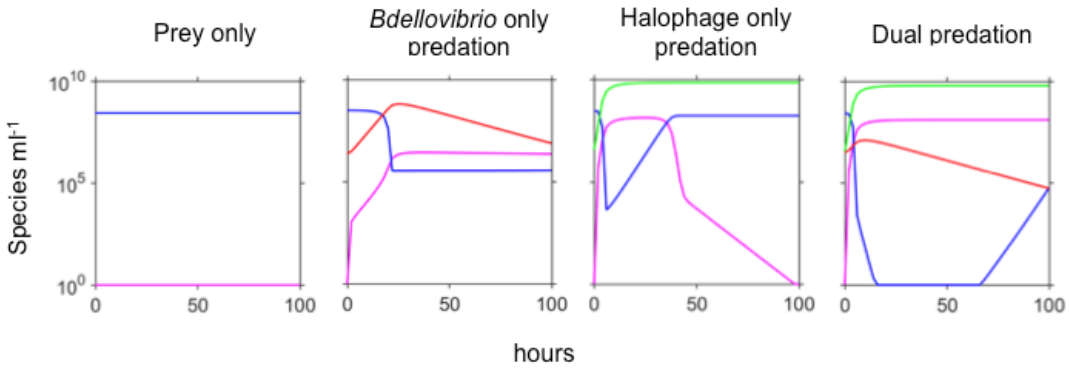

Figure 4.12 – Extending the model simulations to 100 hours

Beyond the 48 h time period of the experiments, the model shows behaviour in line with what might be expected. Most species change little after 48 h. *B. bacteriovorus* numbers continue to decline steadily due to their mortality and prey species numbers in the dual predator scenario eventually rebound (this is unlikely in reality as very low densities would correspond to less than one individual). Simulation based on a 'typical' accepted parameter set from the final (strictest tolerance) generation of running SMC on the most successful model – **N3-SBG-Pii-Vi**. Pink – substrate, Blue – Prey, Red – *B. bacteriovorus*, Green – halo-phage.

4.4 Discussion

Our modelling of dual predation on *E. coli* by *B. bacteriovorus* and a bacteriophage suggested that there were three prey phenotypes, one that could be predated by both predators, another that was resistant to phage predation, but could still be predated by *B. bacteriovorus* and the third had plastic resistance to *B. bacteriovorus* predation, but was still vulnerable to phage. Phage resistance via mutation is a well-established phenomenon (Luria and Delbrück, 1943). Frequently this is due to a mutation in a surface protein that acts as a receptor for the virus (Labrie *et al.*, 2010). This can result in a reduced growth rate, if for example, the mutation is in a nutrient transporter, or in increased susceptibility to antibiotics if an efflux pump is mutated. In this instance the Sockett lab reported that the mutation is in *fhuA*, a transporter of ferric hydroxamate, and so did not result in any reduction in growth as iron was not limiting in the experimental conditions.

Plastic resistance to *B. bacteriovorus* is a little studied phenomenon. Varon (1979) was the first to notice resistance of a prey species to a BALO. Subsequently, Shemesh and Jurkevitch (2004) found that when a population of *Erwinia carotovora* was predated by *B. bacteriovorus* strain SNE a small proportion of the *E. carotovora* survived and could regrow. When fresh *B. bacteriovorus* was added to these survivors they retained their immunity, but if they were grown in the absence of predators the new cultures were completely sensitive to predation. This is consistent with a phenotypic response triggered by either the presence of the *B. bacteriovorus* or by predation, but not with a genetic change that is inherited by subsequent generations. This phenotypic resistance could be the result of changes to the prey cell envelope, either the outer membrane or the peptidoglycan, resulting in reduced attachment of

B. bacteriovorus to the resistant prey or an increase in detachment before penetration occurs. It is known that changes to the lipid A of the prey change its susceptibility to predation. The absence of O-specific side chains increases attachment, whilst the absence of glucosamine reduces it (Varon and Shilo, 1969). Additionally, when *B. bacteriovorus* enters a prey cell it makes several changes to the structure of the prey peptidoglycan, which act as an occupancy signal to other *B. bacteriovorus* cells and prevent wasteful tailgating infections (Lerner *et al.*, 2012). We competed models in which plastic resistance to *B. bacteriovorus* arose and reverted in several different ways. We found that resistance triggered by a signal associated with predation, including *B. bacteriovorus* predation outcompeted intrinsic resistance. We also found that growth coupled reversion to sensitivity matched the data better than intrinsic reversion. This is consistent with a phenotypic response rather than genetically inherited resistance, where new growth would be expected to be resistant and reversion associated with a mutation. It is possible that a chemical released upon lysis of the bdelloplast at the completion of the predation cycle acts as a signal to other prey cells, triggering a stress response, resulting in an alteration to the prey cell envelope, which increases its resistance to predation at a cost of a reduced growth rate. Alternatively it is known that the initial stages of predation, before death of the prey cell, cause a large transcriptional response in *E. coli* prey cells (Lambert, Ivanov, *et al.*, 2010). It is possible that this response causes the secretion of a chemical that acts as a signal to other prey cells triggering a protective response. In either case when the prey is subsequently grown in the absence of predator the signal is no longer produced and the protect response would cease.

The results of the experimental data clearly showed that neither *B. bacteriovorus*, nor the bacteriophage alone was capable of eradicating the *E. coli* population. The bacteriophage caused a large (circa. 5 log units) and rapid drop in *E. coli* density, but this quickly recovered to levels comparable to the starting inoculum. With predation by *B. bacteriovorus* only, the fall in prey numbers was much slower, but did not show signs of a rebound, reaching a plateau approximately 4 log units less than the starting density. In each case the *E. coli* levels never fell below 10^3 cfu ml^{-1}. When combined however the initial rapid fall in prey numbers was followed by a second slower fall to below detection levels, where numbers stayed for the duration of the experiment.

Examining the sub-populations from the modelling simulations (something which would be very difficult to accomplish with live bacteria) offers an explanation for this behaviour. As expected, with the phage only predation the rebound is entirely due to the resistant population, and the sensitive population continues to decline at the same rate until it is below detection levels. With the *B. bacteriovorus* only predation by the end of the experiment the majority of the prey are plastically resistant to *B. bacteriovorus*, but there is also a surviving population of sensitive bacteria. To test the model predictions for sub populations with live bacteria it would be possible to track the bdelloplast population by using a strain of prey cell that expresses a fluorescent protein, and a *B. bacteriovorus* strain that expresses a different fluorescent protein, such as the strains described in Chapter 5. If these strains where observed under a microscope bdelloplasts would have a fluorescence signal consistent with both predator and prey (Kuru *et al.*, 2017). Similarly bacteriophage could either be tagged with a fluorescent marker or radiolabelled

(Hilgard and Stockert, 2000). Given that the mechanism of phage resistance is known it would be possible to track levels of phage resistant prey using quantitative reverse transcriptase polymerase chain reaction (qRT-PCR) to follow the expression levels of the mutated receptor (*fhuA*) (Gommersall *et al.*, 2007). Tracking levels of *B. bacteriovorus* plastic resistant prey however, would require greater knowledge of the resistance mechanism.

It has previously been proposed that *B. bacteriovorus* predation cannot remove prey levels below a certain density because it needs a certain size population of prey in order to allow *B. bacteriovorus* cells to find fresh prey cells before they starve (Hespell *et al.*, 1974). Without disputing this need to find fresh prey, our modelling analysis offers the intriguing possibility of a second reason why *B. bacteriovorus* does not reduce prey populations below a certain level. The presence of the inedible, plastic resistant bacteria acts as a refuge (Alexander, 1981). Growth of these resisters is coupled to their reversion to sensitivity giving a source of fresh sensitive bacteria. In turn these sensitive bacteria are predated by the *B. bacteriovorus* and so their populations levels are in a state of equilibrium. This effect can most clearly be seen by comparing the behaviour of the sensitive prey to the phage resistant population which does not interconvert with the plastic *B. bacteriovorus* resistant population and so does not have this refuge from *B. bacteriovorus* and is reduced to below detection levels. Prey levels in the simulations from Chapter 2 were reduced to much lower densities than seen in the *B. bacteriovorus* only simulations in this chapter, however in that case the model did not include any form of prey resistance.

The sub-populations data also offers insights into the total *E. coli* population levels in the dual predation scenario. The initial rapid fall in *E. coli* density is the

sensitive population being consumed by the phage, and this sub-population continues to drop at the same rate after the initial fall. The second, slower drop is due to the phage resistant prey being consumed by the *B. bacteriovorus.* This is happening at the same time that the phage resistant sub-population was starting its rapid increase in the halo-phage only predation scenario and over ten hours before this population started to decline in the *B. bacteriovorus* only predation. This earlier fall in the phage resistant sub-population in the dual predation scenario is due to the low density of the sensitive prey at this time point, which means the predation effect of *B. bacteriovorus* is focused on the phage resistant sub-population.

Our modelling of dual predation of *E. coli* by both *B. bacteriovorus* and a bacteriophage offers insights into this intriguing system, and helps to explain why the two predators can together reduce the prey population to below detection levels and prevent regrowth of prey over the duration of the experiment. We have also uncovered interesting aspects of the kinetics of predation and potential new insights into the population dynamics.

CHAPTER 5: DEVELOPMENT OF AN ARRAY OF SMALL CHEMOSTATS FOR BACTERIAL PREDATION

5.1 Introduction

The Gram-negative predatory bacterium *Bdellovibrio bacteriovorus* has been proposed as a potential alternative treatment for antibiotic resistant infections and to reduce densities of certain types of bacteria, for example coliforms, in environments such as waste water treatment plants. At the same time, a microbial predator with its high population size and short generation time offers unique opportunities to study predator prey ecology in a controlled environment. To fully exploit this potential however, we need to understand more about *Bdellovibrio* particularly the kinetics of its prey interactions. To date while a few studies have investigated predation by *Bdellovibrio* and like organisms (BALOs) in chemostats (Whitby, 1977; Varon, 1979; Dulos and Marchand, 1984; Varon *et al.*, 1984) most work has been undertaken in either biofilms or batch culture. Both of these systems have significant issues for understanding microbial kinetics. Biofilms are spatially structured environments where conditions and therefore growth and predation kinetics can vary dramatically between different regions. Batch cultures on the other hand are spatially homogeneous, but heterogeneous over time. As nutrients are used up growth conditions and kinetics change, making batch cultures unsuitable for longer term studies. Chemostats by contrast are designed to be spatially homogenous and to have constant inflow of fresh nutrients.

This constant inflow of nutrients means that chemostats can allow microbial communities to be studied in growth phase over extended periods of time. To study many different communities using these however, requires either multiple chemostats, or a long time span. In order to facilitate investigations into microbial

predator-prey dynamics I developed an array of inexpensive, self-built chemostats inspired by work from the Dunham lab (Miller *et al.*, 2013).

There were several requirements made for the chemostats.

1. Easy and relatively inexpensive to construct using materials available to most microbiology labs.
2. Small enough to fit many units into one water bath
3. Able to run reliably for several weeks at a time with minimal issues.
4. When assembled consist of a sealed unit that could be kept free from contamination.
5. All parts of the sealed unit had to be capable of withstanding an autoclave cycle.
6. Ability to enumerate bacterial densities without altering the volume of the chemostat.
7. Ability to inoculate the chemostat chambers without introducing risk of external contamination.
8. Avoid cross-contamination between chemostats.

The development of these chemostats followed an iterative process, whereby a design was constructed and tested initially with water, to check for structural issues with leakage and pressure. Subsequent tests involved first single species of bacteria, followed by a co-culture with a single predator and prey species, and finally co-cultures of a predator with multiple prey species. Issues and problems with a design were noted and improvements made to address these.

To take full advantage of the expanded capacity offered by the chemostat array I also needed to be able to process large numbers of samples in a timely manner.

Traditionally predator and prey densities in *Bdellovibrio* research are enumerated by plating prey bacteria on rich media (such as YT), and counting plaques formed by the predator (Williams, 1987; Shemesh and Jurkevitch, 2004; Kadouri and O'Toole, 2005). This is considered the gold standard method for the most accurate results; however, it has a number of issues which make it less suitable for work with an array of multi-prey species chemostats. Firstly, it is a time-consuming process that limits the number of samples that can be processed. Secondly, samples must be plated and plaqued immediately after sampling and cannot be stored for processing at a future date. Finally, plating on standard rich media such as YT or lysogeny broth (LB) cannot distinguish between different prey species, limiting prey quantification to knowing the total density of bacteria, without any information on the level of contribution from any given species.

The use of chromogenic agars to distinguish between colonies of bacterial species is a long established technique, with different agars being suitable for different purposes (MacConkey, 1905; Mossel *et al.*, 1962; Perry *et al.*, 1999). It is also possible to enumerate bacterial populations without the need for culturing by the use of methods such qualitative polymerase chain reaction (qPCR) and flow cytometry. qPCR has been used previously to enumerate BALO densities either by specifically amplifying the predator DNA and using SYBR green to bind in a non-specific manner (Zheng *et al.*, 2008; Shatzkes *et al.*, 2015) or by using a probe that binds to the amplified DNA only, allowing multiple species to be identified in one reaction (Van Essche, Quirynen, *et al.*, 2009; Van Essche, Sliepen, *et al.*, 2009). More recently flow cytometry assays have been developed for *Bdellovibrio*, using the presence of a fluorescent protein to aid in distinguishing this particularly small bacterium from signal

noise, caused by dust particles (Duncan *et al.*, 2018, 2019). I sought to investigate the use of these methods with a view to developing an assay that was accurate, sensitive, reliable and capable of handling a high throughput of fresh and frozen samples from mixed microbial communities.

To date most research into *Bdellovibrio* has focused on predation of a single prey species. However bacterial infections can involve multiple bacterial species and waste water treatment plants contain many different species. I therefore sought to develop a microbial community of two bacterial species that were potential prey for *Bdellovibrio* and a Gram-positive species that would act as a decoy (Wilkinson, 2001; Hobley *et al.*, 2006; Loozen *et al.*, 2015). As my model predicted that any oscillations were likely to have a period of over one hundred hours (cf. Chapter 2), I wanted to construct a community that could exist stably both in the presence and absence of *Bdellovibrio* for long periods of time. I also sought to ensure that any pair of prey and decoy species could co-exist to enable investigation of individual species interactions.

My research has led to the development of an array of 16 mini chemostats (20 ml volume in a 50 ml vessel) that can be easily and inexpensively constructed within most microbiology laboratories. The chemostats within this array can support single or multiple bacterial species including a predatory bacterium for over a month with minimal numbers of technical failures of individual chemostats. I also constructed a four species microbial community (two Gram-negative prey species, one Gram-positive decoy and a predatory bacterium) that can be co-cultured together for at least a month.

5.2 Methods

5.2.1 Media and strains used in experiments

Escherichia coli (*E. coli*) strain MG1655 (a K-12 derivative) was kindly supplied by Pete Lund (University of Birmingham, UK). Several fluorescent strains of *E. coli* were also used. All fluorescent *E. coli* were strain DH5α with a pBad plasmid encoding for ampicillin resistance as a selection marker, and an arabinose inducible, fluorescent protein (AddGene, Teddington, UK). The fluorescent *E. coli* strains had either mVenus, mOrange2 or mRuby2 as the fluorescent protein. *Pseudomonas putida* (*P. putida*) strain KT2440 with a constitutively expressed, chromosomally inserted, enhanced green fluorescent protein (eGFP) gene was kindly supplied by Victor De Lorenzo (Centro Nacional de Biotechnologica, Spain). iMG1655 and iKT2440 were derivatives evolved in our lab from MG1655 and KT2440 respectively (see results Section 5.3.4.2) as strains that were less prone to clumping under the chemostat conditions used in my experiments. A *Pseudomonas synxantha* strain (NCIMB 10586 DmmpB, DmacpE, mupUJ1), with two mutations that prevented production of mupirocin (*P. synxantha*) was kindly supplied by Chris Thomas (University of Birmingham, UK). *Bacillus subtilis* strain 167 (*B. subtilis*), supplied by the DSMZ strain collection (Leibniz, Germany), was used a non-prey decoy species.

The predator species was either *Bdellovibrio bacteriovorus* strain HD100 (*Bdellovibrio*) or *Bdellovibrio bacteriovorus* strain HD100 with a chromosomal insertion that constitutively expressed the mCherry2 fluorescent protein (mCherry *Bdellovibrio*). Both these strains were kindly supplied to me by the Sockett lab (University of Nottingham, UK).

5.2.2 Culturing methods

Prey and decoy species were maintained using methods previously described (Lambert and Sockett, 2008) in YT broth (8 g l^{-1} tryptone, 5 g l^{-1} bacto peptone, 5 g l^{-1} NaCl, pH 7.5) at 30° C with shaking at 150 rpm. When grown in chemostats prey and decoy species were grown at 30° C in either LB, (10 g l^{-1} tryptone, 5 g l^{-1} yeast extract, 5 g l^{-1} NaCl, pH 7.5) (Sambrook and Russel, 2001), supplemented with 0.1 mM $CaCl_2$ and 2mM $MgCl_2$ or in a minimal medium supplemented with 0.1 mM $CaCl_2$, 2mM $MgCl_2$, 1 ml l^{-1} SL-10 solution (Widdel *et al.*, 1983) (see Table 5.1) and with a carbon source. Two types of minimal media were used for the chemostats, M9 medium (Sambrook and Russel, 2001) (all concentrations are in g l^{-1}: 6 Na_2HPO_4, 3 KH_2PO_4, 0.5 NaCl, 1 NH_4Cl) and Davis Minimal Medium (Eisenstadt *et al.*, 1994) without citrate (DMM) (7 g l^{-1} K_2HPO_4, 2 g l^{-1} KH_2PO_4, 1 g l^{-1} $(NH_4)_2SO_4$).

Tyrosine was added to media before autoclaving (as it did not dissolve at room temperature). All other carbon sources as well as $CaCl_2$ and $MgCl_2$ were created as 100 x stock solutions and filter sterilised through a 0.22 µm filter then added to the medium in a sterile manner post autoclaving. SL-10 solution was also added after autoclaving.

Table 5.1 – Components of SL-10 solution

Component	Quantity (mg l^{-1})
$FeCl_2$	1500
$CoCl_2$	190
$MnCl_2$	100
$ZnCl_2$	70
H_3BO_3	6
Na_2MoO_4	36
$NiCl_2$	24
$CuCl_2$	2

Predators (*Bdellovibrio* and mCherry *Bdellovibrio*) were cultivated using methods previously described (Lambert and Sockett, 2008), 10 ml 4-(2-hydroxyethyl)-

1-piperazineethanesulfonic acid (HEPES), supplemented with 0.25 g l^{-1} $CaCl_2$, 3 ml of a stationary phase culture of *E. coli* MG1655 or *E. coli* iMG1655 and 100 µl of a previous predator lysate were placed in a 25 ml conical flask and incubated at 30° C, 150 rpm for 24 h to give a fresh predator lysate.

5.2.3 Viable counts

Viable counts of predators were obtained by performing a plaquing assay (Lambert and Sockett, 2008), to give a count of plaque forming units (pfu). The sample was first filtered through a 0.45 µm filter to remove any residual prey cells and diluted 10-fold as required to obtain a suitable dilution in HEPES buffer. 5 ml of 0.6% YPSC agar at approximately 55° C was combined with 100 µl of *E. coli* MG1655 or iMG1655 grown to stationary phase and 100 µl of the diluted sample to be assayed for predators and mixed by gentle inversion. This mixture was poured onto a 1% YPSC agar plate and allow to set for 20 minutes before inverting and incubating at 30° C for 3 to 10 days. YPSC agar consists of 1 g l^{-1} yeast extract, 1 g l^{-1} broadbean peptone, 0.5 g l^{-1} sodium acetate, 0.25 g l^{-1} $MgSO_4$ and 10 g l^{-1} technical agar, pH 7.6 (Sockett, R. E. personal communication). Samples were diluted 10-fold in HEPES to obtain useful concentrations of predators (20 – 200 pfu per plate).

Single prey and decoy species were enumerated by plating on 1.5% YT agar. To distinguish between different non-predatory species a modified version of MacConkey agar, without bile salts or crystal violet, was used. This consisted of 17 g l^{-1} bacto peptone, 10 g l^{-1} lactose, 5 g l^{-1} NaCl and 0.033 g l^{-1} neutral red.

5.2.4 qPCR

5.2.4.1 DNA extraction

Samples from chemostats for use in qPCR were routinely stored at -20° C before DNA extraction. Initially DNA was extracted by a simple detergent lysis boil (Reischl *et al.*, 2000). Briefly the culture was centrifuged at 13,000 g for 10 min to pellet. The pellet was resuspended in 200 µl of 1% triton X-100, 0.5% tween 80, 10 mM Tris-HCl (pH 8.0) and 1mM EDTA. The suspension was boiled at 100° C for 10 min, then centrifuged at 13,000 g for 2 min and the resulting supernatant stored at -20° C and used as a DNA template for qPCR.

As the initial extraction method did not produce DNA of a suitable quality and concentration for the subsequent qPCR, four different methods of extracting DNA from bacterial cells were tested on four bacterial samples. Each of the samples contained stationary phase cultures of *E. coli* MG1655, *P. putida* KT2440 and *B. subtilis* and a fresh lysate of *Bdellovibrio* (see 5.2.2). In order to determine if rare constituents of a mixed microbial sample could be detected, each sample consisted of equal amounts by volume (33% v/v each) of three of the bacterial species and a small volume (1% v/v) of the fourth species (see Table 5.2). The first extraction method tested was the original detergent boil lysis with an ethanol precipitation step added. Briefly 200 µl of lysis buffer was used for the initial extraction. After this was completed 400 µl of 100% ethanol and 20 µl sodium acetate were added and the sample incubated at -20° C for 20 min. The sample was then centrifuged at 13,000 g for 10 min and the supernatant discarded. The pellet was washed in 500 µl 100% ethanol and centrifuged

for 5 min at 13,000 g before discarding the supernatant and air drying for 10 min. When dry the pellet was resuspended in 100 µl nuclease free water.

Table 5.2 – Composition of samples used for testing DNA extraction techniques for qPCR.

Sample	*E. coli (%v/v)*	*P. putida (%v/v)*	*B. subtilis (%v/v)*	*Bdellovibrio (%v/v)*
1	33%	33%	33%	1%
2	33%	33%	1%	33%
3	33%	1%	33%	33%
4	1%	33%	33%	33%

The second method used enzymatic lysis, by Proteinase K and lysozyme, and heat to extract the DNA, and spin columns to remove impurities, and was performed using a GenElute bacterial genomic DNA kit (Sigma-Aldrich), following the manufacturer's instructions for Gram-positive bacteria and including RNaseA solution.

The third method used detergent lysis, bead beating and heat to extract the DNA, and precipitation and spin columns to remove impurities and was performed using a DNEasy UltraClean Microbial kit (Qiagen, Manchester, UK), following the manufacturer's instructions.

The final method used detergent and enzymatic lysis, and heat to extract the DNA, and spin columns to remove impurities and was performed using a QIAamp DNA mini kit (Qiagen), following the manufacturer's instructions.

After all extraction methods the resulting supernatant was stored at -20° C until required.

5.2.4.2 Probe based multiplex qPCR

All probe based qPCR assays were performed using an AriaMx machine (Agilent, Stockport, UK), with a reaction volume of 20 µl comprising 10 µl Luna qPCR probe mix (New England Biolabs, Hitchin, UK), 1.8 µl each of *Bdellovibrio* and *E. coli*

forward primer (10 µM) (Integrated DNA Technologies - IDT, Coralville, Iowa, USA), 1 µl each of *Bdellovibrio* and *E. coli* reverse primer (10 µM) (IDT), 0.4 µl each of *Bdellovibrio* and *E. coli* probes (10 µM) (IDT), 1 µl DNA template and 2.6 µl nuclease free water (nH_2O). Genes sequences for all primers and probes are listed in Table 5.3. qPCR reaction conditions were 3 minutes denaturation at 95° C, followed by either 40 or 45 cycles of 5 s at 95° C and 10 s at 60° C to anneal and a final elongation step at 72° C for 10 min. Three technical replicates of all reactions were performed. Primers, probes and reaction conditions were designed and optimised by Bamford (2016).

Table 5.3 – Gene sequences of primers and probes for qPCR

Primers and probes target unique gene sequences from the bacteria I used in multi-species community experiments. F = forward primer, R = reverse prime and P = probe

Organism	Target Gene	Reference		Sequence (5' – 3')	Tm (° C)	GC	Product size (bp)
Bdellovibrio bacteriovorus	16S rRNA	(Van Essche, Sliepen, *et al.*, 2009)	F	GGAGGCAGCAGTAGGGAATA	62.9	55.0%	181
			R	GCTAGGATCCCTCGTCTTACC	62.8	57.1%	
			P	TTCATCACTCACGCGGCGTCGCTG	71.9	62.5%	
Bacillus subtilis	16S rRNA	(Bamford, 2016)	F	CGTGTCGTGAGATGTTGGGT	64.1	55.0%	194
			R	GGTTTCGCTGCCCTTTGTTC	64.1	55.0%	
			P	AGTCCCGCAACGAGCGCAACCCTTGA			
Pseudomonas putida	gryB	(Bamford, 2016)	F	CTCCTCGGAGGTGAAAACCG	64.1	60.0%	187
			R	AGCGTCGATCATCTTGCCAA	64.2	50.0%	
			P	ACCCGAACGAGGCCAAGGCCGTCG	74.9	70.8%	
Escherichia coli	23S rRNA	(Chern *et al.*, 2011)	F	GGTAGAGCACTGTTTTGGCA	62.6	50.0%	81
			R	TGTCTCCCGTGATAACTTTCTC	61.6	45.5%	
			P	TCATCCCGACTTACCAACCCG	65.6	57.1%	

Table 5.4 – Setup of plate for initial qPCR.

Wells with no template control (NTC) are blue, those containing samples of *E. coli* (E) are pink and *Bdellovibrio* (B) are gold. Number refers to the number of times the sample was diluted 10-fold in nuclease free water.

	1	2	3	4	5	6	7	8	9	10	11	12
A	E	E	E	E -1	E -1	E -1	E -2	E -2	E -2	E -3	E -3	E -3
B	E -4	E -4	E -4	E -5	E -5	E -5	E -6	E -6	E -6	E -7	E -7	E -7
C	E -8	E -8	E -8	E -9	E -9	E -9	NTC	NTC	NTC			
D												
E	Bd	Bd	Bd	Bd -1	Bd -1	Bd -1	Bd -2	Bd -2	Bd -2	Bd -3	Bd -3	Bd -3
F	Bd -4	Bd -4	Bd -4	Bd -5	Bd -5	Bd -5	Bd -6	Bd -6	Bd -6	Bd -7	Bd -7	Bd -7
G	Bd -8	Bd -8	Bd -8	Bd -9	Bd -9	Bd -9						
H												

Table 5.5 – Setup of plate for qPCR with sample concentration.

Wells with no template control (NTC) are blue, those containing samples of *E. coli* (E) are pink and *P. putida* (P) are green. Number refers to the number of times the sample was diluted 10-fold in nuclease free water.

	1	2	3	4	5	6	7	8	9	10	11	12
A	E	E -1	E-2	E -3	E -4	E -5	E -6	E -7	E -8	E -9		NTC
B	E	E -1	E -2	E -3	E -4	E -5	E -6	E -7	E -8	E -9		NTC
C	E	E -1	E -2	E -3	E -4	E -5	E-6	E-7	E-8	E-9		NTC
D												
E	P	P-1	P-2	P-3	P-4	P-5	P-6	P-7	P-8	P-9		E-5D
F	P	P-1	P-2	P-3	P-4	P-5	P-6	P-7	P-8	P-9		E-5D
G	P	P-1	P-2	P-3	P-4	P-5	P-6	P-7	P-8	P-9		E-5D
H												

5.2.4.3 SYBR green singleplex qPCR

SYBR based qPCR assays were performed using either an AriaMx machine, or a Roche lightcycler (Roche, Basel, Switzerland). Reactions containing 10 µl Luna qPCR mix (NEB), 0.5 µl of 10 µM each of forward primer for the target bacterium (IDT) and

between 0.4 and 1 µl DNA template make up to a total volume of 20 µl with nH_2O. Sequences for all primers are listed in Table 5.3. qPCR reaction conditions were 3 minutes denaturisation at 95° C, followed by 45 cycles of 5 s at 95° C and 10 s at 60° C to anneal and a final elongation step at 72° C for 10 min. Three technical replicates of all reactions were performed. Primers and probes were designed by Bamford (2016).

Table 5.6 – Setup of plate for SYBR green singleplex qPCR.

Wells with no template control (NTC) are blue, those containing samples of *E. coli* (E) are pink. Number refers to the number of times the sample was diluted 10-fold in nuclease free water. H (high) indicates that 33% of the original bacterial sample volume was from an *E. coli* stationary phase culture. L (low) indicates that 1% volume was *E. coli*. Columns 1-3 are DNA extraction method 1, 4-6 – method 2, 7-9 method 3 and 10-12 method 4

	1	2	3	4	5	6	7	8	9	10	11	12
A	EH	EH	EH	EH	EH	EH	EH	EH	EH	EH	EH	EH
B	EH -1	EH -1	EH -1	EH -1	EH -1	EH -1	EH -1	EH -1	EH -1	EH -1	EH -1	EH -1
C	EL	EL	EL	EL	EL	EL	EL	EL	EL	EL	EL	EL
D	EL -1	EL -1	EL -1	EL -1	EL -1	EL -1	EL -1	EL -1	EL -1	EL -1	EL -1	EL -1
E	EL -2	EL -2	EL -2	EL -2	EL -2	EL -2	EL -2	EL -2	EL -2	EL -2	EL -2	EL- 2
F												
G												
H	NTC	NTC	NTC									

5.2.5 Flow cytometry

All flow cytometry experiments were performed on an Attune NxT flow cytometer (Thermo Fischer Scientific) with blue (480nm excitation) and yellow (561 nm excitation) lasers and BL1 (530/30), YL1 (585/16) and YL2 (620/15) filters. All samples were diluted to a maximum total density of approximately 9 x 10^6 colony forming units (cfu) ml^{-1} in phosphate buffered saline with 1 mM EDTA and 0.01% tween 80. A pure sample of each fluorescent species was used to set a detection

threshold using the signal in the appropriate filter channel for the fluorescent protein being expressed.

5.2.6 Cryo preservation of samples

Cryo stocks of *Bdellovibrio* were made by adding 150 µl 80% glycerol to 750 µl *Bdellovibrio* lysate mixing well and placing in a Nunc vial at –80° C. Cryo stocks of all other cultures were made by centrifuging at 13,000 g for 10 min to pellet and resuspending in 50% glycerol/50% YT before placing in a Nunc vial at -80° C.

5.2.7 Clumping quantifications

Levels of clumping in chemostats were determined after finishing the chemostat experiments. As much of the liquid phase as possible was carefully discarded without disturbing clumps or floating mats of bacterial growth. A tube was weighed and the remainder of the chemostat contents was transferred to this. The tube was spun at 1000 g for 1 minute to separate the clumped material from the liquid phase, while pelleting as few as possible of the planktonic cells. The remaining (still cloudy) liquid phase was discarded and the tube reweighed.

5.3 Results

5.3.1 Chemostat design

The chemostats were based on an existing design (Miller *et al.*, 2013), but adapted to suit the purposes of this study. The development progressed in an iterative manner, where one design was constructed as a prototype and tested. Issues with the design were noted and addressed in subsequent models. There were three main versions of the designs, with minor alterations being made to these (Table 5.7). The first version (Design 1) had many issues, could not be used to culture bacteria and failed within a week. The second version (Design 2) lasted longer, but still had issues which limited run time. The third version (Design 3) addressed these issues with additional improvements that meant chemostat arrays could run for over a month with few failures (Fig. 5.1).

Table 5.7 – Chemostat designs

Model	Air supply	Media supply	Air needle position	Media needle position
1	Branched after hydrator (Fig. 5.8a)	Branched after pump (Fig. 5.6a)	In culture (Fig. 5.3c)	Fully inserted (Fig. 5.3a)
2	Branched after hydrator (Fig. 5.8a)	Branched before pump (Fig. 5.6b)	In culture (Fig. 5.3c)	Just below stopper (Fig. 5.3b)
3	Branched on leaving hydrator (Fig. 5.8b)	Branched before pump (Fig. 5.6b)	In culture (Fig. 5.3c)	Just below stopper (Fig. 5.3b)
4	Branched on leaving hydrator (Fig. 5.8b)	Branched before pump (Fig. 5.6b)	Above level of culture (Fig. 5.3d)	Fully inserted (Fig. 5.3a)

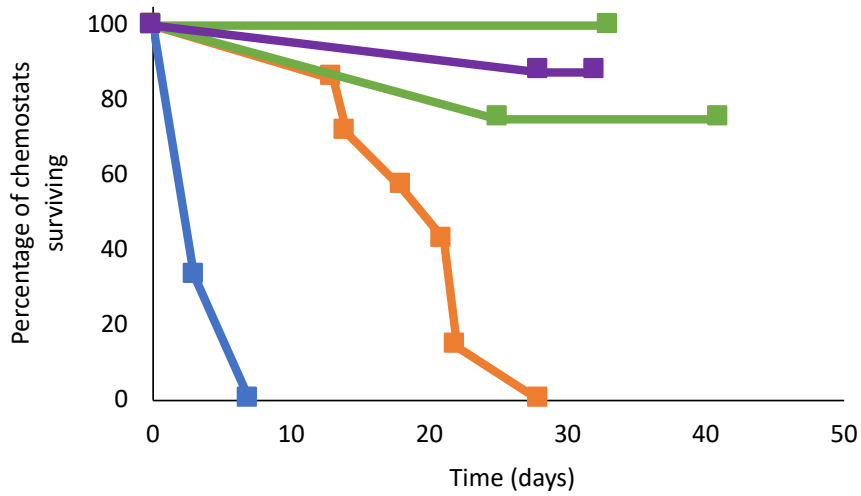

Figure 5.1 – Survival rate of chemostats.

Blue – Design 1, Orange – Design 2, Green Design 3, Purple Design 4. Chemostats were run with up to four aerobic or facultative aerobic bacterial species.

One remaining problem with Design 3 was growth on the media needle, which lead to back growth in the media input tubing (Fig. 5.2). To correct this in Design 4 the air needle was repositioned above the level of the culture (Fig. 5.3d). This did not affect the longevity of the chemostats, but did prevent visible signs of growth on the air and media needles and in the media line.

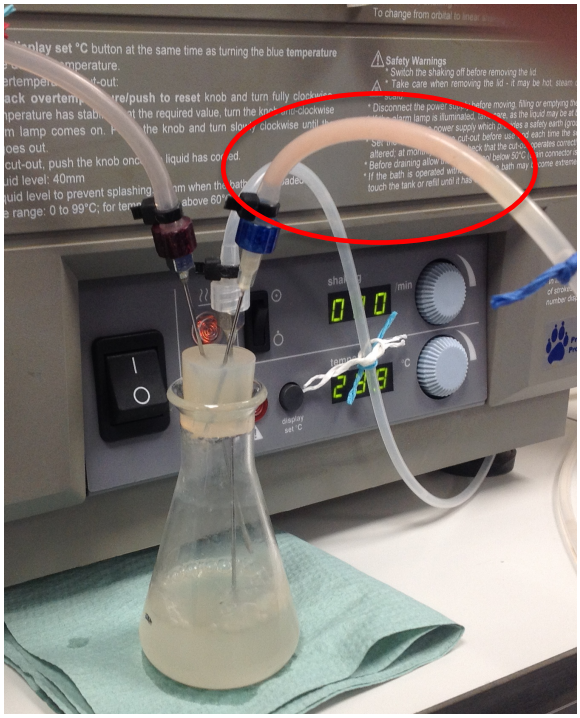

Figure 5.2 – Chemostat with culture

Single chemostat (Design 3) with a bacterial culture. Clear luer lock is the air supply, blue luer lock media and black is the waste efflux. Note the bacterial growth in the media line, as indicated by red ring.

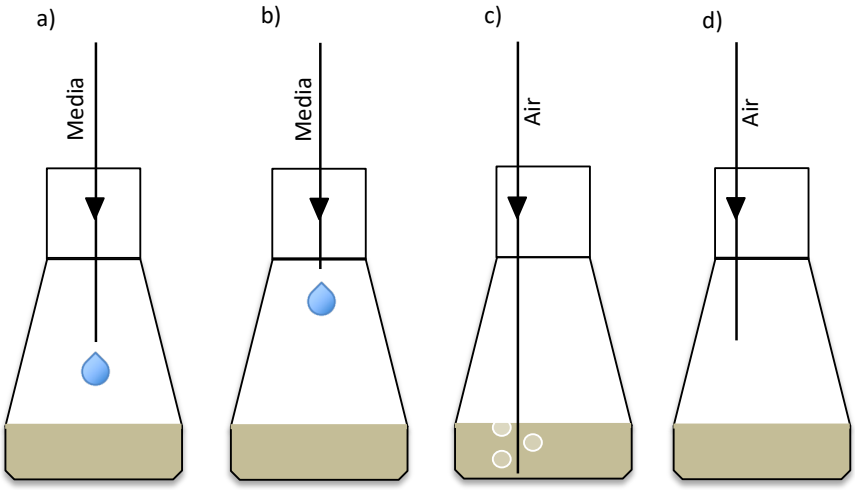

Figure 5.3 – Alternative positions for media and air needles

5.3.1.1 Chemostat vessels

50 ml glass conical flasks were chosen as the main vessels for the chemostats. These could contain a 20 ml volume of liquid with plenty of headspace to facilitate oxygenation of the cultures. After assembly chemostats were autoclaved to sterilise

and placed in a water bath to control temperature and provide an option to stir the vessel contents by shaking. An antimicrobial agent (aqua stabil) was also added to water bath to reduce risk of water contamination due to bacterial or fungal growth over long run times.

5.3.1.2 Flow of liquids and gases into and out of chemostats

The chemostat vessels needed to be sealed to prevent contamination, but still allow controlled access so fresh media and air could enter and excess volume leave the chemostat. To achieve this, I investigated using either a silicone stopper or a septum to seal the top of the flask, through which a set of needles could be inserted to allow for controlled inflow and outflow of liquids and gases (Fig. 5.4). Both of these devices could be autoclaved and each successfully sealed the flask. It was significantly easier to insert the needles through the septums than through the stoppers, however once inserted the needles were not held firmly enough and could move about to an unacceptable extent. Additionally, there appeared to be a loss of pressure in chemostats sealed with septums that did not occur with the stoppers. Because of this I decided to use the stoppers to seal the chemostat vessels.

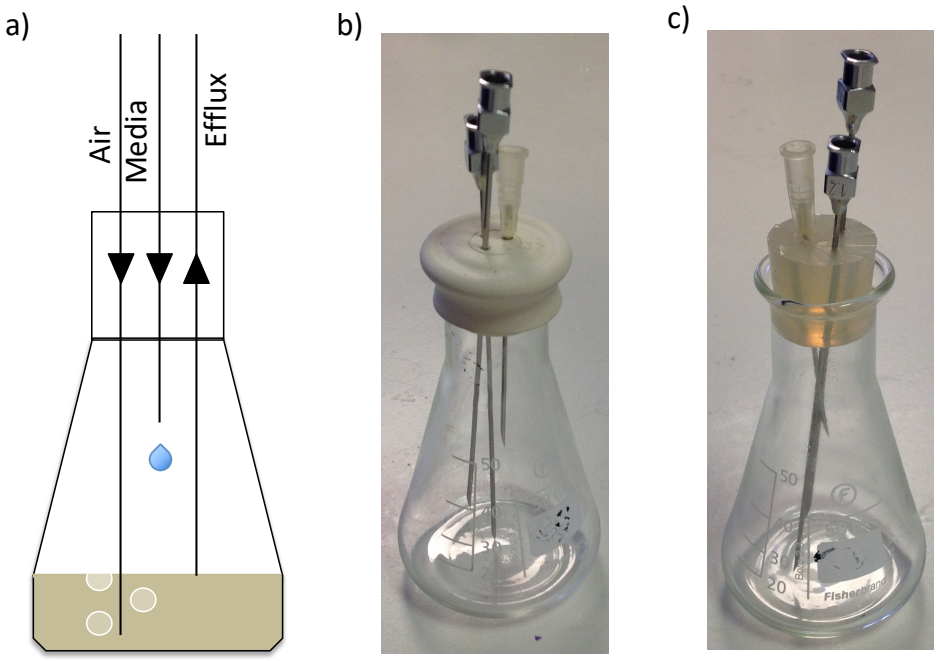

Figure 5.4 – Chemostat vessel design.

Panel (a) - Schematic design of the chemostat (with stirring provided by the air supply) (b) Actual chemostat enclosed with a septum (c) Enclosed by a silicone stopper.

Three sharp pointed needles were needed to deliver liquids and gases to and from the chemostat (Fig. 5.4). These were inserted evenly spaced, through the stopper in the same orientation for each chemostat. The needle used to deliver air into the chemostat was initially chosen to be long enough to reach the bottom of the chemostat so that the air coming into the chemostat could also stir the contents (Fig. 5.3c). For this purpose a 100 mm, 19G steel needle (Unimed, Lausanne, Switzerland) was chosen. The needle proved to be suitable for air delivery and the air supply mixed the contents well, however it also resulted in significant bubbling of the chemostat contents, which helped promote growth on the media needle. To reduce this the position of the needle was adjusted so that it was approximately 1-2 cm over the surface of the liquid (Fig. 5.3d). This allowed for delivery of air to the chemostat with

less bubbling of the vessel contents, resulting in less growth on the air and media needles.

The needle used to supply media to the chemostat needed only to be long enough to go fully through the stopper and a 2”, 19G disposable (Becton Dickenson) needle was used for this purpose. Two positions were compared for this needle (see Fig. 5.3a, b). With the needle pushed fully through the stopper, so that it was as far into the chemostat vessel as possible, it was closer to the culture within the chemostat. This meant it was more exposed to any aerosolised liquids, which could promote bacterial growth on the needle. The alternative position tried was furthest from the culture within the flask, however it resulted in bacterial growth on the stopper around the area of the needle and increased bacterial growth on the needle, which could in turn lead to contamination of the media line (Fig. 5.2). Because of this the fully inserted position was chosen as the optimal position.

The media and air pumped into the chemostat flasks caused pressure within the vessels to increase. To release this pressure, and keep the volume of liquid within the flask constant, a third needle was inserted, through which excess air and liquid could be vented. A 3” 19G steel needle was used for this purpose and positioned so that the tip was level with the top of the liquid when there was 20 ml of liquid culture within the flask.

Initially (Design 1) all needles were connected to tubing using connectors which did not screw into the needles and had no barbs. These quickly disconnected under pressure and were replaced (chemostat models 2 & 3) with autoclavable, nylon luer locks which screwed onto the needles and had barbs on the other end. These were cable tied to 3 mm internal diameter (ID) silicone tubing, which ensured there

was no leakage of liquids, and pressures within the tubing did not cause any of the junctions to disconnect. The luer locks were also colour coded, to allow for quick identification of the needles within an array of chemostats.

5.3.1.3 Chemostats could be mixed with aeration or shaking

When fresh media dropped into my chemostats it created a microenvironment in the region where it landed, where nutrient levels increased transiently. To remove this and ensure the whole chemostat environment remained homogenous it was necessary to ensure through mixing of the chemostat contents. In Design 1, 2 & 3 this mixing was provided by the air entering the chemostat at the bottom of the culture vessel. To confirm that air entry caused thorough mixing of the chemostat contents, a chemostat was constructed and filled with water. Once the air supply to the chemostat had been started a drop of blue dye was added and the time for the dye to be evenly distributed was noted. When the air needle was positioned at the bottom of the flask the dye was distributed throughout the contents of the chemostat within 1 minute of its addition. If the needle was positioned slightly higher within the vessel mixing was only effective above the position of the needle. In Design 4 shaking of the water bath (at 100 rpm) was used to mix the chemostat contents. Again, a drop of blue dye was added to a test chemostat with 20 ml of water and the time for it to be thoroughly mixed noted. Once again, the dye appeared to be evenly distributed over the chemostat contents within one minute. Because shaking of the chemostat contents resulted in changes in the level of the liquid within different parts of the chemostat it caused increased efflux of chemostat content through the efflux needle. However, it proved possible to compensate for this by adjusting the position of the

efflux needle upwards, so that the volume of liquid within the chemostat was maintained at 20 ml. Shaking the chemostats resulted in a mixing of their contents that was comparable to that obtained by mixing through aeration, without any loss of volume control and with the benefit of reduced aerosolisation of the cultures and reduced growth on the air and media delivery needles. Accordingly, mixing of the chemostat contents by shaking is my recommended method and was used in subsequent experiments.

5.3.1.4 Media supply

5.3.1.4.1 Choice of carboy design

Media for the chemostat was supplied from a carboy of between 10 and 20 l capacity. Where possible, components of the media were mixed in the carboy before autoclaving. As some of the components could not be autoclaved, they were instead filter sterilised through a 0.22 µm filter, and added to the chemostat after autoclaving, through the media input tube. Several designs were tried for the carboy (Fig. 5.5). When a side outlet was used it was prone to leakage and the stopper could be lost from the carboy during autoclaving, so a carboy with a single entry at the top was used instead. The stopper of the carboy also had a tube leading to a 0.22 µm filter to allow pressure with the carboy to equilibrate both during autoclaving and whilst the chemostats were running. The third opening was connected on both sides to 8 mm ID silicone tubing through which media was supplied to the chemostats. This tubing needed to be clamped on the outside of the carboy to prevent loss of liquid from the carboy during autoclaving. The external end of this tubing was connected to a female quick connector to allow quick and easy changing of carboy during chemostat running,

if extra media was required. To prevent contamination through this port it was covered with non-absorbent cotton wool and aluminium foil during autoclaving. This carboy designed allowed media to be supplied to the chemostat array for over a month at a time, with minimal risk of contamination.

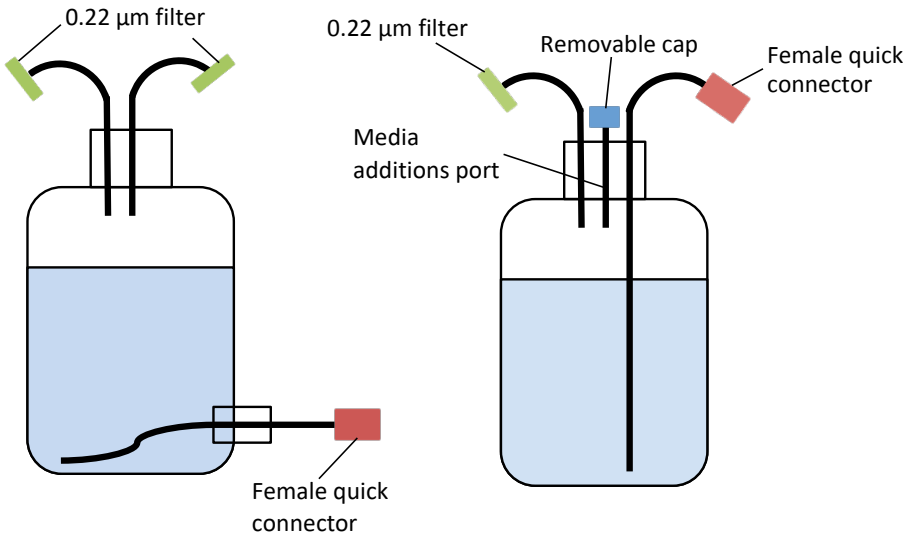

Figure 5.5 – Carboy designs
Left – initial carboy design with a side spout for media delivery to chemostats. Right – Later design without side spout (to avoid issues with leakage) and the inclusion of a glass tube with a metal screw cap as a port for additions of supplements to the media after autoclaving.

5.3.1.4.2 Media flow required a multi-channel pump

To ensure that media flowed into the chemostats at a steady rate it was necessary to control the flow rate using a pump. The use of hydrostatic pressure to supply media, with a clamp on the tubing to control the flow was considered, but was rejected as it was not possible to control the media flow with sufficient accuracy or precision. Additionally, the flow rate would inevitably have changed during the life span of an experiment, as the reduction in media left in the supply vessel (carboy) caused a decrease in hydrostatic pressure that it was not possible to compensate for by adjusting the clamps.

Initially (Design 1) a single channel peristaltic pump was used to supply liquid to multiple chemostats, with the media supply branching after the pump (Fig. 5.6a). Small differences in tubing and/or needles and in the pressure levels within a chemostat, lead to very different flow rates to the chemostats, with some chemostats receiving little or no flow. Attempts to compensate for this, using clamps to help control flow rates, were unsuccessful. Additionally, splitting the tubing after the pump left the system more vulnerable to cross-contamination due to bacterial growth on the media spreading backwards up the media tubing (Fig. 5.2). Therefore, it was deemed that each chemostat needed a separate pump channel (Fig. 5.6b).

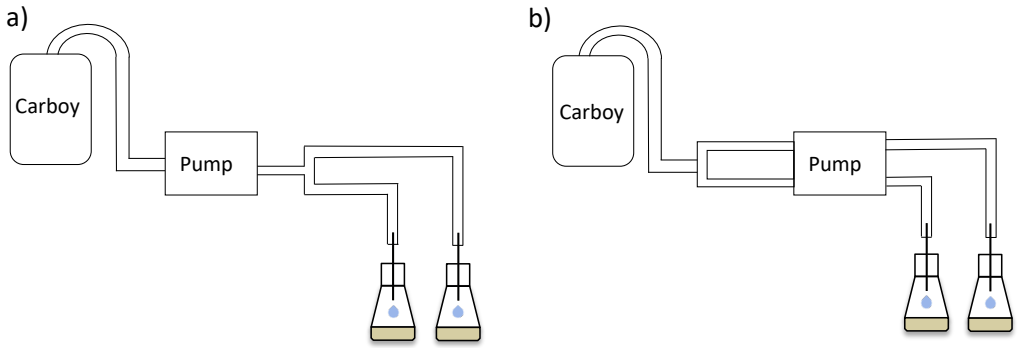

Figure 5.6 – Tubing for chemostat media supply

Panel (a) Design 1 – media tubing was initially split into different tubes for each chemostat after passing through the media pump. This gave issues with increased cross-contamination and uneven flow into each chemostat. Panel (b) Designs 2, 3 & 4 – media tubing was split before the pump and each chemostat had a dedicated pump channel.

A sixteen-channel pump (Watson Marlow, Falmouth, UK) was used for all subsequent experiments.

The pump speed required for a certain flow rate depends on the diameter of tubing used within the pump, with wider tubing giving a faster flow rate for the same pump settings. The pump was calibrated to give a number of different flow rates for two types of tubing. With 0.25 mm tubing the flow rate was 0.26 x the rpm ml h^{-1}. With the 3 mm tubing it was 5 x rpm ml h^{-1}. These flow rates were accurate for faster

flow rates and with short lengths of tubing between the carboy and the pump. Slower flow rates and longer lengths of tubing caused flow rates to become reduced and more erratic over time as air bubbles developed in the tubing (Fig. 5.7).

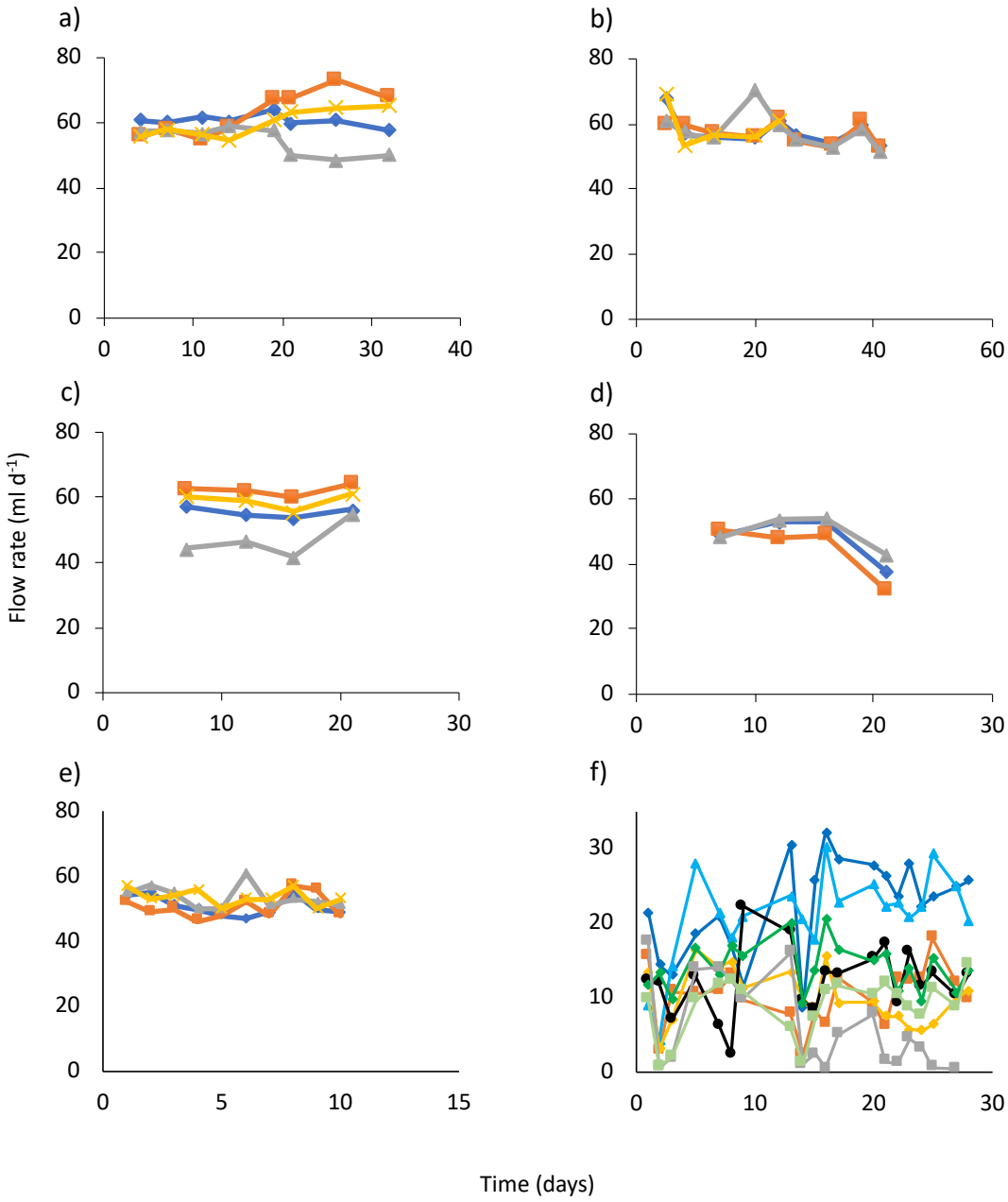

Figure 5.7 – Average chemostat flow rates

Flow rates were calculated from volume collected in waste bottles. Results are from chemostat runs of up to 41 days. Panels (a-e) initially involved an array of 4 chemostats, although in some instances technical issues resulted in the early termination of a chemostat, the target flow rate for these chemostats was 60 ml d^{-1}. Panel (f) had 8 chemostats with a target flow rate of 14.4 ml d^{-1}. Panel (a) *E. coli* MG1655, *P. putida* KT2440 and *B. subtilis* 167. Panel (b) *E. coli* and *P. putida*. Panel (c) *P. putida* and *B. subtilis*. Panel (d) *E. coli* and *B. subtilis*. Panels (e, f) *E. coli*.

5.3.1.4.3 Media tubing

The glass tubes through the carboy stopper were sufficiently large that 6 mm ID silicone tubing was required to ensure a tight fit that prevented any leaks or significant loss of pressure. This was connected to a female quick connector to allow the carboy to be autoclaved separately from the rest of the chemostat setup and allow a smooth and quick change of carboys if additional media was required during a chemostat run. A male quick connector, that fitted into the female quick connector was attached to a second piece of 6 mm ID silicone tubing. This tubing was too large for the pump and would have resulted in too fast a flow rate even on the lowest pump setting. To allow the use of small diameter tubing, the 6 mm ID tubing was connected to a reducing connector, the other end of this was connected to 3 mm ID silicone tubing. For the faster flow rates this diameter tubing was also used within the media pump. For slower flow rates 0.25 mm ID, marprene tubing (Watson Marlow) was used. This was connected to the 3 mm tubing by placing a 0.5" 27G blunt needle in each end of the marprene tubing to which a luer lock was attached. The 3 mm tubing was attached to the luer locks.

5.3.1.5 Aeration of chemostats

5.3.1.5.1 Air supply required an aquarium pump and stone

As the bacteria being cultivated were aerobes or facultative aerobes it was necessary to ensure a constant supply of air to the culture vessels. To ensure there was no loss of culture volume, due to evaporation, the air also needed to be hydrated. Hydration of the air was ensured by pumping it through an aquarium stone in a flask

of water. The aquarium stone ensured the air stream was turned into small bubbles for additional hydration. Hydrated air was then passed through a 0.22 µm, polytetrafluoroethylene (PTFE), autoclavable filter. With Designs 1 and 2 a single air line out of the hydrator was split before delivery to the chemostat vessels. However, this led to issues with cross-contamination between the chemostats, especially if there was any backflow of liquid into the air lines, due to loss of air pressure. To prevent this in Designs 3 and 4 each chemostat had a separate air supply from the hydrator, with its own 0.22 µm filter. (Fig. 5.8). With both systems there was considerable variation in the flow rate of air to each chemostat and the exact flow rate for the air supply was unknown, however each chemostat, including those with the least flow received sufficient air to ensure thorough mixing of the chemostat contents.

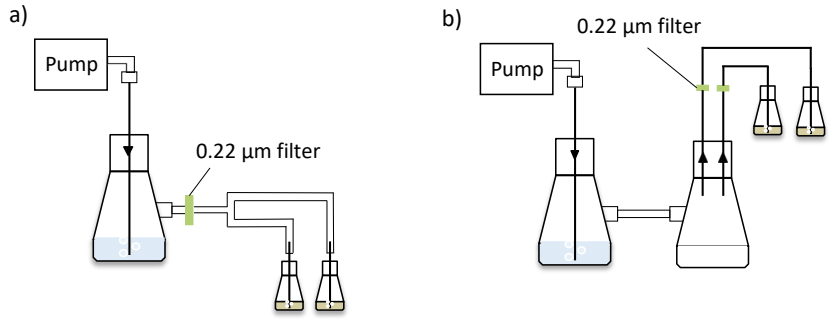

Figure 5.8 – Air supply to chemostats

In Designs 1 and 2 air tubing was split into different tubes for each chemostat after passing through the hydrator and 0.22 µm filter – panel (a). As this gave issues with increased cross-contamination and uneven flow into each chemostat for Designs 3 and 4 the air flow out of the hydrator was directed to a second side-arm flask sealed with a septum. The air was supplied separately to each chemostat by connecting the air tubing for each chemostat to a separate 0.22 µm filter attached to a 2" 19G needle, which was inserted through the septum – panel (b).

5.3.1.6 Pressure within chemostats regulated volume

Excess liquids and gases were expelled from the culture vessel through the efflux needle due to the positive pressure within the chemostat. These then flowed through a section of 3 mm ID silicone tubing connected via a cable tied luer lock to

another 2” 19G disposable needle. This needle was inserted through a size 29 rubber stopper in a 500 ml Duran bottle. A second 2” 19G needle inserted through the stopper and connected on the outside to a 0.22 µm filter via a luer lock and a short piece of 3 mm ID silicone tubing allowed pressure within the bottle to be released without either permitting escape of cultured organisms or external contamination of the waste bottle.

A 500 ml volume bottle was chosen so that it could collect waste from several days of chemostat operation before needing to be emptied. Because the waste bottle had a large volume (500 ml) relative to the chemostat vessel (50 ml) the expansion of air within the bottle during autoclaving could cause a build-up of pressure with the chemostats sufficient to force the stoppers out of the flasks and break the sterile seal. To prevent this the tubing between the two vessels was clamped close to the waste collection bottle prior to autoclaving, forcing the excess pressure to vent via the attached filter.

During long runs of the chemostat arrays there were issues with biofilm growth on the efflux needles, particularly in the absence of predators (which reduced the level of biofilm formation). Despite this, the volume levels, in a majority of chemostats, could be kept constant through the outflow of excess fluids via the efflux needle over the duration of the predation and co-culture experiments.

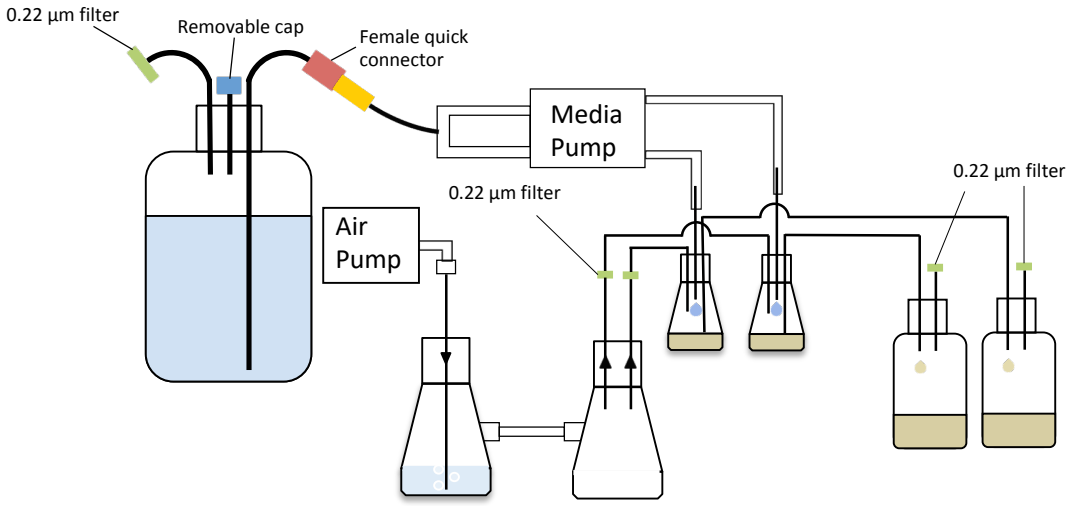

Figure 5.9 – Final chemostat design – Design 4.

5.3.1.7 Chemostats were inoculated by injection

The chemostat apparatus was constructed as a complete unit, then autoclaved, before connecting to the media source. It was then necessary to introduce the bacteria to be cultured within the vessels without causing a loss of sterility. To do this 1 ml of the chosen inoculum was drawn up into a 1 ml syringe, which was then attached to a 1.5" 21G needle and injected into the chemostat flask through the stopper. This successfully introduced the bacteria into the flasks with a minimal risk of contamination.

5.3.1.8 Ongoing issues

5.3.1.8.1 Air and venting filters tended to block

The 0.22 µm filters sterilising the air going into the chemostats tended to clog over time when exposed to damp air, resulting in the system not flowing. This was also true of the filters sealing the waste bottle venting tubes, which were especially prone to clog as the damp air they encountered contained particles of spent media and bacterial cultures. The issue with the air supply filters was a particular problem as

replacement of these came with a high risk of contaminating the chemostats with environmental microbes.

5.3.1.8.2 Biofilms built up on needles

Formation of biofilms on the air, efflux and media needles during the running of a chemostat was a significant issue. The build-up of biofilms meant that the system acted less like an ideal chemostat, especially in the case of the media needle where bacteria growing in the biofilm had preferential access to fresh media and would have reduced the nutrient levels entering the main chemostat liquid phase. Additionally, the physical presence of the biofilm caused blockages that could prevent the flow of liquids or gases within the system. Biofilm build up on the needles was reduced and the lifespan of chemostats increased by the presence of *Bdellovibrio*. Build up on the media and air needles was greatly reduced by altering the position of the air needle from the bottom of the chemostat vessel (Designs 1, 2 & 3) to the air void above the surface of the needle (Design 4) (Fig. 5.3c, d). Build up however, still occurred on the waste needle, which need to be in contact with the surface of the liquid.

5.3.1.8.3 Biofilms grew on chemostat walls

Biofilm growth on the walls of the chemostat vessels meant they acted less like ideal chemostats. The growth increased over the lifetime of a chemostat and was highest when nutrient levels, and therefore overall bacterial density was greatest, while the presence of *Bdellovibrio* acted to reduce wall growth. This reduction in wall growth in the presence of the predator is to be expected, as the concentration of prey there acts as a source of nutrients for the predator. This in turn results in increased predator growth, at the expense of the prey biofilm, as has previously been seen in

other studies (Kadouri and O'Toole, 2005; Núñez *et al.*, 2005). This effectively creates a second compartment within the chemostat vessels that acts as an additional source of both predator and prey.

5.3.1.8.4 Sampling caused blockage of the waste bottle needle

Samples were taken from the waste line by removing the needle from the waste bottle stopper and placing it through the septum of the sampling bottle. After sampling the process was reversed and the needle replaced in the waste bottle stopper. Pushing the needle through this stopper frequently resulted in small pieces of the stopper being retained in the needle, which could cause a blockage of the needle and prevented the chemostat system from flowing.

5.3.2 Quantification of bacteria

When growing a single species monoculture within a chemostat it is sometimes possible to follow growth levels without sampling by monitoring the optical density (OD) of the culture. With co-cultures however, this is not possible as the OD will only give an indication of total biomass, not which species are contributing to it or by how much. Additionally, the same number of viable bacteria of different species can have different biomass and even the same amount of biomass distributed differently can scatter light differently, resulting in a different OD. There is a further problem when using *Bdellovibrio* as these bacteria are so small that they have a negligible effect on the OD at 600 nm (the wavelength at which bacterial growth is commonly monitored). I therefore needed to develop another method for rapid and accurate quantification of multiple bacterial species in co-culture.

5.3.2.1 Sampling

As growth of all species could not be reliably followed using OD and I did not wish to alter the culture volume in the chemostat, the decision was made to sample the waste products coming out of each chemostat. In an ideal chemostat the culture entering the tip of the waste needle is a random sample that is representative of the contents of that vessel at that moment in time. Typically, it took less than 5 seconds for liquids to travel the length of tubing from the waste needle to the sampling bottle, so the bacteria entering the sample should at that moment also be representative of the chemostat contents. A sample size of 1 ml was sufficient for all monitoring purposes. To collect the sample with minimal risk of contamination I used 2 ml glass screw top bottles with a thin silicone septum in the lid (Thermo Fisher Scientific). These were autoclaved to sterilise and dried in a 60° C oven to remove any residual moisture that could dilute samples. The bottles were packed in ice to minimise any metabolic activity during sampling and a drop of 70% ethanol placed on top of the septum to sterilise the needle as it passed through. When sampling, the waste lines were first clamped close to the collection bottle, to prevent flow during transfer from the collection to the sampling bottles. The needle was then carefully withdrawn from the collection bottle, and quickly pushed through the septum of the sampling bottle. The clamp was removed and the lid of the sampling bottle loosened slightly to prevent a build-up of pressure (fully tightening this lid stopped all flow through the waste tubing line). At a flow rate of 2.5 ml h^{-1} it took less than 1 hour to get a sample of between 1 and 1.5 ml. 1 hour was the longest time it was felt appropriate to sample over, as the contents of the chemostat were expected to change over time, and I wanted a sample that was a snapshot of the chemostat contents at one moment in

time, rather than an average over a longer period. Whilst sampling was taking place it was possible to quantify the amount of chemostat waste within each collection bottle, which could then be used to confirm the average flow rate to each chemostat and compare this to the expected flow rate. After sampling the needle transfer process was reversed. This could result in small pieces of the collection bottle stopper being caught in the needle, which in turn impeded flow of liquid from the chemostats to the waste collection. To handle this the chemostats were monitored after sampling for any sign of blockage. If there was an issue a wire pipe cleaner was soaked in 70% ethanol to sterilise and used to clear the needle blockage.

5.3.2.2 Bacterial species can be distinguished on Modified MacConkey agar

It was possible to follow the density of the predators using a plaquing assay, provided the correct dilution could be estimated or a wide range of dilutions were tested. When a single prey species was co-cultured with the *Bdellovibrio* its density could be followed by plating suitable dilutions on to YT agar, and the appropriate dilutions could be determined by measuring the OD. For mixed prey/decoy species however, this would only give the total density of non-predatory bacteria present, and I wished to follow the density of each species separately. To do this I developed a chromogenic medium that was a variant of MacConkey agar, which I refer to as Modified MacConkey Agar (MMA). This has a similar composition to standard MacConkey agar, but the crystal violet and bile salts normally added to inhibit the growth of Gram-positive bacteria were not included to enable growth of *B. subtilis*.

All three prey/decoy species I wished to use, *E. coli*, *P. putida* and *B. subtilis* could grow on this medium. As *E. coli* fermented lactose, it produced a drop in pH

which caused the colony to appear pink. The *P. putida* strain produced glossy colonies and had a chromosomally inserted, constitutively expressed eGFP tag, so colonies were yellow/green in appearance. The *B. subtilis* strain produced white colonies (Fig. 5.10). Whilst this proved effective for determining if all three species were present at similar densities in a co-culture it had limitations. Firstly, whilst most colonies could be definitively assigned to one of the three species, some were ambiguous in phenotype. Secondly, enumeration of both common and rare species (< 1% total cfu) would require a selective medium and plating of multiple dilutions.

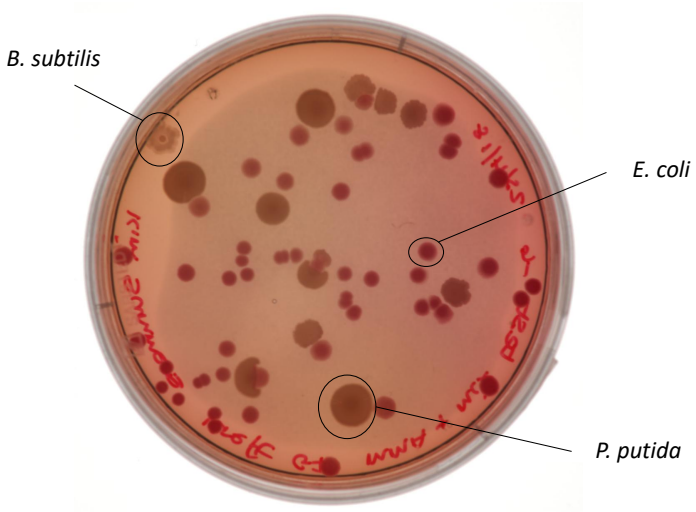

Figure 5.10 - Typical modified MacConkey agar (MMA) plate
Plate was inoculated with a mixed culture of *E. coli, P. putida* and *B. subtilis*

5.3.2.3 qPCR

5.3.2.3.1 Probe based multiplex qPCR was either sensitive or accurate

An attempt was made to construct standard curves for *E. coli* MG1655 and *Bdellovibrio* using the primer and probe sequences listed in Table 5.3. *E. coli* was detected on the FAM channel and *Bdellovibrio* on HEX. *E. coli* MG1655 was grown to an OD of 0.469. *Bdellovibrio* were grown on *P. putida* for three generations, that is a predation lysate (see section 5.2.2) was prepared with *P. putida* as the prey species

and the results of this (after predation was complete) were transferred to a fresh predation lysate, again using *P. putida* as prey and this was repeated three times. This ensured there were no *E. coli* cells present within the lysate, before a growing a fresh lysate on *P. putida* which had a density of 4×10^7 pfu ml^{-1} (as determined by a plaquing assay). DNA was extracted by detergent boil lysis (method 1). After extraction the supernatant was serially diluted 10-fold in nH_2O to create the samples for qPCR. Dilutions below 4.5 log cfu or pfu ml^{-1} could not be distinguished from no template control (NTC) (Fig. 5.11c, d). Above this threshold the PCR cycle in which the fluorescent signal was above the detection threshold (Cq) decreased in a linear manner as the log cfu or pfu ml^{-1} increased (Fig. 5.11a, b). Within the range over which DNA from the samples could be detected (3.7×10^4 to 3.7×10^8 cfu ml^{-1}), *E. coli* DNA was amplified with an efficiency of 105%. For *Bdellovibrio* DNA the efficiency was 101% (over a range of 4×10^5 to 4×10^8 pfu ml^{-1}).

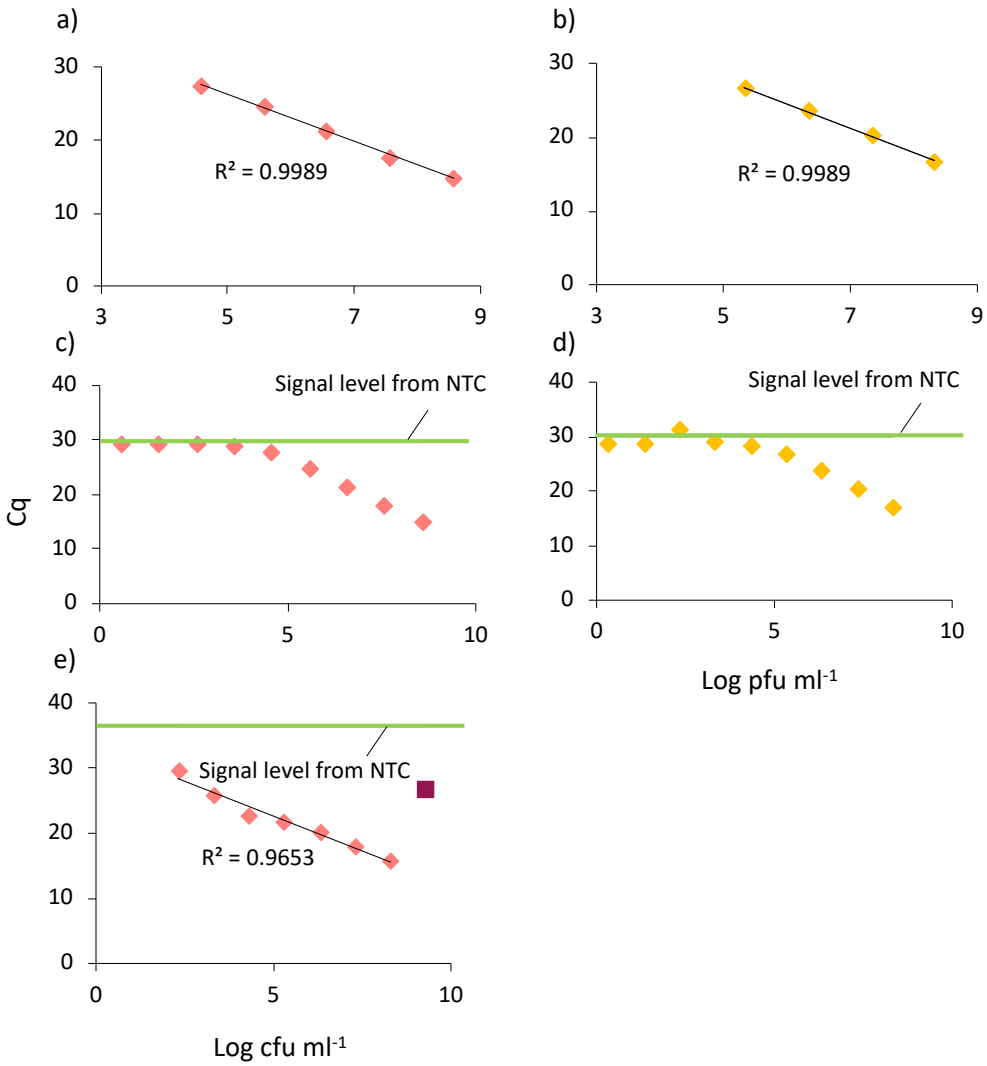

Figure 5.11 - qPCR standard curves

E. coli MG1655 (left side in pink), *Bdellovibrio* (right side in gold). The top row includes only samples with > 4.5 log cfu or pfu ml^{-1} (more dilute samples had a Cq indistinguishable from NTC). The middle row shows all dilutions tested. The bottom row shows samples concentrated by reducing lysis buffer from 200 µl to 20 µl, giving a 10-fold concentration of sample – note the highest sample concentration had an unexpectedly large Cq value (shown as a darker coloured square).

While the standard curve experiment showed that qPCR could accurately quantify the density of a pure culture of bacteria within a certain density range, levels of bacteria in the chemostats were predicted to fall to well below 4 x 10^4 cfu or pfu ml^{-1} on occasions, the limit of detection established. To attempt to lower the limit of detection for the qPCR assay, the concentration of DNA template in each reaction well was increased by decreasing the volume of lysis buffer in which the bacterial pellet

was suspended from 200 µl to 20 µl. *E. coli* MG1655 and *P. putida* were grown to densities of 2.0 x 10^9 and 1.5 x 10^9 cfu ml^{-1} respectively. No signal could be detected from any dilution of *P. putida*. Densities of *E. coli* samples as low as 2.0 x 10^2 cfu ml^{-1} (the lowest value tested) could be distinguished from NTC (Fig. 5.11e). The Cq values for the *E. coli* samples decreased in a linear manner as the log cfu ml^{-1} increased, except for the highest concentration of 2.0 x 10^9 cfu ml^{-1} where the Cq was 26.5. Additionally, the DNA appeared, from the Cq values, to have been amplified with an efficiency of 193%, even after excluding the highest concentration value. This exaggeration of amplification efficiency and the high Cq value observed for the most concentrated sample suggests the presence of high concentrations of inhibitors (Wilson, 1997). These were presumably concentrated along with the DNA, by using a smaller volume of buffer to resuspend the bacterial pellet.

5.3.2.3.2 SYBR green singleplex qPCR

Multiplex qPCR with probes could attempt to quantify densities of all four bacterial species in a single reaction well. There were however drawbacks with this approach. In particular, my model predicted that species densities might vary over several orders of magnitude within the chemostats. This can result in certain species being rare constituents of the total population. If multiplex qPCR was then performed on these samples the more common species would use up all the deoxynucleotides before the rarer populations could be amplified sufficiently to cross the threshold signal level, resulting in a lack of detectable signal from these species. To prevent this issue, I attempted a singleplex qPCR assay where each well contained primers for only a single target species and the probes were replaced by SYBR green which binds to

DNA regardless of sequence. At the same time, I also tested four different methods of extracting DNA from the microbial samples prior to qPCR, in an attempt to maximise the DNA recovery, whilst minimising the presence of compounds likely to inhibit the qPCR reactions.

As with the multiplex probe-based qPCR, the fluorescence signal from all *P. putida* samples was indistinguishable from NTC in the singleplex SYBR based qPCR assay. The *B. subtilis* and *E. coli* primers gave the same pattern of signal for both bacteria and all four extraction methods (Fig. 5.12 and 5.13). The two samples where target bacterial DNA was predicted to be highest (target bacterial culture made up 33% by volume of the total culture on which the extraction was performed) gave the strongest signal (lowest Cq), with the undiluted sample being stronger than the 10-fold diluted. The other three samples all had a similar Cq to each other. In the case of *E. coli* this signal was always indistinguishable from NTC. For the *B. subtilis* the UltraClean kit also gave a signal at the same level as NTC, detergent boil lysis with ethanol precipitation gave a Cq slightly below NTC and the QIAamp DNA mini kit and GenElute kit samples gave the lowest Cq values.

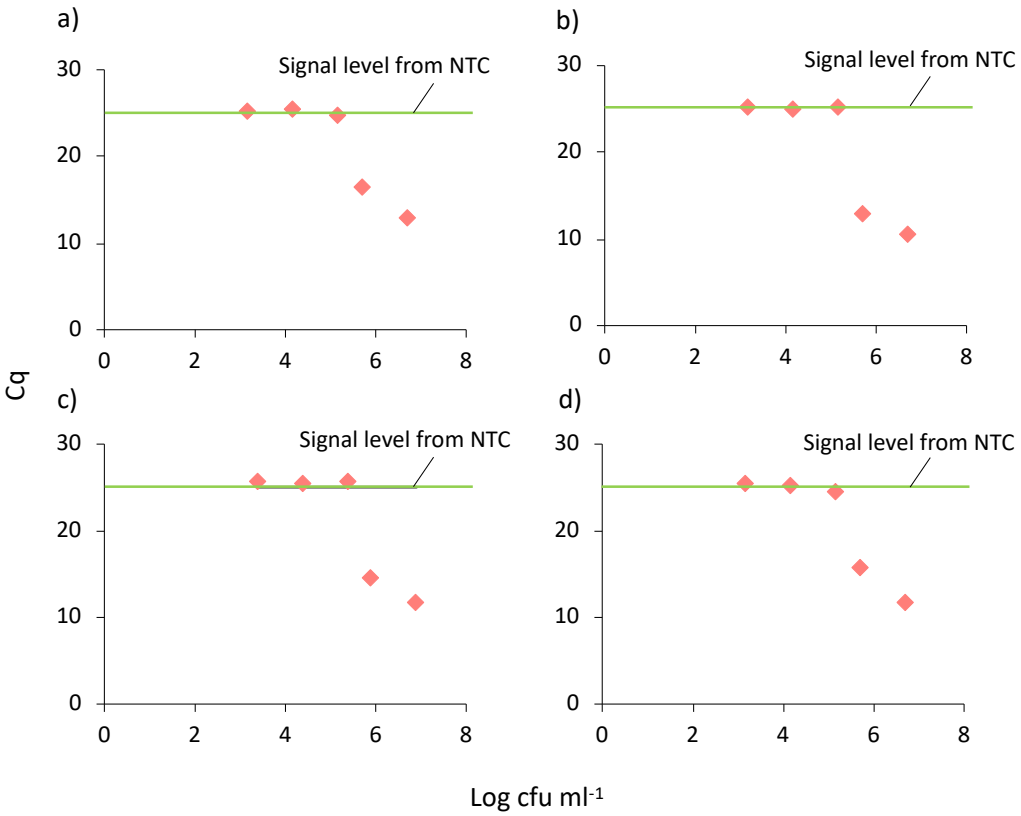

Figure 5.12 - Results of singleplex qPCR for *E. coli*

Results of primers targeting *E. coli* genome on a sample from a mixed microbial community. DNA was extracted by four different methods. Panel (a) DNA extraction method 1 – detergent boil lysis with ethanol precipitation. Panel (b) Method 2 – GenElute enzymatic lysis. Panel (c) Method 3 – DNeasy UltraClean detergent lysis and bead beating with precipitation. Panel (d) Method 4 – QIAamp DNA mini kit detergent and enzymatic lysis.

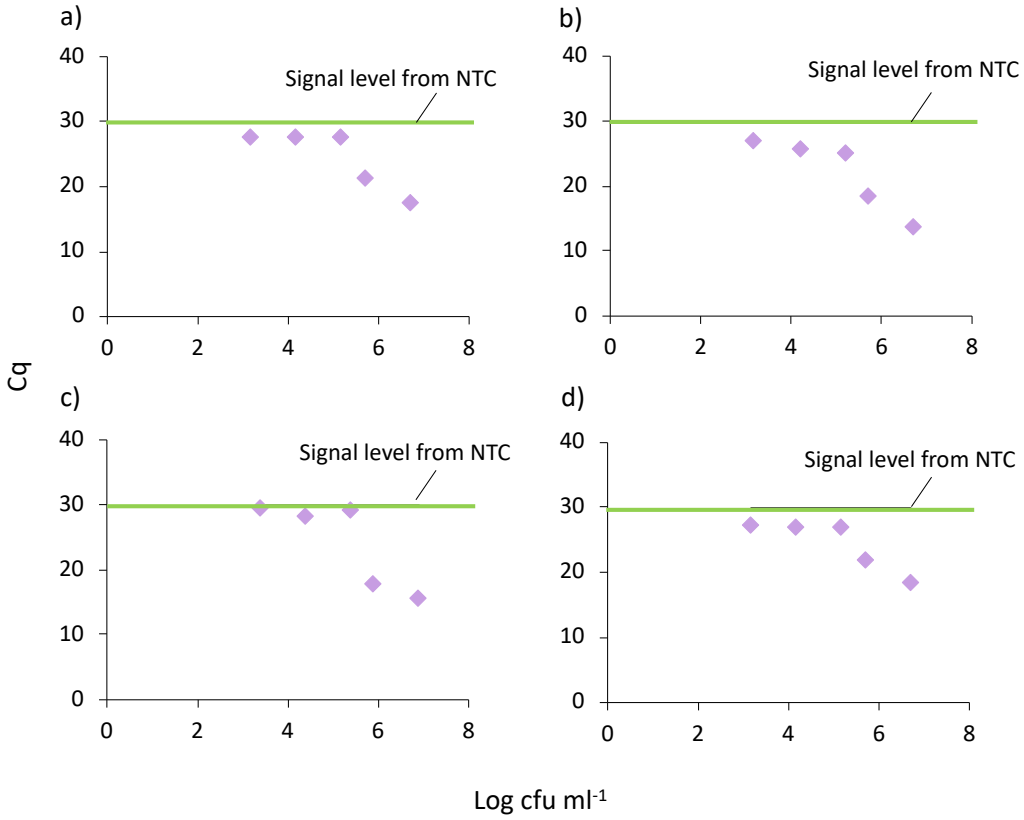

Figure 5.13 - Results of singleplex qPCR for *B. subtilis*

Results of primers targeting *B. subtilis* genome on a sample from a mixed microbial community. DNA was extracted by four different methods. Panel (a) DNA extraction method 1 – detergent boil lysis with ethanol precipitation. Panel (b) Method 2 – GenElute enzymatic lysis. Panel (c) Method 3 – DNeasy UltraClean detergent lysis and bead beating with precipitation. Panel (d) Method 4 – QIAamp DNA mini kit detergent and enzymatic lysis.

5.3.2.3.3 qPCR Summary

Analysis of mixed microbial communities using qPCR proved to be problematic in my hands. Using a probe-based technique and a simple boil lysis it was possible to get an accurate (R^2 = 0.9989, efficiency = 101% to 105%) measure of bacterial densities for pure cultures of *E. coli* MG1655 and *B. bacteriovorus* HD100, down to a density of 3.7 x 10^4 cfu ml^{-1} and 4 x 10^5 pfu ml^{-1} respectively. Attempts to improve this by concentrating samples resulted in a loss of accuracy (R^2 = 0.9653, efficiency = 193%), probably due to increased concentrations of substances that inhibited the PCR reactions. Analysis of mixed microbial cultures using singleplex SYBR based qPCR with

a variety of commercially available kits proved to be even less successful, (Fig. 5.12 and 5.13) regardless of the kit used. Other studies (Zheng *et al.*, 2008; Van Essche, Sliepen, *et al.*, 2009; Iebba *et al.*, 2013) have used qPCR successfully to detect quantities of predatory bacteria in mixed microbial communities. It is therefore entirely possible that with further optimisation this technique could be successfully implemented and should allow for high throughput of samples.

5.3.2.4 Flow cytometry

I tested the ability of the Attune NxT flow cytometer to detect five different strains of fluorescently tagged bacteria (Table 5.8). All five strains could be detected at varying intensities (Fig. 5.14). I found that unsurprisingly, those fluorophores which were encoded on plasmids (and could therefore be expressed in greater numbers) gave the strongest signals. Of these mRuby2 gave the strongest signal and mOrange2 the weakest.

Table 5.8 – Properties of fluorescent strains

Bacterial species	Type of tag	Fluor	Peak emission λ nm	Channel detected	Strength of signal	Spillover?
P. putida	Chromosomal constitutive	eGFP	510	BL1 530±30 nm	Weak to Moderate	No
E. coli	Plasmid inducible	mOrange2	565	YL1 585±16 nm	Strong	Yes
E. coli	Plasmid inducible	mVenus	529	BL1 530±30 nm	Very Strong	No
E. coli	Plasmid inducible	mRuby2	595	YL1 585±16 nm	Extremely Strong	No
Bdellovibrio	Chromosomal constitutive	mCherry2	612	YL2 620±15 nm	Weak to Moderate	Yes

I next checked whether it was possible to distinguish two differently tagged species in a co-culture. For this I chose the mCherry2 tagged *Bdellovibrio* mixed in

equal amounts with either the mVenus tagged *E. coli* or the eGFP tagged *P. putida*. These species were chosen because the channel in which the mCherry2 gave its strongest signal was different from that in which the strongest signal was observed from mVenus and eGFP. With the mVenus/mCherry2 sample it was possible to clearly distinguish the two populations. With the eGFP/mCherry2 sample however the signal of the two fluorescent proteins spilled out of their channels and the populations could not be distinguished, although the use of compensating beads might allow the signals to be differentiated.

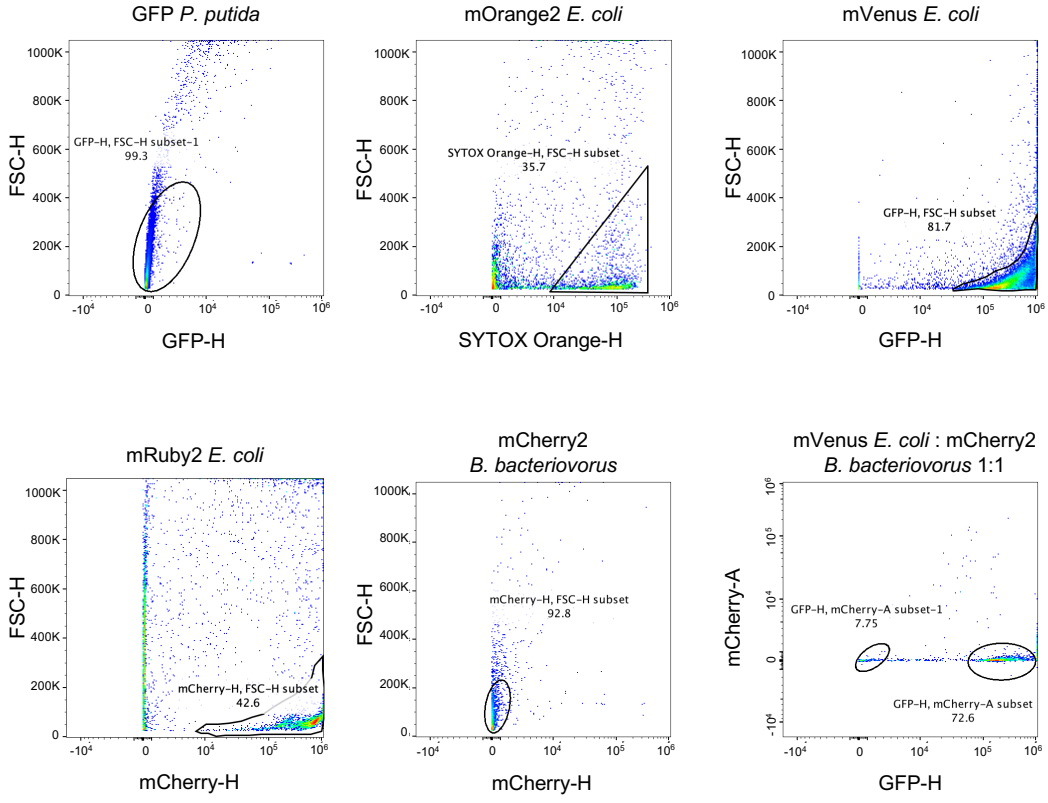

Figure 5.14 – Flow cytometry of predator and prey species

It was possible to detect all the fluorescent strains tested using flow cytometry. The use of a fluorescent tag allowed *Bdellovibrio* cells, which are smaller than prey bacteria, such as *E. coli*, to be distinguished from background noise. Bacteria

expressing certain fluorescent proteins, such as mCherry2 and mVenus could be distinguished using flow cytometry, however care must be taken in choosing suitable combinations of fluorescent tags. Further work is required to determine how accurately flow cytometry can determine bacterial densities in mixed samples, particularly when one species is a very small percentage of the total population, and to determine the minimum density of bacteria that can be accurately quantified.

5.3.3 Microbial community construction

I wished to investigate the effects of adding a bacterial predator to an otherwise stable community, consisting of a small number of prey and non-prey (decoy) bacterial species. To achieve this, I first needed to construct such a community, that could be co-cultured for several weeks in a chemostat, without the loss of any species. The competitive exclusion principle (Hardin, 1960) postulates that each resource within a chemostat can only support a single species. To ensure the survival of all species I therefore needed to provide each of them with an exclusive resource. This was achieved by supplying all nutrients in excess, except for the carbon and energy sources, which were always the limiting nutrients and each of which was exclusive for one of the non-predatory bacterial species I wished to grow.

E. coli, *Pseudomonas putida* (*P. putida*) and *Bacillus subtilis* (*B. subtilis*) were chosen to be the members of the community. All three species are non-pathogenic, motile bacilli of similar size (Brenner *et al.*, 2005; De Vos *et al.*, 2009). *E. coli* (Stolp and Starr, 1963) and *P. putida* (Huang and Starr, 1973) are Gram-negative bacteria known to be predated by *Bdellovibrio* HD100. *B. subtilis* is a Gram-positive bacterium and as such cannot be predated by *Bdellovibrio* and so should act as a decoy species.

A literature search found carbon sources that were predicted to be uniquely utilizable for each bacterial species. For *E. coli* MG1655 this was lactose (Brenner *et al.*, 2005), for *P. putida* KT2440 tyrosine (Nelson *et al.*, 2002) and for *B. subtilis* 167 cellulose (Fisher and Sonenshein, 1991). Additionally, *B. subtilis* 167 is auxotrophic for tryptophan (Zeigler *et al.*, 2008), so for all media in which *B. subtilis* 167 was to be grown tryptophan was included at a concentration of 5 mg l^{-1}.

I attempted to culture all three prey/decoy species together, as well as each combination of species in pairs. In all co-culture experiments I used DMM supplemented with 0.5 g l^{-1} of the carbon source for each of the bacterial species being cultivated, except for tyrosine, which was 0.4 g l^{-1} due to its low solubility.

I initially had four chemostats for each species combination, two of which also had the predator (*Bdellovibrio*) added several days after the prey/decoy species. Chemostats were run for between 21 and 41 days. Species densities were enumerated by a plaquing assay for *Bdellovibrio* and plating on MMA for all other species. Most colonies could be identified but some could not, so the density of that species was underestimated. Despite this issue, I could confirm that in all instances all prey and decoy species initially inoculated into a chemostat survived for the duration of that chemostat (Figs. 5.15, 5.16, 5.17 & 5.18).

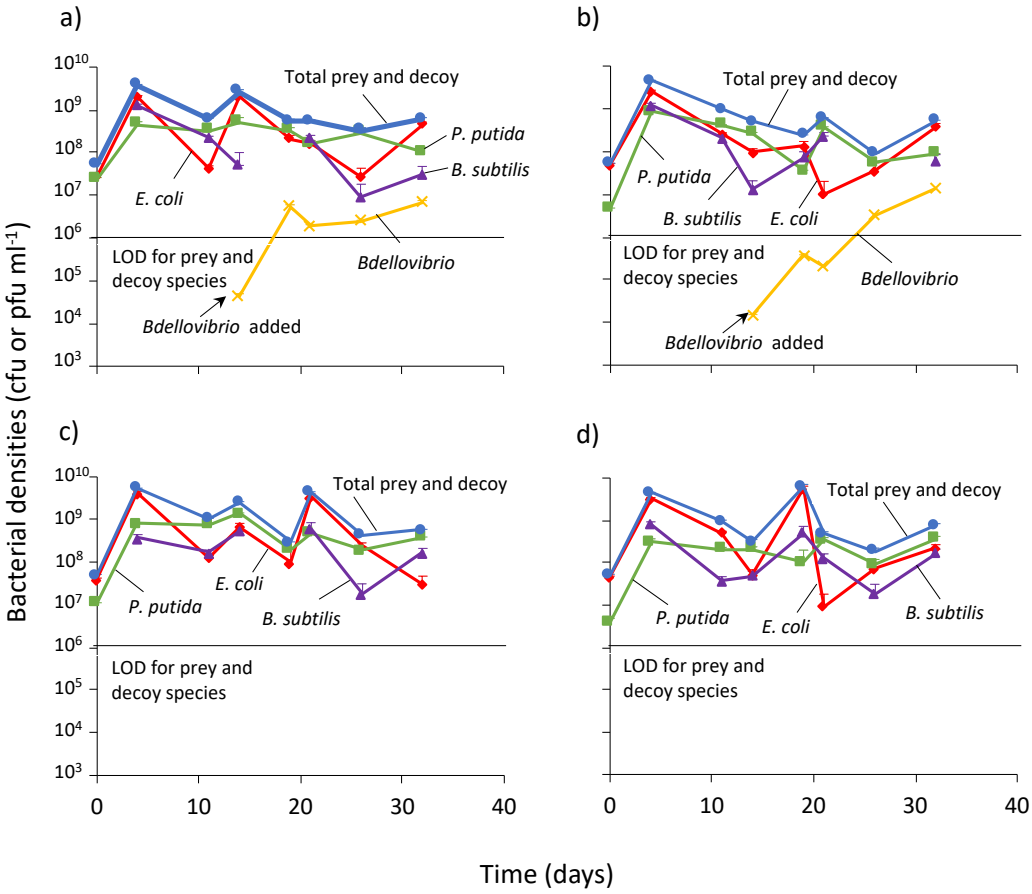

Figure 5.15 – Populations of bacteria in 3 prey/decoy species chemostats.

Red – *E. coli*, green – *P. putida*, purple – *B. subtilis*, yellow – *Bdellovibrio*, blue – total prey and decoy (non-predatory) bacteria. Experiments were conducted using chemostat design 3. Panels (a, b) chemostats were inoculated with *Bdellovibrio*, panels (c, d) chemostats did not contain *Bdellovibrio.* Dilution rate was 0.125 h^{-1}, resulting in a retention time of 8 hours and reservoir carbon source levels were 0.5 g l^{-1} for *E. coli* and *B. subtilis* and 0.4 g l^{-1} for *P. putida*. Limit of detection (LOD) for *Bdellovibrio* was 10^2 pfu ml^{-1}.

Bdellovibrio did best in those chemostats which contained both *E. coli* and *P. putida* (Fig. 5.15a, b, 5.16a, b, 5.17a, b & 5.18a, b). In the *E. coli, P. putida and B. subtilis* chemostats *Bdellovibrio* increased from an initial density of less than 10^5 pfu ml^{-1} to over 10^7 pfu ml^{-1} (Fig. 5.15a, b). In the chemostats without *B. subtilis*, the *Bdellovibrio* density initially dropped to below detection levels before rebounding to over 10^7 pfu ml^{-1} (Fig. 5.16a, b). When the chemostats contained only *P. putida* and *B. subtilis* the *Bdellovibrio* did less well, with densities declining from over 2 x 10^5 pfu ml^{-1} to under 3 x 10^3 pfu ml^{-1} and in one instance being below detection levels (Fig. 5.17a, b). It

should be noted however, that this experiment was terminated after 20 days, 5 days after the *Bdellovibrio* had been added and at the comparable time in the *E. coli* and *P. putida* chemostats the *Bdellovibrio* had also dropped to below detection levels before recovering and it is entirely possible that had the *P. putida* and *B. subtilis* chemostats been run for another seven to ten days the density of *Bdellovibrio* would have also recovered here. When *E. coli* was the sole prey species and *B. subtilis* was present as a decoy the *Bdellovibrio* densities were lowest, as they were only detected at one time point (the point of initial inoculation) in one chemostat of the two inoculated (Fig. 5.18a, b). These chemostats were however also terminated at twenty days, five days after *Bdellovibrio* inoculation.

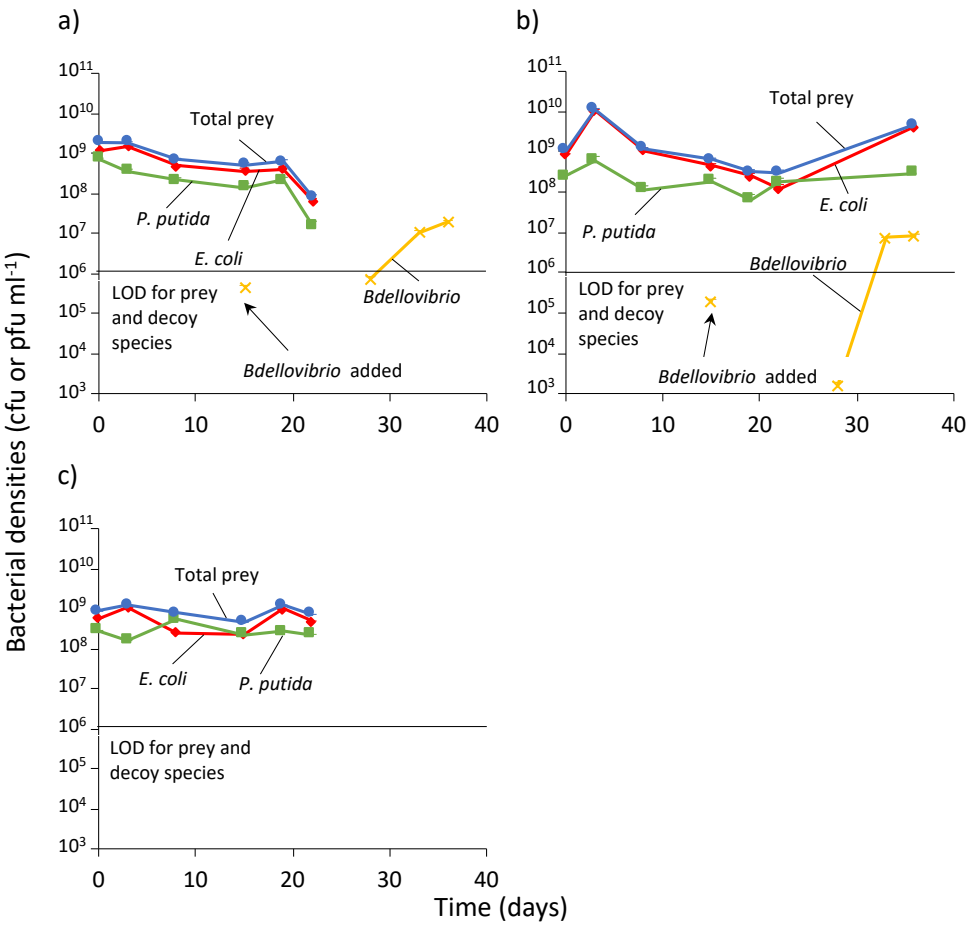

Figure 5.16 – Populations of bacteria in *E. coli* and *P. putida* chemostats.

Red – *E. coli*, green – *P. putida*, yellow – *Bdellovibrio*, blue – total prey bacteria. Experiments were conducted using chemostat design 3. Panels (a, b) chemostats were inoculated with *Bdellovibrio*, panel (c) chemostat did not contain *Bdellovibrio*. The prey density counts for days 28 and 33 are absent because of contamination of the HEPES buffer used to dilute samples. The densities for day 36 are also missing from panels (a, c) because the density of prey on plates from this timepoint was too high to count. Dilution rate was 0.125 h^{-1}, resulting in a retention time of 8 hours and reservoir carbon source levels were 0.5 g l^{-1} for *E. coli* and 0.4 g l^{-1} for *P. putida*. Limit of detection (LOD) for *Bdellovibrio* was 10^2 pfu ml^{-1}.

Assuming an average burst size of *Bdellovibrio* from an *E. coli* cell is 3.5 (Seidler and Starr, 1969a) and 4.8 from a *P. putida* (Matin and Rittenberg, 1972) gives an average burst size over the two prey of 4.15. To achieve a population of 1 x 10^7 pfu ml^{-1} (the maximum density of *Bdellovibrio* observed in my chemostats) would therefore require the consumption of 2.4 x 10^6 cfu ml^{-1} (1 x 10^7 / 4.15) prey cells (Table 5.9). Given that the density of total prey and decoy bacteria in the chemostats was in the region of 1 x 10^9 cfu ml^{-1} it is not surprising that there was little or no difference in the

total prey/decoy densities between those chemostats with and those without predator. What is more surprising, is that the predator did not grow to considerably higher densities.

Table 5.9 – Conversion factors between glucose concentration, *E. coli* density and *Bdellovibrio* density

Glucose concentration (g l^{-1})	Density of *E. coli* (cfu ml^{-1})	Density of *Bdellovibrio* (pfu ml^{-1})
0.05	1.1×10^8	3.9×10^8
0.4	8.9×10^8	3.1×10^9
0.5	1.1×10^9	3.9×10^9
1	2.2×10^9	7.8×10^9

With mixed cultures it was not always possible to identify bacterial colonies, which meant that following trends in the density of any non-predatory species was challenging. With the three prey and decoy species chemostats the total density of non-predatory species increased from an initial value of just under 10^8 cfu ml^{-1} to about 4×10^9 cfu ml^{-1}, then fluctuated by 1 to 1½ log units. The chemostats inoculated with *Bdellovibrio* had on average half a log unit fewer non-predatory bacteria than those without *Bdellovibrio* (Fig. 5.15), although this difference was not significant ($P = 0.17$).

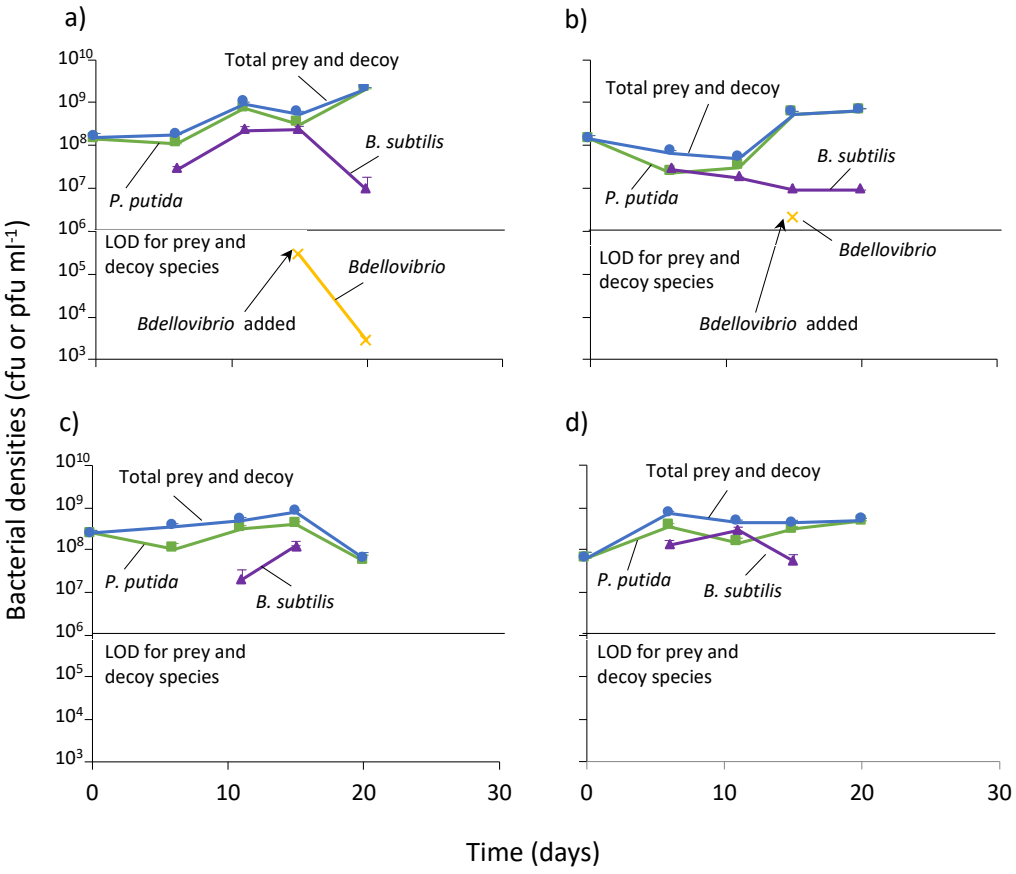

Figure 5.17 – Populations of bacteria in *P. putida* and *B. subtilis* chemostats.
Green – *P. putida*, purple – *B. subtilis*, yellow – *Bdellovibrio*, blue – total prey/decoy bacteria. Experiments conducted using chemostat design 3. Panels (a, b) chemostats were inoculated with *Bdellovibrio* panels (c, d) chemostats did not contain *Bdellovibrio*. Dilution rate was 0.125 h^{-1}, resulting in a retention time of 8 hours and reservoir carbon source levels were 0.5 g l^{-1} for *B. subtilis* and 0.4 g l^{-1} for *P. putida*. Limit of detection (LOD) for *Bdellovibrio* was 10^2 pfu ml^{-1}.

With the *E. coli* and *P. putida* chemostats the total prey bacteria density was initially around 1 x 10^9 cfu ml^{-1}. Due to contamination of the HEPES buffer used to dilute samples, several bacterial counts for these chemostats were unobtainable. In the chemostat without *Bdellovibrio* total bacterial densities fluctuated by 0.4 log units around the initial population size, but showed no consistent trend (Fig. 5.16). In the chemostats with *Bdellovibrio* the fluctuations were greater (1.4 to 1.6 log units).

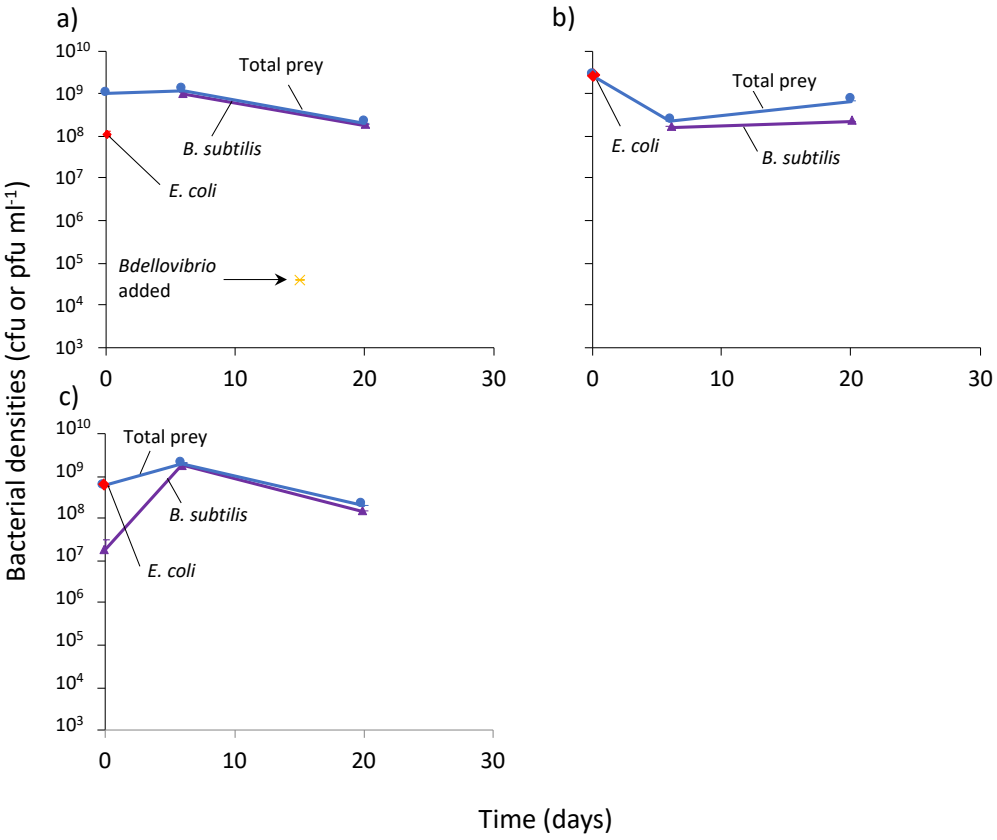

Figure 5.18 - Populations of bacteria in *E. coli* and *B. subtilis* chemostats.

Red – *E. coli*, purple – *B. subtilis*, yellow – *Bdellovibrio*, blue – total prey/decoy bacteria. Experiments conducted using chemostat design 3. Panels (a, b) chemostats were inoculated with *Bdellovibrio*, panel (c) chemostat did not contain *Bdellovibrio*. Dilution rate was 0.125 h^{-1}, resulting in a retention time of 8 hours and reservoir carbon source levels were 0.5 g l^{-1} for *E. coli* and *B. subtilis*. Limit of detection (LOD) for *Bdellovibrio* was 10^2 pfu ml^{-1}.

While it was encouraging that the bacterial species could survive together with or without the presence of the predator, I noted that in all chemostats containing both *E. coli* and *P. putida* there was considerable clumping (Fig. 5.19).

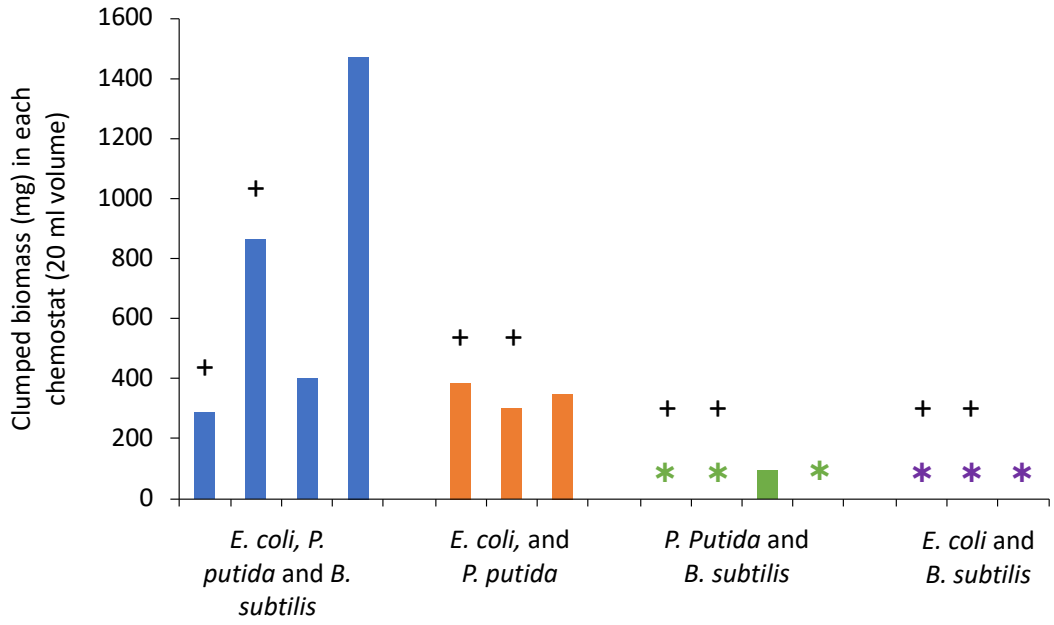

Figure 5.19 – Clumping levels observed in multiple-species chemostats.
Clumping was quantified at the end of the chemostat run. '*' indicates that any clumped material was below detection limits. '+' indicates that *Bdellovibrio* was also cultured in the chemostat. Chemostat design 3 was used for these experiments.

5.3.4 Clumping reduction

5.3.4.1 Clumping reduction experiment 1 – Single stage chemostats

When *E. coli* MG1655 and *P. putida* KT2440 were co-cultured in a chemostat there was considerable clumping observed in the form of floating mats of bacteria. This clumping occurred regardless of the presence or absence of *Bdellovibrio* and was exacerbated by the addition of *B. subtilis*. The presence of large amounts of clumped material meant the vessels were no longer acting as ideal chemostats or reasonable approximations of these. To reduce the levels of clumped material I attempted to evolve bacterial strains that did not clump when cultured together. The strains I evolved needed to be capable of growing on their chosen carbon source (lactose for *E. coli* and tyrosine for the *Pseudomonad*) at 30° C (the temperature used for predation experiments). They also had to be capable of growing in co-culture with

each other and with *B. subtilis*. Growing in a chemostat generally selects for cells that have a means to avoid being washed out, such as forming a biofilm. I reasoned that cells growing planktonically in the liquid phase of the chemostat however, were less likely to be strong biofilm formers or clumpers. I therefore co-cultured various strains of *E. coli* and *Pseudomonads,* along with *B. subtilis,* in DMM with their unique carbon source, in a chemostat at 30° C for one week, before transferring 1 ml of the liquid phase to a fresh chemostat. As well as attempting to evolve the strains of *E. coli* (MG1655) and *P. putida* (KT2440) previously used, I also wished to test a number of other strains to determine if any of these produced less clumped material, or could be evolved to do so. For this purpose, I obtained a TRADIS library of *E. coli* (Langridge *et al.*, 2009), which whilst undoubtably containing some strains that were stronger biofilm formers, might also have strains that would be less likely to clump under my experimental conditions. For the *Pseudomonad*, I was not able to obtain a TRADIS library for *P. putida*, so instead tested a single strain of a different species of *Pseudomonad*. I chose a strain of *P. synxantha* for this, as it was phylogenetically similar to *P. putida* and capable of utilising tyrosine as a carbon source. Wild type *P. synxantha* produces the antibiotic mupirocin, so I obtained a strain with two independent mutations that prevented mupirocin production, to reduce the likelihood of reversion to wild type and antibiotic production. Strains of *E. coli* and species of *Pseudomonad* were tested in combination as detailed in Table 5.10. When the samples were transferred a cryo stock was made of the contents of each chemostat and the amount of clumping in the chemostats was quantified.

Table 5.10 – Strains used in anti-clumping chemostats

Each chemostat contained either *E. coli* MG1655 or an *E. coli* TRADIS library, and one *Pseudomonad*, as well as *B. subtilis*. Each bacterial combination was run in two chemostats as technical replicates.

Chemostat	*E. coli* strain	*Pseudomonad*
1	TRADIS library	*P. synxantha*
2	TRADIS library	*P. synxantha*
3	TRADIS library	*P. putida* KT2440
4	TRADIS library	*P. putida* KT2440
5	MG1655	*P. synxantha*
6	MG1655	*P. synxantha*
7	MG1655	*P. putida* KT2440
8	MG1655	*P. putida* KT2440

Chemostats with the TRADIS library of *E. coli* initially had significantly more clumping than those with MG1655 ($P = 0.0052$) (Fig. 5.20). This was not surprising given that amongst the library there was likely to be some mutants that were strong biofilm formers, and these would likely be at an advantage in a chemostat, as they would be less likely to be washed out. After two weeks of running, clumping levels in all chemostats had dropped significantly below their starting levels ($P = 0.008$), but one week later, clumping levels in all chemostats rebounded ($P = 0.014$). After another week levels in three of the chemostats fell, while in the other five chemostats they went up further. At this stage there was no significant difference between those chemostats containing the TRADIS library and those with the MG1655 strain. At no time point were there any significant differences between those chemostats with *P. putida* and those with *P. synxantha*.

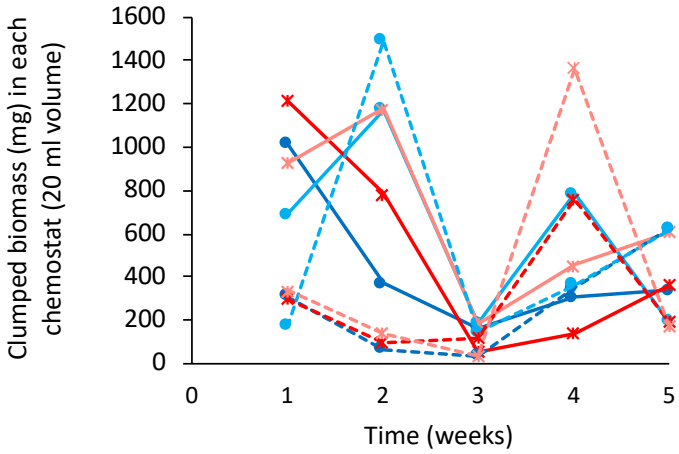

Figure 5.20 – Clumping levels in single stage chemostats with serial transfer.
Clumping was quantified at the time of transfer. Blue – *P. synxantha*, Red – *P. putida* KT2440, solid lines – TRADIS library of *E. coli*, dashed lines – *E. coli* MG1655. Different shades of a colour indicate replicate chemostats. Experiments conducted using chemostat design 3.

5.3.4.2 Clumping reduction experiment two stage chemostats

As the experiments to evolve non-clumping strains in a single stage chemostat showed only limited success, I decided to attempt to evolve the strains in a two stage chemostat. In this arrangement two chemostat vessels were used in series. The efflux from the first vessel was the media inflow to the second vessel. Initially, I attempted to use the pump to control media flow between the vessels, however this resulted in the media not flowing properly. Hence, the media pump was only used to control the flow into the first vessel.

Samples taken during clumping reduction experiment 1 were used to inoculate the two stage chemostats. I considered using sample point 3 as the inoculum, as it had the lowest levels of clumping, but decided against this, as when I had used this inoculum previously (during clumping reduction experiment 1) clumping with the chemostat had gotten worse not better by sample point 4 , and I was concerned that this pattern might be repeated. Instead, I used sample point 2, as in experiment 1

chemostats inoculated with these samples had improved (reduced clumping levels) by the next sampling point.

The chemostats were run for eleven days at the end of which the levels of clumping in both stage vessels was quantified and the contents of the chemostats cryo preserved. In all instances there was less clumping in the second stage vessels than in the first stage (P = 0.0033) (Fig. 5.21). There were no statistically significant differences between the TRADIS *E. coli* and MG1655 *E. coli* second stage chemostat vessels or between the *P. synxantha* and *P. putida* vessels. The lowest clumping levels were observed in one of the MG1655 and *P. putida* and one of the TRADIS *E. coli* and *P. synxantha* chemostats. Of the two, the MG1655/*P. putida* chemostat had consistently shown less signs of clumping throughout the running of the chemostats. Accordingly, a sample of this chemostat was streaked out to single colonies on YT agar. Cryo stocks were made of one isolated *P. putida* and one *E. coli* colony. These strains were termed iMG1655 and iKT2440.

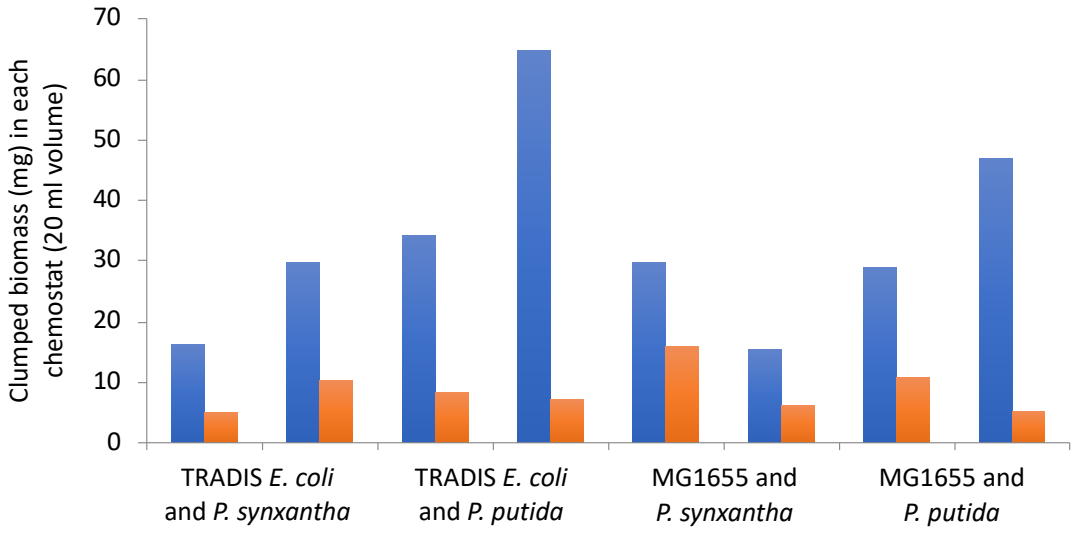

Figure 5.21 – Clumping levels of two stage chemostats

Clumping was quantified after running the chemostats for eleven days. Blue – first stage vessels, red – second stage vessels. Experiments conducted using chemostat design 3.

5.3.5 Predation in a chemostat

5.3.5.1 Bdellovibrio can replicate within a chemostat

Initial predation experiments were performed to determine how long *Bdellovibrio* could survive in a chemostat with *E. coli* strain MG1655 as prey. An array of four chemostats was used, two of which had M9 medium, supplemented with 1 g l^{-1} glucose and two had DMM, supplemented with 0.5 g l^{-1} glucose. The media pump was set to a flow rate of 2.5 ml h^{-1}, equivalent to a dilution rate of 0.125 h^{-1}, and an 8 h retention time. All chemostats were inoculated with 1 ml of approximately 1 x 10^9 cfu ml^{-1} *E. coli* MG1655 grown to stationary phase in YT. The media pump was stopped for 48 hours to allow *E. coli* to adapt to the new medium (I had previously observed long lag phases). After this time both M9 chemostats and one DMM chemostat were inoculated with 1 ml of approximately 1 x 10^7 pfu ml^{-1} *Bdellovibrio* HD100. The final DMM chemostat was left predator free as a control.

In all chemostats inoculated with *Bdellovibrio* they were still detectable for 6 days, after that levels of *Bdellovibrio* dropped below detection levels, but in both M9 chemostats (with higher nutrient levels) the density of predators rebounded after another 5 days (Fig. 5.22). This behaviour was similar to that seen in chemostats with *E. coli* and *P. putida*, but not *B. subtilis* (Fig. 5.16). In the lower nutrient level, DMM chemostat there was no sign of recovery at day 11, but it is possible that given further time a recovery would have been observed. It should also be noted that over the three days preceding the drop in predator levels there was a drop of 1.8 log units in the *E. coli* densities in the lower glucose concentration (DMM) chemostat.

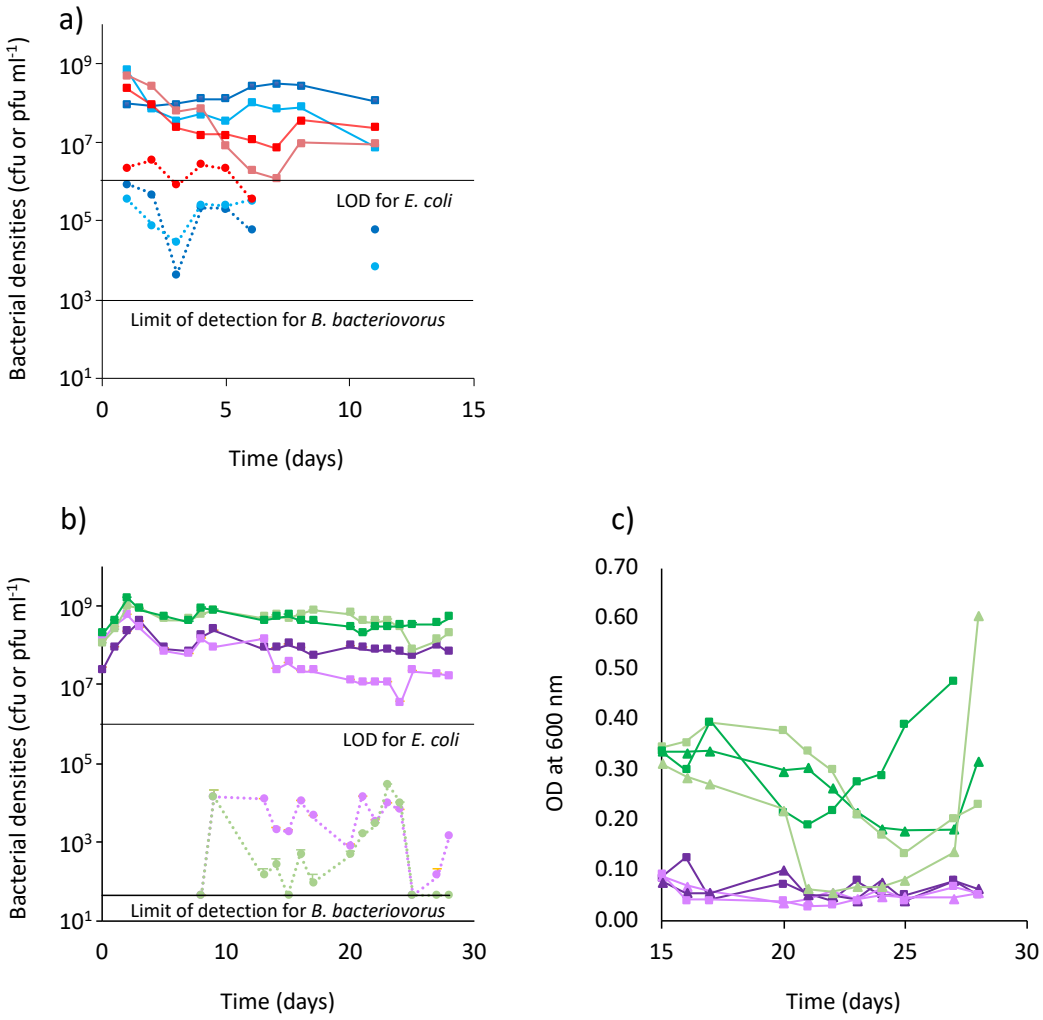

Figure 5.22 – Levels of *Bdellovibrio* and *E. coli* in glucose limited chemostats

Panel (a) represents one experiment where only viable counts were available, panels (b) and (c) are a second experiment with both viable counts and OD measurements. Blue lines are chemostats with M9 minimal medium and 1 g l^{-1} glucose, all other chemostats have DMM with different glucose levels red lines = 0.5 g l^{-1}, green lines = 0.4 g l^{-1}, purple lines = 0.05 g l^{-1}. Solid lines are *E. coli* counts and dotted lines are *Bdellovibrio*. In panels (b) and (c) pale shades indicate predators were added to the chemostat, darker shades indicate no predators. In panel (c) triangular markers indicate a replicate chemostat for which viable counts were not available. Panel (a) the *E. coli* strain was MG1655 and dilution rate was 0.125 h^{-1}, panels (b, c) *E. coli* strain was iMG1655 and dilution rate was 0.03 h^{-1}. Chemostat design 3 was used for the experiment in panel (a) and design 4 was used for the experiment in panels (b, c).

The density of *E. coli* in all four chemostats was similar for the first four days. From day five onwards however, levels were lower in the lower (0.5 g l^{-1}) glucose DMM chemostats than in the higher (1 g l^{-1}) glucose M9 chemostats (P = 0.0047). *E. coli* density was also lower from day five onwards in one replicate higher nutrient chemostat than the other (P = 0.014), despite the fact that conditions in the two

chemostats were supposedly identical. *E. coli* densities in the two lower nutrient chemostats were not statistically different from each other over this period (P = 0.061), despite there being predators present in only one of these chemostats.

Linear regression of the *E. coli* and *Bdellovibrio* densities was attempted, but a single straight line was generally of poor fit to the data (R^2 = 0.0031 to 0.7322).

5.3.5.2 Effect of predation was greater at lower nutrient levels

Further predation experiments were conducted at a lower dilution rate of 0.03 h^{-1}, equivalent to a 33 h retention time and with two inflow substrate concentrations, 0.4 g l^{-1} and 0.05 g l^{-1} glucose (Fig. 5.22b, c). These values were chosen because my model predicted, that at the lower nutrient level, a steady state co-existence of predator and prey should be observed, while at the higher concentration oscillations should occur (cf. Fig. 2.3). DMM medium was used for these experiments as it gave more consistent growth than M9 medium. I also used iMG1655 as the prey strain, as this had evolved to be less prone to clumping, and mCherry *Bdellovibrio* as the predator.

Surprisingly the chemostats with the two lowest glucose concentrations (0.4 g l^{-1} and 0.05 g l^{-1}) had the highest *E. coli* densities. It should be noted that Design 3 was used for the experiments with the two highest glucose concentrations (0.5 g l^{-1} and 1 g l^{-1}) and there was heavy growth on both the air and media needles, probably due to the bubbling of the media. This mean that bacteria growing on, and potentially within the media needle were likely to have consumed nutrients within the medium before it reached the chemostat thereby potentially reducing the glucose levels available to the planktonic culture. For the lower glucose concentration experiments Design 4 was

used and there was no bubbling and no growth was seen on either the air or media needles even after four weeks of running. There was also a noticeable reduction in biofilm growth on the walls of the chemostats vessels in the lower glucose concentration experiments. Assuming the yield of *E. coli* growing on glucose is 0.4444 mg dry biomass per mg glucose (Kreft *et al.*, 1998), and that an *E. coli* has a volume of 1 fl (Kubitschek and Friske, 1986), 20% of which is dry mass then 0.4 mg l^{-1} glucose should give 0.4 x 0.4444 = 0.18 mg dry mass *E. coli* ml^{-1} or 8.9 x 10^8 cfu ml^{-1} (Table 5.9). This is in reasonable agreement with the density of *E. coli* in the Design 4 chemostats, but the density in the Design 3 chemostats is below what would be expected. This cannot be solely due to biomass being converted into *Bdellovibrio* as this would have resulted in a much higher density of *Bdellovibrio* (Table 5.9).

Within the Design 4 chemostats (Fig. 5.21b), higher nutrient levels had consistently higher bacterial densities. In the lowest nutrient level (0.04 g l^{-1} glucose) chemostats, *E. coli* density in the chemostat inoculated with *Bdellovibrio* (predator) dropped below the predator free chemostat six days after inoculation, and remained lower for the duration of the chemostat run. With the higher nutrient levels, the effects of predation were less detectable.

5.3.5.3 Chemostat results could not be well fitted to the theoretical model

Attempts were made to fit the results of the single prey (*E. coli*) chemostats to my theoretical model using the Sequential Monte Carlo – Approximate Bayesian Computational (SMC-ABC) methodology described in Chapter 4. For the chemostats with both predator and prey species, three models were competed. Model 1 assumed that predators were present, but did not predate prey. Predators in this model were

subject to mortality and dilution as previously described in Chapters 2 and 4. Prey grew normally as previous described. Model 2 was the standard predation model described in Chapter 2. Model 3 also included plastic resistance to predation as described in Chapter 4, following the signal-driven conversion to resistance and growth coupled back-conversion to a sensitive phenotype (see model **N3-SBG-Pii-Vi** in Chapter 4, but without phages or the phage resistant phenotype). In all instances the no predation model was rapidly outcompeted and eliminated. Depending on the data being fitted, the levels of support varied from 100% for Model 2 to 100% for Model 3 and all combinations in between. After fitting, a typical dataset was chosen by principal component analysis (see Chapter 4) and compared to the experimental data. With the no persistence model, this gave a fit for the *E. coli* of either constant increase or decrease in biomass and did not match any fluctuations. With the persister model there was an initial decline in *E. coli* density, followed by a plateau, that was not a good match to the experimental data. For the *Bdellovibrio* the pattern of the model varied depending on the experimental data, but was never a good fit. Fig. 5.23 shows a typical fit to data from a Design 3 chemostat with M9 medium, 1 g l^{-1} glucose and *E. coli* and *Bdellovibrio* (Fig. 5.21). The model shows the *E. coli* density in constant decline, while the *Bdellovibrio* density, after an initial small rise drops down to almost zero, with no sign of recovery.

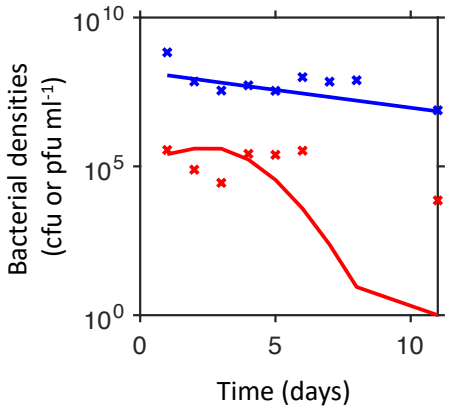

Figure 5.23 – 'Typical' model fit to experimental chemostat data

Blue – Prey, Red – *B. bacteriovorus*. Solid lines are simulation results, symbols are experimental data.

The model developed in Chapter 2 was not a good fit for the experimental data collected in this chapter. This was likely due to the experimental vessels not behaving as ideal chemostats, with in particular biofilm growth on the walls of vessels and on all needles, especially the media needle. Adaptation of the model to include a separate compartment for biofilm growth, such as a Freter model (Freter *et al.*, 1983), might yield a better fit.

5.4 Discussion

I have developed an array of mini chemostats inspired by the work of Miller et al. (2013) and adapted their design for use with multispecies bacterial communities, including predators. I made several changes, most importantly I found that having the air needle fully inserted into the culture media caused bubbling of the bacteria and heavy growth on both the air and media needles. This in turn resulted in blockages that limited the lifespan of the chemostats. The growth on the media needle also led to growth in the media tubing connected to the needle, which over time started to spread backwards along the tubing (at a rate of 10 – 20 mm per week) (Fig. 5.2). To reduce this, I moved the air needle to be above the level of the liquid culture and mixed the chemostat contents via shaking of the water bath. This method ensured through mixing of the liquid contents of the chemostat on the same timescale as provided by bubbling, however aeration may be less effective. Good aeration is important as three of the species cultured, *Bdellovibrio* (Hespell, 1976), *P. putida* (Belda *et al.*, 2016) and *B. subtilis* (Sonenshein *et al.*, 1993) are commonly considered to be obligate aerobes. Additionally, whilst *E. coli* is a facultative anaerobe, low oxygen levels are likely to result in a transition from respiration to mixed acid fermentation, which will again affect growth rates and yields. I did not monitor oxygen levels within the chemostats, as traditional oxygen probes would be challenging to incorporate into the chemostat design, although alternative methods of measuring oxygen, such as the optical monitoring of oxygen sensitive fluorescent sensors (Klein *et al.*, 2013) are available. It is also possible to measure the effects of oxygen limitation, in chemostats containing *E. coli*, by measuring the acidification of the media due to the products of

mixed acid fermentation such as formate, lactate, ethanol and acetate, in the culture (or samples from the waste line) using a methyl red test (Clark and Lubs, 1915).

As well as developing a chemostat array I also sought to create a stable multispecies community that could co-exist both in the presence and absence of *Bdellovibrio*. I found that while all the species could co-exist, when *E. coli* and *P. putida* were co-cultured large amounts of clumped material, in the form of floating mats of bacteria accumulated. This may be the result of a stress response on the part of one or both of the bacteria. *P. putida* KT2440 is known to have a type 6 secretion system, which it uses to target other bacteria, including *E. coli* (Bernal *et al.*, 2017). While this did not allow *P. putida* to eliminate *E. coli* in my chemostats it is certainly possible that it could be responsible for inducing a stress response pathway and stress responses in *E. coli* are known to induce aggregation and increased biofilm formation (Adnan *et al.*, 2010). To reduce the problems with clumping I attempted to evolve non-clumping mutants of *E. coli* and either *P. putida* or its relative *P. synxantha*. The result was a pair of strains which I have termed iMG1655 and iKT2440 which clumped less when co-cultured (Fig. 5.21).

In order to take full advantage of the additional capacity provided by a chemostat array I investigated various methods of enumerating the densities of bacteria in my microbial communities. I tested three different methods, traditional plating and plaquing, but with a chromogenic medium that could distinguish bacterial species, qPCR and flow cytometry. Enumerating viable counts via plating and plaquing has long been the gold standard method for research into *Bdellovibrio* (Williams, 1987; Shemesh and Jurkevitch, 2004; Kadouri and O'Toole, 2005). Unlike molecular methods such as qPCR, viable counts only include culturable cells. This is important when

investigating *Bdellovibrio* because it is a bacterium with an unusually high mortality rate (Hespell *et al.*, 1974) and because a recently invaded bdelloplast is likely to still contain significant amounts of prey DNA, but it should no longer be counted as a prey cell. Viable counts are however, time consuming, limiting throughput, and are unsuited for multiple non-predatory species. The chromogenic media did allow me to distinguish most colonies, however there was a level of ambiguity in identifying some colonies and it would need to be replaced by selective media to enumerate species that are a rare (< 1%) component of the community, as otherwise dilutions which contained any of the rare species would result in a lawn of the more common species. Automation such as spiral platting can reduce plating times, but to my knowledge no automated techniques exist for plaquing assays.

qPCR has several advantages over culturing techniques. Samples for qPCR can be frozen and processed in bulk later. It is also significantly faster to perform than plating and plaquing and different species can be clearly distinguished even when they are a small component of the whole community. qPCR has been used successfully in a number of studies on *Bdellovibrio* and other BALOs (Zheng *et al.*, 2008; Van Essche, Sliepen, *et al.*, 2009; Chen *et al.*, 2018). In my hands, however, the qPCR assay tended to be somewhat unreliable and there was a trade-off between sensitivity and accuracy.

Flow cytometry has recently started to be used with *Bdellovibrio* (Duncan *et al.*, 2018, 2019). Bacterially produced fluorescent proteins allow similarly sized strains of bacteria to be distinguished and are particularly important for *Bdellovibrio* as they help to differentiate signal from this particularly small bacterium from noise. I attempted to identify mCherry2 tagged *Bdellovibrio*, eGFP *P. putida* and *E. coli* with

several different fluorescent proteins using flow cytometry. In single culture all these bacteria could be detected and in a dual culture it was possible to tell mCherry2 tagged *Bdellovibrio* from *E. coli* with mVenus. Ordinarily flow cytometry requires fresh cultures meaning samples cannot be stored, but the addition of formaldehyde to fix bacteria offers the possibility of storage for future processing. The downside of this is that formaldehyde fixation can increase autofluorescence, which may mask the signal from the fluorescent tags (Billinton and Knight, 2001).

I developed a small scale chemostat array that can run reliably for over a month without significant issues; although, as evidence by the fluctuations in bacterial densities (Fig. 5.15 c, d & Fig. 5.22 a, b), this did not give the sort of results expected from an ideal chemostat in the absence of predators. There are several possible reasons for this. Firstly, it is possible that samples taken from the waste line of the chemostat were not an accurate reflection of the contents of the vessel. This could be compensated for by sampling directly from the vessel using a needle inserted through the stopper, however, this would disturb the volume of the vessel and would pose a risk of contamination. Secondly, in the multispecies communities, where species numbers were enumerated by colony counting, it was not always possible to accurately assign a species designation to all colonies. This issue could be resolved either by using selective media, on which only one species could grow, instead of distinguishing species by their appearance on non-selective media, or by the further development of molecular methods such as qPCR or flow cytometry. Thirdly, in the multispecies communities there may have been interactions between non-predatory species that caused numbers to fluctuate. An example of this was seen in the presence of rafts of floating bacteria in the vessels containing both *E. coli* and *P. putida*. This

clumping was reduced, but not entirely eliminated, by the evolution of strains iMG1655 and iKT2440 (section 5.3.4), but other less obvious interactions could have been occurring. Finally, there was growth both on the walls of the vessels and on the needles suppling media and air, and removing waste. These biofilms would have acted as a source of bacteria, particularly in the case of the needles, where aggregates were especially prone to periodically being dislodged. Additionally, growth on the media needle would have reduced the levels of nutrients reaching the liquid cultures. Adjusting the chemostat design to have the air needle above the level of the culture (Fig. 5.3 d) prevented visible growth of biofilms on the air and media needles, however the waste needle still needed to be in contact with the culture. Growth on the walls of the vessels could be reduced by the addition of a surfactant, such as tween or by coating the walls of the vessels to make them more resistant to colonisation.

I have also developed a four species community, including a predatory bacterium, that can be cultivated within these chemostats and can co-exist for at least 30 days. Additionally, I evolved two members of this community to reduce their levels of clumping. I have shown that *Bdellovibrio* can survive for long periods within my chemostats. Finally, I have worked on improving enumeration of multi-species cultures to facilitate high-throughput processing of samples. Whilst the results from the qPCR assay were disappointing initial results from the flow cytometry were promising. It was possible to detect the *Bdellovibrio* despite their particularly small size and different bacteria could be distinguished based on the fluorescent protein they produced.

5.5 Future prospects

Firstly, now that I have evolved strains of *E. coli* and *P. putida* that should clump less in chemostats, these should be used in new multi-prey/decoy species chemostats. These should give better results as without mats of floating bacteria they will be closer to an ideal chemostat. The reduction of growth on the media needle and in the media inflow tube from repositioning to air needle to prevent bubbling will also help in this regard.

Secondly, as the *Bdellovibrio* was generally present at low densities, relative to the prey and decoy species, it had little impact on prey densities. While it would have be expected that the population of *Bdellovibrio* would have grown rapidly in the presence of excess prey it did not, and it would be interesting to see how it responds to lower densities of prey, which can be accomplished by reducing the concentration of the carbon source for the prey species.

Thirdly, given that prey was present in excess there must have been some other factor limiting either absolute population size or the population growth rate of the *Bdellovibrio*. One possibility is that there was insufficient oxygen in the chemostats. It would be possible to use an oxygen sensitive fluorescent sensor in the chemostats to monitor the oxygen levels. Alternatively, a methyl red test could be conducted on the contents of chemostats that contained *E. coli* to check for acidification due to mixed acid fermentation products which will accumulate in the absence of sufficient oxygen.

Fourthly, there were issues with running the chemostats at very low dilution rates, especially as the small volume of the chemostats resulted in particularly slow flow rates. At these low flow rates, the media tubing can develop air bubbles which

interrupt the media flow. Additionally, the use of a peristaltic pump to control the flow means that the media is delivered in discrete drops rather than a more continuous flow meaning nutrient levels in the chemostat can fluctuate. The use of a syringe pump for media delivery and larger chemostats vessels should be investigated as means to improve this issue.

Finally, attempts to fit variants of the model developed in Chapter 2, to the data I gathered from running the chemostat arrays, did not result in a good fit to the data. It possible to fit variants of that model to experimental datasets of *Bdellovibrio* predation, as this was done successfully with an experimental dataset collected by the Sockett lab, as detailed in Chapter 4. That dataset consisted of substantially more data points and was of a much higher time resolution. Further experiments should concentrate on generating larger datasets to give the model fitting the best chance of getting a good fit to the data. Further development of the flow cytometry assay should help with this. Using formaldehyde to fix samples would mean that they can be stored for processing and do not have to be processed immediately after sampling, although this may give issues with autofluorescence.

CHAPTER 6: CONCLUSIONS

B. bacteriovorus is an intriguing Gram-negative bacterium, with a highly unusual predatory lifestyle. It holds promise both as an alternative treatment for antibiotic resistant infections, and as a model system for understanding predator prey dynamics and ecology in microbes, and more generally. Fully exploiting this potential requires the application and integration of many different techniques. In this thesis I have adapted and explored two previously underexploited methods of investigating *B. bacteriovorus* predation, the use of mathematical models and predation within chemostats.

Mathematical models have a long history in predator prey ecology (Edelstein-Keshet, 2005). Models of microbial predator prey systems have mostly focused on either phage (Krysiak-Baltyn *et al.*, 2016) or protists (Curds and Bazin, 1980), while models of bacterial predators are less common (Wilkinson, 2006). In this work, I developed a family of mathematical models to explore predation by *B. bacteriovorus*. The most biological relevant of these models included predator mortality, which has been previously documented (Hespell *et al.*, 1974), a discrete bdelloplast stage and Holling type II saturating kinetics for the predator (which was the predation kinetic type that best matched the model fitting to experimental data). Using this model, I explored bacterial predation under a wide range of conditions, many of which would have been difficult or impossible to investigate experimentally, such as varying the predator attack rate constant, mortality and bdelloplast maturation rate.

This model was also used as a base for model fitting to an experimental dataset, collected by the Sockett lab at the University of Nottingham (Hobley *et al.*, 2019). This detailed the predation in isolation and combination of *E. coli* by *B. bacteriovorus* and a bacteriophage. This model fitting, gave insights into details of

predation kinetics and how different resistance phenotypes could arise. It also improved the estimates of various parameters and these parameters were used in the theoretical modelling in Chapter 2.

To attempt to verify the findings of my model, I developed an array of small self-constructed chemostats, and a stable four species bacterial community. I used these to run experiments with multiple combinations of bacteria, under different nutrient levels and dilution rates, to test the predictions of the model.

My mathematical model predicted that *B. bacteriovorus* predating a single prey species is a system that is prone to extreme oscillations, that would in a natural environment, result in the extinction of the predator. As such it could only survive permanently within a very narrow range of conditions. Increasing nutrient concentrations narrowed this survival range. Previous models of microbial predator prey interactions in chemostats, including those with *B. bacteriovorus* as the predator, also showed a tendency to extreme oscillations, especially for higher nutrient concentrations (Crowley *et al.*, 1980; Nisbet *et al.*, 1983; Wilkinson, 2001). Only the group of Varon studied this experimentally in chemostats with a *B. bacteriovorus* like predator (BM4) and *Photobacterium leiognathi* E28 as prey. They did observe oscillations, albeit less extreme ones than those seen in my model (Varon, 1979; Varon *et al.*, 1984). They also found that BM4 could survive in a chemostat with a prey density of 2-5 x 10^4 colony forming units (cfu) ml^{-1} (Varon *et al.*, 1984), substantially less than the 7 x 10^5 cfu ml^{-1} predicted by their model (Varon and Zeigler, 1978) and less still than the 4.4 x 10^6 cfu ml^{-1} minimum required for survival in our model. In contrast Keya and Alexander (Keya and Alexander, 1974) found *B. bacteriovorus* strain

PF13, isolated from soil, would only replicate in the presence of at least 3 x 10^7 cfu ml^{-1} of its *Rhizobium* prey.

Given the likelihood of extreme oscillations predicted by the model it is surprising that *B. bacteriovorus* is ubiquitous in non-marine and *B. bacteriovorus* like organisms are ubiquitous in marine environments (Shilo and Bruff, 1965; Williams, 1987; Williams, Schoeffield, *et al.*, 1995; Shemesh and Jurkevitch, 2004). This suggests that there must be other forces at work stabilising population numbers. One possibility is that *B. bacteriovorus* is a hotspot organism targeting regions of high prey density and structured environments, such as biofilms, and migrates from these regions to neighbouring areas with lower prey densities, where it is a transitory visitor. Biofilms represent a lush resource grouping for *B. bacteriovorus*. It possesses the lytic enzymes needed to chew the extracellular matrix that holds cells within the biofilm, and can likely derive valuable nutrients from this (Im *et al.*, 2018). *B. bacteriovorus* can predate the metabolically inactive cells found deeper within biofilms and its gliding motility allows it to move within the biofilm (Lambert *et al.*, 2011). Indeed, there is ample evidence that *B. bacteriovorus* is a hotspot organism. Higher numbers are found in sewage rather than in rivers (Dias and Bhat, 1965; Seliavko and Lambina, 1985), and downstream of sewage treatment plants rather than upstream (Staples and Fry, 1973) or in sewage treated rather than untreated soils (Klein and Casida, 1967). *B. bacteriovorus* are likewise more common in trickling filter biofilms than in their inflow (Fry and Staples, 1976). Prey rich rhizospheres support greater *B. bacteriovorus* numbers than bulk soil (Jurkevitch *et al.*, 2000). Eutrophic lakes have higher predatory densities than oligotrophic lakes (Chauhan *et al.*, 2009). *B. bacteriovorus* like

organisms are more abundant in marine sediments than the water column and much higher in oyster shell biofilms (Williams, Kelley, *et al.*, 1995).

While it is clear that *B. bacteriovorus* is present in prey rich natural habitats, our model predicts that in these nutrient enriched regions there will be a narrow range of conditions under which the predator can survive over long time periods. This is due to a paradox of enrichment effect (Rosenzweig, 1971) where high levels of nutrients destabilise predator prey communities leading to extreme oscillations, periods of dangerously low predator and prey densities and eventual local extinction. This narrow survival range, combined with the fact that *B. bacteriovorus* was outcompeted by a typical bacteriophage under conditions tested in both Chapters 2 and 4, and that in natural conditions it also has to compete for resource with protists, offers a potential explanation of why it has to be a semi-generalist predator.

Indeed in natural environments phage greatly outnumber *B. bacteriovorus* (Stolp, 1973; Kutter and Sulakvelidze, 2004) (this comparison is reasonable assuming that *B. bacteriovorus* in total can prey on about half of all bacteria that phage in total can prey on). This is in spite of the fact that bacteriophage have several disadvantages compared to *B. bacteriovorus*, which were not included in my models. Firstly, bacteriophage require metabolically active prey, while *B. bacteriovorus* can predate both active and dormant cells (Varon and Shilo, 1969), which can be found in biofilms growing on surfaces in nutrient rich environments. Secondly, while phenotypic persistence to *B. bacteriovorus* attack has been observed (Shemesh and Jurkevitch, 2004), stable, genetically inheritable resistance to *B. bacteriovorus* has not been seen. In contrast, phage resistance is well known (Luria and Delbrück, 1943). Thirdly, half of all sequenced bacterial genomes contain a CRISPR-CAS system (Koonin and Wolf,

2015), which acts as an adaptive immune system, and many bacteria also have restriction modification systems which digest viral DNA (Bayliss *et al.*, 2006). Finally, *B. bacteriovorus* is highly motile and possesses chemotaxis genes that likely allow it to locate regions of high prey density (Straley and Conti, 1977; Lambert *et al.*, 2003), potentially allowing the predator to move from hotspot to hotspot as resources are used up and prey becomes scarce. Despite all of these advantages, *B. bacteriovorus* is still massively outnumbered by the total population of phages. Taken together, these results suggest that for long-term survival *B. bacteriovorus* needs to be a semi-generalist predator and indeed *B. bacteriovorus* and other like organisms (BALOs) are known to have wide prey ranges (Stolp and Starr, 1963; Jurkevitch *et al.*, 2000; Dashiff *et al.*, 2010; Feng *et al.*, 2016).

My modelling of dual predation on *E. coli* by *B. bacteriovorus* and a bacteriophage showed a synergy of action between the two predators. The bacteriophage acted fastest and reduced the density of prey by about five orders of magnitude. The remaining prey that were resistant to phage predation, could still be predated by *B. bacteriovorus* and were thus removed down to levels that were below detection limits. Resistance to predation is a known issue with phage therapy (Abedon *et al.*, 2011) and is a well-studied phenomenon (Luria and Delbrück, 1943). In contrast to phage resistance, plastic resistance to *B. bacteriovorus* is much less well understood. To investigate possible causes, I competed different models for generating and removing plastic resistance to *B. bacteriovorus*. Resistance arising due to a signal caused by predation from *B. bacteriovorus* (and possibly also bacteriophage) outcompeted intrinsic resistance. The data also supported reversion to sensitivity being coupled to growth over intrinsic reversion, consistent with a

phenotypic response, not genetically inherited resistance, where new growth would be expected to be resistant and reversion occur via a mutation.

In both Chapters 2 and 4 I also investigated whether predation rates saturate at high prey densities. I found that at the densities used in both chapters, bacteriophage predation did not saturate, but *B. bacteriovorus* predation did. This is consistent with *B. bacteriovorus* taking about 30 minutes to penetrate a prey cell (Varon and Shilo, 1968). At high prey density where encounters with prey are common, this handling time limits the maximum attack rate of the predator (Jeschke *et al.*, 2002). Most mathematical models of *B. bacteriovorus* predation have a non-saturating predation rate (Varon and Zeigler, 1978; Crowley *et al.*, 1980; Hobley *et al.*, 2006; Baker *et al.*, 2017; Said *et al.*, 2019). Only my model, described in Chapter 2 and Chapter 4, and one of the models by Wilkinson (2001), use saturating kinetics, which I have found produces a better match to the data. Prior to this study there was very little information on the kinetic parameters for a saturating attack rate for *B. bacteriovorus*. By reanalysing data from Varon and Zeigler (1978), on predation of *photobacterium leiognathi* E28 by BALO BM4, I calculated an estimate for these values (see Chapter 2). In Chapter 4 I discovered values for the attack rate constant of 0.33 bdelloplasts *B. bacteriovorus*$^{-1}$ h^{-1} (0.31 to 0.43, 25th to 75th percentile) and a half-saturation constant of 3.2 x 10^6 prey cells ml^{-1} (2.5 x 10^6 to 4.2 x 10^6, 25th to 75th percentile) based on *B. bacteriovorus* HD100 predating *E. coli* S-17.

My chemostat array permitted testing of multiple growth conditions and bacterial communities, including predators in parallel. The results of these chemostat experiments demonstrated that *B. bacteriovorus* HD100 could survive in a chemostat for at least 21 days (at which time the experiment was terminated, although there was

no reason to suppose the *B. bacteriovorus* population could not have survived substantially longer). Whitby (1977) was able to keep *B. bacteriovorus* strain 6-5-S alive on a diet of *Spirillum serpens* for a similar period of time, but had to use a complex medium, as the minimal medium suitable for *S. serpens* did not support predation by *B. bacteriovorus*. At faster dilutions rates (0.1 to 0.3 h^{-1}) he observed oscillations in the densities of predator and prey with a period in the order of 100 hours. At a lower dilution rate (0.05 h^{-1}) the predator and prey came to a co-existing steady state.

Varon and co-workers (Varon, 1979; Varon *et al.*, 1984) studied the marine BALO BM4 predating a luminescent prey *Photobacterium leiognathi* E28 in a complex medium (MPY) at a dilution rate of 0.1 h^{-1} for 13 days. When nutrient levels were sufficiently high to support 1 x 10^8 cfu ml^{-1} of prey cells they observed two cycles of oscillations with large and irregular amplitude and a period of ~50 to 100 h. They also found that after six days of co-culture a predation resistant genotype of the prey, which was darker in colour and had a slower growth rate emerged. At lower nutrient levels the period of oscillation increased and the amplitude decreased, giving less obvious oscillations. A further reduction in nutrients led to either stable co-existence of predator and prey or washout of the predator in a stochastic manner.

Dulos and Marchand (1984) were the only group to previously use a minimal medium and a strain of *E. coli* as the prey species. They maintained *B. bacteriovorus* strain X-Ty in energetically open (chemostat) conditions, and at low dilution rates (0.014 h^{-1} to 0.08 h^{-1}), for up to 14 days. However, they also reported that the system was unstable and results were not reproducible between experiments. They found that, as previously reported (Huang and Starr, 1973), a deficiency in calcium ions hampered predation. In contrast to the previous experiments, they struggled to get

either predator survival or oscillations of predator and prey. In order to observe oscillations, they had to resort to using large inocula of both predator and prey, and the resulting system was still unstable, resulting in damped oscillations and experimental results that were quantitatively unrepeatable.

In contrast to Dulos and Marchand, I could reliably get *B. bacteriovorus* to survive for over a month in my small minimal media chemostats, even when operating at a similar low dilution rate of 0.03 h^{-1}. Occasionally, densities of *B. bacteriovorus* dropped below detection levels, sometimes for several days, but usually recovering (Fig. 5.16a, b). Like Dulos and Marchand, I found that patterns of population densities were often not quantitatively reproducible, to the extent that two replicate chemostats could give population densities that were 1 to 2 log orders different from each other. Unlike Varon and co-workers and the experiments of Whitby, and in contrast to the predictions of my model, I did not see sustained oscillations with repeated oscillatory cycles. However, both Whitby and Varon used different strains of predator and prey and had undefined complex media for bacterial growth, while I used a defined minimal media.

The differences in media and prey strain are important because my model predicts that there are optimal values, with narrow ranges, for many factors, including nutrient levels, which are dependent on the medium used, and prey size, prey growth rate, predator attack rate constant and BALO burst size, all of which are affected by the choice of prey and strain of predator. Increased nutrients levels in particular were shown to destabilise my chemostat model predator prey system in a paradox of enrichment (Rosenzweig, 1971). While a predator that kills its prey too efficiently

overexploits its own resource, and can lead to a tragedy of the commons (Hardin, 1968).

While it was clear that *B. bacteriovorus* could survive for substantial periods of time in my chemostats, it did not eliminate the prey species (indeed had it done so it would itself have starved, and been lost from the chemostats). This is consistent with other reports (Hespell *et al.*, 1974; Varon *et al.*, 1984) that *B. bacteriovorus* is unable to reduce prey densities below a certain level and has implications for its use as a therapeutic. It may be that when there is a single prey species *B. bacteriovorus* is most effective in combination with another anti-microbial agent. Previous work has indicated a synergy between *B. bacteriovorus* and the vertebrate immune system (Willis *et al.*, 2016) and this may also be a reason behind other successful trials in live animal models (Chu and Zhu, 2009; Atterbury *et al.*, 2011; Guo *et al.*, 2016; Shatzkes *et al.*, 2016; Findlay *et al.*, 2019). Evidence of the effectiveness of another treatment combination comes from my modelling of dual predation of *E. coli* by *B. bacteriovorus* and a bacteriophage, which showed the combined effect of the two predators was sufficient to eliminate the prey when neither predator could do so alone.

In more complex microbial communities with additional prey, decoy or predatory species, the situation becomes less clear. The presence of a secondary prey species for a generalist predator to consume may act to boost predator numbers, allowing the predator to eliminate one of the prey types. This effect has been observed in insects (Harmon and Andow, 2003), protists (Mallory *et al.*, 1983) and even polyvalent bacteriophages (Yu *et al.*, 2017) as well as *B. bacteriovorus* (Johnke *et al.*, 2017). By contrast, the presence of a decoy species can reduce the efficiency of the predator in locating prey and has been predicted to stabilise a chemostat system

(Wilkinson, 2001). No previous study investigated the effect of a decoy species on bacterial predation experimentally in a chemostat. The multiple species chemostat experiments detailed in this thesis were intended to test whether the species could co-exist over a period of at least a few weeks and in this regard they were successful. However, further, more detailed experiments would be needed to elucidate details of the effects of alternative prey and decoy species.

In conclusion, my investigations predict *B. bacteriovorus* predation yields a system that is prone to extreme, destabilising oscillations. This, together with the fact that *B. bacteriovorus* and other BALOs need to compete with specialist bacteriophage means they need to be semi-generalist predators with a wide prey range in order to survive long term in natural environments. Additionally, they should be hotspot specialists capable of migrating between regions of high prey density which they can likely detect through chemotaxis (Lambert *et al.*, 2003; Chauhan and Williams, 2006). This has implications for the use of *B. bacteriovorus*, either as a therapeutic in agriculture and aquaculture, or to reduce numbers of pathogens in an environmental setting. BALOs are likely to be most effective when there are alternative prey species present that may act to boost predator numbers, or when a second type of predator, such as bacteriophage is present and can acts synergistically with the BALO.

6.1 Future prospects

In order to fully exploit the chemostats developed in this study, the methods of quantifying densities of individual species in a co-culture need to be improved. When this is done, it should be possible to carry out investigations into the effects of prey density and diversity on bacterial predation. These should include:

1. Under which conditions are oscillations triggered and what is the nature of these oscillations?
2. Do alternative prey boost predator numbers and cause one prey species to be eliminated from the chemostat? And if so, under which conditions?
3. Do decoy species reduce the efficiency of the predator? And if so, does this allow survival of a prey species under conditions where it would otherwise become extinct?
4. Do the experimental results differ from those predicted by the model, and if so, where do they differ and what is the reason for these differences? This information should result in the production of a better model.

Future developments of the model are likely to include:

1. The addition of alternative prey and decoy species.
2. The addition of a secondary compartment to account for wall growth (Freter *et al.*, 1983), as this is one area where my small chemostats differ from an ideal chemostat.
3. The development of an individual-based model of microbial predation to explore how stochasticity affects model outcomes and whether this stabilises a system that is otherwise prone to extreme oscillations.

BIBLIOGRAPHY

Abedon, S.T., Kuhl, S.J., Blasdel, B.G., and Kutter, E.M. (2011) Phage treatment of human infections. *Bacteriophage* **1**: 66–85.

Adnan, M., Morton, G., Singh, J., and Hadi, S. (2010) Contribution of *rpoS* and *bolA* genes in biofilm formation in *Escherichia coli* K-12 MG1655. *Mol Cell Biochem* **342**: 207–213.

Alexander, M. (1981) Why microbial predators and parasites do not eliminate their prey and hosts. *Annu Rev Microbiol* **35**: 113–33.

Allee, W.C. and Bowen, E.S. (1932) Studies in animal aggregations: mass protection against colloidal silver among goldfishes. *J Exp Zool* **61**: 185–207.

Arcilla, M.S., van Hattem, J.M., Matamaros, S., Melles, D.C., Penders, J., and de Jong, M.D. (2016) Dissemination of the mcr-1 colistin resistance gene. *Lancet Infect Dis* **16**: 292–293.

Arditi, R. and Ginzburg, L.R. (1989) Coupling in predator-prey dynamics : Ratio-dependence. *J Theor Biol* **139**: 311–326.

Atterbury, R.J., Hobley, L., Till, R., Lambert, C., Capeness, M.J., Lerner, T.R., et al. (2011) Effects of orally administered *Bdellovibrio bacteriovorus* on the well-being and *Salmonella* colonization of young chicks. *Appl Environ Microbiol* **77**: 5794–803.

Azam, F., Fenchel, T., Field, J.G., Gray, J.S., Meyer-Reil, L.A., and Thingstad, F. (1983) The ecological role of water-column microbes in the sea. *Mar Ecol Prog Ser* **10**: 257–263.

Baker, M., Negus, D., Raghunathan, D., Radford, P.M., Moore, C., Clark, G., et al. (2017) Measuring and modelling the response of Klebsiella pneumoniae KPC prey to Bdellovibrio bacteriovorus predation, in human serum and defined buffer. *Sci Rep* **7**: 1–18.

Bamford, K. (2016) Development of a quantitative PCR for the enumeration of *Bdellovibrionaceae* in single and mixed cultures.

Bayliss, C.D., Callaghan, M.J., and Moxon, E.R. (2006) High allelic diversity in the methyltransferase gene of a phase variable type III restriction-modification system has implications for the fitness of *Haemophilus influenzae*. *Nucleic Acids Res* **34**: 4046–59.

Becks, L., Hilker, F.M., Malchow, H., Jürgens, K., and Arndt, H. (2005) Experimental demonstration of chaos in a microbial food web. *Nature* **435**: 1226–9.

Beebe, J.M. (1941) Studies on the *myxobacteria*: I, distribution in Iowa soils and description of a new species; II, *Myxobacteria* as bacterial parasites; III, The morphology and cytology of *Myxococcus xanthus* sp. n.

Belda, E., van Heck, R.G.A., José Lopez-Sanchez, M., Cruveiller, S., Barbe, V., Fraser, C.M., et al. (2016) The revisited genome of *Pseudomonas putida* KT2440 enlightens its value as a robust metabolic chassis. *Environ Microbiol* **18**: 3403–3424.

Berleman, J.E., Chumley, T., Cheung, P., and Kirby, J.R. (2006) Rippling is a predatory behavior in *Myxococcus xanthus*. *J Bacteriol* **188**: 5888–5895.

Bernal, P., Allsopp, L.P., Filloux, A., and Llamas, M.A. (2017) The *Pseudomonas putida* T6SS is a plant warden against phytopathogens. *ISME J* **11**: 972–987.

Berryman, A.A. (1992) The origins and evolution of predator-prey theory. *Ecology* **73**: 1530–1535.

Bigger, M. (1973) An investigation by fourier analysis into the interaction between coffee leaf-miners and their larval parasites. *J Anim Ecol* **42**: 417–434.

Billinton, N. and Knight, A.W. (2001) Seeing the wood through the trees: A review of techniques for distinguishing green fluorescent protein from endogenous autofluorescence. *Anal Biochem* **291**: 175–197.

Blake, W. (1794) Songs of experience.

Bohannan, B.J.M. and Lenski, R.E. (2000) Linking genetic change to community evolution: insights from studies of bacteria and bacteriophage. *Ecol Lett* **3**: 362–377.

Brenner, D.J., Krieg, N.R., Staley, J.T., Garrity, G.M., Boone, D.R., De Vos, P., et al. (2005) Bergey's manual® of systematic bacteriology, second edition, volume two: the Proteobacteria part B the gammaproteobacteria.

Burnham, J.C., Hashimoto, T., and Conti, S.F. (1970) Ultrastructure and cell division of a facultatively parasitic strain of *Bdellovibrio bacteriovorus*. *J Bacteriol* **101**: 997–1004.

Capeness, M.J., Lambert, C., Lovering, A.L., Till, R., Uchida, K., Chaudhuri, R., et al. (2013) Activity of *Bdellovibrio* hit locus proteins, Bd0108 and Bd0109, links Type IVa pilus extrusion/retraction status to prey-independent growth signalling. *PLoS One* **8**: e79759.

Chauhan, A., Cherrier, J., and Williams, H.N. (2009) Impact of sideways and bottom-up control factors on bacterial community succession over a tidal cycle. *Proc Natl Acad Sci U S A* **106**: 4301–6.

Chauhan, A. and Williams, H.N. (2006) Response of *Bdellovibrio* and like organisms (BALOs) to the migration of naturally occurring bacteria to chemoattractants. *Curr Microbiol* **53**: 516–522.

Chen, H., Athar, R., Zheng, G., and Williams, H.N. (2011) Prey bacteria shape the community structure of their predators. *ISME J* **5**: 1314–22.

Chen, H., Laws, E.A., Martin, J.L., Berhane, T.-K., Gulig, P.A., and Williams, H.N. (2018) Relative contributions of *Halobacteriovorax* and bacteriophage to bacterial cell death under various environmental conditions. *MBio* **9**: e01202-18.

Chern, E.C., Siefring, S., Paar, J., Doolittle, M., and Haugland, R.A. (2011) Comparison of quantitative PCR assays for *Escherichia coli* targeting ribosomal RNA and single copy genes. *Lett Appl Microbiol* **52**: 298–306.

Chu, W.H. and Zhu, W. (2009) Isolation of *Bdellovibrio* as biological therapeutic agents used for the treatment of *Aeromonas hydrophila* infection in fish. *Zoonoses Public Health* **57**: 258–264.

Clark, W.M. and Lubs, H.A. (1915) The differentiation of bacteria of the *Colonaerogenes* family by the use of indicators. *J Infect Dis* **17**: 160–173.

Cotter, T.W. and Thomashow, M.F. (1992) Identification of a *Bdellovibrio bacteriovorus* genetic locus, hit, associated with the host-independent phenotype. *J Bacteriol* **174**: 6018–6024.

Cover, W.H., Martinez, R.J., and Rittenberg, S.C. (1984) Permeability of the boundary layers of *Bdellovibrio bacteriovorus 109J* and its bdelloplasts to small hydrophilic molecules. *J Bacteriol* **157**: 385–390.

Cremer, J., Arnoldini, M., and Hwa, T. (2017) Effect of water flow and chemical environment on microbiota growth and composition in the human colon. *Proc Natl Acad Sci U S A* **114**: 6438–6443.

Crowley, P.H., Straley, S.C., Craig, R.J., Culin, J.D., Fu, Y.T., Hayden, T.L., et al. (1980) A model of prey bacteria, predator bacteria, and bacteriophage in continuous culture. *J Theor Biol* **86**: 377–400.

Curds, C.R. and Bazin, M.J. (1980) Protozoan predation in batch and continuous cultures. In, Droop,M.R. and Jannasch,H.W. (eds), *Advances in Aquatic Microbiology*. Academic Press, pp. 115–176.

Dashiff, A., Junka, R.A., Libera, M., and Kadouri, D.E. (2010) Predation of human pathogens by the predatory bacteria *Micavibrio aeruginosavorus* and *Bdellovibrio bacteriovorus*. *J Appl Microbiol* **110**: 431–444.

Dattner, I., Miller, E., Petrenko, M., Kadouri, D.E., Jurkevitch, E., and Huppert, A. (2017) Modelling and parameter inference of predator–prey dynamics in heterogeneous environments using the direct integral approach. *J R Soc Interface* **14**:.

Dias, F.F. and Bhat, J. V (1965) Microbial ecology of activated sludge. II. bacteriophages, *Bdellovibrio*, coliforms, and other organisms. *Appl Microbiol* **13**: 257–261.

Diedrich, D.L., Denny, C.F., Hashimoto, T., and Conti, S.F. (1970) Facultatively parasitic strain of *Bdellovibrio bacteriovorus*. *J Bacteriol* **101**: 997–1004.

Donze, D., Mayo, J.A., and Diedrich, D.L. (1991) Relationships among the *Bdellovibrios* revealed by partial sequences of 16S ribosomal RNA. *Curr Microbiol* **23**: 115–119.

Dulos, E. and Marchand, A. (1984) Oscillations des densitiés de population du couple bactérien proie-prédateur *Escherichia coli-Bdellovibrio bacteriovorus*: Etude expérimental et modèle théorique. *Ann l'Institut Pasteur / Microbiol* **135**: 271–295.

Duncan, M.C., Forbes, J.C., Nguyen, Y., Shull, L.M., Gillette, R.K., Lazinski, D.W., et al. (2018) *Vibrio cholerae* motility exerts drag force to impede attack by the bacterial predator *Bdellovibrio bacteriovorus*. *Nat Commun* **9**: 4757.

Duncan, M.C., Gillette, R.K., Maglasang, M.A., Corn, E.A., Tai, A.K., Lazinski, D.W., et al. (2019) High-throughput analysis of gene function in the bacterial predator *Bdellovibrio bacteriovorus*. *MBio* **10**: 1–12.

Dunlap, P. V. (1985) Osmotic control of luminescence and growth in *Photobacterium leiognathi* from ponyfish light organs. *Arch Microbiol* **141**: 44–50.

Edelstein-Keshet, L. (2005) Mathematical models in biology, Society for Industrial and Applied Mathematics.

Eisenstadt, E., Carlton, B.C., and Brown, B.J. (1994) Gene mutation. In, *Methods for general and molecular bacteriology*. Washington, DC: American Society for Microbiology, pp. 297–316.

Elton, C. (1942) Voles, mice and lemmings. Problems in population dynamics.

Emmert, E.A.B., Haupt, Z.M., Pflaum, K.M., Lasbury, J.L., McGrath, J.P., Collins, A.E., and Briand, C.H. (2014) *Bdellovibrio bacteriovorus* protects *Caenorhabditis elegans* from bacterial pathogens. *Fine Focus*.

Van Essche, M., Quirynen, M., Sliepen, I., Van Eldere, J., and Teughels, W. (2009) *Bdellovibrio bacteriovorus* attacks *Aggregatibacter actinomycetemcomitans*. *J Dent Res* **88**: 182–6.

Van Essche, M., Sliepen, I., Loozen, G., Van Eldere, J., Quirynen, M., Davidov, Y., et al. (2009) Development and performance of a quantitative PCR for the enumeration of *Bdellovibrionaceae*. *Environ Microbiol Rep* **1**: 228–233.

Evans, K.J., Lambert, C., and Sockett, R.E. (2007) Predation by *Bdellovibrio bacteriovorus HD100* requires type IV pili. *J Bacteriol* **189**: 4850–4859.

Feng, S., Tan, C.H., Cohen, Y., and Rice, S.A. (2016) Isolation of *Bdellovibrio bacteriovorus* from a tropical wastewater treatment plant and predation of mixed species biofilms assembled by the native community members. *Environ Microbiol*.

Fenton, A.K. (2010) Roles of cytoskeletal proteins in the predatory life cycle of *Bdellovibrio bacteriovorus*.

Findlay, J.S., Flick-Smith, H.C., Keyser, E., Cooper, I.A., Williamson, E.D., and Oyston, P.C.F. (2019) Predatory bacteria can protect SKH-1 mice from a lethal plague challenge. *Sci Rep* **9**: 7225.

Fisher, S.H. and Sonenshein, A.L. (1991) Control of carbon and nitrogen metabolism in *Bacillus subtilis*. *Annu Rev Microbiol* **45**: 107–35.

Freter, R., Brickner, H., Fekete, J., Vickerman, M.M., and Carey, K.E. (1983) Survival and implantation of *Escherichia coli* in the intestinal tract. *Infect Immun* **39**: 686–703.

Fry, J.C. and Staples, D.G. (1976) Distribution of *Bdellovibrio bacteriovorus* in sewage works, river water, and sediments. *Appl Environ Microbiol* **31**: 469–474.

Fuhrman, J.A. and Noble, R.T. (1995) Viruses and protists cause similar bacterial mortality in coastal seawater. *Limnol Oceanogr* **40**: 1236–1242.

Gallet, R., Tully, T., and Evans, M.E.K. (2009) Ecological conditions affect evolutionary trajectory in a predator-prey system. *Evolution (N Y)* **63**: 641–651.

Gause, G.F. (1934) The struggle for existence, New York: Hafner Publishing Company.

Ginzburg, L.R. and Akçakaya, R.H. (1992) Consequences of ratio-dependent predation for steady-state properties of ecosystems. *Ecology* **73**: 1536–1543.

Giovannoni, S.J., Tripp, H.J., Givan, S., Podar, M., Vergin, K.L., Baptista, D., et al. (2005) Genetics: Genome streamlining in a cosmopolitan oceanic bacterium. *Science (80-)* **309**: 1242–1245.

Gommersall, L.M., Arya, M., Patel, P.S., and Patel, H.R.H. (2007) Quantitative reverse transcriptase polymerase chain reaction. In, Patel,H.R.H., Arya,M., and Shergill,I.S. (eds), *Basic Science Techniques in Clinical Practice*. London: Springer London, pp. 66–85.

Gompertz, B. (1825) On the nature of the function expressive of the law of human mortality , and on a new mode of determining the value of life contingencies. **115**: 513–583.

Guo, Y., Yan, L., and Cai, J. (2016) Effects of *Bdellovibrio* and like organisms on survival and growth performance of juvenile turbot, *Scophthalmus maximus*. *J World Aquac Soc* **47**: 633–645.

Gupta, S., Tang, C., Tran, M., and Kadouri, D.E. (2016) Effect of predatory bacteria on human cell lines. *PLoS One* **11**: e0161242.

Hadas, H., Einav, M., Fishov, L., and Zaritsky, A. (1997) Bacteriophage T4 development depends on the physiology of its host *Escherichia coli*. *Microbiology* **143**: 179–185.

Hagen, K.S. and Franz, J.M. (1973) A history of biological control. *Hist Entomol Annu Rev Palo Alto, CA* 433–476.

Halton, J.H. (1960) Sequential Monte Carlo. *Math Proceeding Cambridge Philos Soc* **58**: 57–78.

Hardin, G. (1960) The competitive exclusion principle. *Science (80-)* **131**: 1292–1297.

Hardin, G. (1968) The tragedy of the commons. The population problem has no technical solution; it requires a fundamental extension in morality. *Science* **162**: 1243–8.

Harmon, J.P. and Andow, D.A. (2003) Alternative foods as a mechanism to enhance a generalist ladybird's predation of target prey. *Proc first Int Symp Biol Control arthropods* 244–249.

Henze, M., Grady, C.P.L., Gujer, W., Marais, G.V.R., and Matsuo, T. (1987) A general model for single-sludge wastewater treatment systems. *Water Res* **21**: 505–515.

Hespell, R.B. (1976) Glycolytic and tricarboxylic acid cycle enzyme activities during intraperiplasmic growth of *Bdellovibrio bacteriovorus* on *Escherichia coli*. *J Bacteriol* **128**: 677–80.

Hespell, R.B., Miozzari, G.F., and Rittenberg, S.C. (1975) Ribonucleic acid destruction and synthesis during intraperiplasmic growth of *Bdellovibrio bacteriovorus*. *J Bacteriol* **123**: 481–91.

Hespell, R.B., Thomashow, M.F., and Rittenberg, S.C. (1974) Changes in cell composition and viability of *Bdellovibrio bacteriovorus* during starvation. *Arch Microbiol* **97**: 313–327.

Hilgard, P. and Stockert, R. (2000) Heparan sulfate proteoglycans initiate dengue virus infection of hepatocytes. *Hepatology* **32**: 1069–1077.

Hobley, L., King, J.R., and Sockett, R.E. (2006) *Bdellovibrio* predation in the presence of decoys: Three-way bacterial interactions revealed by mathematical and experimental analyses. *Appl Environ Microbiol* **72**: 6757–6765.

Hobley, L., Till, R., Milner, D.S., Atterbury, R.J., Stroud, A., Capeness, M.J., et al. (2019) Dataset of dual predation by bacteriophage and *Bdellovibrio* on *Escherichia coli*.

Hol, F.J.H., Rotem, O., Jurkevitch, E., Dekker, C., and Koster, D.A. (2016) Bacterial predator–prey dynamics in microscale patchy landscapes. *Proc R Soc B Biol Sci* **283**: 1–9.

Holling, C.S. (1959a) Some characteristics of simple types of predation and parasitism. *Can Entomol* **XCI**: 385–398.

Holling, C.S. (1959b) The components of predation as revealed by a study of small mammal predation of the European Pine Sawfly. *Can Entomol* **91**: 234–261.

Hopf, E. (1948) A mathematical example displaying features of turbulence. *Commun Pure Appl Math* **1**: 303–322.

Huang, J.C.C. and Starr, M.P. (1973) Effects of calcium and magnesium ions and host viability on growth of *Bdellovibrios*. *Antonie Van Leeuwenhoek* **39**: 151–167.

Huffaker, C.B., Shea, K.P., and Herman, S.G. (1963) Experimental studies on predation: Complex dispersion and levels of food in an acarine predator-prey interaction. *J Agric Sci* **34**: 305–330.

Iebba, V., Santangelo, F., Totino, V., Nicoletti, M., Gagliardi, A., De Biase, R.V., et al. (2013) Higher prevalence and abundance of *Bdellovibrio bacteriovorus* in the human gut of healthy subjects. *PLoS One* **8**: e61608.

Im, H., Choi, S.Y., Son, S., and Mitchell, R.J. (2017) Combined application of bacterial predation and violacein to kill polymicrobial pathogenic communities. *Sci Rep* **7**: 1–10.

Im, H., Dwidar, M., and Mitchell, R.J. (2018) *Bdellovibrio bacteriovorus HD100*, a predator of Gram-negative bacteria, benefits energetically from *Staphylococcus aureus* biofilms

without predation. *ISME J* **12**: 2090–2095.

Jannasch, H.W. (1969) Estimations of bacterial growth rates in natural waters. *J Bacteriol* **99**: 156–160.

Jansen, V.A.A. and Sigmund, K. (1998) Shaken not stirred: on permanence in ecological communities. *Theor Popul Biol* **54**: 195–201.

Jeschke, J.M., Kopp, M., and Tollrian, R. (2004) Consumer-food systems: why type I functional responses are exclusive to filter feeders. *Biol Rev* **79**: 337–349.

Jeschke, J.M., Kopp, M., and Tollrian, R. (2002) Predator functional responses: Discriminating between handling and digesting prey. *Ecol Monogr* **72**: 95–112.

Johnke, J., Baron, M., Leeuw, M. de, Kushmaro, A., Jurkevitch, E., Harms, H., and Chatzinotas, A. (2017) A generalist protist predator enables coexistence in multitrophic predator-prey systems containing a phage and the bacterial predator *Bdellovibrio*. *Front Ecol Evol* **5**: 124.

Jurkevitch, E., Minz, D., Ramati, B., and Barel, G. (2000) Prey range characterization, ribotyping, and diversity of soil and rhizosphere *Bdellovibrio spp*. isolated on phytopathogenic bacteria. *Appl Environ Microbiol* **66**: 2365–71.

Kadouri, D.E. and O'Toole, G.A. (2005) Susceptibility of biofilms to *Bdellovibrio bacteriovorus* attack. *Appl Environ Microbiol* **71**: 4044–4051.

Kessel, M. and Shilo, M. (1976) Relationship of *Bdellovibrio* elongation and fission to host cell size. *J Bacteriol* **128**: 477–80.

Keya, S.O. and Alexander, M. (1974) Regulation of parasitism by host density: the *Bdellovibrio-Rhizobium* interrelationship. *Soil Biol Biochem* **7**: 231–237.

Klein, D.A. and Casida, L.E.J. (1967) Occurrence and enumeration of *Bdellovibrio bacteriovorus* in soil capable of parasitizing *Escherichia coli* and indigenous soil bacteria. *Can J Microbiol* **13**: 1235–41.

Klein, T., Schneider, K., and Heinzle, E. (2013) A system of miniaturized stirred bioreactors for parallel continuous cultivation of yeast with online measurement of dissolved oxygen and off-gas. *Biotechnol Bioeng* **110**: 535–542.

Koonin, E. V. and Wolf, Y.I. (2015) Evolution of the CRISPR-Cas adaptive immunity systems in prokaryotes: models and observations on virus–host coevolution. *Mol Biosyst* **11**: 20–27.

Koval, S.F. and Bayer, M.E. (1997) Bacterial capsules: no barrier against *Bdellovibrio bacteriovorus*. *Microbiology* **143**: 749–753.

Koval, S.F. and Hynes, S.H. (1991) Effect of paracrystalline protein surface layers on predation by *Bdellovibrio bacteriovorus*. *J Bacteriol* **173**: 2244–2249.

Koval, S.F., Hynes, S.H., Flannagan, R.S., Pasternak, Z., Davidov, Y., and Jurkevitch, E. (2013) *Bdellovibrio exovorus* sp. nov., a novel predator of *Caulobacter crescentus*. *Int J Syst Evol Microbiol* **63**: 146–151.

Krebs, C.J., Boonstra, R., Stan, B., and Sinclair, A.R.E. (2001) What drives the 10-year cycle of Snowshoe hares? *Bioscience* **51**: 25–35.

Kreft, J.-U., Booth, G., and Wimpenny, J.W.T. (1998) BacSim, a simulator for individual-based modelling of bacterial colony growth. *Microbiology* **144**: 3275–3287.

Krysiak-Baltyn, K., Martin, G.J.O., Stickland, A.D., Scales, P.J., and Gras, S.L. (2016)

Computational models of populations of bacteria and lytic phage. *Crit Rev Microbiol* **42**: 942–968.

Kubitschek, H.E. and Friske, J.A. (1986) Determination of bacterial cell volume with the Coulter Counter. *J Bacteriol* **168**: 1466–7.

Kuru, E., Lambert, C., Rittichier, J., Till, R., Ducret, A., Derouaux, A., et al. (2017) Fluorescent D-amino-acids reveal bi-cellular cell wall modifications important for *Bdellovibrio bacteriovorus* predation. *Nat Microbiol* 1.

Kutter, E.M. and Sulakvelidze, A. (2004) Bacteriophages biology and applications. In, Kutter,E. and Sulakvelidze,A. (eds), *Bacteriophages Biology and Applications*. Boca Raton: CRC Press, pp. 1–4.

Labrie, S.J., Samson, J.E., and Moineau, S. (2010) Bacteriophage resistance mechanisms. *Nat Rev Microbiol* **8**: 317–327.

Lamarre, A.G., Straley, S.C., and Conti, S.F. (1977) Chemotaxis toward amino acids by *Bdellovibrio bacteriovorus*. *J Bacteriol* **131**: 201–207.

Lambert, C., Chang, C.-Y., Capeness, M.J., and Sockett, R.E. (2010) The first bite — profiling the predatosome in the bacterial pathogen Bdellovibrio. *PLoS One* **5**: e8599.

Lambert, C., Evans, K.J., Till, R., Hobley, L., Capeness, M.J., Rendulic, S., et al. (2006) Characterizing the flagellar filament and the role of motility in bacterial prey-penetration by *Bdellovibrio bacteriovorus*. *Mol Microbiol* **60**: 274–86.

Lambert, C., Fenton, A.K., Hobley, L., and Sockett, R.E. (2011) Predatory *Bdellovibrio* bacteria use gliding motility to scout for prey on surfaces. *J Bacteriol* **193**: 3139–41.

Lambert, C., Ivanov, P., and Sockett, R.E. (2010) A transcriptional "scream" early response of *E. coli* prey to predatory invasion by *Bdellovibrio*. *Curr Microbiol*.

Lambert, C., Morehouse, K.A., Chang, C.-Y., and Sockett, R.E. (2006) *Bdellovibrio*: growth and development during the predatory cycle. *Curr Opin Microbiol* **9**: 639–644.

Lambert, C., Smith, M.C.M., and Sockett, R.E. (2003) A novel assay to monitor predator-prey interactions for *Bdellovibrio bacteriovorus 109 J* reveals a role for methyl-accepting chemotaxis proteins in predation. *Environ Microbiol* **5**: 127–132.

Lambert, C. and Sockett, R.E. (2008) Laboratory maintenance of *Bdellovibrio*. *Curr Protoc Microbiol* **Chapter 1**: Unit 1B.1.

Lambina, V.A., Afinogenova, A. V., Romaĭ Penabad, S., Konovalova, S.M., and Pushkareva, A.P. (1982) *Micavibrio admirandus* gen. et sp. nov. *Mikrobiologiia* **51**: 114–7.

Langridge, G.C., Phan, M.D., Turner, D.J., Perkins, T.T., Parts, L., Haase, J., et al. (2009) Simultaneous assay of every *Salmonella Typhi* gene using one million transposon mutants. *Genome Res* **19**: 2308–2316.

Lenz, R.W. and Hespell, R.B. (1978) Attempts to grow *Bdellovibrios* micurgically-injected into animal cells. *Arch Microbiol* **119**: 245–248.

Lerner, T.R., Lovering, A.L., Bui, N.K., Uchida, K., Aizawa, S., Vollmer, W., and Sockett, R.E. (2012) Specialized peptidoglycan hydrolases sculpt the intra-bacterial niche of predatory *Bdellovibrio* and increase population fitness. *PLoS Pathog* **8**:.

Leslie, P.H. (1948) Some further notes on the use of matrices in population mathematics. *Biometrika* **35**: 213–245.

Levin, B.R., Stewart, F.M., and Chao, L. (1977) Resource-limited growth, competition, and

predation: a model and experimental studies with bacteria and bacteriophage. *Am Nat* **111**: 3–24.

Li, H., Chen, C., Sun, Q., Liu, R., and Cai, J. (2014) *Bdellovibrio* and like organisms enhanced growth and survival of *Penaeus monodon* and altered bacterial community structures in its rearing water. *Appl Environ Microbiol* **80**: 6346–54.

Loozen, G., Boon, N., Pauwels, M., Slomka, V., Rodrigues Herrero, E., Quirynen, M., and Teughels, W. (2015) Effect of *Bdellovibrio bacteriovorus* HD100 on multispecies oral communities. *Anaerobe* **35**: 45–53.

Lotka, A.J. (1925) Elements of physical biology. *Am J Public Health* **15**: 812.

Luck, R.F. (1990) Evaluation of natural enemies for biological control: A behavioral approach. *Trends Ecol Evol* **5**: 196–199.

Luckinbill, L.S. (1973) Coexistence in laboratory populations of *Paramecium Aurelia* and Its predator *Didinium Nasutum*. *Ecology* **54**: 1320–1327.

Luria, S.E. and Delbrück, M. (1943) Mutations of bacteria from virus sensitivity to virus resistance. *Genetics* **28**: 491–511.

MacConkey, A. (1905) Lactose-fermenting bacteria in faeces. *J Hyg (Lond)* **5**: 333–379.

Maclulich, D.A. (1936) Fluctuations in numbers of varying hares. *Science (80-)* **83**: 162.

Maki, N., Gestwicki, J.E., Lake, E.M., Kiessling, L.L., and Adler, J. (2000) Motility and chemotaxis of filamentous cells of *Escherichia coli*. *J Bacteriol* **182**: 4337–4342.

Makowski, Ł., Trojanowski, D., Till, R., Lambert, C., Lowry, R.C., Sockett, R.E., and Zakrzewska-Czerwińska, J. (2019) Dynamics of chromosome replication and its relationship to predatory attack lifestyles in *Bdellovibrio bacteriovorus*. *bioRxiv*.

Mallory, L.M., Yuk, C.-S.S., Liang, L.-N.N., and Alexander, M. (1983) Alternative prey: a mechanism for elimination of bacterial species by protozoa. *Appl Environ Microbiol* **46**: 1073–1079.

Marbach, A., Varon, M., and Shilo, M. (1976) Properties of marine *Bdellovibrios*. *Microb Ecol* **2**: 284–295.

Matin, A. and Rittenberg, S.C. (1972) Kinetics of deoxyribonucleic acid destruction and synthesis during growth of *Bdellovibrio bacteriovorus* strain 109D on *Pseudomonas putida* and *Escherichia coli*. *J Bacteriol* **111**: 664–673.

May, R.M. (1972) Limit cycles in predator-prey models. *Science (80-)* **177**: 900–902.

Mckay, M.D., Beckman, R.J., and Conover, W.J. (1979) Comparison of three methods for selecting values of input variables in the analysis of output from a computer code a comparison of three methods for selecting values of input variables in the analysis of output from a computer code. *Technometrics* **21**: 239–245.

Miller, A.W., Befort, C., Kerr, E.O., and Dunham, M.J. (2013) Design and use of multiplexed chemostat arrays. *J Vis Exp* e50262.

Milner, D.S., Till, R., Cadby, I.T., Lovering, A.L., Basford, S.M., Saxon, E.B., et al. (2014) Ras GTPase-like protein *MglA*, a controller of bacterial social-motility in *Myxobacteria*, has evolved to control bacterial predation by *Bdellovibrio*. *PLoS Genet* **10**: e1004253.

Monnappa, A.K., Bari, W., Choi, S.Y., and Mitchell, R.J. (2016) Investigating the responses of human epithelial cells to predatory bacteria. *Sci Rep* **6**: 33485.

Monod, J. (1949) The growth of bacterial cultures. *Annu Rev Microbiol* **3**: 371–394.

Mossel, D.A., Mengerink, W.H., and Scholts, H.H. (1962) Use of a modified MacConkey agar medium for the selective growth and enumeration of *Enterobacteriaceae*. *J Bacteriol* **84**: 381.

Nelson, K.E., Weinel, C., Paulsen, I.T., Dodson, R.J., Hilbert, H., Martins dos Santos, V.A.P., et al. (2002) Complete genome sequence and comparative analysis of the metabolically versatile *Pseudomonas putida* KT2440. *Environ Microbiol* **4**: 799–808.

Nisbet, R.M., Cunningham, A., and Gurney, W.S. (1983) Endogenous metabolism and the stability of microbial prey-predator systems. *Biotechnol Bioeng* **25**: 301–306.

Núñez, M.E., Martin, M.O., Chan, P.H., and Spain, E.M. (2005) Predation, death, and survival in a biofilm: *Bdellovibrio* investigated by atomic force microscopy. *Colloids Surfaces B Biointerfaces* **42**: 263–271.

Núñez, M.E., Martin, M.O., Duong, L.K., Ly, E., and Spain, E.M. (2003) Investigations into the life cycle of the bacterial predator *Bdellovibrio bacteriovorus* 109J at an interface by atomic force microscopy. *Biophys J* **84**: 3379–3388.

Paine, R.T. (1969) A note on trophic complexity and community stability. *Am Nat* **103**: 91–93.

Pérez, J., Moraleda-Muñoz, A., Marcos-Torres, F.J., and Muñoz-Dorado, J. (2016) Bacterial predation: 75 years and counting! *Environ Microbiol* **18**: 766–779.

Perry, J.D., Ford, M., Taylor, J., Jones, A.L., Freeman, R., and Gould, F.K. (1999) ABC medium, a new chromogenic agar for selective isolation of *Salmonella* spp. *J Clin Microbiol* **37**: 766–768.

Piñeiro, S.A., Sahaniuk, G.E., Romberg, E., and Williams, H.N. (2004) Predation pattern and phylogenetic analysis of *Bdellovibrionaceae* from the Great Salt Lake, Utah. *Curr Microbiol* **48**: 113–117.

Proctor, L.M. and Fuhrman, J.A. (1990) Viral mortality of marine bacteria and cyanobacteria. *Nature* **343**: 60–62.

Raghunathan, D., Radford, P.M., Gell, C., Negus, D., Moore, C., Till, R., et al. (2019) Engulfment, persistence and fate of Bdellovibrio bacteriovorus predators inside human phagocytic cells informs their future therapeutic potential. *Sci Rep* **9**: 1–16.

Reischl, U., Linde, H.-J., Metz, M., Leppmeier, B., and Lehn, N. (2000) Rapid identification of methicillin-resistant *Staphylococcus aureus* and simultaneous species confirmation using real-time fluorescence PCR. *J Clin Microbiol* **38**: 2429–2433.

Rendulic, S., Jagtap, P., Rosinus, A., Eppinger, M., Baar, C., Lanz, C., et al. (2004) A predator unmasked: life cycle of *Bdellovibrio bacteriovorus* from a genomic perspective. *Science (80-)* **303**: 689–693.

Rittenberg, S.C. and Shilo, M. (1970) Early host damage in the infection cycle of *Bdellovibrio bacteriovorus*. *J Bacteriol* **102**: 149–60.

Romanowski, E.G., Stella, N.A., Brothers, K.M., Yates, K.A., Funderburgh, M.L., Funderburgh, J.L., et al. (2016) Predatory bacteria are nontoxic to the rabbit ocular surface. *Sci Rep* **6**: 30987.

Romo, A.J., Ruby, E.G., and Saier, M.H.J. (1992) Effect of *Bdellovibrio bacteriovorus* infection on the phosphoenolpyruvate:sugar phosphotransferase system in *Escherichia coli* : evidence for activation of cytoplasmic proteolysis. *Res Microbiol Paris* **143**: 5–14.

Rosenzweig, M.L. (1971) Paradox of enrichment: destabilization of exploitation

ecosystems in ecological time. *Science* **171**: 385–7.

Rosenzweig, M.L. (1969) Why the Prey Curve Has a Hump. *Am Nat* **103**: 81–87.

Rosenzweig, M.L. and MacArthur, R.H. (1963) Graphical representation and stability conditions of predator-prey Interactions. *Am Nat* **97**: 209–223.

Rosenzweig, R.F., Sharp, R.R., Treves, D.S., and Adams, J. (1994) Microbial evolution in a simple unstructured environment: Genetic differentiation in *Escherichia coli*. *Genetics* **137**: 903–917.

Rotem, O., Pasternak, Z., and Jurkevitch, E. (2014) *Bdellovibrio* and like organisms. In, *The Prokaryotes*. Berlin, Heidelberg: Springer, pp. 3–17.

Russo, R., Kolesnikova, I., Kim, T., Gupta, S., Pericleous, A., Kadouri, D.E., and Connell, N.D. (2018) Susceptibility of virulent *Yersinia pestis* bacteria to predator bacteria in the lungs of mice. *Microorganisms* **7**: 2.

Said, N., Chatzinotas, A., and Schmidt, M. (2019) Have an ion on it: The life-cycle of *Bdellovibrio bacteriovorus* viewed by helium-ion microscopy. *Adv Biosyst* **3**: 1800250.

Sambrook, J. and Russel, D.W. (2001) Molecular cloning: A laboratory manual, Cold Spring Harbour: Cold Spring Harbor Laboratory Press.

Saxon, E.B., Jackson, R.W., Bhumbra, S., Smith, T., and Sockett, R.E. (2014) *Bdellovibrio bacteriovorus HD100* guards against *Pseudomonas tolaasii* brown-blotch lesions on the surface of post-harvest *Agaricus bisporus* supermarket mushrooms. *BMC Microbiol* **14**: 163.

Scherff, R.H. (1973) Control of bacterial blight of soybean by *Bdellovibrio bacteriovorus*. *Phytopathology* **63**: 400–402.

Schulz, H.N., Brinkhoff, T., Ferdelman, T.G., Hernández Mariné, M., Teske, A., and Jørgensen, B.B. (1999) Dense populations of a giant sulfur bacterium in namibian shelf sediments. *Science (80-)* **284**: 493–495.

Schwudke, D., Linscheid, M.W., Strauch, E., Appel, B., Zahringer, U., Moll, H., et al. (2003) The obligate predatory *Bdellovibrio bacteriovorus* possesses a neutral lipid A containing alpha-D-Mannoses that replace phosphate residues: similarities and differences between the lipid As and the lipopolysaccharides of the wild type strain B. b. *J Biol Chem* **278**: 27502–12.

Seidler, R.J. and Starr, M.P. (1969a) Factors affecting the intracellular parasitic growth of *Bdellovibrio bacteriovorus* developing within *Escherichia coli*. *J Bacteriol* **97**: 912–23.

Seidler, R.J. and Starr, M.P. (1969b) Isolation and characterization of host-independent *Bdellovibrios*. *J Bacteriol* **100**: 769–785.

Seliavko, A. V. and Lambina, V.A. (1985) Distribution of microorganisms lysing *Pseudomonas aeruginosa* and *Staphylococcus aureus* in the system of sewage waters. *Nauchnye Doki Vyss Shkoly Biol Nauk* **4**: 84–8.

Shampine, L.F. and Reichelt, M.W. (1997) The MATLAB ode suite. *SIAM J Sci Comput* **18**: 1–22.

Shanks, R.M.Q., Davra, V.R., Romanowski, E.G., Brothers, K.M., Stella, N.A., Godboley, D., and Kadouri, D.E. (2013) An eye to a kill: using predatory bacteria to control Gram-negative pathogens associated with Oocular infections. *PLoS One* **8**: e66723.

Shatzkes, K., Chae, R., Tang, C., Ramirez, G.C., Mukherjee, S., Tsenova, L., et al. (2015) Examining the safety of respiratory and intravenous inoculation of *Bdellovibrio*

bacteriovorus and *Micavibrio aeruginosavorus* in a mouse model. *Sci Rep* **5**: 12899.

Shatzkes, K., Singleton, E., Tang, C., Zuena, M., Shukla, S., Gupta, S., et al. (2016) Predatory bacteria attenuate *Klebsiella pneumoniae* burden in rat lungs. *MBio* **7**: e01847-16.

Shatzkes, K., Tang, C., Singleton, E., Shukla, S., Zuena, M., Gupta, S., et al. (2017) Effect of predatory bacteria on the gut bacterial microbiota in rats. *Sci Rep* **7**: 43483.

Shemesh, Y. and Jurkevitch, E. (2004) Plastic phenotypic resistance to predation by *Bdellovibrio* and like organisms in bacterial prey. *Environ Microbiol* **6**: 12–18.

Shilo, M. and Bruff, B. (1965) Lysis of Gram-negative bacteria by host-independent ectoparasitic *Bdellovibrio bacteriovorus* isolates. *J Gen Microbiol* **40**: 317–28.

Sockett, R.E. (2009) Predatory lifestyle of *Bdellovibrio bacteriovorus*. *Annu Rev Microbiol* **63**: 523–539.

Sockett, R.E. and Lambert, C. (2004) *Bdellovibrio* as therapeutic agents: a predatory renaissance? *Nat Rev Microbiol* **2**: 669–75.

Sonenshein, A.L., Hoch, J.A., and Richard, L. eds. (1993) *Bacillus subtilis* and other Gram-positive bacteria - biochemistry, physiology, and molecular genetics.

Staples, D.G. and Fry, J.C. (1973) Factors which influence the enumeration of *Bdellovibrio bacteriovorus* in sewage and river water. *J Appl Bacteriol* **36**: 1–11.

Starr, M.P. and Baigent, N.L. (1966) Parasitic interaction of *Bdellovibrio bacteriovorus* with other bacteria. *J Bacteriol* **91**: 2006–2017.

Stent, G.S. and Wollman, E.L. (1952) On the two-step nature of bacteriophage adsorption. *Biochim Biophys Acta* **8**: 260–269.

Stolp, H. (1973) The *Bdellovibrios*: Bacterial parasites of bacteria. *Annu Rev Phytopathol* **11**: 53–76.

Stolp, H. and Petzold, H. (1962) Untersuchungen über einen obligat parasitischen Mikroorganismus mit lytischer Aktivität für *Pseudomonas*-Bakterien. *J Phytopathol* **45**: 864.

Stolp, H. and Starr, M.P. (1963) *Bdellovibrio bacteriovorus* gen. et sp. n., a predatory, ectoparasitic, and bacteriolytic microorganism. *Antonie Van Leeuwenhoek* **29**: 217–248.

Straley, S.C. and Conti, S.F. (1977) Chemotaxis by *Bdellovibrio bacteriovorus* toward prey. *J Bacteriol* **132**: 628–40.

Straley, S.C., Conti, S.F., and Morgan, T.H. (1974) Chemotaxis in *Bdellovibrio bacteriovorus*. *J Bacteriol* **120**: 549–551.

Straley, S.C., Lamarre, A.G., Lawrence, L.J., and Conti, S.F. (1979) Chemotaxis of *Bdellovibrio bacteriovorus* toward pure compounds. *J Bacteriol* **140**: 634–642.

Thomashow, M.F. and Rittenberg, S.C. (1978a) Intraperiplasmic growth of *Bdellovibrio bacteriovorus 109J*: attachment of long-chain fatty acids to *Escherichia coli* peptidoglycan. *J Bacteriol* **135**: 1015–23.

Thomashow, M.F. and Rittenberg, S.C. (1978b) Intraperiplasmic growth of *Bdellovibrio bacteriovorus 109J*: N-deacetylation of *Escherichia coli* peptidoglycan amino sugars. *J Bacteriol* **135**: 1008–14.

Thomashow, M.F. and Rittenberg, S.C. (1978c) Intraperiplasmic growth of *Bdellovibrio bacteriovorus 109J*: solubilization of *Escherichia coli* peptidoglycan. *J Bacteriol* **135**: 998–

1007.

Toni, T., Welch, D., Strelkowa, N., Ipsen, A., and Stumpf, M.P.H. (2009) Approximate Bayesian computation scheme for parameter inference and model selection in dynamical systems. *J R Soc Interface* **6**: 187–202.

Turnbull, A.L. and Chant, D.A. (1961) The practice and theory of biological control of insects in Canada. *Can J Zool* **39**: 697–753.

Varon, M. (1979) Selection of predation-resistant bacteria in continuous culture. *Nature* **277**: 386–388.

Varon, M., Fine, M., and Stein, A. (1984) The maintenance of *Bdellovibrio* at low prey density. *Microb Ecol* **10**: 95–98.

Varon, M. and Seijffers, J. (1975) Symbiosis independent and symbiosis incompetent mutants of *Bdellovibrio bacteriovorus 109J*. *J Bacteriol* **124**: 1191–1197.

Varon, M. and Shilo, M. (1969) Attachment of *Bdellovibrio bacteriovorus* to cell wall mutants of *Salmonella spp*. and *Escherichia coli*. *J Bacteriol* **97**: 977–979.

Varon, M. and Shilo, M. (1968) Interaction of *Bdellovibrio bacteriovorus* and host bacteria. I. Kinetic studies of attachment and invasion of *Escherichia coli B* by *Bdellovibrio bacteriovorus*. *J Bacteriol* **95**: 744–53.

Varon, M. and Zeigler, B.P. (1978) Bacterial predator-prey interaction at low prey density. *Appl Environ Microbiol* **36**: 11–17.

Verhulst, P.-F. (1838) Notice sur la loi que la population suit dans son accroissement. *Corresp Math Phys* **10**: 113–126.

Volterra, V. (1926) Fluctuations in the abundance of a species considered mathematically. *Nature* **118**: 558–560.

De Vos, P., Garrity, G.M., Jones, D., Krieg, N.R., Ludwig, W., Rainey, F.A., et al. (2009) Bergey's Manual® of systematic bacteriology, second edition, volume three: the Firmicutes, Second. Springer.

Whitby, G.E. (1977) *Bdellovibrio bacteriovorus* 6-5-S and *Aquaspirillum serpens* Vhl in continuous culture.

Widdel, F., Kohring, G.-W., and Mayer, F. (1983) Studies on dissimilatory sulfate-reducing bacteria that decompose fatty acids. *Arch Microbiol* **134**: 286–294.

Wilkinson, M.H.F. (2006) Mathematical modelling of predatory prokaryotes. In, Jurkevitch,E. (ed), *Predatory Prokaryotes*., pp. 94–130.

Wilkinson, M.H.F. (2001) Predation in the presence of decoys: an inhibitory factor on pathogen control by bacteriophages or *Bdellovibrios* in dense and diverse ecosystems. *J Theor Biol* **208**: 27–36.

Williams, H.N. (1987) The recovery of high numbers of *Bdellovibrios* from the surface water micro layer. *Can J Microbiol* **33**:.

Williams, H.N., Falkler, J.W.A., and Shay, D.E. (1982) Seasonal distribution of *Bdellovibrios* at the mouth of the Patuxent river in the Chesapeake bay. *Can J Microbiol* **28**: 111–116.

Williams, H.N., Kelley, J.I., Baer, M.L., and Turng, B.-F. (1995) The association of *Bdellovibrios* with surfaces in the aquatic environment. *Can J Biochem* **41**: 1142–1147.

Williams, H.N., Lymperopoulou, D.S., Athar, R., Chauhan, A., Dickerson, T.L., Chen, H., et

al. (2016) *Halobacteriovorax*, an underestimated predator on bacteria: potential impact relative to viruses on bacterial mortality. *ISME J* **10**: 491–499.

Williams, H.N., Schoeffield, A.J., Guether, D., Kelley, J.I., Shah, D., and Falkler, J.W.A. (1995) Recovery of Bdellovibrios from submerged surfaces and other aquatic habitats. *Microb Ecol* **29**: 39–48.

Willis, A.R., Moore, C., Mazon-Moya, M., Krokowski, S., Lambert, C., Till, R., et al. (2016) Injections of predatory bacteria work alongside host immune cells to treat *Shigella* infection in zebrafish larvae. *Curr Biol* **26**: 1–9.

Wilson, I.G. (1997) Inhibition and facilitation of nucleic acid amplification. *Appl Environ Microbiol* **63**: 3741–3751.

Yu, P., Mathieu, J., Yang, Y., and Alvarez, P.J.J.J. (2017) Suppression of enteric bacteria by bacteriophages: Importance of phage polyvalence in the presence of soil bacteria. *Environ Sci Technol* **51**: 5270–5278.

Zeigler, D.R., Prágai, Z., Rodriguez, S., Chevreux, B., Muffler, A., Albert, T., et al. (2008) The origins of 168, W23, and other *Bacillus subtilis* legacy strains. *J Bacteriol* **190**: 6983–95.

Zheng, G., Wang, C., Williams, H.N., and Piñeiro, S.A. (2008) Development and evaluation of a quantitative real-time PCR assay for the detection of saltwater *Bacteriovorax*. *Environ Microbiol* **10**: 2515–2526.

Zusman, D.R., Scott, A.E., Yang, Z., and Kirby, J.R. (2007) Chemosensory pathways, motility and development in *Myxococcus xanthus*. *Nat Rev Microbiol* **5**: 862–872.

APPENDIX A

Dual Predation by Bacteriophage and *Bdellovibrio* Can Eradicate *E. coli* Prey in Situations Where Single Predation Cannot

Laura Hobley,[a*] J. Kimberley Summers,[b] Rob Till,[a] David S. Milner,[a*] Robert J. Atterbury,[a*] Amy Stroud,[a] Michael J. Capeness,[a*] Stephanie Gray,[a] Andreas Leidenroth,[a] Carey Lambert,[a] Ian Connerton,[c] Jamie Twycross,[d] Michelle Baker,[a*] Jess Tyson,[a] Jan-Ulrich Kreft,[b#] R. Elizabeth Sockett[a#]

[a]School of Life Sciences, University of Nottingham, Nottingham, UK

[b]Institute of Microbiology and Infection & Centre for Computational Biology & School of Biosciences, University of Birmingham, Birmingham, UK

[c]School of Biosciences, University of Nottingham, Loughborough, UK

[d]School of Computer Science, University of Nottingham, Nottingham, UK

Running head: Phage-*Bdellovibrio* co-predation

Address correspondence to R. Elizabeth Sockett liz.sockett@nottingham.ac.uk and Jan-Ulrich Kreft J.Kreft@bham.ac.uk

L.H. and J.K.S. contributed equally to this work

* Present Address: Laura Hobley, School of Biosciences, University of Nottingham, Loughborough, UK; Michelle Baker, School of Biosciences, University of Nottingham, Loughborough, UK; David S. Milner, School of Biosciences, University of Exeter, Exeter, UK; Robert J. Atterbury, School of Veterinary Medicine and Science, University of Nottingham, Loughborough, UK; Michael J. Capeness, School of Biological Sciences, University of Edinburgh, Edinburgh, UK.

Word Count: Abstract: 250. Importance: 142. Main text: 6458

ABSTRACT

Bacteria are preyed upon by diverse microbial predators including bacteriophage and predatory bacteria, such as *Bdellovibrio bacteriovorus*. Whilst bacteriophage are used as antimicrobial therapies in Eastern Europe, and are being applied for compassionate use in the United States, predatory bacteria are only just beginning to reveal their potential therapeutic uses. However, predation by either predator type can falter due to different adaptations arising in the prey bacteria. When testing poultry farm wastewater for novel *Bdellovibrio* isolates on *E. coli* prey lawns, individual composite plaques were isolated, containing both an RTP-like-phage and a *B. bacteriovorus* strain and showing central prey lysis and halos of extra lysis. Combining the purified phage with a lab strain of *B. bacteriovorus* HD100 recapitulated halo-ed plaques, and increased killing of the *E. coli* prey in liquid culture, showing effective side-by-side action of these predators, compared to their actions alone. Using Approximate Bayesian Computation to select the best fitting from a variety of different mathematical models demonstrated that the experimental data could only be explained by assuming the existence of three prey phenotypes: (1) sensitive to both predators, (2) genetically resistant to phage only and (3) plastic resistant to *B. bacteriovorus* only. Although each predator reduces prey availability for the other, high phage numbers did not abolish *B. bacteriovorus* predation so both predators are competent to co-exist and are causing different selective pressures on the bacterial surface while, in tandem, controlling prey bacterial numbers efficiently. This suggests that combinatorial predator therapy could overcome problems of phage resistance.

IMPORTANCE

With increasing levels of antibiotic resistance being reported, the development of alternative therapies is urgently needed. Two potential alternatives discussed are bacteriophage and predatory bacteria. Whilst bacteriophage therapy has long been used in Eastern Europe, and is now seeing limited compassionate use in the West; prey/host specificity and the rapid acquisition of bacterial resistance to bacteriophage are major practical considerations. Predatory bacteria are of increasing interest due to their broad Gram-negative bacterial prey range, and the lack of simple resistance mechanisms. Here, a bacteriophage and a strain of *Bdellovibrio bacteriovorus*, isolated from the same environmental sample, preyed side-by-side on a population of *E. coli* causing significantly greater decrease in prey numbers than either alone. Such combinatorial predator therapy may have greater potential than individual predators as prey surface changes selected for by each predator do not protect prey against the other predator.

KEYWORDS *Bdellovibrio*, bacteriophage, RTP phage, predation, co-operation, predator prey models, mathematical modelling, Approximate Bayesian Computation

INTRODUCTION

Rapidly rising levels of antimicrobial resistance in Gram-negative bacterial pathogens has highlighted the urgent need for the development of alternative forms of antibacterial therapies (1) and the World Health Organisation has listed several as critically urgent for new therapeutics. Many Gram-negative pathogens can be killed by a variety of bacteriophage ('phage') and by predatory bacteria including *Bdellovibrio bacteriovorus* (2, 3). Bacteriophage have been used regularly in Eastern Europe and Russia as antimicrobial therapies (4). However, the development of bacterial resistance to bacteriophage can occur rapidly both *in vitro* and *in vivo* by receptor gene mutations (5-7), leading to the requirement for, and development of, phage cocktails for therapeutic purposes, including recent compassionate treatment use (8, 9). *Bdellovibrio* have recently been the subject of a number of *in vivo* studies to test their efficacy in animals (10-12), but have yet to be trialled for use in humans. Unlike bacteriophage, there are no known simple receptor gene mechanisms for resistance.

Bacteriophage are obligate intracellular predators that can be found in environments wherever susceptible bacteria are available; over 95% of phage isolates described to date belong to the order Caudovirales or "tailed phage" (13). The tails of these phage attach to receptors on the surface of the host bacterium including flagella (14), lipopolysaccharide (15) or outer membrane proteins (16). Due to the specific nature of the receptor for phage attachment, the host range of each phage is typically quite small, determined by the prevalence and conservation of phage receptors in bacterial populations (17). The cellular machinery of the bacterium is rapidly hijacked by the phage, after injection of the viral genome, and redirected to synthesize and

assemble new phage virions that are released to start a new infection cycle (2). Host resistance against bacteriophage infection falls within four general categories: inhibition of adsorption; blocking injection of the viral genome; recognition and restriction modification of bacterial DNA and inhibition of the transcription and replication of phage DNA (18, 19)

B. bacteriovorus predation is a biphasic process, consisting of a flagellate, rapidly swimming phase, before colliding with, attaching to and invading Gram-negative bacteria (which can be either actively growing or in stationary phase) (20). *B. bacteriovorus* invade prey cells by interacting with the outer membrane, creating a pore in the outer membrane and wall, through which they enter into the prey cell periplasm, sealing the pore behind them, forming a rounded structure called a bdelloplast (20). Unlike bacteriophage, which hijack prey replication machinery for their own replication, *Bdellovibrio* invasion results in the rapid death of the prey cell (20, 21). Periplasmic *Bdellovibrio* secrete many enzymes into the prey cell cytoplasm, using the cytoplasmic contents for growth. The *Bdellovibrio* elongates, divides into multiple progeny cells, lyses the prey bdelloplast and is released (22).

By growing intracellularly, the *Bdellovibrio* is within an enclosed niche and does not have to compete with other bacteria for resources. The only known protection against predation is the synthesis of a paracrystalline S-layer by prey cells, however, *Bdellovibrio* are still able to prey on S-layer+ cells should there be any patchiness to the S-layer (23). It has been observed that, in laboratory culture, not all prey bacteria are killed by *Bdellovibrio*, a small population exhibits a “plastic” resistance phenotype; when removed from predators and allowed to grow, the resulting cells are as sensitive to *Bdellovibrio* predation as the original prey population (24). Prey resistance to

antibiotics does not result in resistance to *Bdellovibrio* predation as has been shown in multiple studies looking at drug-resistant Gram-negative pathogens (25, 26). Although well-known for their predatory nature, *B. bacteriovorus* are not obligate predators, approximately one in a million *Bdellovibrio* from a predatory culture can be grown axenically, prey/host-independently (HI), on complex media without prey (27).

Mathematical modelling of bacterial predation is being increasingly applied to understanding predation kinetics of either bacteriophage or *Bdellovibrio;* however modelling of predation by both types of predators on the same prey species has not yet been reported. Bacteriophage predation has been the subject of numerous studies, reviewed in (7, 28), with the models becoming increasingly complex through the inclusion of the effects of the rise of prey resistance (6), altered nutrient availability, multiple bacterial species and more (28). Modelling of *Bdellovibrio* predation is more limited, having started from the original Lotka-Volterra equations (29), via considering a delay between prey death and predator birth (30) to models that consider the bdelloplast stage as a separate population rather than just as a delay (31-34). Few papers considered decoys (33, 34) and one of these integrated experiments and adjusted the model to match the experiments (33). Other models considered the effect of a refuge on predation (32), the effect of serum and "plastic" resistance of prey to *Bdellovibrio* on predation (31), or how predation efficiency depends on prey size and other factors (35).

Here, during sampling standing water on a poultry farm for novel *Bdellovibrio* isolates, single halo-ed plaques were observed on *E. coli* prey lawns. Within each halo-ed plaque was both a predatory *Bdellovibrio bacteriovorus* and a co-isolated bacteriophage. In this paper we use 'prey' as a unified term that encompasses both

prey for *Bdellovibrio* and host for bacteriophage, as in this work a single bacterium, *E. coli*, acts as both prey and host and we are comparing the action of two different predators.

The phage genome was partially sequenced and shown to be homologous to that of a rosette-tailed-phage (RTP) (36). The RTP phage family differ in tail structure, but are related to the T1 phages, the receptor for some of which is a component of the *E. coli* outer membrane and host-resistance is reported to arise frequently (36).

Our experimental analysis of predation kinetics revealed that when both predators were combined in one culture with *E. coli* prey, complete prey lysis was achieved in 48 hours. This was in contrast to cultures containing either of the single predators where prey remained; with phage alone the remaining prey were phage-resistant, whilst with *Bdellovibrio* alone a subpopulation of prey remained but no acquisition of genetic resistance occurred. Mathematical modelling of this experimental system revealed that both phage resistance and the plastic resistance to *Bdellovibrio* predation arose in the *E. coli* prey population, and that the two predators were most likely acting independently and competitively rather than cooperatively. This work shows that two bacterial predators can be co-isolated from the environment, co-exist in lab cultures, and when applied in combination can result in greater killing of the prey bacterial population than by either predator alone; suggesting that *Bdellovibrio*-phage combinations may be a successful approach towards therapeutic antibacterials.

RESULTS

Isolation of environmental *B. bacteriovorus* and associated bacteriophage.

When isolating *Bdellovibrio* from 0.45 μm filtrates of standing water on a poultry farm, one isolate rapidly lysed offered *E. coli* lab cultures, and repeatedly produced plaques with large "halos" around them on prey lawns (Fig. 1A). These plaques contained characteristic small, highly-motile *B. bacteriovorus*-like bacteria (Fig. 1B), and "bdelloplasts" - infected *E. coli* prey cells containing live *B. bacteriovorus*. Sequencing and alignment of the 16S rRNA gene amplified from predatory *Bdellovibrio* purified from a single isolated "halo-ed" plaque showed that the *Bdellovibrio* was a member of the *B. bacteriovorus* species, and its 16S rRNA sequence (GenBank accession no: GQ427200.1) to be 99% identical to that of the type strain HD100 (37). Therefore the isolated *Bdellovibrio* was named *B. bacteriovorus* angelus, due to the initial halo-ed appearance of the plaques from which it was isolated.

Predatory cultures derived from individual "halo-ed" plaques, when filtered through 0.22 μm filters, which retain *B. bacteriovorus*, were found to contain an agent that lysed *E. coli* giving different cell debris (without the rounded bdelloplasts). The concentrated filtrate showed several prominent protein bands on SDS PAGE (Fig. S1A). One of these bands (of approximately 30 kDa) was found, by MALDI QToF MS, (Fig. S1B) to contain 5 peptides which were homologous to the 34 kDa protein RTP27 (GenBank accession no: CAJ42231.1) of a rosette-tailed phage (RTP) of *E. coli* (36). Simultaneous electron microscopy of the 0.22 μm filtrate revealed many phage particles with curved tails that resembled RTP, without such a pronounced rosette on the tail (Fig. 1C). The phage was given the abbreviated name "halo" and the 46 kDa double stranded DNA phage genome was purified and 7 kb of it was sequenced (GenBank GQ495225.1 bacteriophage halo named RES2009a) and compared in BLAST to other phage genomes. The best matches were to phage genomes belonging to the

"rtpvirus" genus, including the characterised RTP phage (EMBL AM156909.1) (36). The phage halo was plaque-purified away from the *B. bacteriovorus*, using a kanamycin resistant *E. coli* as prey (as *B. bacteriovorus* angelus was found to be kanamycin sensitive - as is the type strain HD100) and so was inhibited from predatorily replicating in the Kn^R *E. coli* in the presence of the antibiotic).

Thus *B. bacteriovorus* angelus and bacteriophage halo had been co-isolated, from the same environment, via single "halo-ed" plaques in bacterial prey lawns, in which both predators were preying, side by side, upon the same offered *E. coli* population and thus it is possible that they prey similarly in the natural environment.

***E. coli* resistance to bacteriophage halo occurred rapidly.**

Rapid phage resistance was observed in *E. coli* S17-1 cultures that were preyed upon by the bacteriophage halo alone; with a persistent level of *E. coli* remaining after 16 hours of infection (see Fig. 2B for an example from later growth experiments). Two independently-derived phage-resistant *E. coli* cultures, (F & G), were isolated by plating out the remaining *E. coli* prey cells from these 16 hour cultures – preyed upon by the phage alone. The two isolates were verified as being phage-resistant by being tested for phage predation again. Genome sequencing of each isolate, alongside the original *E. coli* S17-1 strain used in the experiments, was performed to identify the mutations that resulted in phage resistance. This revealed (Table 1) that two different IS4 transposase insertions had occurred and been selected for in the genomes of resistant strains F and G within the same gene - encoding the ligand-gated outer membrane porin FhuA responsible for ferric hydroxamate uptake through the outer

membrane (36). The FhuA protein is known to act as a receptor for other phages and is likely to be the receptor for phage halo (38).

The two halo-phage resistant *E. coli* derivatives grew at similar rates to the parental *E. coli* S17-1 strain. Using the phage resistant *E. coli* as prey in lawns in overlay plates allowed for plaque formation by, and subsequent purification of, the *B. bacteriovorus* angelus isolate away from the phage (Fig. S2A), as phage resistance did not confer any resistance to predation by *B. bacteriovorus*.

We also verified (data not shown) that *B. bacteriovorus* is not susceptible to lytic or lysogenic infection by bacteriophage halo in two tests. Firstly, using host-independent derivatives of both *B. bacteriovorus* angelus and HD100 (isolate HID13 (21)) as prey in lawns onto which bacteriophage halo was added. No zones of clearing were observed, even after prolonged incubation. Secondly, after addition of bacteriophage to liquid cultures of pure attack-phase *B. bacteriovorus* angelus, or HD100, no evidence of phage infection was seen when observed microscopically or enumerated. Thus *B. bacteriovorus* itself is not susceptible to the bacteriophage halo during either predatory or prey-independent lifecycles.

Experimental predation by combined *B. bacteriovorus* HD100 and halo-phage predators eradicates *E. coli* prey unlike single predators.

To test the effects of predation by the two predators on a single prey population at the same time, the kinetics of predation by equal numbers of phage alone, *B. bacteriovorus* alone and *B. bacteriovorus* plus phage on *E. coli* S17-1 was measured alongside an *E. coli* with buffer control (Fig. 2A-D) using methods as detailed below. We had found no specific association between the phage and the

environmental *B. bacteriovorus* co-isolate as mixing the purified halo phage and pure *B. bacteriovorus* angelus or *B. bacteriovorus* HD100 suspensions together both reconstituted halo-ed plaques on a lawn of *E. coli* prey. Having noted that predation rates in liquid cultures of each of the two *B. bacteriovorus* strains angelus and HD100 were the same, but that HD100 forms larger (and hence more visible and countable) plaques, the HD100 strain was used in predation kinetics studies on *E. coli* with or without the phage.

As phage are usually grown in log-phase prey cultures in broth and *B. bacteriovorus* on stationary phase prey in calcium HEPES buffer, a "compromise" late log-phase *E. coli* prey, of starting OD_{600nm} 0.75, was used with a mean initial *E. coli* population of 2.9×10^8 cfu/ml. Deliberate inclusion of an equal volume of background YT medium used for the *E. coli* pre-culture in the CaHEPES buffer gave a low nutrient environment, which allowed for *E. coli* viability throughout the 48 hour test period (Fig. 2B).

The overall kinetics of the 48 hour experiments were followed by optical density at 600 nm (OD_{600}; Fig. 2A) and viable counts (Fig. 2B,C,D), which indicated that, during the first 24 hour period, *E. coli* was killed more slowly by *B. bacteriovorus*, than when preyed upon by both *B. bacteriovorus* and bacteriophage halo together (Fig. 2B). When incubated solely with the bacteriophage halo, the *E. coli* numbers decreased rapidly, reaching the lowest prey density of 2.1×10^3 cfu/ml at 6-8 hours; after which the *E. coli* population began to rise, due to the increase in phage resistant cells within the prey population (Fig. 2B). Interestingly, when the prey were incubated with both the phage and the *B. bacteriovorus*, this increase in prey numbers did not occur,

instead the *E. coli* population was eradicated after 14 hours, dropping to below detectable numbers (less than 10 cfu/ml) (Fig. 2B). The phage and *B. bacteriovorus* population numbers were lower (by 10-fold and 100-fold respectively at the 48 hour timepoints) in the combined culture, likely due to the reduced numbers of prey available to each predator population (Fig. 2C and D). It was noteworthy that adding an equal number of 5×10^6 pfu/ml of the other predator, each with the potential to kill and remove an *E. coli* cell from the available prey pool, caused 10 fold less reduction in phage numbers than in *B. bacteriovorus* numbers. This may be due to more rapid kinetics of *E. coli* predation by phage versus the slower kinetics of killing by *B. bacteriovorus*. As the emergence of genetic or plastic resistance, respectively to the two different predators, would be expected to have a major effect, we modelled these processes mathematically to investigate them further.

Mathematical modelling of co-predation. Modelling started from a one prey and one predator model (35). A bacteriophage was added as a second predator to build the base model of the experimental system (Fig. 3). This base model has one (*E.coli*) prey type (N) and two consumers of the prey, the Predator *B. bacteriovorus* (P) and the Virus bacteriophage halo (V). Both attack and enter the prey to form a distinct stage, thereby removing prey and predator from their respective populations. When *B. bacteriovorus* enters the prey, a bdelloplast (B) is formed. When the phage infects the prey, an Infected prey (I) is formed. Upon lysis of B or I, resources enabling regrowth of prey called M for Medium are released, together with the respective predator offspring.

The combined resource M is needed because the experimental data shows regrowth of *E. coli* during halophage predation (Fig. 2B). Altogether, the base model (Fig 3A) has 6 variables shown as circles. Processes are shown as arrows and terms of the equations in Fig. 3. These are: (i) prey growth by consumption of medium, (ii) predation of prey by available *B. bacteriovorus* to yield the Bdelloplast, (iii) predation by free bacteriophage halo (virus) to yield the Infected prey, (iv) maturation (replication and development) of *B. bacteriovorus* within the bdelloplast, (v) maturation of the bacteriophage (virus) within the Infected prey, (vi) lysis of bdelloplast which yields free replicated *B. bacteriovorus* and releases nutrients which replenish Medium, (vii) lysis of Infected prey which yields free Virus and also releases nutrients which replenish Medium. The nutrients remaining were not sufficient to produce further whole progeny *B. bacteriovorus* or more phage, but will be a small residue of what did constitute the original prey cell as most nutrients were used in producing *B. bacteriovorus* or phage progeny. As mentioned above the Medium does allow some limited growth of the prey.

We also included (viii) mortality for *B. bacteriovorus* as this was evident from Fig. 2C and is well known from the literature (33, 39). We did not include mortality for *E. coli* and the halophage since the data showed no evidence for this during the 48 h experimental time-period (no statistically significant trend; Fig. 2B and D).

From this base model (Fig 3), we generated a family of related models, adding additional variables and processes step by step and testing different mechanisms for the transitions between entities (Fig. 4). We then used Bayesian inference to select, in several stages, the model variant that best fitted the population dynamics observed in the experiments (Fig. 5, see also Fig. S6 demonstrating reproducibility). A full

description of the model variants and the Approximate Bayesian Computation process for model selection and parameter inference is given in Supplemental Text.

Competing the top level model variants with one, two, three or four prey types (Fig. 4C) gave clear results (Fig. 5A). The model variant N1 with prey sensitive to both predators (N_S) and variant N2 with only N_S and bacteriophage resistant prey (N_R) were not supported by the experimental data at all. The variant N3 with N_S, N_R and prey exhibiting the "plastic" phenotypic resistance to *B. bacteriovorus* predation (N_P), was best supported by the experimental data, while variant N4 including the double resistant prey (N_D) was less supported (Fig. 5A). N3 and N4 are nested models with the same number of parameters, so fitting variant N4 is not intrinsically more difficult. Using the parameter values generated by fitting either of the variants N3 or N4, predicted similarly low levels of double resistant prey at the end of the experiment when applied to the equations of variant N4. Variant N4 fitted to all data predicted 0.26 cfu/ml while the same variant using parameters from fitting variant N3 to all data predicted 0.0084 cfu/ml. Both are well below the detection threshold in the experiments (10 cfu/ml). Variant N4 predicts double resistance to occur, albeit at a very low level, however the data could not provide information to constrain this density. Due to these considerations and the aim to choose the minimal adequate model, the N3 model variant was selected for further study.

After selecting this three prey type N3 model, we tested various sub-models based on different ways in which the sensitive prey type converts to the type with plastic phenotypic resistance to *B. bacteriovorus* and back (Fig. 4Di). The simplest assumption is that forward and backward conversion occur spontaneously at certain rates, without any external triggers (intrinsic conversion both ways, variant I). This was

not supported by the data (Fig. 5B). Another model variant replaces the intrinsic back conversion with a growth-coupled conversion (variant IG). This variant was well supported by the data. A third variant replaces the intrinsic conversion by a signal-triggered conversion to plastic resistance (variant S). At this initial stage in the modelling, the signal was assumed to be generated by the lysis of bdelloplasts and phage infected cells. Plastic resistance has been previously described (24) as developing to *B. bacteriovorus* in predatory cultures, due to (as yet unidentified) molecular signals changing prey metabolism/development but it is not due to genetic changes in the prey as when those prey are grown in new cultures and re-challenged with *B. bacteriovorus* they are susceptible once more (21). This variant S had some support from the data (Fig. 5B). Hence, we tested whether a combination of the two supported variants would fit better. This combined variant SG, with signal triggered conversion to plastic resistance plus growth-coupled back conversion, was better supported by the data than its parental variants (Fig. 5C).

Following this, we compared variants where the source of the signal was interaction of prey with phage only, or *B. bacteriovorus* only, or both (Fig. 5D). Since there was no evidence for phage involvement, and the two variants with *B. bacteriovorus* involvement were about equally supported, we concluded that *B. bacteriovorus* interaction with prey was sufficient to generate the signal for plastic resistance.

Likewise, we looked in the model at different ways in which the phage resistant prey arise (Fig. 4Dii). We compared the simpler sub-models where some phage resistant prey are already present at the beginning of the experiment, as in the classic fluctuation test of Luria and Delbrück (40), or only develop as *de novo* mutations

during the experiment with the combined sub-model that had both pre-existing and *de novo* mutations. This combined model variant was best supported by the data and *de novo* developing mutations alone are insufficient to explain the data (Fig. 5E).

Modelling predation-rate saturation

After finding the 'best' or most appropriate model variant for prey type conversions, we looked at the low level model variants (Fig. 4E) where details of the model are varied but not the number of prey types and their conversion. One such detail is whether the predation rate saturates at higher prey density or not (Fig. 4E). Only the variant assuming no saturation of predation rate for the phage but saturation of predation rate for *B. bacteriovorus* was supported by the data (Fig. 5F). This does not mean that phage predation would not saturate at higher prey densities than we investigated in this study, but that the bacterial predator saturates at lower prey densities than the phage (see parameters in Table S1). This is expected as the longer the prey 'handling time' for a predator, the more its response will saturate when prey becomes abundant (41). It is well known that *B. bacteriovorus* takes longer to attach and enter its prey periplasm than phage (20) and our results support this (42). Lack of saturation facilitates the observed rapid initial prey killing by phage (Fig. 2). We did not consider saturation effects at high phage densities in this study because there was little information in the data from experiments that concentrated on later timepoints and the rise of phage resistance to parameterise phage saturation (there is only a brief interval with high phage density while sensitive prey are available, see Fig. 2B & D). We did however model different initial prey densities as shown in Figure S8, see below.

The final model shows effective side-by-side action of dual predators.

The final, most appropriate model variant was then fitted to all the data (Fig. 6A-D). We explain in Supplemental Text how we used Principal Component Analysis to objectively select a typical parameter set out of the hundreds of accepted fits. The final model fits the prey dynamics well, apart from the exact kinetics of the decline of prey in the presence of *B. bacteriovorus* as the only predator (Fig. 6B) where prey density does not drop as gradually in the model as in the experiments. Despite trying many variants of prey type conversions, we could not find any variant that would give a better fit to this more gradual decline of prey without making the fit to other parts of the data much worse, so Fig. 6A-D shows the best fit we could obtain.

We also compared the fit of this final model to all data (Fig. 6A-D) with the fit of the same model to all data, excluding that from two predators acting on one prey (Fig. 6E-H). The two fits are almost the same. This means that the experimental results can be explained without invoking any direct interactions between the two predators.

Dependence on initial densities.

To understand the dependence of predation success on the initial densities of prey and predators, we used the model to predict the outcome if we varied one population at a time, increasing as well as decreasing initial densities 10-fold (Fig. S8). The time series of the three related traces (10-fold lower, normal, 10-fold higher initial densities) showed similar qualitative behaviour for cases with prey only and prey with a single predator. Here, the three traces either converged in the end or their separation was less than the 10-fold initial separation. Prey could survive during dual predation if (i) the initial density of prey was too high, or (ii) the initial density of *B.*

bacteriovorus was too low or (iii) the initial density of the phage was too high (Fig. S8F-H). The model can thus identify suitable densities of the predators to add for effective predation.

Modelling reveals interactions of sub-populations of predators and prey

The modelling allowed insights into the different sub-populations that comprised the observed total bacterial populations (Fig. 6I-L). In the simulated *B. bacteriovorus*-only predation, the *B. bacteriovorus* population is evenly split between free *B. bacteriovorus* and bdelloplasts from 2 to 20 hours. Afterwards, the bdelloplasts decline exponentially while free *B. bacteriovorus* increase a little (due to progeny release from bdelloplasts) and then decline again due to their mortality (Fig. 6J). Both the fully-susceptible and phage-resistant prey populations plummet at 20 hours, when the plastic resistant prey has reached a plateau (Fig. 6J). In the simulated phage-only predation, sensitive prey rapidly dropped in the first 6 hours, afterwards the phage resistant prey increased exponentially until reaching a plateau (Fig. 6K). In the simulated dual predation, the phage is mostly responsible for the rapid drop of the susceptible prey and the removal of the intermittently arising plastic *B. bacteriovorus* resistant prey, whilst *B. bacteriovorus* is responsible for the removal of the phage resistant prey. All three prey populations are eradicated by the two predators together (Fig. 6K).

DISCUSSION

When attempting to isolate *Bdellovibrio* strains from environmental sources, a sample of chicken farm wastewater gave halo-ed plaques on lawns of *E. coli*, due to the combined predation by the new strain of *B. bacteriovorus*, which we named angelus, and an RTP-like bacteriophage, which we named halo. The combined predation was also produced by the addition of bacteriophage halo to lab strain *B. bacteriovorus* HD100. We combined both experimental and mathematical modelling approaches to unravel the dynamics of this combinatorial predation, showing that a combination of two microbial predators eradicated a single pathogenic bacterial species in conditions when each alone did not. The modelling suggested that *B. bacteriovorus* killed all the phage resistant prey types and the phage halo killed all the plastically *B. bacteriovorus*-resistant prey. This suggests that combinatorial predator therapy may be one approach to tackle the problem of phage resistance in phage therapy treatments.

Although found co-associated in nature, the RTP-family phage halo did not attach to, lyse or lysogenise the *B. bacteriovorus*, but was found to prey alongside it on *E. coli* in experimental lawns, producing the halo-ed plaques.

There were several possibilities for how the combined predators were behaving in the mixed cultures – were they acting independently on the prey, in competition with each other at overlapping receptor sites, were the phage aiding in some way predation by the *Bdellovibrio,* or *vice versa,* was the phage acting as an opportunistic passenger, or were there subsets of the prey population that were susceptible to predation by each? The mathematical modelling allowed investigation of this beyond experimental limits. The model selection results revealed the presence

of three subsets of the prey population, those susceptible to both predators, and those resistant to predation by either the phage or the *Bdellovibrio.*

The final model gave a good fit to the co-predation experimental data. Moreover, when fitted to just the data sets containing the prey only and the single predators, the resulting parameter values gave a very similar fit to the experimental data for the combined predation conditions. As the final model does not contain any terms for direct interactions between the two predators, combined with the fact that fitting to single predator data predicts the combined predation results, we conclude that the two predators act independently.

One question did remain to why did we isolate halo-ed plaques from the environment which contained both predators, if they can operate independently? Clearly during our dual predation experiments a final yield of c1 × 10^{10} phage were present from a prey population which yielded c1 × 10^{6} *B. bacteriovorus*, so phage were in 10,000 fold excess. High phage abundance was probably the reason for their presence in each plaque. The rapid accumulation of phage resistant populations of *E. coli*, preyed upon by phage, provides no barrier to *B. bacteriovorus* predation so does not prevent co-occurrence.

Purification of each predator made it possible to study their individual and combined effects in ways not possible in other studies (43). Employing a low-nutrient environment allowed predation by each predator, and allowed sustained viability of the *E. coli* population over the 48 hours of investigation. Experimental predation by the *Bdellovibrio* alone resulted in a gradual decrease in prey numbers from 1.2 × 10^{9} cfu/ml to a minimum of 2.0 × 10^{4} cfu/ml (Fig. 2). This is consistent with other reports of *Bdellovibrio* predation on a variety of different prey species where complete killing

of the prey population was not observed (26, 31, 33). The modelling revealed that a subpopulation of prey arose that would exhibit a "plastic" resistance to *Bdellovibrio* predation, a form of resistance that is not genetically encoded, and is also not passed to daughter cells, consistent with the "plastic" resistance phenotype previously reported (24). It had previously been hypothesised (24) that this resistance would arise due to the release of a molecular signal from the lysis of the bdelloplast, and the modelling supports such a mechanism. This "plastic" resistance may pose a problem if considering the therapeutic application of *Bdellovibrio* (3), as it may limit the reduction of pathogen numbers, although the immune system has been shown to act synergistically *in vivo* (12). In addition, physiological state of prey (leading to plastic resistance or not) may be different in the *in vivo* growth conditions. Our modelling predicts that, in a dual predation setting, the balance between applied predator numbers is important and that adding sufficient but not excess phage with *B. bacteriovorus* gives the best outcome.

Predation by the phage alone resulted in a 10-fold larger (but transient) decrease of the prey population to 2.1×10^3 cfu/ml (seen at 6 hours, Fig. 2B), before phage-resistant prey growth resulted in a final prey population at 48 hours similar to the starting population. The model assumed the presence of a small fraction of phage resistant prey at the beginning of the experiment; the median value of this fraction was 2.6×10^{-6} after fitting (Table S1). This is similar in order of magnitude to previously reported values for *E. coli* (5, 40). The model evaluations indicated that the rise in bacteriophage-resistant prey resulted both from growth of this initial, resistant population and spontaneous mutations arising in members of the initially phage-sensitive prey population. Both were selected for during the time course of the

experiment. Replication of the phage-resistant prey resulted in the production of phage-resistant progeny, consistent with resistance being the result of genetic mutation. Sequencing of the phage resistant genomes points to the absence of the ferric hydroxamate uptake, FhuA, protein as the reason for *E. coli* resistance to phage halo. This mutation would have little fitness effect in the iron-containing environment of our experimentation and given additional routes of iron uptake by *E. coli*.

The most noteworthy result of our study was the eradication of *E. coli* prey (reduction below detectable levels of less than 10 cells/ml) when preyed upon by both the *B. bacteriovorus* and the phage together (Fig. 2). The modelling revealed that the two predators were not interacting directly with each other as the experimental results could be recapitulated by the model using the data from the individual predators, without the need for the inclusion of any terms for direct interactions between predators. This suggests the potential for this phenomenon to be replicated for other combinations of Gram-negative prey, *B. bacteriovorus* and prey-specific bacteriophage, something that should be further investigated (beyond the scope of this paper). Such combinatorial predator therapy could be considered as a future alternative antibacterial treatment reducing bacterial numbers to lower levels than achievable with single predators alone, and reducing the selection for single predator-specific resistance.

MATERIALS AND METHODS

Bacterial strains, maintenance and isolation. *E. coli* S17-1 (44) prey were grown for 16 hours in YT broth (45) at 37^{o}C with shaking at 200 rpm to late-log phase for use in predatory *Bdellovibrio* cultures (see below for predation kinetics description). *B. bacteriovorus* predatory cultures were set up as previously described and consisted of a mixture of Calcium HEPES buffer, *E. coli* culture and a previous *B. bacteriovorus* culture in a 50:3:1 v:v:v ratio (45) at 29^{o}C with shaking at 200 rpm. Where stated, the *B. bacteriovorus* type strain HD100 (37, 46) was used for comparison. Host-independent (HI) *B. bacteriovorus* were grown as described in (45, 47), the HD100 derivative HID13 was described in (21) and the angelus HI strain was obtained as part of this study.

Bdellovibrio bacteriovorus strain angelus and bacteriophage halo were co-isolated using *E. coli* S17-1 as prey on YPSC double-layer agar plates as described previously (45). The bacteriophage halo was purified from the mixed phage-*B. bacteriovorus* cultures by growing the phage on *E. coli* S17-1 containing the plasmid pZMR100 (48) to confer resistance to kanamycin, which was added at 50 µg/ml, killing the Kn^{S} *B. bacteriovorus* angelus, using repeated rounds of plaque purification on YPSC overlay plates (45, 49). Phage resistant *E. coli* S17-1 were obtained by plating *E. coli* cells remaining in pure bacteriophage halo infection cultures and screening resultant isolates by addition of bacteriophage halo. These phage resistant *E. coli* (two strains F & G) were used to purify the *B. bacteriovorus* angelus from the originally mixed phage and *B. bacteriovorus* co-cultures, again using rounds of plaque purification. The resulting purified *B. bacteriovorus* angelus produced small plaques (smaller than those

produced by the type strain HD100 under matched conditions) on both the phage resistant and original phage-sensitive *E. coli*.

***Bdellovibrio* DNA purification and 16S rRNA sequencing.** To phylogenetically characterise the pure *Bdellovibrio* strain isolated in the co-culture, *Bdellovibrio* genomic DNA was purified from 0.45µm filtered host-dependently grown (before and after separation from the associated phage) and unfiltered host-independently grown *B*. *bacteriovorus* angelus using the Genelute Bacterial Genomic DNA Kit (Sigma) following the manufacturer's instructions. The full-length 16S rRNA gene was amplified from a total of 11 individual genomic DNA samples using Phusion high-fidelity polymerase (Finnzymes) following the manufacturer's guidelines using general bacterial primers 8F (50) and 1492r (51). Purified PCR products were sent for sequencing at MWG Biotech Ltd, and the full length double-stranded sequence was aligned to that of the *Bdellovibrio bacteriovorus* type strain HD100 (37).

Phage preparation and protein identification. Phage preparations were made by addition of bacteriophage halo (purified as described above and in the results) to a mid-log phase culture of *E. coli* S17-1 (pZMR100) and incubated at 29^{o}C. When the optical density (OD) of the culture at 600 nm dropped to half that of the starting OD, chloroform was added and the phage particles were collected using PEG precipitation as described for lambda phage (52).

Phage preparations were run on standard 12.5% acrylamide SDS polyacrylamide gels (53) to examine their protein content; a single band was excised

and analysed by MALDI QToF MS, and the resulting peptide reads compared to existing sequences in NCBI databases for the most significant hits.

Phage and prey genomic DNA purification and sequencing. Bacteriophage halo genomic DNA was extracted from the above phage preparations using the Qiagen Lambda Maxi Kit (Qiagen) following the manufacturer's instructions from step 6 to step 15. Harvested DNA was resuspended in a final volume of 1 ml 10 mM Tris, 1 mM EDTA pH 7.5. Restriction-digested fragments of phage genomic DNA were cloned into pUC19 (54) and sent for sequencing at MWG Biotech Ltd using standard pUC19 primers M13uni(-21) and M13rev(-29). To complete the phage sequence contig, unsequenced regions of cloned fragments were PCR amplified using KOD high-fidelity polymerase, and purified PCR products sent for sequencing. A 7 kb contig of phage genomic DNA was fully sequenced, compared to other phage genomes by DNA and protein BLASTs at NCBI, and deposited in GenBank under accession number GQ495225.

E. coli S17-1 genomic DNA was prepared using a Sigma GenElute Bacterial Genomic DNA kit (Sigma- Aldrich Co, St Louis), from 16 hour overnight cultures of wild type and phage resistant strains F and G. MinION and Illumina HiSeq platforms were used to sequence the genome of *E. coli* S17-1 (4,772,290 nucleotides). Long-read sequences from the MinION were used as a scaffold for Illumina data consisting of 4.6 million paired-end sequence reads with lengths of 250 bp. Sequence assembly was performed using CLC Genomics Workbench version 11.0.1 (Qiagen, Aarhus, Denmark). The genome sequence is available under GenBank accession number CP040667. Phage resistant genome sequences

were assembled using the *E. coli* S17-1 chromosome as template from Illumina HiSeq data composed of 0.8 and 3.5 million paired-end sequence reads of 250 bp for mutants F and G respectively. These data also included the DNA sequence of plasmid pZMR100 (5,580 nucleotides).

Electron microscopy. *B. bacteriovorus* cells and phage preparations were visualised using transmission electron microscopy. 15 µl of sample was placed on a carbon formvar grid (Agar Scientific) for five minutes before being removed and 15 µl of 0.5% Uranyl Acetate added for 1 minute before the grid was dried. Samples were imaged using a JEOL JEM1010 electron microscope.

Predation kinetics experiments. Predation kinetics were assayed as described and reasoned in the results: experimental measurements were taken in triplicate and viable counting was used to enumerate phage, *B. bacteriovorus* and *E. coli*. Two separate biological repeats of the experiment were run over 48 hours, with enumerations of all three populations every two hours by a team of four people.

The starting prey cultures had to be established by experimentation to produce prey cells that were suitable for both *B. bacteriovorus* and phage predation. In the lab, *B. bacteriovorus* predation is usually studied using stationary-phase prey, whilst phage predation typically requires exponentially-growing prey; here our setup resulted in late-log phase prey cells that were preyed upon by both predators. *E. coli* S17-1 prey cells were pre-grown for 16 hours shaken at 37°C in YT broth. They were added, still in the YT broth, to 100 ml of calcium HEPES buffer (2 mM $CaCl_2$ 25 mM HEPES pH 7.8) to give a final OD_{600nm} of 0.75 units (typically 20ml of overnight culture

added to 100 ml buffer), resulting in an average starting *E. coli* prey population in the experimental cultures of 2.9×10^8 cfu/ml.

Into 100 ml of this prey suspension, 2 ml of an attack-phase culture of *B. bacteriovorus* HD100 was added (or 2 ml calcium HEPES buffer to *B. bacteriovorus* free controls) giving an average starting *B. bacteriovorus* count in the experimental cultures of 2.8×10^6 pfu/ml. To this, 20 µl of a pure preparation of the halo-phage was added, giving an average starting count in the experimental cultures of 3.7×10^6 pfu/ml. Cultures were incubated at 29°C with shaking at 200 rpm, and samples taken every 2 hours.

At each timepoint, OD_{600nm} was measured and samples plated onto the appropriate agar plates for enumeration of *E. coli* (YT), bacteriophage halo (YPSC with kanamycin at 50 µg/ml, with S17-1 pZMR100 prey) and *B. bacteriovorus* HD100 (YPSC with phage-resistant S17-1 as prey).

Mathematical modelling. A family of ordinary differential equation (ODE) models were developed to describe the population dynamics. ODEs were ideal as the experimental data are at the population rather than the individual level and the ODE model can be solved rapidly (this is important as we had to simulate the model millions of times for the model selection and parameter inference). Fig. 3 visualizes the variables, their interactions and the equations of the base model with one prey type. Fig. 4 does the same for the final model as well as explaining the different model variants. Parameters are defined in Table S1. The full sets of equations and details on the ODE solver are given in Supplemental Text. Each model variant was fitted to the experimental data shown in Fig. 2. A Bayesian framework for model selection and

parameter inference was used to obtain estimates of the uncertainty of the model and parameters. As explicit likelihood functions cannot be derived, an Approximate Bayesian Computation (ABC) with Sequential Monte Carlo (ABC-SMC) algorithm was used as described by Stumpf and co-workers (55), for details of the procedure see Supplemental Text. Figs. S3 and S4 show how the fit improves with decreasing tolerance and Fig. S5 shows how the accepted parameter ranges narrow down increasingly from the broad priors. The objective choice of typical parameter sets via PCA is shown in Fig. S7. The open source code for running the simulations and the model selection and fitting are available as Supplemental Code.

Accession numbers. The nucleotide sequences derived in this work have been deposited with GenBank. The bacteriophage halo partial genome sequence has accession number GQ495225.1 https://www.ncbi.nlm.nih.gov/nuccore/GQ495225 and the *B. bacteriovorus* angelus full-length 16S rRNA sequence has accession number GQ427200.1 https://www.ncbi.nlm.nih.gov/nuccore/GQ427200.1/.

The *E. coli* wild type strain S17-1 genome sequence was deposited with the accession number CP040667.1 https://www.ncbi.nlm.nih.gov/nuccore/NZ_CP040667.1

SUPPLEMENTAL CODE for Modelling:

https://github.com/kreft/predatorprey

FIG S1 –S8

TABLE S1, PDF file

ACKNOWLEDGEMENTS

This work was carried out with contributions by many workers on the multi-day live experimentation and modelling sides. We thank Kevin Bailey for MALDI QToF MS analysis and peptide identification, Angus Davison and Richard Woods for helpful advice, Iain G. Johnston for guidance using ABC and Marilyn Whitworth for technical support. L.H., C.L., M.J.C., R.J.A. and R.T. were supported by HFSP grant RGP57/2005 and Biotechnology and Biological Sciences Research Council (BBSRC) UK grant BB/G003092/1. D.S.M., A.S., M.J.C., S.G. and A.L. were undergraduate students at University of Nottingham. D.S.M. was supported by a Nuffield Foundation undergraduate summer bursary and A.L. by an SGM undergraduate summer bursary. J.K.S. was supported by a BBSRC funded, Midlands Integrative Biosciences Training Partnership (MIBTP) PhD studentship. M.B., J.T., J.Tw. were supported by US Army Research Office and the Defense Advanced Research Projects Agency under Cooperative Agreement Number W911NF-15-2-0028 to R.E.S. The views and conclusions contained in this document are those of the authors and should not be interpreted as representing the official policies, either expressed or implied, of the Army Research Office, DARPA, or the U.S. Government.

AUTHOR CONTRIBUTIONS

R.E.S devised the experimental work with L.H. and R.T. Live experimental data collection was carried out by a group of experimental researchers: L.H., R.T., D.S.M., R.J.A., A.S., M.J.C., S.G. and A.L. J.K.S. and J.U.K. devised and J.K.S. carried out the modelling work with inputs from M.B., J.T. and J.Tw. C.L. and J.T. did nucleic acid sequencing and I.C. annotated and deposited the *E. coli* genome sequence. R.E.S., J.K.S., L.H., J.T. and J.U.K. drafted the manuscript with comments from M.B. All authors gave final approval for publication.

REFERENCES

1. Allen HK, Trachsel J, Looft T, Casey TA. 2014. Finding alternatives to antibiotics. Ann N Y Acad Sci 1323:91-100.
2. Lederberg J. 1996. Smaller fleas ... ad infinitum: therapeutic bacteriophage redux. Proc Natl Acad Sci U S A 93:3167-8.
3. Negus D, Moore C, Baker M, Raghunathan D, Tyson J, Sockett RE. 2017. Predator Versus Pathogen: How Does Predatory Bdellovibrio bacteriovorus Interface with the Challenges of Killing Gram-Negative Pathogens in a Host Setting? Annu Rev Microbiol 71:441-457.
4. Kakasis A, Panitsa G. 2018. Bacteriophage therapy as an alternative treatment for human infections. A comprehensive review. Int J Antimicrob Agents doi:10.1016/j.ijantimicag.2018.09.004.
5. Oechslin F. 2018. Resistance Development to Bacteriophages Occurring during Bacteriophage Therapy. Viruses 10.
6. Cairns BJ, Timms AR, Jansen VA, Connerton IF, Payne RJ. 2009. Quantitative models of in vitro bacteriophage-host dynamics and their application to phage therapy. PLoS Pathog 5:e1000253.
7. Weitz J. 2016. Quantitative Viral Ecology: Dynamics of Viruses and Their Microbial Hosts. Princeton University Press.
8. Gu J, Liu X, Li Y, Han W, Lei L, Yang Y, Zhao H, Gao Y, Song J, Lu R, Sun C, Feng X. 2012. A method for generation phage cocktail with great therapeutic potential. PLoS One 7:e31698.
9. Schooley RT, Biswas B, Gill JJ, Hernandez-Morales A, Lancaster J, Lessor L, Barr JJ, Reed SL, Rohwer F, Benler S, Segall AM, Taplitz R, Smith DM, Kerr K, Kumaraswamy M, Nizet V, Lin L, McCauley MD, Strathdee SA, Benson CA, Pope RK, Leroux BM, Picel AC, Mateczun AJ, Cilwa KE, Regeimbal JM, Estrella LA, Wolfe DM, Henry MS, Quinones J, Salka S, Bishop-Lilly KA, Young R, Hamilton T. 2017. Development and Use of Personalized Bacteriophage-Based Therapeutic Cocktails To Treat a Patient with a Disseminated Resistant Acinetobacter baumannii Infection. Antimicrob Agents Chemother 61.
10. Atterbury RJ, Hobley L, Till R, Lambert C, Capeness MJ, Lerner TR, Fenton AK, Barrow P, Sockett RE. 2011. Effects of orally administered Bdellovibrio bacteriovorus on the well-being and Salmonella colonization of young chicks. Appl Environ Microbiol 77:5794-803.
11. Shatzkes K, Singleton E, Tang C, Zuena M, Shukla S, Gupta S, Dharani S, Onyile O, Rinaggio J, Connell ND, Kadouri DE. 2016. Predatory Bacteria Attenuate Klebsiella pneumoniae Burden in Rat Lungs. MBio 7.
12. Willis AR, Moore C, Mazon-Moya M, Krokowski S, Lambert C, Till R, Mostowy S, Sockett RE. 2016. Injections of Predatory Bacteria Work Alongside Host Immune Cells to Treat Shigella Infection in Zebrafish Larvae. Curr Biol 26:3343-3351.
13. Ackermann HW. 2006. Classification of bacteriophages., p 8-16. *In* Calendar R (ed), The Bacteriophages. Oxford University Press, New York.
14. Shea TB, Seaman E. 1984. SP3: a flagellotropic bacteriophage of Bacillus subtilis. J Gen Virol 65 (Pt 11):2073-6.

15. Susskind MM, Botstein D. 1978. Molecular genetics of bacteriophage P22. Microbiol Rev 42:385-413.
16. Randall-Hazelbauer L, Schwartz M. 1973. Isolation of the bacteriophage lambda receptor from Escherichia coli. J Bacteriol 116:1436-46.
17. Koskella B, Meaden S. 2013. Understanding bacteriophage specificity in natural microbial communities. Viruses 5:806-23.
18. Coffey A, Ross RP. 2002. Bacteriophage-resistance systems in dairy starter strains: molecular analysis to application. Antonie Van Leeuwenhoek 82:303-21.
19. Stern A, Sorek R. 2011. The phage-host arms race: shaping the evolution of microbes. Bioessays 33:43-51.
20. Sockett RE. 2009. Predatory lifestyle of Bdellovibrio bacteriovorus. Annu Rev Microbiol 63:523-39.
21. Lambert C, Chang CY, Capeness MJ, Sockett RE. 2010. The first bite--profiling the predatosome in the bacterial pathogen Bdellovibrio. PLoS One 5:e8599.
22. Fenton AK, Kanna M, Woods RD, Aizawa SI, Sockett RE. 2010. Shadowing the actions of a predator: backlit fluorescent microscopy reveals synchronous nonbinary septation of predatory Bdellovibrio inside prey and exit through discrete bdelloplast pores. J Bacteriol 192:6329-35.
23. Koval SF, Hynes SH. 1991. Effect of paracrystalline protein surface layers on predation by Bdellovibrio bacteriovorus. J Bacteriol 173:2244-9.
24. Shemesh Y, Jurkevitch E. 2004. Plastic phenotypic resistance to predation by Bdellovibrio and like organisms in bacterial prey. Environ Microbiol 6:12-8.
25. Kadouri DE, To K, Shanks RM, Doi Y. 2013. Predatory bacteria: a potential ally against multidrug-resistant Gram-negative pathogens. PLoS One 8:e63397.
26. Sun Y, Ye J, Hou Y, Chen H, Cao J, Zhou T. 2017. Predation Efficacy of Bdellovibrio bacteriovorus on Multidrug-Resistant Clinical Pathogens and Their Corresponding Biofilms. Jpn J Infect Dis 70:485-489.
27. Cotter TW, Thomashow MF. 1992. Identification of a Bdellovibrio bacteriovorus genetic locus, hit, associated with the host-independent phenotype. J Bacteriol 174:6018-24.
28. Krysiak-Baltyn K, Martin GJ, Stickland AD, Scales PJ, Gras SL. 2016. Computational models of populations of bacteria and lytic phage. Crit Rev Microbiol 42:942-68.
29. Varon M, Zeigler BP. 1978. Bacterial predator-prey interaction at low prey density. Appl Environ Microbiol 36:11-7.
30. Crowley PH, Straley SC, Craig RJ, Culin JD, Fu YT, Hayden TL, Robinson TA, Straley JP. 1980. A Model of Prey Bacteria, Predator Bacteria, and Bacteriophage in Continuous Culture. Journal of Theoretical Biology 86:377-400.
31. Baker M, Negus D, Raghunathan D, Radford P, Moore C, Clark G, Diggle M, Tyson J, Twycross J, Sockett RE. 2017. Measuring and modelling the response of Klebsiella pneumoniae KPC prey to Bdellovibrio bacteriovorus predation, in human serum and defined buffer. Sci Rep 7:8329.
32. Dattner I, Miller E, Petrenko M, Kadouri DE, Jurkevitch E, Huppert A. 2017. Modelling and parameter inference of predator-prey dynamics in heterogeneous environments using the direct integral approach. J R Soc Interface 14.

33. Hobley L, King JR, Sockett RE. 2006. Bdellovibrio predation in the presence of decoys: Three-way bacterial interactions revealed by mathematical and experimental analyses. Appl Environ Microbiol 72:6757-65.
34. Wilkinson MH. 2001. Predation in the presence of decoys: an inhibitory factor on pathogen control by bacteriophages or bdellovibrios in dense and diverse ecosystems. J Theor Biol 208:27-36.
35. Summers JK, Kreft, J.U. 2019. Predation strategies of the bacterium Bdellovibrio bacteriovorus result in bottlenecks, overexploitation, minimal and optimal prey sizes. bioRxiv 621490.
36. Wietzorrek A, Schwarz H, Herrmann C, Braun V. 2006. The genome of the novel phage Rtp, with a rosette-like tail tip, is homologous to the genome of phage T1. J Bacteriol 188:1419-36.
37. Rendulic S, Jagtap P, Rosinus A, Eppinger M, Baar C, Lanz C, Keller H, Lambert C, Evans KJ, Goesmann A, Meyer F, Sockett RE, Schuster SC. 2004. A predator unmasked: life cycle of Bdellovibrio bacteriovorus from a genomic perspective. Science 303:689-92.
38. Feucht A, Heinzelmann G, Heller KJ. 1989. Irreversible binding of bacteriophage T5 to its FhuA receptor protein is associated with covalent cross-linking of 3 copies of tail protein pb4. FEBS Lett 255:435-40.
39. Hespell RB, Rosson RA, Thomashow MF, Rittenberg SC. 1973. Respiration of Bdellovibrio bacteriovorus strain 109J and its energy substrates for intraperiplasmic growth. J Bacteriol 113:1280-8.
40. Luria SE, Delbruck M. 1943. Mutations of Bacteria from Virus Sensitivity to Virus Resistance. Genetics 28:491-511.
41. Jeschke JM, Kopp M, Tollrian R. 2002. Predator functional responses: Discriminating between handling and digesting prey. Ecological Monographs 72:95-112.
42. Wilkinson MHF. 2006. Mathematical Modelling of Predatory Prokaryotes. *In* Jurkevitch E (ed), Predatory Prokaryotes. Springer, Berlin, Heidelberg.
43. Chen H, Laws EA, Martin JL, Berhane TK, Gulig PA, Williams HN. 2018. Relative Contributions of Halobacteriovorax and Bacteriophage to Bacterial Cell Death under Various Environmental Conditions. MBio 9.
44. Simon R, Priefer U, Puhler A. 1983. A Broad Host Range Mobilization System for Invivo Genetic-Engineering - Transposon Mutagenesis in Gram-Negative Bacteria. Bio-Technology 1:784-791.
45. Lambert C, Sockett RE. 2008. Laboratory maintenance of Bdellovibrio. Curr Protoc Microbiol Chapter 7:Unit 7B 2.
46. Stolp H, Starr MP. 1963. Bdellovibrio Bacteriovorus Gen. Et Sp. N., a Predatory, Ectoparasitic, and Bacteriolytic Microorganism. Antonie Van Leeuwenhoek 29:217-48.
47. Evans KJ, Lambert C, Sockett RE. 2007. Predation by Bdellovibrio bacteriovorus HD100 requires type IV pili. J Bacteriol 189:4850-9.
48. Rogers M, Ekaterinaki N, Nimmo E, Sherratt D. 1986. Analysis of Tn7 transposition. Mol Gen Genet 205:550-6.
49. Lambert C, Smith MC, Sockett RE. 2003. A novel assay to monitor predator-prey interactions for Bdellovibrio bacteriovorus 109 J reveals a role for methyl-accepting chemotaxis proteins in predation. Environ Microbiol 5:127-32.
50. Hicks RE, Amann RI, Stahl DA. 1992. Dual staining of natural bacterioplankton with 4',6-diamidino-2-phenylindole and fluorescent

oligonucleotide probes targeting kingdom-level 16S rRNA sequences. Appl Environ Microbiol 58:2158-63.
51. Kane MD, Poulsen LK, Stahl DA. 1993. Monitoring the enrichment and isolation of sulfate-reducing bacteria by using oligonucleotide hybridization probes designed from environmentally derived 16S rRNA sequences. Appl Environ Microbiol 59:682-6.
52. Perbal B. 1988. A Practical Guide to Molecular Cloning, 2 ed. Wiley Interscience.
53. Laemmli UK. 1970. Cleavage of structural proteins during the assembly of the head of bacteriophage T4. Nature 227:680-5.
54. Yanisch-Perron C, Vieira J, Messing J. 1985. Improved M13 phage cloning vectors and host strains: nucleotide sequences of the M13mp18 and pUC19 vectors. Gene 33:103-19.
55. Toni T, Welch D, Strelkowa N, Ipsen A, Stumpf MP. 2009. Approximate Bayesian computation scheme for parameter inference and model selection in dynamical systems. J R Soc Interface 6:187-202.

Figure Legends

Fig. 1. Unique halo-ed plaque morphology from which the co-isolated novel *B. bacteriovorus* angelus and bacteriophage halo were identified by electron microscopy. (A) Halo-ed plaques containing both *B. bacteriovorus* angelus and bacteriophage halo on lawns of *E. coli* in YPSC double-layer agar plates. Scale bar = 1 cm. **(B)** Electron microscopy of *B. bacteriovorus* angelus, stained with 0.5% URA pH 4.0. Scale bar = 500 nm. **(C)** Electron microscopy of a 0.22 μm filtrate of a predatory culture, showing the presence of phage particles with curved tails resembling bacteriophage RTP. Phage were stained with 0.5% URA pH 4.0. Scale bar = 50 nm

Fig. 2. Kinetics of predation. Measured over 48 hours on late log-phase *E. coli* S17-1 by bacteriophage halo alone (green), *B. bacteriovorus* HD100 alone (red); both bacteriophage halo and *B. bacteriovorus* HD100 combined (purple) versus *E. coli* plus buffer control (blue). **(A)** *E. coli* measured by optical density (OD_{600nm}) (*B. bacteriovorus* are too small to register at OD_{600nm}). **(B)** *E. coli* viable counts. **(C)** *B. bacteriovorus* HD100 enumeration by plaque counts. **(D)** bacteriophage halo enumeration by plaque counts.

Fig. 3. Base model with one prey type. (A) Diagram of the model variables (populations and chemicals) in circles and their positive or negative interactions. The arrow colours match the colours of the terms in the equations in panel (B) and the roman numerals refer to the list of processes in the main text. **(B)** The set of differential equations defining the base model.

Fig. 4. Final model and model variants. (A) Diagram of the final model variables (populations and chemicals) and their positive or negative interactions. The arrow colours match the colours of the terms in the equations in panel (B). **(B)** The set of differential equations defining the final model. **(C)** Top level model variants with different prey phenotypes (models N1, N2, N3, N4). **(D)** Mid level

model variants – **(Di)** methods of development of plastic resistance to *B. bacteriovorus*, **(Dii)** methods of development of phage resistance. **(E)** Low level model variants – predation rate either saturates at high prey densities or not (can differ between *B. bacteriovorus* and phage).

Fig. 5. Hierarchical model selection process. This infers which model variants from Fig. 4 are best supported by the data (frequency of a variant winning out of 1000). **(A)** Competition of models with different number of prey phenotypes. N1: one prey type sensitive to both predators (N_S), N2: two prey types, N_S and phage resistant prey (N_R), N3: three prey types, N_S and N_R and prey with plastic phenotypic resistance to *B. bacteriovorus* (N_P). N4: four prey types, N_S, N_R, N_P and prey with dual resistance (N_D). **(B)** Competition of models with different ways of converting between sensitive prey (N_S) and plastic resistant prey (N_P) but the same saturating *B. bacteriovorus* attack rate (Pii) and non-saturating phage attack rate (Vi). N3-IG-Pii-Vi: N_S intrinsically (spontaneously) converts to N_P and back conversion is coupled to growth. N3-S-Pii-Vi: N_S conversion to N_P is triggered by a signal and back conversion is spontaneous. N3-I-Pii-Vi: spontaneous conversion both ways. **(C)** The combined variant from panel (B) is in the middle and its 'parent' variants on either side. N3-SG-Pii-Vi: N_S conversion to N_P is triggered by a signal and back conversion is coupled to growth. **(D)** Model variants, derived from the combined model in panel (C), but differing in the way the signal is produced. N3-SBG-Pii-Vi: Signal derives from interaction of prey and *B. bacteriovorus* only. N3-SG-Pii-Vi: Signal derives from interaction of prey with both predators. N3-SVG-Pii-Vi: Signal derives from prey interaction with virus (phage) only. **(E)** Different ways of generating phage resistance. Phage resistant prey were already present initially or prey developed resistance *de novo* or both. **(F)** Model variants, based on N3-SBG from panel (D), but differing in attack rate saturation. Pii: *B. bacteriovorus* attack rate saturates at high prey density while Pi does not saturate. Likewise with Vii and Vi for the virus (phage). **(G)** Mortality of *B. bacteriovorus* (phage assumed to be stable) was either set to Hespell et al. (1974) or fitted by the ABC-SMC method. Less decisive competitions (B-D) were repeated 10 times, see Fig. S6.

Fig. 6. Comparison of experimental data (mean values) with fits of the best model variant (from Fig. 5). The model was either fitted using **(A-D)** all experimental data or **(E-H)** all data without dual predation and then used to predict the outcome of dual predation (shown in H). The parameter values for each case are given in Table S1. Experimental data is shown by symbols, lines represent model simulations. **(A-H)** Blue: *E. coli* prey, Red: *B. bacteriovorus*, Green: bacteriophage halo, Pink: medium (not experimentally measured). **(I-L)** Dynamics of the sub-populations of prey and predators predicted by the model that was fitted to all data, corresponding to panels (A-D). **(I-L)** Blue: *E. coli* prey: solid line – susceptible prey N_S, dotted line – plastic resistant prey N_P, dashed line – bacteriophage resistant prey N_R. Red: *B. bacteriovorus*: solid line – free *B. bacteriovorus* P, dashed line – bdelloplasts B. Green: bacteriophage halo: solid line – free bacteriophage V, dashed line – bacteriophage-infected cells I. Pink: medium.

Table Legends

Table 1. Mutational changes present in the genome sequences of the bacteriophage resistant mutants

Supplemental Legends

Table S1. Description of model parameters with their symbols and units. The ranges used for parameter fitting (priors) and results of ABC-SMC fitting are also given. Typical fitted parameters were identified using PCA, see Supplemental text and Fig. S7 for an explanation.

Fig. S1. Isolation and peptide analysis of a bacteriophage halo protein from the 0.22µm filtrate. **(A)** SDS-page analysis of the purified bacteriophage halo showing multiple protein bands. The highlighted ~30 kDa band was extracted and analysed by MALDI QToF MS, showing homology to protein RTP27 of the rosette-tailed bacteriophage RTP. **(B)** Five peptides (bold) found by MALDI QToF MS analysis of the 30 kDa protein from panel (A) with homology to the 34 kDa protein RTP27 (GenBank accession no: CAJ42231.1, EMBL Accession Number AM156909.1) of a rosette-tailed phage (RTP) of *E. coli* (32).

Fig. S2. Plaque morphology from *E. coli* lawns on agar overlay plates of **(A)** purified *B. bacteriovorus* angelus alone after 6 days incubation and **(B)** when co-cultured with bacteriophage halo after 1 day of incubation, showing differences in plaque dimensions (bracketed on plate images taken at identical magnification), morphology and speed of plaque formation.

Fig. S3. The fit of the final model improves from generation to generation in the ABC-SMC method Each generation lowered the threshold for accepting a fit. In the final generation, all accepted fits have a similar distance between simulated and experimental data, showing that fits with further reduced distance did not occur. None of the accepted fits in the first generation would have been accepted in the last generation. The x axis has no meaning and is simply used to spread out the data. See Supplemental Text for the distance measure.

Fig. S4. Improved model fit. The fit of the final model to all data improves over the generations, showing a subset of the generations in Fig. S3.

Fig. S5. Convergence of fitted parameters from generation to generation, We started from the uniform priors to the values after the final generation 12. Parameters that are better informed by the experimental data reach a more narrow spread of fitted values. Medians and quartiles from the final generation are shown in Supplemental Table S1. Note the log scale for the parameters.

Fig. S6. Box plots showing the variation amongst the 10 repeats of model selection. We repeated the model selection procedure shown in Fig. 4B-D ten times because finding 1,000 acceptable parameter sets with a Monte Carlo method could lead to some variation between runs of the ABC-SMC algorithm and it is good to check whether these difference are large. Box plots show the variation

amongst the 10 repeats. We only show repeats for sub-model selections where the outcome was not 100% in favour of one model variant. The Bayes factor is the ratio of the times model X was accepted versus model Y.

Fig. S7. Objective selection of a typical parameter set. Selection was from the hundreds of parameter sets that gave acceptable fits and were nearly equally good (see Fig. S3). Principal Component Analysis (PCA) was used to find the centre of the cloud of parameter sets in 15 dimensional parameter space. Four parameter sets that were closest to the centre were picked and used to run simulations. Results of these 4 simulations were indistinguishable by eye and one of these 4 parameter sets was then chosen as 'typical' and used in Fig. 5 and reported in Table S1.

Fig. S8. Effect of varying initial densities. The model was simulated using the typical parameter values fitted to all data in Table S1 , with either initial values from the experimental data (solid lines), one order of magnitude higher than these values (dashed lines) or one order of magnitude lower (dotted lines). Blue: *E. coli* prey, Red: *B. bacteriovorus*, Green: bacteriophage halo, Pink: medium. **(A)** Effects of initial prey density on prey only scenario. **(B-C)** Effects of varying either initial prey **(B)** or initial *Bdellovibrio* **(C)** densities on *Bdellovibrio* only predation. **(D-E)** Effects of varying either initial prey **(D)** or initial halophage **(E)** densities on halophage only predation. **(F-H)** Effects of varying either initial prey **(F)**, initial *Bdellovibrio* **(G)** or initial halophage **(H)** densities on dual predation.